The development of next-generation small volume biophysical screening for the early assessment of monoclonal antibody manufacturability

Jay Ketan Kong Joshi

Department of Biochemical Engineering

University College London

A thesis submitted to University College London for the degree of Doctor of Philosophy

September 2019

Declaration

I, Jay Joshi, confirm that the work presented in this thesis is my own. Where information has been derived from other sources, I confirm that this has been indicated in the thesis.

Signature:

Date:

Dedicated to my family.

Acknowledgements

As my years studying in the Department of Biochemical Engineering in UCL comes to an end, I am thankful for all the good friends I have made and all the support I have received. From BEng to PhD, these really have been some great years!

Firstly, I would like to thank Prof. Paul Dalby for his knowledge, supervision, guidance and advice throughout the project. Dr. Samir Aoudjane and Dr. John Hales, I am grateful for the time spent training me on all the equipment and data analysis for everything fluorescence.

I would like to thank everyone in BioPharm Process Research at GSK, especially Rachana Shah, Marisa Barnard and Mike Molloy. Without their perseverance, direction and support, this project would not nearly have been as enjoyable, or possible. I am thankful for all the guidance throughout the process of material generation and the characterisation of the monoclonal antibodies. I would also like to thank Sheun Oshinbolu for her “unofficial supervision” through the project.

I wish to acknowledge the Biotechnology and Biological Sciences Research Council (BBSRC) for the continued sponsorship and for making the entire project possible.

To all my friends who have supported me throughout the project, the discussions, catch-up lunches and board games. It has all made my experience at UCL a fantastic one!

To Dada and Dadi, I hope to continue to make you proud.

Finally, I would like to thank my family. Papa and Mama, you are my role models and I am always grateful for your guidance through life. You have shaped me into the person I am today, I can’t thank you enough for everything you have given for me. Dev, thank you for being there, taking me out and reminding me to have fun!

Abstract

The ever-growing need to characterise manufacturability is a key driver for a therapeutic's success. Early information can reduce costs massively and speed up a product's delivery to market. Current monoclonal antibody (mAb) methods are limited by the amount of material required and the time it takes to gain valuable information. The formation of aggregates poses a significant hindrance to biopharmaceutical companies.

This project aims to develop a novel assay sequence to forecast the manufacturability of a mAb by predicting its propensity to aggregate from low populations. The assay will form part of a biophysical screening process in order to de-risk lead candidates.

A panel of six mAb candidates were characterised using currently employed techniques: SEC, DLS and AUC. The limitations were evaluated for each technique. An extensive literature review was conducted to select novel methods to explore as potential replacements for the current methods. After ranking each potential method based on several criteria, fluorescence-based methods were chosen to investigate further.

Several fluorescence techniques were evaluated: fluorescence intensity (FLI), red-edge excitation shift (REES) and time-correlated single photon counting (TCSPC). After evaluating each technique, a 14-day time-course study, where samples were isothermally held at elevated temperatures, was carried out to mimic the current lead panel screening. Spearman's ranking was used to compare the novel techniques to SEC. The earliest time-point at which each technique could detect aggregation of mAbs, formed the basis for a 4-hour time-course study. REES and TCSPC were successful in detecting the aggregation propensity of mAbs. Each technique's ability to detect concentration-dependent aggregation was also evaluated. TCSPC was successful in identifying the aggregation-prone mAbs from their time-decays, and the impact of different buffers.

Finally, a novel assay, using a combination of TCSPC (emission at 330 nm and 395 nm) and REES, was proposed as a method to obtain fast information (<1 minute) on mAbs from low volumes (< 20 µL).

Impact Statement

There is an escalating need for assays capable of characterising early mAb aggregation. Currently, SEC, DLS and AUC are used to identify aggregate-prone molecules. These techniques require relatively long sample times, limiting their screening capabilities.

This project intended to reduce the resources required to get new biopharmaceuticals to market by detecting aggregates from low volumes in shorter times. A fluorescence-based assay based on a combination of techniques was achieved and successfully reduced the time and volume required to identify an aggregate prone mAb within a 4-hour timeframe and across a range of concentrations. The assay is useful to both academia and the biopharmaceutical industry by reducing costs, both in generating enough sample and in time.

The novel fluorescence-based assay could provide:

- Support for the advancement of an in-silico prediction tool based on the protein sequence by providing large datasets on mAb behaviour and propensity to aggregate.
- The basis for a fully automated high-throughput tool for early mAb characterisation by implementing robotics reducing the need for manual tasks.
- Faster decision-making when selecting potential candidate molecules.

The impact of this research could accelerate a more comprehensive understanding of mAb structure and behaviour, and aid to increase the amount of more stable biopharmaceuticals to patients.

Table of contents

List of figures

List of tables

Nomenclature

A	Amplitude
A_{280}	Absorbance at 280nm
AF4	Asymmetric-Flow Field-Flow Fractionation
arb.units	Arbitrary units
AUC	Analytical Ultra-Centrifugation
c	Concentration
CARS	Coherent Anti-Stokes Raman Spectroscopy
CD	Circular Dichroism
CE	Capillary Electrophoresis
CHO	Chinese Hamster Ovary
CIP	Clean-In-Place
CPS	Counts per second
CSM	Centre of Spectral Mass
CUB	Clarified Unprocessed Bulk
D	Translational Diffusion
d_i	Difference between rankings
DCB	Developmental Cell Bank
DLS	Dynamic Light Scattering
DSP	Downstream Processing
F	Final State
f_x	Fluorescence intensity at emission x
FEL	Free Electron Landscape
FFF	Field Flow Fractionation
FLI	Total Fluorescence Intensity
FTIR	Fourier Transform Infrared
GSK	GlaxoSmithKline

HEK	Human Embryonic Kidney
IFE	Inner Filter Effect
IgG	Immunoglobulin
K	Boltzmann constant
l	Pathlength
LED	Light Emitting Diode
LPR	Lead Panel Ranking
MALS	Multi-Angle-Static Light Scattering
mAb or MAb	Monoclonal antibody
MCB	Master Cell Bank
MFI	Micro-Flow Imaging
MS	Mass Spectroscopy
mW	Molecular Weight
N	Native State
n	Number of Data Points
nm	Nanometre
ns	Nanosecond
NTA	Nanoparticle Tracking Analysis
PAGE	Polyacrylamide Gel Electrophoresis
PMT	Photomultiplier Tube
QUBES	Quantitative Understanding of Biomolecular Edge Shift
R	Curvature of exponential
r_h	Hydrodynamic radius
r_s	Spearman's Ranking Coefficient
REES	Red Edge Excitation Shift
RMM	Resonant Mass Measurement
rpm	Revolutions Per Minute

S_x	Singlet electron state (x=state)
SDS	Sodium Dodecyl Sulphate
SEC	Size Exclusion Chromatography
SLS	Static Light Scattering
SPR	Surface Plasmon Resonance
t	Time
T	Temperature
TCSPC	Time Correlated Single Photon Counting
TRF	Time Resolved Fluorescence
Trp	Tryptophan
U	Intermediate State
UCL	University College London
UPLC	Ultra High-Pressure Liquid Chromatography
USP	Upstream Processing
UV	Ultraviolet
UV-Vis	Ultraviolet-Visible
WCB	Working Cell Bank
XRD	X-Ray Diffraction

λ	Wavelength
ε	Extinction Coefficient
τ	Time Decay
η	Viscosity

Chapter 1

Introduction and Literature Review

1.1 Introduction

1.1.1 Overview of Industry

The success of biopharmaceuticals (or biologics), pharmaceutical drug products manufactured from biological sources, has continued to radically impact the industry while representing some of the best modern scientific accomplishments. Since the first recombinant biologic, insulin, was approved in 1982 by the U.S. Food and Drug Administration (FDA), research and development investment has sharply risen (Yuraszeck & Gibbs 2016). Biologics are now used throughout the healthcare industry and are one of the most effective clinical treatments for a wide range of diseases such as, cancers and autoimmune disorders. General benefits of biologics over conventional small molecule counterparts of higher target specificity and activity, reduced side effects, and lower dose requirements explain their attraction and shift of pharmaceutical companies focus towards biologics (Kesik-Brodacka 2017; Craik et al. 2013). For these reasons, and the addition of development costs being similar for biologics and small-molecules, it is clear to see that biologics may dominate the healthcare industry in the future (Yuraszeck & Gibbs 2016).

Since the commercialisation of insulin, biopharmaceuticals have transformed the treatment of various serious and chronic diseases, while taking the place of many traditional small-molecule drugs as the top selling drugs. In 2015, biopharmaceutical revenues were estimated to be 23% of the global pharmaceutical market at $288 billion accounting for 7 of the top 10 listed drugs (Subramaniam 2016). Additionally, as of 2015, there were over 900 biologics in preclinical and clinical development, making it clear that biologics will keep on playing a larger role in years to come (Yuraszeck & Gibbs 2016). The biopharmaceutical market is expected to reach over $380 billion in revenue in 2024 (Tsumoto et al. 2019).

The success rate for biologics is around 11.5% from clinical phase 1 to approval compared to 6.2% success in small molecules (Thomas et al. 2016). As biologics start to cover a larger share of the pharmaceutical market, it is imperative that a better understanding is required during the development process. While some principles of small-molecule development are used in the development of biologics, there is a variety of unique considerations that must be accounted for.

Biologics are typically large molecules that can be roughly 100-1000 times larger than small molecules (Misra 2012). Small molecules are generally well characterised and can be easily purified. On the other hand, biologics are produced as a mixture of molecules, making them more difficult to fully characterise. Biologics are inherently more complex, in part due to the formation of the varying polymeric chains (Kesik-Brodacka 2017). Due

to biological variances in expression systems and process conditions used in the manufacture processes, variability can occur. This may result in variations between batches (Weise et al. 2014). Consequently, batch-to-batch variability must be monitored to ensure a degree of conformance. Biologics also have the potential to illicit an immunogenic response. Small variations in the active ingredient structure and process related impurities can cause this (Kessler et al. 2006; Committee for Medicinal Products for Human use (CHMP) 2007).

The ability for a biopharmaceutical company to predict problems with a biologic molecule is key to its success in the market. With growing pressures on companies, efforts are being made to increase the number of potential therapeutics going through to market and increase the information known about the molecule, while decreasing time to market and development costs. A key factor in this is the use of high-throughput analytical methods, which play a key role in better decision making (Oshinbolu et al. 2018).

1.1.2 Monoclonal Antibodies

Monoclonal antibodies (mAbs) remain the top selling and largest class of biopharmaceuticals, doubling in size in the last 5 years (Grilo & Mantalaris 2019; Tsumoto et al. 2019; Kesik-Brodacka 2017; Walsh 2018). Since the first FDA-approved mAb in 1986 (muromonab), the mAb market has gained a lot of traction in the biopharmaceutical market (Ecker et al. 2015). Between 2002 and 2012, an average of 1.6 mAbs per year were approved. Since 2013, 31 new mAbs and 10 biosimilars have been approved, giving a total of 64 mAbs and 11 biosimilars in use by 2017. This has been helped by the EU and USA regulatory bodies streamlining approvals and increased interest (Tsumoto et al. 2019; Grilo & Mantalaris 2019). As of 2017, 22 companies were developing and manufacturing mAbs commercially, with 7 of those dominating the market with an 87% market share. Genentech (Roche Group) currently lead with 31% of sales and 11 approved mAbs (Grilo & Mantalaris 2019). Some of the top selling mAbs include: Humira®, Remicade® , Rituxan® , Herceptin® and Avastin® (Ecker et al. 2015).

Figure 1 shows the growth in the number of humanised and human antibodies growing dramatically year on year, pushing the contribution of mAbs in the biopharmaceutical sector (Tsumoto et al. 2019).

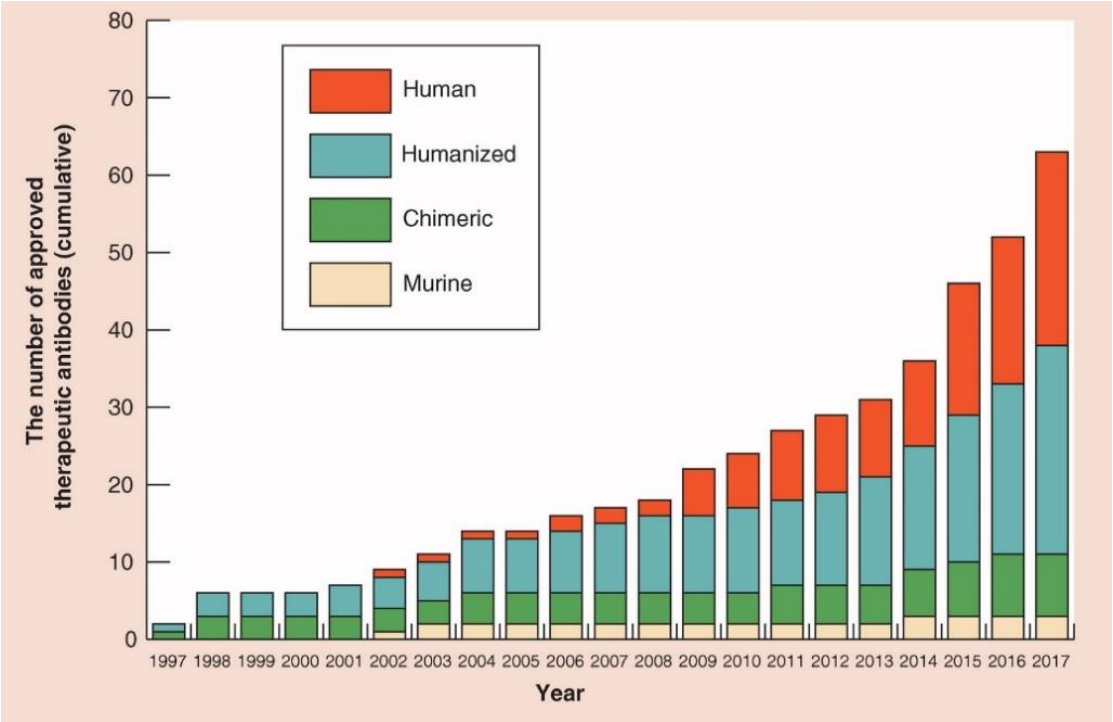

Figure 1 The growth of US FDA-approved therapeutic monoclonal antibodies between 1997 and 2017 (Tsumoto et al. 2019)

Therapeutic mAbs, also known as immunoglobulins (Ig), are large Y-shaped proteins made from 2 light chains and 2 heavy chains linked together with a disulphide bond. In each chain, a variable and a constant domain is found. Three complementary determining regions (CDR) are responsible for antibody specificity. The whole structure can then be divided into: two antigen-binding fragments (Fab) containing 1 light chain, 1 variable heavy domain and 1 constant heavy domain, and 1 crystallisable fragment (Fc) containing the heavy chains (Le Basle et al. 2020). Figure 2 shows the general antibody structure. Monoclonal antibodies can have various sources. Murine antibodies are produced from rodents. In order to reduce immunogenicity, genetic engineering attempts to generate chimeric antibodies. These contain human constant domains with mouse variable domains, retaining the specificity. Over time the CDRs from murine antibodies are grafted onto a human variable region, creating humanised antibodies. Lastly, a fully human antibody are produced without additions to the antibody from a foreign source (Morrison et al. 1984; Hwang & Foote 2005).

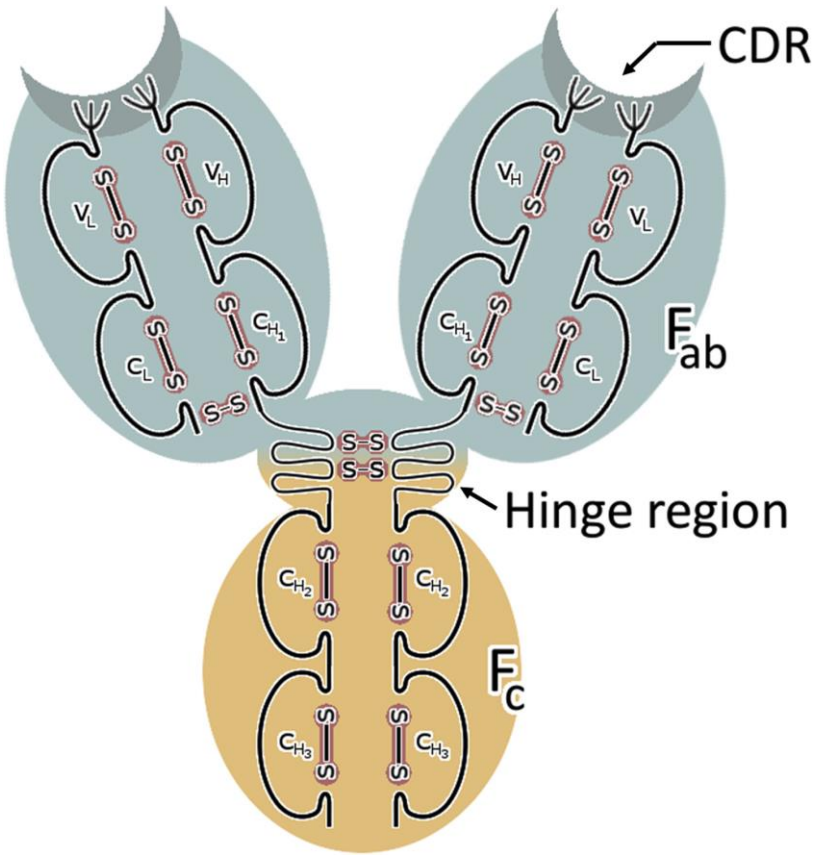

Figure 2 Antibody structure. Fc – crystallisable fragment; Fab – antigen binding fragment; V – variable domain; C – Constant; L - Light chain; H – Heavy chain; S-S – disulphide bond (Le Basle et al. 2020).

Monoclonal antibodies work with the immune system to destroy pathogens by specifically binding via the Fab regions, to the antigen which is a unique molecule on a pathogen. The Fab regions are located at the tips of the Y shape. These are connected to the fragment crystallisable (Fc) region at the stem of the Y shape. The Fc region interacts with effector cell receptors or complementary proteins, allowing the activation of the immune system, prompting a physiological response.

Immunoglobulins (Ig) can be divided into five classes or isotypes, IgA, IgD, IgE, IgM and IgG, based on their constant regions, or multimer assembly (Wang et al. 2007). The most abundant and widely used as therapeutics are IgGs, with 79% being IgG1 and at least 70% having a kappa light chain. IgGs are monomeric and have a molecular weight of around 150kDa. There are 4 subclasses of IgG (1-4), each containing a different heavy chain (Wang et al. 2007). Almost 84% of mAbs approved in 2017 were fully human or humanised.

There is a clear preference for mammalian cell expression, with 61 out of 66 commercial bioprocesses using this expression system. Chinese Hamster Ovary Cell (CHO) based systems are the most commonly used, with over 84% of mAbs approved use the system (Walsh 2018). Their popularity is mainly due to their ability to ensure therapeutic efficacy

by producing glycosylation patterns, high expression, the ability to grow in chemically-defined media, and to guarantee a suitable half-life within the human body (Grilo & Mantalaris 2019; Kelley 2009). HEK293 cells (Human Embryonic Kidney cells) are typically used in the research and development process as they can product material faster, albeit at much lower titres.

1.1.2.1 Monoclonal Antibody Development

Typically, the best mAb must be selected before process development. Initial stages involve screening compound libraries, around 10^6, to find the mAbs with the highest binding affinity to a given antigen (Razinkov et al. 2013). Material for this is generally produced in low expression fast growing cells such as HEK-293 (Spidel et al. 2016). These are then typically ranked, with the top 20-30 mAbs being taken forward (Razinkov et al. 2013). In the past the best binding mAbs would progress in the development process, with an entire process being developed around it (Smith 2007).

Companies are increasingly focussing on assessing manufacturability in a bid to decrease costs at early stages. A wide variety of orthogonal analytical techniques are used to evaluate mAb behaviour under a range of process conditions. The elimination of bad performing mAbs saves enormous material costs and helps get more mAbs to market quicker. This involves characterising the lead panel to de-risk and test developability. From this additional information and a solid understanding of how the mAbs will behave during manufacture and storage, a lead mAb will be chosen (Razinkov et al. 2013).

Resources and efforts have been made to introduce a low-volume, robust, accurate, high-throughput and appropriate analytical tests in order to predict how mAbs behave during the characterisation stage (LeSaout et al. 2015).

Currently, high material requirements (20 mg of material), slow material generation, sample handling, and rigid concentration ranges are bottlenecks in the development process.

1.1.2.2 Monoclonal Antibody Manufacture

Since 1986, the bioprocessing technologies and manufacturing processes for mAbs has greatly evolved. Driven by traditionally low titres and high demand, large manufacturing facilities were built, containing huge vessels of 10,000 L tanks or more. Today, as titres have increased, there is a large production capacity excess, which has led to companies

struggling how best to use it (Kelley 2009). This has opened the field to other, more efficient technologies.

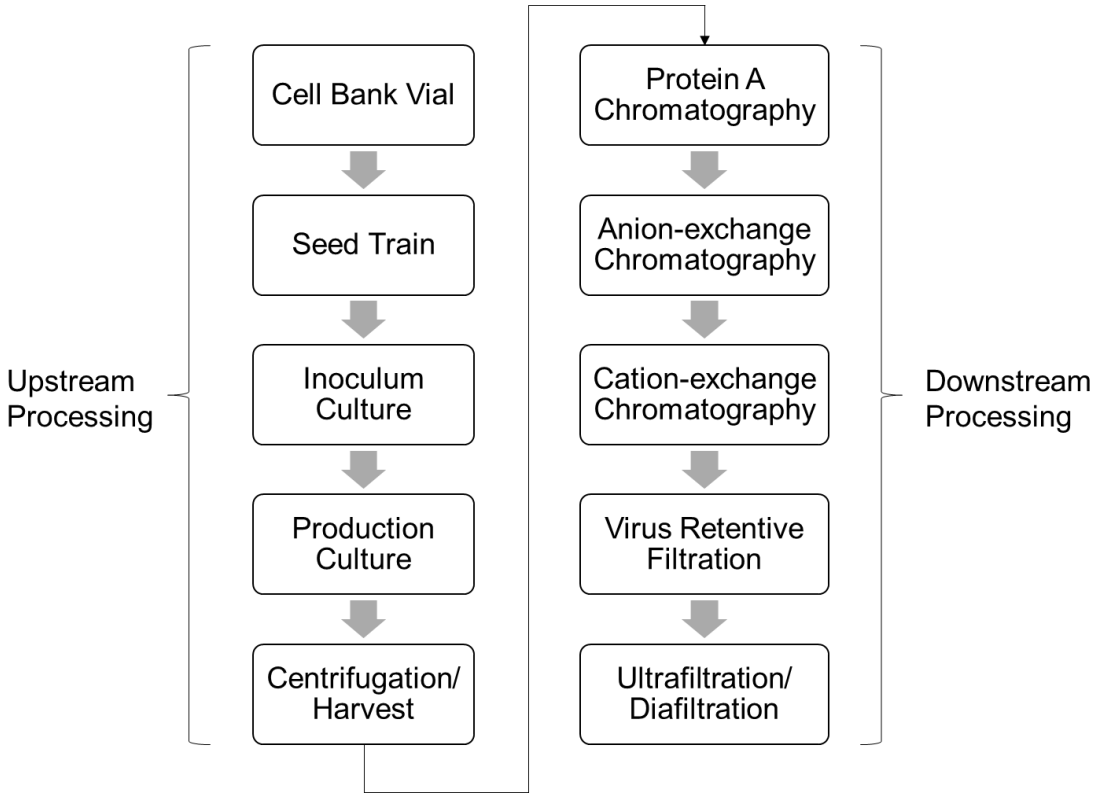

Figure 3 Typical bioprocess flowsheet for recombinant therapeutic monoclonal antibody production. Adapted from (Kelley 2009).

The traditional mAb manufacture process (Figure 3) starts by growing suspended mammalian cells in bioreactors of a specified volume for production. A majority of commercial cell lines derive from a few cell lines, mainly CHO cells, as mentioned previously (Wurm 2004). During the 7- to 14-day production phase, typically operated in fed-batch mode, nutrients are added. The recombinant therapeutic is expressed during this stage at titres of 1-10 mg/mL (Kunert & Reinhart 2016). After production, the cell broth is separated from the cells using centrifugation and then clarified further by depth filtration. The mAb is captured using Protein A chromatography, which elutes at a low pH that also doubles as a viral inactivation step. Anion- and Cation-exchange chromatography are used to further polish and purify to meet requirements. A viral retentive filtration step is used to ensure safety followed by an ultrafiltration/diafiltration step to formulate and concentrate the product (Kelley 2009).

1.1.2.2 Monoclonal Antibody Instability

Despite the advantages of therapeutic mAbs over small-molecule therapeutics, their highly complex macromolecular structure creates numerous difficulties during manufacture, storage, and application. Monoclonal antibody instability are prone to two

types of degradation, physical and chemical (Wang et al. 2007). Due to the inherent dangers from changes in protein structure ranging from reduced drug efficacy to causing an immunogenic response, a standard therapeutic protein must be free from all degradants in formulation and stable for up to two years to be approved (Cleland et al. 1993).

Chemical instability can cause changes in the structure, resulting in completely new entities being formed or the loss of protein activity. Common causes of chemical instability are: deamidation and oxidation. Deamidation is one of the most common chemical degradation pathways. It is caused by the cleavage of the amides glutamine and asparagine. They are converted to acid forms, changing the charge profile (Wang et al. 2007; Cleland et al. 1993; Tous et al. 2005). Deamidation can cause immunogenicity and is the most common reason for heterogeneity in mAbs and is known to cause aggregation (Manning et al. 2010). Oxidation can lead to the deactivation or loss of protein activity. Oxidation can affect methionine, tyrosine, tryptophan, histidine, and cysteine. Although not as predominant as deamidation, oxidation commonly occurs during mAb storage (Wang et al. 2007).

Physical instability can be shown via two pathways: denaturation and aggregation. Protein denaturation can occur under a number of conditions including temperature changes, agitation, and various process stages (Paborji et al. 1994; Wang et al. 2007; Harrison et al. 1998; Vlasak & Ionescu 2011). Protein aggregation is one of the most common consequences of physical instabilities. Non-native protein aggregates occur as protein-protein interactions cause the formation larger structures. Aggregates can greatly reduce activity. They are typically observed at all process stages and are thought to be a dominant cause of immunogenicity (Wang et al. 2007). One of the great challenges facing the industry is concentration dependent aggregation, that proves to be a problem when reaching high concentration formulations (Shire et al. 2004).

In general, the stability of a mAb is dependent on the environment. During fermentation, purification, formulation and storage, a mAb will be applied to many stresses such as: pH changes, buffer agents, concentration changes, temperature changes, shear stresses, freeze/thawing, excipients and being in contact with different materials (Wang et al. 2007).

1.1.3 Monoclonal Antibody Aggregation

1.1.3.1 Overview of Aggregation

Aggregation is the most common and unpredictable form of instability, that poses one of the biggest problems in the development of therapeutic mAbs, as it can occur at all

stages in the therapeutic protein's life cycle (Hernandez 2015; Lowe et al. 2011). Aggregates can form during upstream and downstream processing, during fill-finish formulation operations, shipping and storage (Moussa et al. 2016). Aggregates can cause major problems, from eliciting an immunological response to reducing potency (Wang et al. 2007; Lowe et al. 2011).

Protein aggregation is a process in which a given protein molecule interacts self-associates (Li et al. 2016). Proteins are in a constant equilibrium between folded and partially-unfolded states (James & Tawfik 2003). Under stress, the folded state can destabilise and/or the partially-unfolded state can become more stable (Chiti & Dobson 2009). In its partially unfolded state, proteins can self-associate forming aggregates. For aggregation to occur, key residues (known as "hot-spots") must be exposed due to unfolding. Folding is a fundamental process for biological functionality and is the mechanism in which a protein self-assembles into a specific three-dimensional structure, known as the "native state". Proteins in their native state have the lowest free energy and the most stable conformation (Dobson & Karplus 1999). This stable conformation is preserved via a range of interactions: hydrogen bonds, van der Waals and hydrophobic interactions (Fink 1998; Vendruscolo & Paci 2003). Non-native aggregates can form, which are thermodynamically stable and are irreversible (Dobson 2003). They are highly undesirable for the biopharmaceutical industry (Kalonia et al. 2016). At a physiochemical level, aggregation can occur through one or more different pathways. The first is self-association of a folded protein, where colloidal interactions form with minimal structural change. The second is self-association of non-native proteins where they are partially or totally unfolded. The last is where covalent reactions bind monomers together (Moussa et al. 2016).

Protein aggregates can be defined as protein species of higher molecular weight (oligomers/ multimers) than what was intended and desired (monomer). The term "aggregate" is characteristically a broad term covering all loosely defined oligomers formed by covalent bonds or non-covalent interactions (Philo 2003; Cromwell et al. 2006; Mahler et al. 2009). Table 1 summarises the aggregation types and classifications. Aggregates can take on various forms and sizes ranging from dimers to visible particles. They can be detrimental to a process, and most importantly to a patient. Consequently, this has drawn a huge amount of research interest in both academia and industry and overseen by regulatory bodies. Detection, quantification and characterisation are key areas in characterising protein aggregation (Wang 2005; Berkowitz et al. 2012; Den Engelsman et al. 2011; Razinkov et al. 2013). Several reviews highlight the various techniques used to characterise aggregates (Sharma & Kalonia 2010; Razinkov et al. 2013; Schein 2010; Den Engelsman et al. 2011).

Table 1 Summary of aggregation types and classifications (Sharma & Kalonia 2010; Mahler et al. 2009)

Aggregate Category	Aggregate Type	Definition
Conformation	Native	Properly folded and/or assembled into operative functional state
	Non-native or unfolded	Protein shows largely altered structure to native.
Linkage	Covalent	Proteins held together by covalent links (e.g. disulphide linkages through free groups), so will not usually dissociate in chemical denaturant.
	Physical	Proteins held together by physical interactions (e.g. hydrogen bonding, van der Waals interactions), so would usually dissociate in chemical denaturant.
Reversibility	Reversible	Protein aggregate dissociates when solution condition reverts to initial formation.
	Irreversible	Protein aggregate remains associated in higher-order state when solution condition reverts to initial.
Size	Soluble (<100 nm)	Aggregates are not visible to under a microscope. Typically passes through a 0.2 µm filter.
	Sub-visible (Micron to Submicron) (1-100 µm to 100-1000 nm)	Typically, 0.1 µm to 100 µm in size. These aggregates may be visible in higher concentrations by microscopy.
	Visible (>100 µm)	Aggregates that are larger than 100 µm in size are visible to the naked eye.

1.1.3.2 Mechanisms of Aggregation

Aggregation propensity is thought to be a function of many different conditions: temperature, pH, ionic strength, mechanical agitation, light and excipients (Kalonia et al.

2016). Aggregation can also be pre-defined by the intrinsic properties of the protein, down to the primary sequence level (Li et al. 2016). When the protein experiences a form of conformational change from its monomer form, aggregation prone residues drive strong inter-molecular interactions. These residues are typically located in aggregation-prone regions (APRs), of which there are may be several in a typical mAb would contain more than one (Wu et al. 2014). Due to this, aggregation occurs through several intermediate states (Vermeer & Norde 2000). Most APRs in proteins are located in their hydrophobic core (Ventura et al. 2002).

External stresses introduce the mAb, in its partially unfolded state, to several pathways leading to different fates, as depicted in Figure 4. The populations of all the species depends on their kinetic and thermodynamic stabilities under a given set of conditions.

$$N \rightleftharpoons U \rightarrow F \tag{1.1}$$

Traditionally protein aggregation mechanisms are interpreted using the Lumry-Eyring two-step model (equation 1.1), which suggests a reversible conformational change in the protein is followed by an immediate self-association step, where N is the native protein, U is the unfolded state at equilibrium and F is the final state. The equilibrium between N and U is influenced by external stress such as heat or agitation and F is typically an aggregate (Philo & Arakawa 2009; Chi et al. 2003; Kalonia et al. 2016).

The kinetics in the model are sensitive to the fraction of partially unfolded states due to second order concentration dependence. This means that protein conformational stability can be used to understand aggregation (Kalonia et al. 2016). The Lumry-Eyring model has also been built upon to better show the kinetics (Andrews & Roberts 2007).

Contrarily, there have been some examples of native proteins associating before any conformational changes (Chi et al. 2003; Banks et al. 2012). Experimentally, it has proved challenging to measure the concentration of the intermediate species because of its reversibility and thermodynamic instability causing them to only exist temporarily in small quantities (Li et al. 2016).

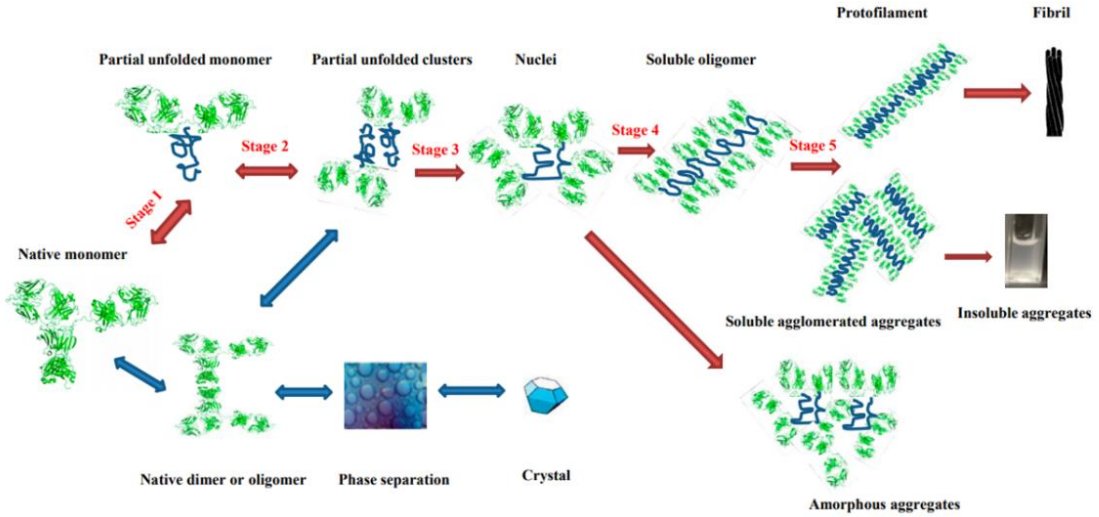

Figure 4 The process of monoclonal antibody unfolding and aggregation. The red arrows show non-native aggregation. The blue arrows show native aggregation. The arrows are directional, with bidirectional arrows showing a reversible process (Li et al. 2016).

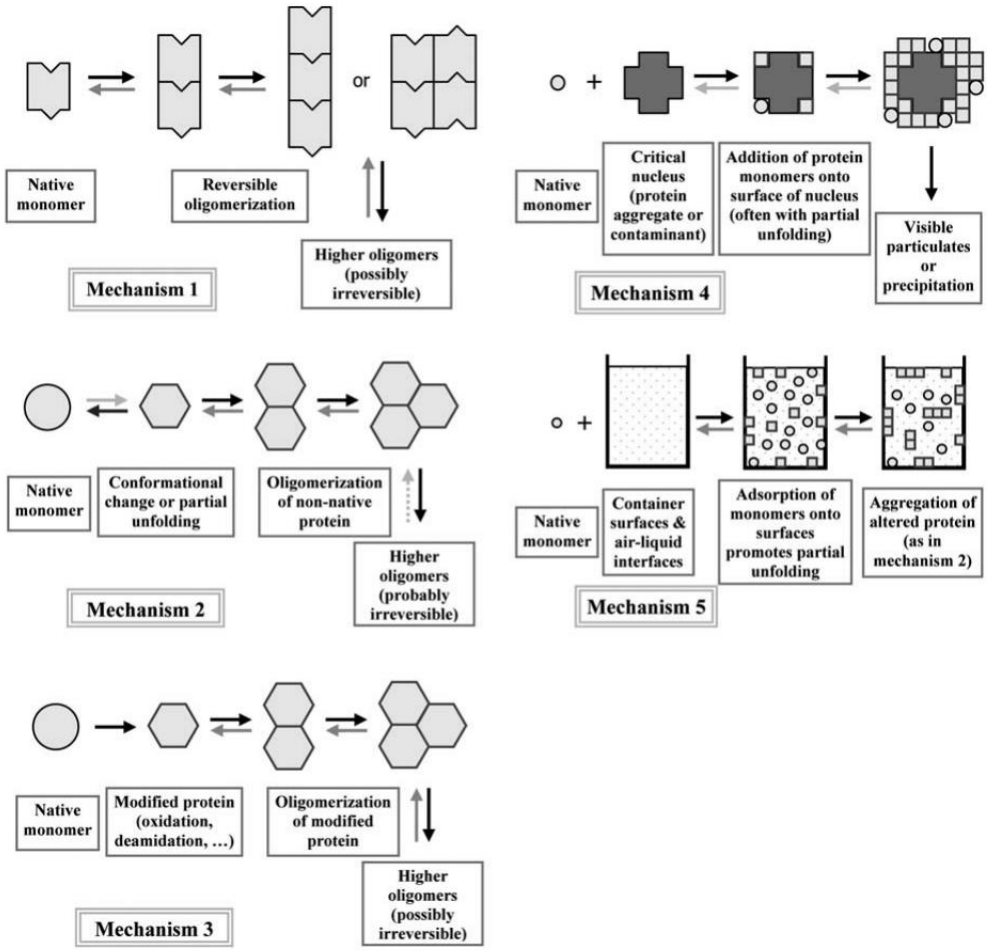

Figure 5 Schematic diagram of common aggregation mechanisms. Mechanism 1 – Reversible association of the native monomer. Mechanism 2 – Aggregation of conformationally-altered monomer. Mechanism 3 – Aggregation of chemically-modified product. Mechanism 4 – Nucleation-controlled aggregation. Mechanism 5 – Surface-induced aggregation. (Philo & Arakawa 2009)

Philo and Arakawa, 2009, describe five distinct aggregation mechanisms (illustrated by):

Reversible association of the native monomer (mechanism 1; Figure 5) suggests that the monomer surface is self-complementary and so will readily self-associate. This forms small reversible oligomers (Philo & Arakawa 2009; Bickel et al. 2016). An example of interleukin-1 receptor antagonist (rhIL-1RA) has shown reversible dimerization at high concentrations, followed by the formation of irreversible aggregates (Alford et al. 2008).

Aggregation of conformationally-altered monomer (mechanism 2; Figure 5) where a native monomer undergoes a conformational change (partial unfolding) which then associates with other unfolded monomers to form small aggregates. A monomer may undergo this change due to external stresses. This mechanism is the most common, as described by the Lumry-Eyring model previously. Several reviews suggest this is the most common and dominant mechanism (Philo & Arakawa 2009; Chi et al. 2003; Wang 2005; Krishnamurthy & Manning 2002).

Aggregation of chemically modified monomers (mechanism 3; Figure 5) is a variant of the conformational change mechanism. Chemical degradation like oxidation of methionine, deamidation or hydrolysis, can cause surface or electric changes causing aggregation (Philo & Arakawa 2009). Aggregates of this kind can be particularly immunogenic (Hermeling et al. 2006).

A common mechanism observed in the formation (mechanism 4; Figure 5) of very large aggregates, visible particulates and precipitates, is nucleation-controlled aggregation (Chi et al. 2003; Philo & Arakawa 2009). Typically, in this mechanism, monomers do not tend to form small aggregates, as it is thermodynamically unfavourable. Instead, if an aggregate reaches a certain size, in this case the critical nucleus, the addition of monomers is strongly favoured. This leads to the formation of much larger aggregate species. This mechanism tends to show a lag phase where no aggregates can be observed for a long period of time, followed by their sudden appearance (Philo & Arakawa 2009).

The final mechanism is surface-induced aggregation (mechanism 5; Figure 5). The monomer undergoes a conformational change which then aggregates. This mechanism could be observed when freeze-thawing, as the monomer binds to the surface of ice crystals (Philo & Arakawa 2009) .

Determining aggregation propensity is a key step in process development. Current efforts require generating large amounts of data over a long period of time to estimate the level of aggregation a mAb may display, thereby accounting for the protracted time it takes for a lead molecule to go through development. This highlights the need for an

early screening platform to accurately detect aggregate propensity to aid rapid decision making (Lauer et al. 2012).

Aggregation also occurs during formulation and administration. At high concentrations of >100 mg/mL, typical of sub-cutaneous administration, mAbs can be more prone to aggregate (Shire 2009; Daugherty & Mrsny 2006). This often forms from native, or native-like conformations, without the need for unfolding or destabilisation (Garcia-Pardo et al. 2014).

The largest challenge when dealing with protein aggregates is that no single technique can analyse all forms and sizes. Additionally, there is no consensus on how to mitigate aggregation (Hernandez 2015). Therefore, typically the choice of technique is determined by the characteristics and size of aggregates, based on prior knowledge. In the absence of this, orthogonal methods must be used to gain as much information as possible about the type of aggregation forming (Sharma & Kalonia 2010; Mahler et al. 2009).

A protein may aggregate by many different mechanisms or pathways depending on its environment. Temperature, mechanical stress, freezing and thawing, protein concentration, solvent and surface effects or chemical modifications to the protein may stimulate aggregation, summarised in Table 2.

Table 2 Summary of factors that influence protein aggregation

Factor	Influence	Reference
Temperature	• Due to low thermodynamic stability, a slight change can alter the globular conformation (essential for biological function). If the protein unfolds it can lead to aggregation • Temperature can increase rate of reactions such as oxidation. • For long term storage, freezing may be required. This can introduce chemical and physical complications such as crystallisation and adsorption to containers	(Chi et al. 2003) (Mahler et al. 2009)
Solution pH and Salt type	• Typically, proteins are stable within a limited pH range. Outside this, aggregation can quickly occur. • In acidic conditions protein cleavage can occur, where in alkali solutions deamidation and oxidation can occur.	(Chi et al. 2003) (Mahler et al. 2009)
Agitation	• Agitation is very likely to induce aggregation. Pumping, stirring, or shaking during the process can be a source of agitation- cavitation, shearing, localised thermal effects or interface effects. • These effects are hard to measure.	(Mahler et al. 2009)
Protein concentration	• Particularly problematic at low volumes and high protein concentrations, that is required during analysis. • High concentrations (>5 mg/mL) can cause molecular crowding. • Low concentrations (<1 mg/mL) can cause weak reversible interactions.	(He et al. 2013) (Mahler et al. 2009) (Shire 2009) (Daugherty & Mrsny 2006)
Chemical modification	• This includes deamidation, oxidation, glycosylation, hydrolysis • Any modification to the protein can cause knock on effects leading to aggregation	(Amin et al. 2014)

1.1.3.3 Aggregation Prediction

The complexity of antibodies allied with the variety of mechanisms by which they can aggregate and added unpredictability of aggregation, make predictions of mAb behaviour and aggregation propensity very difficult.

Historically, the industry has used trial and error, screening different buffers, salts, additives to alter solubility and stress conditions to assess aggregation. This is costly and time-consuming (Gil-Garcia et al. 2018).

Now, different experimental approaches to assess stability used have included: measurements of conformational stability and aggregation onset temperatures in temperature ramping studies; accelerated stability; and behaviour under light exposure, agitation, and freeze-thaw. These methods use changes in a therapeutic protein's physical form to predict aggregation propensity and long term stability (Wang & Roberts 2010). However, these techniques have met with uncertainty due to the level of human judgement involved in decision making. Instead, mathematical models are also being evaluated (Maddux et al. 2014).

In silico (computational) models are increasing in popularity for screening molecules for their aggregation propensity, as derived from large data sets and historical data of known characteristics. The aim of these is to predict how a therapeutic will behave based on its sequence data and known aggregation-prone features. These are limited as huge data banks are required over time (Lauer et al. 2012; Fernandez-Escamilla et al. 2004; Tartaglia et al. 2008; Maddux et al. 2014; Gil-Garcia et al. 2018).

Gil-Garcia et al. (2018) have identified that a computational approach must also be able to rank a therapeutic based on aggregation propensity and solubility to improve a therapeutic's success. This aims to decrease time and money, by examining a myriad of protein variants before any experiments are required. In this case, the top-ranking therapeutics would then undergo biophysical characterisation to assess aggregation propensity. They developed a program called AGGRESCAN 3D (A3D) which predicts aggregation based on structure and protein surface.

Solubis, a recent program that combines aggregation and solubility prediction using the protein sequence, and a statistical thermodynamic algorithm called TANGO (Fernandez-Escamilla et al. 2004), which calculates intrinsic aggregation propensity, have shown some success. It uses a scoring system to assess risk for antibody aggregation in native conditions (van der Kant et al. 2017). Other various *in silico* tools include: CamSol (Wolf Pérez et al. 2019); Modular (Sormanni et al. 2018); and PASTA (Trovato et al. 2007).

These novel approaches highlight the need for a low volume, high-throughput and fast method of aggregate detection, in order to generate the required data, required to build

a model. This strategy aims to predict aggregation in early phases of development to de-risk candidates for failure at later stages (Wolf Pérez et al. 2019). Novel prediction tools aim to assess developability, the likelihood of a successful development of a lead candidate into a stable, manufacturable and safe drug (Jarasch et al. 2015).

1.2 Biophysical Analysis Technique Review

Currently, mAb aggregation is characterised using various biophysical methods. This section aims to cover the principles of current techniques used to detect aggregation throughout this project. Emphasis on throughput and low-volume analysis was used.

The techniques discussed in this section were selected by triaging all available and viable technologies from literature using a Red/Amber/Green (RAG) system (see Materials and Methods).

1.2.1 Current techniques to measure mAb aggregation

1.2.1.1 Size Exclusion Chromatography (SEC)

SEC (also known as gel filtration chromatography) is a chromatographic method used to separate soluble molecules or species or entities based on their particle size or hydrodynamic volume. A stationary phase, made from inert porous beads, form a packed bed. This is equilibrated with a running buffer, which is used throughout the process (GE Healthcare n.d.). Two methods of SEC can be employed, preparative and analytical.

Preparative SEC is a low-resolution size-based separation technique that is used to isolate a molecule from a mixture. Sample volumes of around 0.5% to 4% of the total column volume is used at low flow rates, on long columns (around 60 cm). Particles of >12 µm are used. This method was not used during this project, as it is typically used as a finishing step during purification (GE Healthcare n.d.).

Analytical SEC is a high-resolution size-based separation technique that does not use fractionation. Selective detectors, typically on-line UV-vis spectroscopy (measuring absorbance at 215 nm or 280 nm), are connected to check the quality of the sample. Small sample volumes (<0.5% of the total column volume) is applied in columns of around 15-30cm.Particle size of the beads are around 4-12 µm, which provide high resolution (GE Healthcare n.d.). This technique was used in the project.

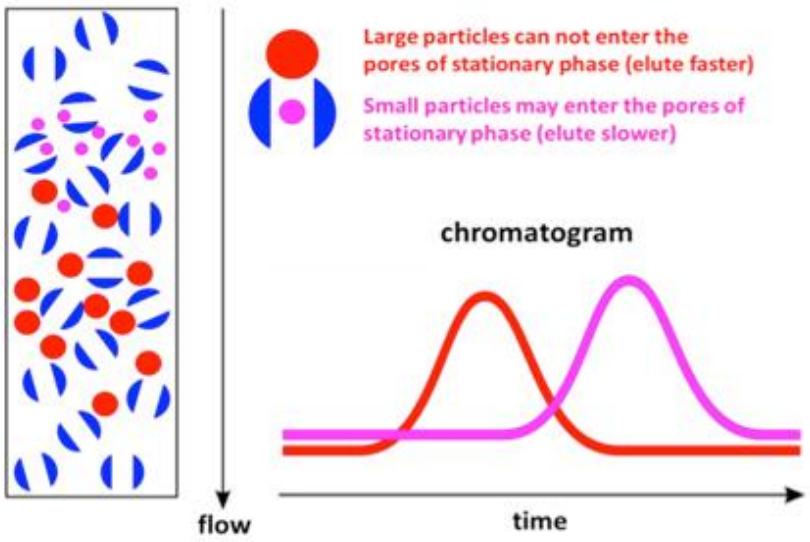

Figure 6 A schematic to show the principles of SEC. The larger molecules cannot enter the pores on the stationary phase so they elute faster through the column (red chromatogram). The smaller molecules enter the matrix eluting slower (pink chromatogram) (Creative Proteomics 2020).

Results from SEC are expressed as a chromatogram, showing peaks of different species as they elute from the column. Figure 6 shows the principles of SEC. The sample enters a column; difference sized molecules will have different elution rates. In this example, the mobile phase contains molecules of two sizes, large molecular weight and low molecular weight. The stationary phase is a matrix of a defined pore size (Fekete et al.

2018). The large molecules do not enter the pores of the stationary phase, as they are simply too big. Therefore, larger molecules elute faster. Low molecular weight species, smaller molecules, become trapped in the pores of the stationary phase. Hence, elution is slower (Mori & Barth 2013). The chromatogram shows the elution peaks with the colours corresponding to the path and elution times of the different sized molecules, with smaller molecules appearing later. For analytical SEC, analysis time typically takes around 25 to 40 minutes (Fekete et al. 2018). Each peak is integrated and calculated as a percentage of the total. This assigns a quantitative measurement to the concentration of aggregates, fragments, and monomer in the sample. Sample concentrations for analytical SEC are around 1 mg/mL.

Analytical SEC is arguably the most used method to characterise mAb aggregation. It is simple, robust, low cost, requires a low amount of sample, is easy-to-use, and can be a high-throughput method (Berkowitz et al. 2012; Hong et al. 2012; Mori & Barth 2013). It can also be used to quantify the amount of aggregates present. Typically used to monitor irreversible soluble aggregates, it can also be employed to characterise protein self-association. It cannot measure insoluble aggregates on its own, and it assumes that these are removed via filtration or centrifugation during sample preparation (Sharma & Kalonia 2010; Mahler et al. 2009).

Often combined with light scattering technologies, one belief is that irreversible soluble aggregates in the oligomer range can be best quantified by multi-angle static light scattering (MALS) coupled with SEC (Hernandez 2015).

Ultra High-Performance Liquid Chromatography (UPLC), allowing a dramatic increase in efficiency and the resolution of separations for proteins. Brought on by the industry's need for fast and efficient procedures for analysis of many samples, UPLC is growing as a viable method to bypass current limitations. UPLC allows an improves resolution, shorter processing time and requires less sample (Fekete & Guillarme 2014). State-of-the-art columns are now packed with sub-3 µm porous particles, and take around 4-8 minutes for analysis (Fekete et al. 2018).

SEC does have limitations, hindering its use as a gold standard analysis tool. For example, due to the dilution of the sample, aggregates may dissociate, creating problems with detection with reversible aggregates. There is also a chance for aggregates to interact with the matrix leading to an underestimation of the real level of aggregation. (Philo et al. 2006; Hong et al. 2012).

1.2.1.2 Light Scattering

Light scattering is a technique used to detect and characterise soluble aggregates between 1-100 µm in real-time to measure kinetics. Light scattering is used to: determine

absolute molar mass and size without reference to standards; gain a better understanding of conformation and particles; and give a good product differentiation in protein aggregation (Johann 2012; Oliva et al. 2004).

Light scattering is caused by light being scattered by particles in solution. The intensity of the scattered light depends on the particle size to incident light wavelength ratio. The smaller the particles, the shorter the wavelength value (Mahler et al. 2009). Rayleigh scattering is elastic scatting from small particles which results in radiation being scattered uniformly in all directions. It is wavelength dependent, with smaller wavelengths scattered more. Mie scattering is the elastic scattering which occurs from larger molecules, comparable or larger than the wavelength of incident light. The result is a non-uniform scattering, not dependent on wavelength (Stetefeld et al. 2016; Stokes 1845; Mie 1908).

The advantages of light scattering are that no dilution is required to prepare the sample. Samples should be optically clear to avoid backscattering as large particles like dust can inhibit good data. Therefore, it is crucial to remove these particles by filtration or centrifugation, provided that sample preparation does not result in artificial results (Mahler et al. 2009).

There are two main types of light scattering techniques: static light scattering and dynamic light scattering. Both techniques characterise different aspects of aggregation, and so are presented as two different technologies.

Dynamic Light Scattering (DLS)

DLS a technique used to determine the size of particles (sub-micron scale) in solution. It measures diffusion rather than the size to produce a sum of exponentials weighted regarding to frequency and scattering intensity. The short term intensity fluctuations with the scattered light arise because of small particles (<5 um) are in constant motion (Mahler et al. 2009). DLS works by measuring the Brownian motion of the particle. Brownian motion is the random movement of particles due to collisions with the solvent surrounding them. The Brownian motion is slower for larger species, so the speed is inversely proportional to the particle size (see Figure 7) (Wyatt Technology 2016)**.** Scattered light can allow the detection of particles between 1 nm to 1000 nm. Intensity fluctuations are used to obtain the Brownian motion and particle size is determined by using the Stokes-Einstein relationship (equation 1.2), where: d(H) = hydrodynamic diameter; K = Boltzmann’s constant; D= translational diffusion coeffiicient; T = absolute temperature; and η = viscosity.

$$d(H) = \frac{kT}{3\pi\eta D} \tag{1.2}$$

The particle size distribution is given by using an autocorrelation function (Jose et al. 2019).

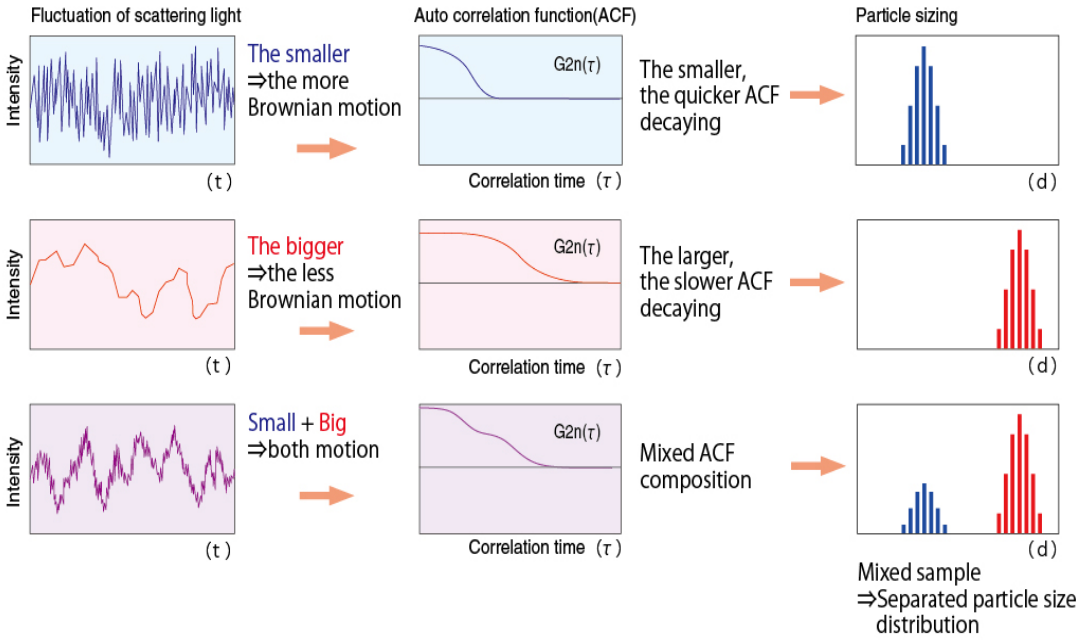

Figure 7 The theory of DLS. The fluctuations due to particles moving are autocorrelated. The decay rate can be presented as peaks between certain diameters of a hydrodynamic radius. The larger the particle, implying mAb aggregates, the less Brownian motion is experienced, and therefore the system can identify its size and distribution (Otsuka Electronics Co. 2015).

The advantages of DLS include that it requires no extensive sample preparation, it is non-invasive and measures in native conditions at varying concentrations (Jose et al. 2019). It has been used in the studies of many different proteins and is a widely-used method in industry (Demeule et al. 2007; Mahler et al. 2005; Ye 2006; Gun'ko et al. 2003).

Despite its widespread use, DLS is sensitive to bubbles, temperature, dust and very large aggregates, which can give misleading results. Surrounding particles can also cause secondary scattering. Filtration can remove this but there is a risk of retaining aggregates and changing particle distribution. Additionally, diluting a sample can cause the dissociation of reversible aggregates (Shire et al. 2004). DLS also has limited resolution, sometimes failing to distinguish between monomer and dimer/ oligomers well, resulting in wider peaks (Jose et al. 2019).

DLS is also sensitive to temperature variations, measurement time, rheology, protein concentration range, non-spherical particle shapes and mathematical model error used for hydrodynamic radii or polydispersity of a sample. DLS results can be biased from large particles, semi-quantitative and unsuitable in polydisperse samples (Hamrang et al. 2013).

Overall DLS is a good tool to better characterise aggregates where dilution occurs, from SEC or FFF for example, causing aggregate dissociation or to be measured under different conditions and is able to be automated using a high throughput plate reader (Hernandez 2015).

Static Light Scattering (SLS)

SLS has been used for decades to determine radii of biological macromolecules such as protein aggregates in solution. It works by elastic scattering, which happens when a laser beam hits a particle. The particle's electrons then re-emit the radiation at the same frequency in all directions (Mahler et al. 2009).

Proteins with a high fluorescence background can be examined with SLS to determine aggregation (Senisterra & Finerty 2009). SLS can be used as a plate-based method (Goldberg et al. 2011). Goldberg et al. show that SLS can be used to measure mAb stability for formulation design.

1.2.1.3 Analytical Ultra Centrifugation (AUC)

AUC is being used to characterise biopharmaceutical proteins as it can accommodate for a wide range of sample concentrations and it is sensitive to small amounts of aggregates. It is considered the industry gold standard (Lebowitz et al. 2002)**.** It relies on centrifugal force to separate molecules based on mass, size and shape, measuring sedimentation velocity (Schuck et al. 2017). The results obtained also depend on a comparison to a standard. It is able to cover a large range of molecules (Philo et al. 2006). Optical detectors, such as fluorescence and absorbance, are used. Absorbance detectors allow characterisation from low concentrations and fluorescence detectors measures fluorescent labels in very dilute samples allowing high concentration studies (Mahler et al. 2009). The most widely used software for estimating distribution of sedimentation coefficients and protein aggregates is SEDFIT (Schuck et al. 2017).

AUC is advantageous as there is no preparation for samples, no matrix, native condition measurement and can operate using a wide range of buffers (Philo et al. 2006; Healey et al. 2018). This allows AUC to measure the protein aggregates without alteration to the original solvent (Gabrielson et al. 2007; Laue & Stafford 1999)**.** AUC is an orthogonal method to SEC and can deliver a thorough representation of the quantity of aggregation (Hernandez 2015).

However, AUC is not a high-throughput technique, as it requires lengthy periods of time (roughly 8 hours) to run a sample and can only handle a few samples at a time (Lebowitz et al. 2002). It also requires highly specialised equipment, trained operators and analysts and increased validation requirements, all leading to increased cost (Philo et al. 2006). Reproducibility and precision can be an issue (Mahler et al. 2009). AUC cannot detect low levels of proteins well and therefore is typically run at higher concentrations. One other drawback, in comparison to SEC, is that it relies on fitting data, rather than giving an absolute value.

In industry, SEC, DLS and AUC are typically used to evaluate mAb aggregation. The current shortcomings with respect to throughput have been briefly highlighted.

The following techniques have received growing interest within industry to augment and/or replace the existing technologies.

1.2.2 Fluorescence-based techniques to measure mAb aggregation

Fluorescence offers a sensitive technique to detect and characterise even trace amounts of aggregates. The key advantages fluorescence offers include high sensitivity, non-destructiveness, and the ability to take real time measurements, allowing early and fast detection (Poole et al. 2012).

Fluorescence occurs in certain molecules that contain fluorophores. A fluorophore is a fluorescent compound that can absorb energy from a photon (entering an excited state) and re-emit light in the fluorescence range as it relaxes back to the ground state in a process that typically lasts femtoseconds (Lichtman & Conchello 2005).

This occurs in three steps:

- Excitation: When a sample is subjected to a beam of light of a certain wavelength, the photon is absorbed by the fluorophore, which raises it from the ground, to the excited state (Lakowitz 2006). Light is emitted from a monochromator, an optical device that transmits light at a specific wavelength, chosen from a wide range of wavelengths of several hundred nanometres (Thompson & Scarlata 2017). An excitation spectrum varies the excitation wavelength and measures intensity at a fixed emission. As a molecule must absorb first to then fluoresce, the excitation spectrum is usually similar to the absorbance spectrum (Figure 8).
- Excited-State Lifetime: The fluorophore exists in an excited state for a finite amount of time, typically between 1-10 ns. In this time, it is subjected to possible interactions within its environment leading to energy dissipation at this stage (Lakowitz 2006)

- Emission: To return to its ground state, a photon is emitted. Due to energy dissipation during the Excited-state lifetime, the emitted photon is of lower energy and therefore emitted at a longer wavelength. The difference between the excitation maxima and emission maxima wavelength is known as the Stokes Shift. This shift is fundamental to the sensitivity of fluorescence techniques (Lakowitz 2006). An emission spectrum, with a fixed excitation wavelength is normally measured (Thompson & Scarlata 2017).

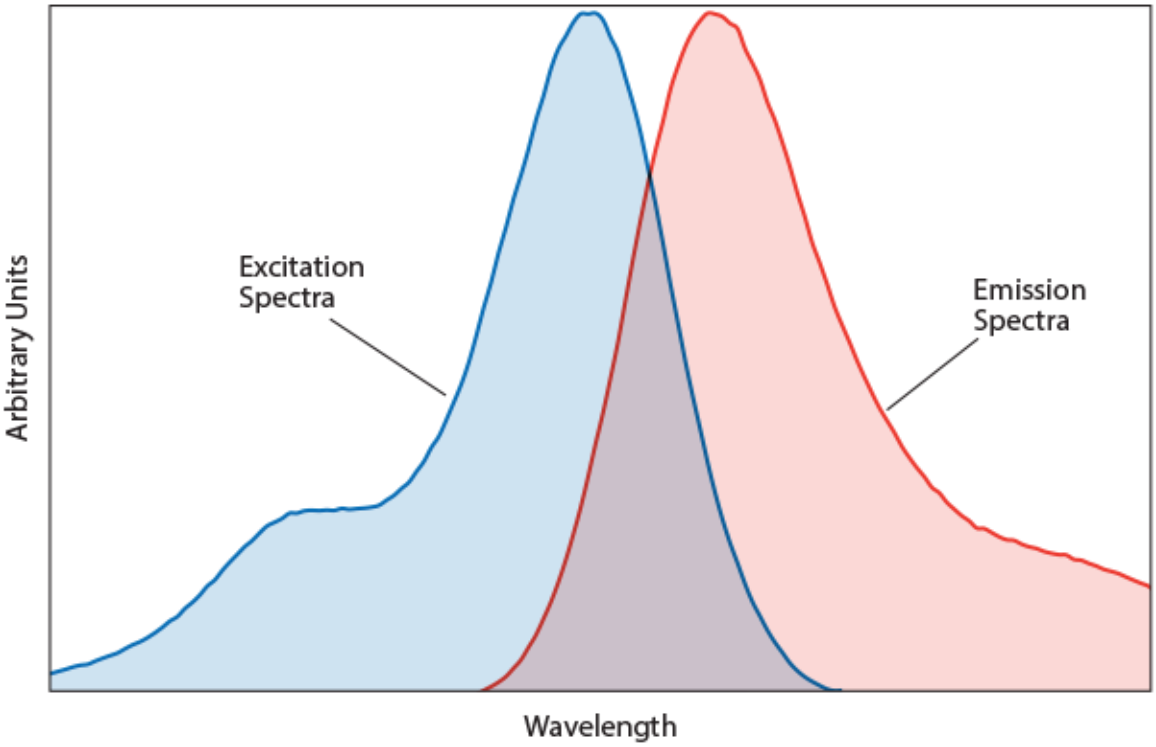

Figure 8 A schematic illustration showing the excitation and emission spectra from fluorescence. The difference between the peak maxima indicates the Stokes shift (Chroma Technology Corporation 2016)

An understanding of the process of excitation and emission in fluorescence spectroscopy can be illustrated using Jablonski diagrams, which show the electronic states of a molecule and transitions between them.This was first proposed by Alexander Jablonski in 1935. It provides a valuable approach to understanding the process of excitation and emission transition between them. Figure 9 shows three diagrams showing how the Jablonski diagram is used.

The left side of the diagrams show the singlet states. A singlet state is one in which two electrons in a single orbital spin in opposite directions cancelling each of the magnetic moments. S_0 represents the ground state. This is the normal state showing the energy of a molecule that is not excited by light. S_1 and S_2 are excited singlet states; here the outermost electron moves to a different orbital when excited. S_2 has the highest energy, followed by S_1 and then S_0.

When a fluorophore absorbs excitation light, energy from the photon is transferred to it causing it to move from the ground state to an excited singlet state depending on the amount of energy transferred. The molecule undergoes a change in vibration and rotation. The probability that a photon will absorb a photon is called the molar extinction coefficient (Lichtman & Conchello 2005; Lakowicz 2006; Thompson & Scarlata 2017).

Once a molecule is in the excited state, there are several pathways by which it can lose the absorbed energy and return to its ground state (Figure 9 c). Internal conversion is the transition between orbital states, S_2 to S_1 for example. No energy is lost as low vibrational energy of a higher electronic state goes to a high vibrational mode in a lower electronic state. During vibrational relaxation, vibrational energy is transferred to nearby molecules, typically solvent molecules. This does not lead to emission of photons. Both processes take picoseconds and bring the molecule back to S_1 (Lichtman & Conchello 2005; Lakowicz 2006; Thompson & Scarlata 2017).

In fluorophores, the energy difference between the S_1 singlet and S_0 ground singlet state is released as a photon. This is the favoured path. The energy released is usually less than the energy absorbed, due to internal conversion and vibrational relaxation. This difference in energy leads to the Stokes shift. Larger Stokes shifts are advantageous as there is a bigger difference between excitation and emission wavelengths. In rare cases, the emitted light can occur at shorter wavelengths as a minority of ground states can be in a higher vibrational state at S_0, causing a larger jump to S_1. This accounts for the overlap between the excitation and emission spectra. Another reason for the overlap could be that multiple fluorophores are excited simultaneously (Lichtman & Conchello 2005).

Figure 9 b shows the range of wavelengths that the emitted photon can have, as an emission spectrum.

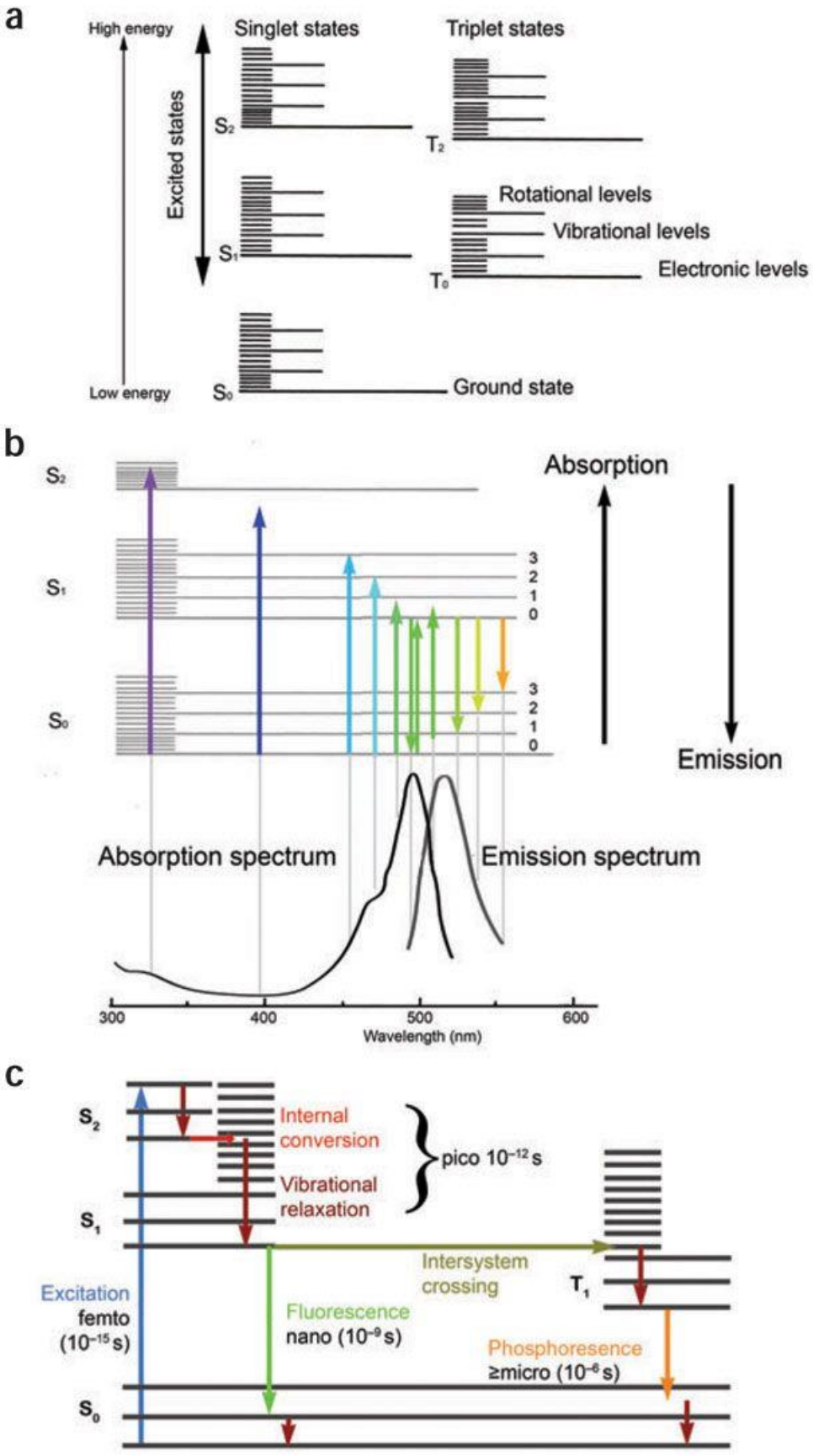

Figure 9 Jablonski diagrams showing the:. (a) energy states of a molecule; (b) spectral characteristics related to excitation/absorbance and emission spectra; and. (c) The steps in fluorescence excitation and emission. From Lichtman & Conchello 2005.

When a fluorophore is continuously exposed to excitation light, it can sometimes become irreversibly damaged in the excited state. This is known as photo-bleaching. Photobleaching is caused by photo-induced chemical destruction of the fluorophore from excitation radiation (Lakowitz 2006; Vincente et al. 2007). This lowers the amount of emission light and can result in the loss of potentially useful information, so caution is required when taking repeated measurements (Vincente et al. 2007; Song et al. 1995). High intensities cause higher levels of photobleaching (Marcu et al. 1999). Some specialised techniques such as fluorescence recovery after photobleaching (FRAP) have been used to analyse protein dynamics based on fluorescent recovery kinetics after photobleaching (Chapeau et al. 2016; Soumpasis 1983). The degree of damage from photobleaching can also be affected by the level of oxygen in a sample or the chemical microenvironment (Song et al. 1995). It is generally good practice to obtain a photobleaching curve for long term studies using fluorescence (Vincente et al. 2007).

Photobleaching should not be confused with fluorescence decay. Fluorescence decay involves the shift of a fluorophore from a high energy state to a lower energy state, in which it can be excited again. With fluorescence decay, the fluorophore may or may not be damaged in the process (Vincente et al. 2007).

Fluorescence based technology is normally used to detect changes in protein conformation, interactions and folding/unfolding as a result of certain stresses (temperature, pH and solute). It is a non-invasive method, which can analyse samples from long-term studies. Fluorescence has been used in fluorescence lifetime studies and anisotropy measurements, which provide further information on protein conformation (Fowler et al. 2002; Owicki 2000; Wriggers n.d.).

Fluorescence can be measured either intrinsically, where the naturally found fluorophores are used, or extrinsically, where the use of a fluorescent dye is applied to boost emission intensity.

1.2.2.1 Intrinsic Fluorescence

Intrinsic fluorescence offers little sample preparation and can measure aggregation under many conditions it would experience in the manufacture process. It is fast and rapid detection makes it a powerful technique.

There are three naturally fluorescent aromatic amino acids that can be used for intrinsic fluorescence detection as most proteins contain at least one of; tryptophan (Trp), tyrosine (Tyr) and phenylalanine (Phe). Table 3 shows the quantum yield, excitation and emission wavelengths and fluorescence lifetime for each of the three fluorescent amino acids. Quantum yield is the ratio of emitted photons to excited photons (Lakowicz 2006).

Table 3 Fluorescence parameters of Tyrosine, Tryptophan and Phenylalanine in Water at pH 7 (Lakowicz, 2006).

Amino Acid	Quantum Yield	Excitation (nm)	Emission (nm)	Lifetime (ns)
Tyrosine	0.14	275	304	3.6
Tryptophan	0.13	295	354	3.1
Phenylalanine	0.02	260	282	6.8

Tryptophan is the most commonly used amino acid for excitation due to its prevalence in many proteins (Möller & Denicola 2002; Yammine et al. 2019; Teale & Weber 1957). Tryptophan is a large hydrophobic amino acid that is generally buried or partially buried in proteins. The polar-NH group in tryptophan can form hydrogen bonds as well as giving it the largest nonpolar accessible surface area of all amino acids (Chothia 1976). This makes tryptophan unique and it can be used as it is localised for monitoring conformation and dynamics of proteins (Chattopadhyay & Haldar 2014).

There is little absorption at 295 nm excitation by other amino acids, so it can be measured selectively (Yammine et al. 2019). Tryptophan has an indole group which is responsible for UV absorption and emission (Chattopadhyay & Haldar 2014). Certain structural changes due to aggregation, unfolding or conformational can cause a reduction in tryptophan emission intensity and a shift in peak wavelength (Yammine et al. 2019; Möller & Denicola 2002). A decrease in fluorescence intensity, coupled with a blue shift in peak maxima to lower wavelengths is usually observed when there is an increase in hydrophobicity around a tryptophan site (Yammine et al. 2019).

Due to the relatively low quantum yield, phenylalanine is not used experimentally as it gives a low fluorescence intensity signal (Lakowitz 2006; Poole et al. 2012; Teale & Weber 1957). Tyrosine is also not often used, despite its relatively high quantum yield, as it tends to be quenched naturally, lowering its fluorescence intensity (Yammine et al. 2019; Teale & Weber 1957; Möller & Denicola 2002).

Fluorescence techniques such as steady state fluorescence and time-correlated single-photon counting (TCSPC) can be used to measure protein aggregation (Palais et al. 2009).

1.2.2.2 Steady State Fluorescence

This is the easiest method in terms of data acquisition and analysis, and the most used fluorescence method. Molecules are selectively excited by using a specific wavelength. Commercial fluorescence spectrometers use monochromators to achieve this. Figure 10 shows the workings of fluorescence spectroscopy.

A sample is illuminated by a light source for a longer period than the fluorescence lifetime. A commonly used light source is an arc Xenon lamp or an LED light of a specific wavelength. The amount of light to the sample is influenced by the slit width. Light excites the sample and the emission light is measured perpendicular to the excitation. This stops interference to the detector from excitation light. Specific emission wavelengths are measured. The light is then detected by a photomultiplier tube (PMT). A PMT is a device that converts incident photons into electrical signals, where light amount is proportional to the current generated, and is capable of detecting single photons (Lakowicz 2006).

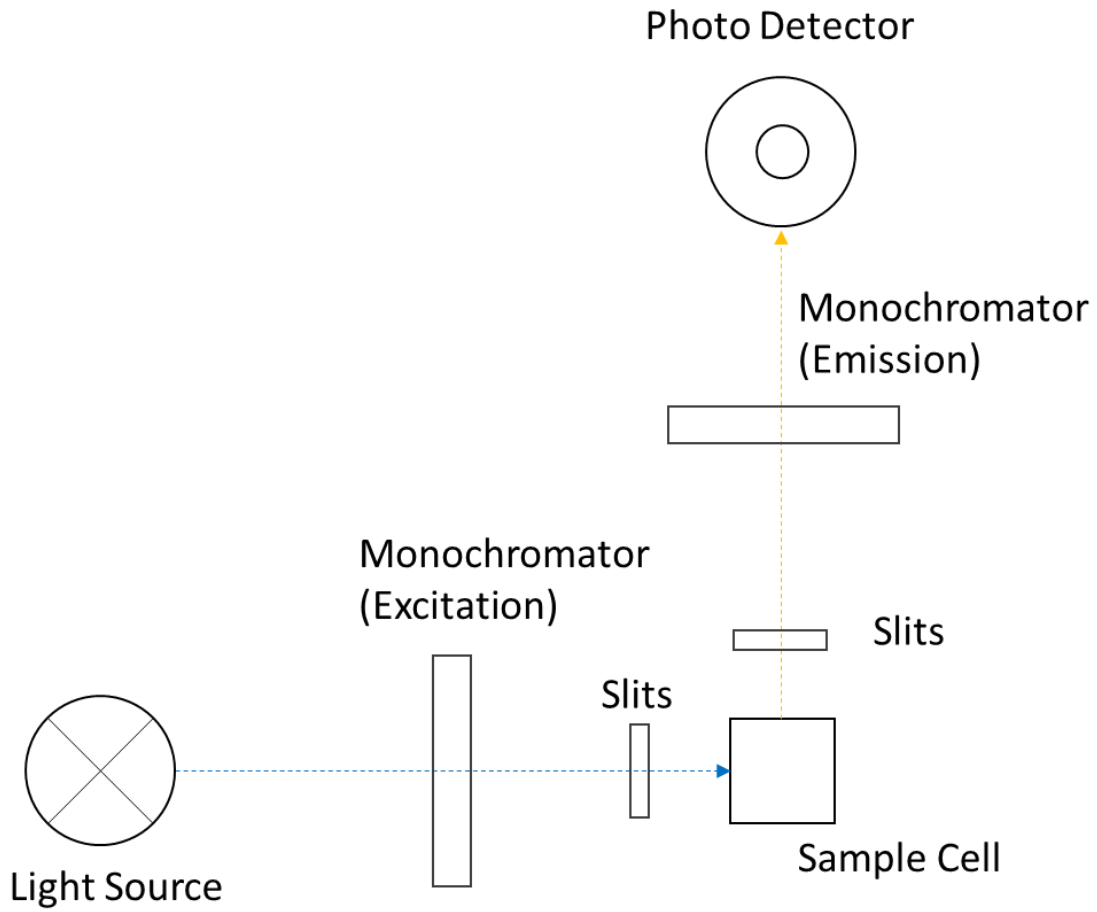

Figure 10 Schematic of fluorescence spectrometer. Select wavelengths are chosen by the excitation monochromator from a light source. Slits vary to allow a light to pass, with smaller slits allowing less light. This is used to change intensity to avoid saturating the detector. Light passes through the sample and is excited. The emission monochromator allows specific wavelengths to be detected.

Two spectra, excitation and emission can be measured. Typically, the spectra are plotted as fluorescence intensity against wavelength. Fluorescent intensity is an arbitrary unit as this can depend on many factors such as sample and the instrument (Poole et al. 2012; Munishkina & Fink 2007; Lindgren et al. 2005).

Excitation Spectra

Fluorescence excitation spectra show the change of fluorescence intensity, with changing excitation wavelength. The emission monochromator is fixed to a known wavelength, with the excitation monochromator scanning across a range of wavelengths. Excitation spectra is generally the same as the absorption spectra and is used to find the excitation maxima (Poole et al. 2012; Lakowicz 2006).

Emission Spectra

This is the more commonly used method. The sample is excited at a fixed wavelength (usually to excite tryptophan) and the emission is measured. As aggregation occurs, it can lead to protein unfolding. This leaves the hydrophobic regions exposed to the aqueous exterior. The less compact structure causes a red shift in the peak maxima and a decrease in fluorescence intensity. However, the intensity is also sensitive to band-pass settings, fluorophores, quantum yield, uniformity of the light and the detection system. Some machines correct for these automatically but care should be taken when measuring raw fluorescence intensity (Poole et al. 2012; Lakowicz 2006). The intensity is found by taking the sum of all emissions.

Different analysis techniques can be used to compare different samples and to evaluate aggregation.

Fluorescence Intensity (FLI)

When measuring the fluorescence intensity for a protein, typically tryptophan is excited at around 280 nm, with the emission peak maximum (λ_{max}) tending to be around 300-350 nm. Intensity is the amount of photon counts at a certain emission wavelength. The total fluorescence intensity is found by integrating the emission or excitation spectrum. To compare the emission spectra of different samples, or the same sample under different conditions, measurements are typically normalised (Lakowicz 2006).

One method used is fluorescence intensity ratio. This method uses the ratio of two points to indicate or highlight changes. This negates any fluctuations between day to day measurements, helps to avoid fluctuations in day-to-day measurements and helps to highlight shape changes more clearly.

1.2.2.3 Red-Edge Excitation Shift (REES)

Red edge excitation shift is increasingly being used to examine protein folding, structure, and dynamics. REES is the shift in wavelength of the emission maxima peak towards higher wavelengths (red shift). This is caused by a shift in excitation wavelength towards the red edge of the absorption spectrum (Chattopadhyay & Haldar 2014; Lakowicz & Keating-Nakamoto 1984; Demchenko 2008). REES comes from the photo selection of

conformational states echoed by different solvent-solute interaction energies (Jones et al. 2017).

REES comes from the relatively slow rates of solvent (water most commonly) relaxation around an excited state fluorophore in the protein. Therefore, REES depends on the motion restricting environment forced on the surrounding solvent molecules. The magnitude of REES gives a good measure of the rigidity of the fluorophores surrounding region (Chattopadhyay & Haldar 2014).

Tryptophan REES has been used to report on intramolecular protein dynamics and examines the ruggedness of the free energy landscape (FEL) (Catici et al. 2016). FEL for a protein describes its structure as a multidimensional energy surface and is the equilibrium of the conformational states that a protein can adopt, affected by vibrational free energy (Jones et al. 2017). With a larger REES effect, there is a larger amount of discrete species present in the equilibrium of conformational states. This suggests a more flexible protein (Catici et al. 2016).

The REES effect is used to provide a quantitative understanding of biomolecular edge shift (QUBES). QUBES allows REES measurements gathered to give a 2D spectral fingerprint. This allows a comparison to a reference fingerprint, giving an understanding of the different conformational states in the protein sample in different conditions. These conformations can relate to aggregation, unfolding and stability (Pudney 2017). Figure 11 shows a rough interpretation of the REES data analysis.

REES can be found by implementing various data analysis techniques (Pudney 2017). First, the emission wavelength, λ_{Em} (nm), and excitation wavelength, $\lambda_{Ex,}$ (nm) are plotted against one another (Figure 11 A), from exciting and measuring the emission over a range. The change in centre of spectral mass (CSM) then can be found from equation 1.3:

$$CSM = \frac{\Sigma(f_i . \lambda_{Em})}{f_i} \tag{1.3}$$

Where f_i is the total intensity at a certain excitation and λ_{Em} is the emission wavelength. All the CSMs are plotted against their respective excitation wavelengths (Figure 11 B). The curve is then fitted, giving an exponential equation.

QUBES parameters are found from the equation below:

$$y = CSM_0 + Ae^{R\Delta\lambda_{Ex}} \tag{1.4}$$

Where CSM_0 is the CSM independent of excitation wavelength (λ_{Ex}), as determined by the amplitude (A) of an exponential with a curvature (R). The magnitude of A and R are used to characterise the REES effect. Using the ratio, A/R, samples can be compared. QUBES can be used to reflect and differentiate mAb unfolding and early aggregate formation. A larger A/R value, increased A and decreased R, leads to a more pronounced REES effect, with more flexible protein and therefore more conformational states (Jones et al. 2017; Pudney 2017). Jones et al. (2017) show that protein flexibility is affected strongly by temperature. This approach is used as it is allows for faster data processing than fitting to a Gaussian model because of its lower dimensionality (Pudney 2017).

REES has been used historically to examine proteins in their native conformation. Studies now apply this to study various conformational changes, such as native to unfolded, denatured or aggregated states (Chattopadhyay & Haldar 2014; Demchenko 2002; Demchenko 2008; Haldar et al. 2011; Raghuraman et al. 2005). REES has many advantages including: fast data acquisition (<2 minute); amenability to proteins with multiple tryptophan residues; use in native buffer conditions; measurements are non-destructive; and that a lot of information can be obtained from a single measurement. In addition, QUBES is shown to be a promising method for detecting protein aggregates (Pudney 2017).

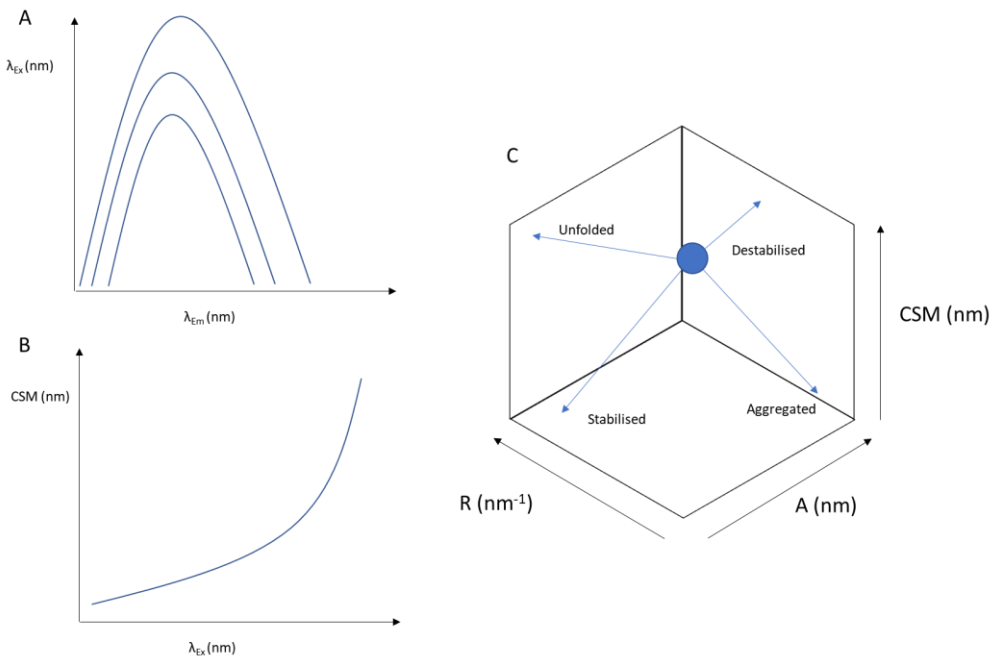

Figure 11 The effects of edge shift. (A) Combined emission and excitation spectra give a high information fluorescence data set for a protein. The intensity and peak position suggest the number of Trp residues, the degree of their exposure, photoselection of conformations and energy transfer. From this plot, CSM can be found from the emission maxima (B) The resulting plot from plotting CSM data against excitation wavelength. Data is fitted to the QUBES equation. (C) A 3D plot using parameters from QUBES equation. Their direction is based on empirical data from Pudney 2017. Plots adapted from Pudney 2017.

1.2.2.4 Time Resolved Fluorescence (TRF)

The fluorescence lifetime can deliver more information than steady state measurements as only the intensity-weighted average of the decay process is used. Lifetime measurements allow a better understanding of the local environment to better understand aggregation (Poole et al. 2012).

TRF is used to measure and monitor molecular interactions and motions, which occur in extremely short time frames (picosecond to nanosecond range). It is applied to biomolecules to analyse their structure and dynamics (Millar 1996; Lakowicz 2006).

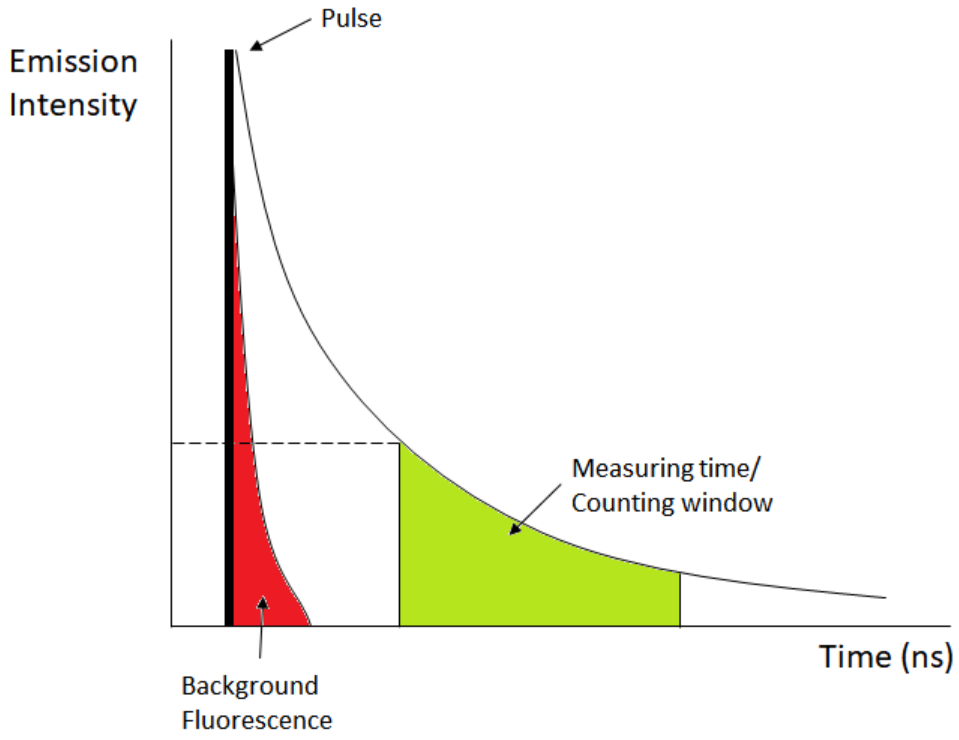

Figure 12 Schematic illustration of the decay of fluorescence as a function of time in TRF. A pulse excites a sample. As a pulse is not perfect, background fluorescence occurs. A delay is incorporated to avoid this. As the fluorophore decays and releases an emission photon, and measurement occurs during the gate time or counting window. Adapted from (Agenet et al. 2012).

TRF is measured by exciting a fluorophore at a set excitation wavelength, typically using a laser. TRF measures the decay of total fluorescent intensity following a pulse to excite the fluorophore. A delay time is used before the data collection of emission intensity to avoid background fluorescence caused by the light pulse. Measurement occurs during the counting window, or gate time. Pulses are repeated as cycles and photons are measured over time to map out the fluorescence decay. This can be shown in Figure 12. This reflects the average time that the molecule remains in its excited state. In principle, the larger the molecule, the longer the fluorescence decays (Poole et al. 2012; Lakowicz 2006; Millar 1996).

1.2.2.5 Time-Correlated Single Photon Counting (TCSPC)

TCSPC is considered a faster, version of TRF. However, for many years it has been considered as the most sensitive fluorescence lifetime method (Peronio et al. 2015). TCSPC works by exciting the protein by using a light source, an LED or a laser is used as it can be quickly pulsed. As the protein emits photons, a detector measures the arrival time, relative to the reference signal (pulse of light). The detector is usually a PMT. It is a repetitive technique, which accumulates data to create a histogram, based on time bins of a set time period, showing counts against time. Figure 13 shows the measurements obtained.

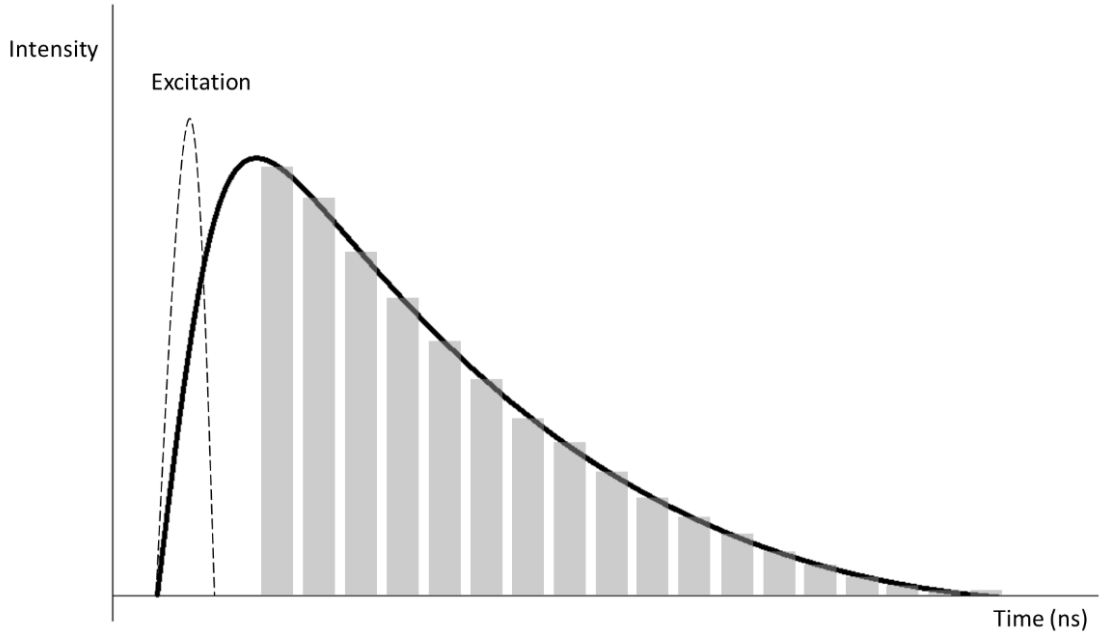

Figure 13 Basic illustration of TCSPC. The sample is excited by a fixed wavelength light source and the first emitted photon is collected, with the time recorded. This repeats until a stop parameter is met. The histogram created from "time bins" shown as grey bars. The black line represents the fit from the measured decay. From this, the fluorescence decay can be obtained. Image adapted from Wang et al. 2011.

TCSPC analyses the return of a molecules from its excited state to back to ground state (Kapusta et al. 2007; Wahl 2014a; Becker 2005). Fluorescence decay has the major advantage of being an absolute measurement, rather than the relative steady state fluorescence intensity. It is also concentration independent and unaffected by photobleaching (Lakowicz 2006). Fluorescence lifetime is intrinsic to the fluorophore and will not depend on the method of measurement. It is sensitive to fluorophore structure, surrounding environment and temperature (Berezin & Achilefu 2010).

The histogram data is fitted and usually follows an exponential decay, see equation 1.5.

$$y = y_0 + A_1 e^{\left(-\frac{t}{\tau_1}\right)} \tag{1.5}$$

A is the preexponential decay (the intensity at time zero), t is the time measurement of the decay and τ is the time decay or fluorescence lifetime. A prompt is taken before measurements and a deconvolution function can be implemented to correct for wide excitation pulses. Fluorescence decay typically lasts from a few picoseconds to tens of nanoseconds (Wahl 2014a).

A low probability of registering one photon per pulse cycle is essential to ensure that the histogram represents what would constitute an accurate time decay if only one photon were shot. Sometimes due to a detector's dead times, where it cannot process another photon for a few nanoseconds yet multiple photons can come through. This is shown in Figure 14. This causes the system to register an artificially quick time leading to an over-representation of early photons. This is called pile-up. Therefore, it is imperative to keep the probability of multiple photons appearing per cycle down (Wahl 2014a). TCSPC avoids time gating and can yield a near-perfect counting (Becker 2005; Wahl 2014b).

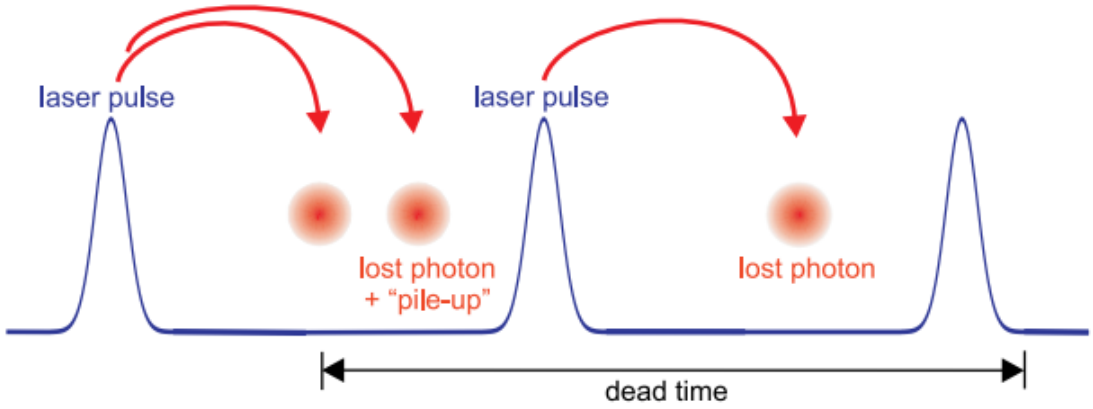

Figure 14 The distortion of a TCSPC measurement caused by pile-up and dead time (Wahl 2014a).

1.2.2.6 High Concentrations and the Inner Filter Effect

At lower concentrations, fluorescence intensity is proportional to the concentration of the fluorophore. This is only valid for cases where there is little to no absorption. Intensity can be reduced by any compound that would absorb either excitation or emission energy from photons. As the concentration increases, this proportionality becomes non-linear (Lakowicz 2006).

At higher concentrations, the fluorophore can absorb energy from emitted photons from the same fluorophore on another molecule. This results in a complete reduction in fluorescence intensity due to a phenomenon called the "Inner Filter Effect" (IFE). The absorption of the incident light is referred to as "primary inner filter effect". Reabsorption of emitted light is "secondary inner filter effect". This hinders fluorescence use for

quantitative purposes (Lakowicz 2006; Kubista et al. 1994; Yuan & Walt 1987; Chen et al. 2018).

Due to the IFE, fluorescence struggles to measure across a dynamic concentration range, thereby limiting its capabilities for measuring concentration-dependent aggregate formation.

Various tools and approaches have been tested to correct for this, ranging from simple mathematical correction factors, to using smaller pathlengths or novel cuvettes (Chen et al. 2018; Kubista et al. 1994).

1.2.3 Other Techniques

1.2.3.1 Raman Spectroscopy

Raman spectroscopy is a type of vibrational spectroscopy (He et al. 2013; Liu et al. 2011). A useful method for analysing protein secondary structure, Raman scattering uses Raman spectroscopy characteristics (rapid, cheap, non-invasive, able to work at high concentrations and non-destructive) (Hamrang et al. 2013).

Raman scattering is a phenomenon in which inelastic light scattering is frequency shifted from that of the incident light. The laser light interacts with molecular vibrations, changing the energy in the light. A small fraction of the laser light is scattered at higher or lower frequencies than the incidence beam. The shifts in frequency from Raman scattered light parallels the frequency of molecular vibrations (Jakubek et al. 2018; Schein 2010).

The frequencies and intensities of the vibration bands are used to determine a protein's conformation and environment (Schein 2010; Jakubek et al. 2018). Raman spectroscopy can select certain amino acid side chains, such as tryptophan and tyrosine (Oladepo et al. 2012; Tuma 2005).

Raman spectroscopy has been adapted to microwell plate technology. One advantage Raman gives over other techniques is that it suffers less from water interference. Raman spectroscopy also benefits from requiring little sample preparation and fast measurement (<5 mins). However, protein specific signals are usually weak and this can result in inconclusive results (He et al. 2013). Several techniques have been attempted to address the weak Raman signal (Das & Agrawal 2011; Li et al. 2012; Zhou et al. 2012).

1.3 Orthogonal Approach to Analysis

As aggregates vary in size by multiple orders of magnitude and form by different mechanisms, an orthogonal approach is required given that no single instrument can assess all forms of aggregates at once. Therefore, the industry has adopted orthogonal approaches.

Orthogonal methods are independent methods that differ in their physical measuring principles, used to measure aspects of a sample. An example for protein aggregates could be microscopy, chromatography or centrifugation (Den Engelsman et al. 2011; Temel et al. 2016; Mahler et al. 2009). Figure 15 shows a typical orthogonal approach to measure aggregates.

The use of orthogonal methods to evaluate data on a case-by-case basis allows a broader assessment of which techniques work best. Orthogonal method is using a combination or a variety of different techniques, each measuring a certain aspect using its own measuring technique. The European Medicines Agency (EMEA) for the production and quality control of monoclonal antibodies and related substances suggests this practice (Mahler et al. 2009).

A good example of this would be SEC. Long considered being a major tool in determining protein aggregation, regulatory bodies are increasingly asking that SEC is coupled with others to validate the accuracy. Typically, AUC or Alternative Flow Field-Flow Fractionation (AF4) are used, as they give an extra assurance that the SEC data is accurate (Berkowitz et al. 2012).

To detect aggregate forms in the range between SEC, AUC and AF4 ranges (up to a few million Daltons) and light obscuration and visible methods (largest particles above 10 µm) techniques such as DLS or Micro Flow Imaging (MFI) are used, to cover the range between 0.1 µm and 10 µm (sub-visible and sub-micron particles). Using a number of techniques to cover the limitations of the previous allows a wider and more accurate picture of the molecule, leading to a safer product overall (Berkowitz et al. 2012; Carpenter et al. 2016; Carpenter et al. 2009).

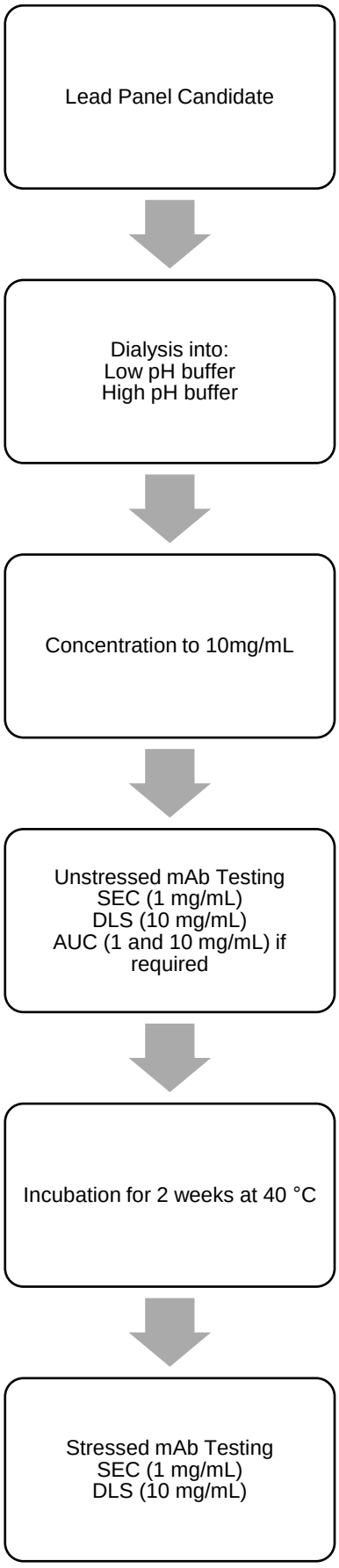

Figure 15 Typical approach to biophysical characterisation to support candidate selection (GSK).

1.4 Thesis Overview

1.4.1 Thesis Aim

The project aimed to develop a novel assay screen for use as a method to predict mAb aggregation from low concentrations and low volumes of material.

This screen aims to apply novel orthogonal techniques to an industrial use. The assay will be used as part of the biophysical screening process in order to de-risk candidates to predict manufacturability and assess developability. The assay aims to speed up current drug development by reducing the gap between discovery of a therapeutic and its manufacture.

Once the assay has been developed, it will be used to identify trends in the sequence, which may be used to forecast aggregation. For this, it must be high throughput to assess a myriad of mAbs.

The new assay must deliver the best information about a mAb using the investigated techniques (in combination with each other). It must be highly sensitive using small amounts of material and be robust to work effectively at low volumes to predict behaviour at higher concentrations well.

A novel assay screen will be evaluated based on the following criteria:

- Ability to detect aggregates to the same level as SEC, DLS and AUC
- Ability to identify species previously undetected by current methods (smaller aggregates or different conformations)
- Increased speed of measurements to increase throughput
- Ability to detect small aggregates (dimers, trimers) and differentiate to monomer form in low populations (concentrations) earlier in time and in low volumes.

1.4.2 Thesis Objectives

Objective 1*:* Material generation and select appropriate methods to investigate monoclonal antibody aggregation at low volumes.

A selection of model monoclonal antibodies will be generated and characterised following standard BioPharm procedures. Bottlenecks will be identified throughout the process. Following this, an extensive literature review will be carried out in order to assess the best methods available to detect protein aggregation at low volumes. There are many techniques, with extensive literature, available. The best suited techniques will be taken forward for the project.

A mAb panel, with positive and negative controls will be generated. Typically, SEC and DLS (and in some cases AUC) are used as orthogonal techniques to assess therapeutic antibodies stability over time and in different concentrations. SEC and DLS focus on assessing the effects of temperature and concentration stresses on the molecule. The initial objective will be to establish different techniques on samples from the lead panel (provided by GlaxoSmithKline, UK) and comparing them to SEC and DLS. The techniques that can correctly identify the same information as currently used methods are carried forward.

An approach to increasing throughput is to reduce the amount of material required as the material generation process is time and cost consuming. An immediate reduction in volume and concentration can increase the amount of mAbs that reach the lead panel and allow more information to be obtained in a shorter period.

***Objective 2**:* Early identification of aggregation-prone monoclonal antibodies.

A 2-week accelerated stability study using thermal stress, can evaluate long-term storage. If successful, the selected techniques will be used in a time-course study, to identify early signs of aggregation or unfolding. The earliest time point where the methods can distinguish the behaviour of each mAb is then investigated further. Reducing time in the isothermal hold can improve throughput. Information from each method can help to understand mAb behaviour and aid in the prediction of aggregation. An investigation into the novel methods' ability to detect concentration dependent aggregation will also be conducted.

Chapter 2

Materials and Methods

2.1 Rationale for cell lines, mAbs and buffers

2.1.1 Cell Line

A key decision was to select which expression platform to use. This was important to weigh factors such as titres and production times when selecting the best method. In this work, two options were considered: CHO cells and HEK cells.

CHO cells offered higher titres, which would allow for all the material required for the project and a consistent product during the project. Training support from the GSK BioPharm Process Research team was available. HEK cells offered much faster material generation, but with a lower yield. Currently, HEK cells are typically used during discovery work to rapidly produce small amounts of material.

CHO was selected for material generation due to ease of support and training, and the opportunity to make all required material required for the project. It was also the best choice for assessing any screening platform as it would be indicative of real-life samples.

HEK cell derived product was considered later in the project due to availability of material from terminated projects. Table 4 briefly summarises the differences between the cell lines (Steger et al. 2016).

Table 4 Rationale summary for CHO and HEK expression systems (Steger et al. 2016).

	CHO	**HEK**
Expected Yield	>1g/L	<0.4g/L
Growth	Slow	Fast
Total time for material	1.5-2 months	2-3 weeks

2.1.2 Monoclonal Antibodies

Six monoclonal antibodies were selected to test out the capabilities of each analytical technique, and to act as controls. The mAbs are terminated projects obtained from the lead panel ranking (LPR) studies in BioPharm Research, GSK. Permissions were obtained to use the molecules. The aggregation profile was based on historical GSK data. Table 5 shows a summary of the mAbs used for the project and the rational for their selection.

Table 5 Summary of the mAbs used throughout the project. mAbs were provided by BioPharm Research, GSK. Aggregation profile based on historical data from Lead Panel Ranking by GSK.

Molecules	Aggregation
mAb A	Negative control in acetate and phosphate buffers. Passed LPR
mAb B	Positive control for small aggregates in high pH buffer)
mAb C	Positive control for concentration dependent aggregation (1 vs. 10 mg/mL in low pH buffer)
mAb D	Negative control in low and high pH buffers
mAb E	Precipitation sometimes seen in high pH buffer
mAb F	Positive control for concentration dependent aggregation (1 vs. 10 mg/mL in low pH buffer)

mAb A was selected to be the negative control. It passed the LPR and was manufacturable. In historical GSK tests, it showed less than 5% aggregates in both the low and high pH buffers by SEC after 14 days of thermally stressing at 40°C.

mAb B was selected to be the positive control, exhibiting over 20% aggregation in the high pH buffer after 14 days held at 40°C as determined by SEC. It showed less than 5% in the low pH in SEC. This mAb was selected to represent a typical mAb which would aggregate in storage.

mAb C was also selected as a positive control. In SEC, at 1 mg/mL it showed little aggregation before and after thermally stressing. In DLS, at 10 mg/mL, mAb C showed high amounts of aggregation in the unstressed samples only in the low pH buffer, indicative of concentration dependent aggregation. This was confirmed by AUC, which showed over 70% small aggregates at 10 mg/mL in the low pH buffer.

mAbs D, E and F were added to the panel after A, B and C were characterised and tested.

mAb D was selected as it showed very little aggregation after thermal stressing and so was chosen as a secondary negative control.

mAb E was selected as was shown to precipitate in the high pH buffer over time. This mAb had initially passed the LPR tests after stressing and only precipitated in some

samples. Therefore, it was not carried through and acted as an unknown for the purposes of the project.

Mab F exhibited a very similar aggregation profile to mAb C but to a higher degree. This mAb was selected as a back-up to mAb C and as a worst case mAb.

2.1.3 Buffers

The buffers were selected to mimic the current biophysical screening process. The exact composition of the buffers is confidential.

Phosphate Buffer (High pH buffer): Selected to provide unfavourable conditions for the antibody. To examine the manufacturability, pH 7.5 was chosen as it is the highest pH a mAb would experience during downstream processing. It is also selected as it can be used to evaluate behaviour in the pH of blood (Rosenthal 1947). As part of the lead panel ranking if a molecule does not fare well, recommendations to DSP and serum stability are made.

Acetate Buffer (Low pH buffer): Selected as it gives favourable conditions, used in many formulation buffers. It is expected that the monomers will be most stable in these conditions. pH 5 is the lower end that the mAbs would experience for prolonged amounts of time and so will be useful to evaluate manufacturability.

2.2 Materials and Methods

Note: Some information regarding proprietary materials and methods have been redacted as stated in the NDA signed between UCL and GSK.

2.2.1 Material Generation

Standard industry protocols were followed to generate material. The process was written up in the electronic lab notebook (eLNB). Owing to the commercially sensitive process, certain elements of the process have been omitted from this report.

mAbs A, B and C were generated for this project. mAbs D, E and F were provided by GSK in PBS buffer which was dialysed into acetate and phosphate buffers for the purposes of this project.

2.2.1.1 Cell Culture

To produce the antibodies for the assays, CHO cells were cultured. Vials of frozen transfected CHO cells (stored in liquid nitrogen), were obtained from BioPharm Research, GSK. Following the revival protocol, the cells were thawed ready for growth in shake flasks (Corning). Passages took place every 3-4 days, scaling up the volume up to 1 L to enough create cells for inoculating the production flasks. mAbs were cultured in GSK proprietary chemically defined serum free media. A developmental cell bank (DCB) was made, by freezing a section of the shake flasks cell culture. This enabled material production later if required. Once scale up was completed, the shake flasks were passaged into production flasks. In total three production flasks (600 mL cell culture volume in 1 L flasks) were made for antibody A and eight were made for antibody B and C.

The production run lasted 10 days or more, with a supplement feed on day 7. However, the run was cut short due to a power supply interruption. Enough material was still obtained from the production process. Cell culture titre, viability and metabolites were observed to monitor the health of the cells, the productivity and to examine if any contamination has occurred.

Viable cell counts were determined using the Vi-CELL XR Cell Counter (Beckman Coulter). Using a dilution factor of 2, 500 μL of cells and 500 μL TryplE Express (Invitrogen) was taken and incubated for 10minutes at 37 ºC before analysis on the Vi-CELL. IgG titre, glucose and lactate during production was found using the Cedex Bio HT Analyzer (Roche). IgG titre during shake flask culture and production was determined using the IMMAGE Immunochem system/ Nephelometer (Beckman Coulter). Five hundred microliters of cells were centrifuged at 13200 rpm for 2 minutes before loading onto the Cedex and the Nephelometer (250 μL into each).

2.2.1.2 Harvest

On day 10 of production, the cell culture was harvested using a Pall Allegro Filtration System. The system is a two-step filtration, first through a 0.4 µm, then a sterile 0.2 µm filter. A Watson-Marlow 505S peristaltic pump was used to maintain sterility and to minimise mechanical stress on the product. The clarified unprocessed bulk (CUB) was stored at 4 °C until purification.

2.2.1.3 Purification

The mAbs were purified from the CUB by protein A affinity chromatography using MabSelect SuRe (GE Healthcare) on an AKTA Avant system. The protein A eluate was then collected in a cooled area, to maintain stability during the overnight purification. A small sample was collected for pre-neutralisation aggregation evaluation in SEC.

The protein eluate was then neutralised by adding Tris Hydrochloric acid buffer (pH 7.45). Once neutralised, the eluate was filtered through a 0.22 µm sterile filter (Nalgene) and stored at 4 °C. SEC was run for a sample from the neutralised product.

Table 6 shows the summary of the buffers used for protein A affinity-based purification. The exact buffer compositions are commercially sensitive and key information has been redacted.

Table 6 Buffers used for Protein A purification

Buffer	**Composition**
Equilibration	Tris HCL (Neutral pH)
Wash	High salt wash
Elution	Acetate base (Low pH)
Clean in Place (CIP)	Sodium Hydroxide (pH >11)
CIP Strip	Acetic Acid (pH<3)
Storage	20% Ethanol

2.2.1.4 Quality check

The molecular weights of the produced mAbs were measured using reduced mass spectrometry. Ten microliters of 1 M DTT (reducing agent) was added to 100 µL of 1 mg/mL sample and incubated at 37 °C for 60 minutes. An Agilent Poroshell 300SB-C8 5 µm column with an injection volume of 10 µL. The open access mass spectroscopy system (ESI-TOF-LCT, Waters) at GSK was used. The observed value was compared to the theoretical to determine if the correct molecule was made.

2.2.1.5 Concentration step

The neutralised protein A eluate was concentrated using a Millipore centrifugal filtration unit at 3000 g. The buffer passes through a membrane to concentrate the remaining product to 10 mg/mL. For larger volumes, the filtration unit was topped up after 30 minutes to enable a continuous concentration. The concentrated solution was removed, and the membrane was washed to ensure maximum recovery. Once the concentration reached 11 mg/mL, all material was collected and stored in the fridge at 4 °C.

2.2.1.6 Dialysis

Each mAb molecule (A-F) was dialysed into two buffers: Phosphate buffer and Acetate buffer by injecting the concentrated sample, into a Pierce Slide A-lyser dialysis cassette,. This was submerged in an excess of either Acetate or Phosphate buffer (1800 mL) and left to stir at 4 °C overnight. The dialysed materials were collected into 15 mL tubes to create stock solutions. Buffers were prepared by Sodexo on GSK site..

2.2.1.7 Material stocks

A series of stock solutions were created from the 10 mg/mL dialysed material. This was done via serial dilutions, with the appropriate buffer, into 1 mL vials. The concentrations chosen were: 0.01, 0.1, 0.5, 1.0, 5.0 and 10.0 mg/mL.

The stock solutions were created for use in multiple analytic techniques. Vials of 1 mL at 10 mg/mL are to be frozen for long-term storage by freezing at -80 °C. All concentrations were validated using the Nanodrop spectrometer 1000. The extinction coefficients for mAb A, B and C are 14.40, 15.40 and 13.90, respectively. Two microliters are loaded onto the Nanodrop and a UV measurement at 280 nm was taken.

2.2.1.8 Storage

To ensure the safe long-term storage of the antibodies, a freeze-thaw study was conducted. This enabled confidence in the storage method and long-term storage during the project.

One millilitre aliquots of the three antibodies in both buffers were made at 10 mg/mL. SEC and DLS were performed to evaluate the baseline. The samples were then frozen at -80 °C and left to thaw in room temperature. SEC and DLS were then carried out. Vials were frozen again, ending cycle 1. This was repeated 2 more times. The results from SEC and DLS were compared to ensure no major increase in aggregation and that long-term storage was possible. Samples when used for testing were thawed at room temperature and not used again to avoid additional levels of aggregation from freeze-thawing.

2.2.1.9 Material Transfer

Material was transferred to UCL using GSK's delivery service. Vials of 1 mL, of the three molecules in different buffers and concentrations were shipped using next day service. They were transported at 4 ºC and frozen on the day of arrival.

2.2.2 Experimental Analytical Techniques

Analytical techniques to investigate aggregation were selected using a RAG (Red-Amber-Green) ranking system created for this project, based on expert opinion from academia and industry, and first-hand experience. Green indicates a suitable technique; Amber indicates a possibility and Red indicates that the technique is not suitable. A list of current and novel techniques was created based on an extensive literature review, with the advantages and disadvantages, ability to be Microfluidic and possibility of being a flow-through method, listed alongside. The list was evaluated by supervisors with a ranking, according to opinion, assigned to each technique. The agreed methods were taken forward for investigation.

2.2.2.1 SEC

SEC analysis was performed on an open access system maintained by a member of GSK Analytics. The SEC-HPLC uses a silica-based TSK-Gel G3000SWXL (7.8 x 300 mm) column, from TOSOH Bioscience, on an Agilent 1100 series HPLC valve system using a UV detector at 214 nm and 280 nm. The running buffer is composed of sodium phosphate and sodium chloride, pH 6.7, with a flow rate of 1.0 mL/min was employed. Samples were loaded into a 100 µL vial and stored in a cooled sample tray. Ten microlitre injection volume is loaded onto the column and the average run time was 16 min. Chromatograms are viewed and peak integration was analysed using the ChromView software. Measurements were taken in triplicate, with the mean taken. Reintegration offline was performed where required.

2.2.2.2 DLS

One hundred microlitres of 10 mg/mL sample in native buffer is loaded into each well of a Corning 96-well clear polystyrene plate which was then sealed to stop evaporation. Samples are run in triplicate and read using a Wyatt DynaPro Plate Reader II. A 30-minute wait time was included, to ensure the temperature reached 25 °C. Ten acquisitions are taken for each sample. After finishing the measurements, the plate was cooled until collection. Data was analysed using the Dynamics software. Samples were recovered. The hydrodynamic radius for a typical mAb is generally around 5-7 nm. A larger hydrodynamic radius (8-500 nm) indicates anything from dimers to small aggregates.

2.2.2.3 AUC

AUC was used only after SEC and DLS analysis found anomalies or indicated concentration dependent aggregation. AUC was performed using a Beckman Optima XL-1 system, which utilises the ProteomeLab software for data acquisition and Sedfit software for data analysis. One hundred microlitres of 10 mg/mL mAb solutions were loaded into a sample chamber, with 100µL of buffer into the buffer chamber. Larger volumes are used for low concentration samples to ensure a suitable pathlength. Temperature was equilibrated in a vacuum to 20 ºC before running. 7 samples at a time can be run, due to limited availability of AUC cells. Readings are measured using a monochromatic light source. AUC is run at 30,000 rpm. Typically, 300 reading scans are taken, with the first 10 and last 100 excluded from analysis. Sedimentation coefficient acts as a measurement of size, which is then converted into an estimated molecular weight (MW). A typical mAb is around 150 kDa.

2.2.2.4 Fluorescence Intensity

Fluorescence intensity measurements were taken using a FluoroMax-4 spectrofluorometer from (Horiba, Kyoto, Japan). The FluoroMax-4 was turned on and left to warm up for 60 minutes prior to any measurements. FluorEssence software is used for data acquisition. OriginPro software (OriginLab) is used for data processing. Water Raman was taken to ensure the lamp is fully warmed up and calibrated. Two millilitres of water in a quartz cuvette with a 10 mm path length (Hellma) was excited at 350 nm with a 5 nm bandpass. Emission is taken from 365-450 nm at increments of 1 nm. The expected emission peak is 397 nm. Measurements were taken at room temperature.

Three cuvettes were used during the experiment, depending on the situation. The three cuvettes are:

- 100 µL Ultra-Micro Far UV quartz cuvette with a 10 mm by 2 mm window (Hellma). Used in initial experiments.
- 12 µL Ultra-Micro Far UV quartz cuvette with a 1.5 mm by 1.5 mm window (Hellma). Used in time-course experiments.
- MicroSense microlitre TrayCell (0.7-10 µL sample size) (Hellma). Used in high concentration studies due to small pathlength.

Fluorescence Intensity was measured by exciting a sample at 280 nm. An emission spectrum was taken from 290 nm to 500 nm at increments of 1nm and an integration time of 0.1 s. Slit widths were set at 2.5 nm to lower the amount of light coming through. This was done to avoid counts surpassing 2 million counts, the point where a detector becomes saturated. A connected water bath was used to keep the system at 22 °C.

Fluorescence intensity (f_i) was calculated by taking the counts at certain emission wavelengths. Total fluorescence intensity, equation 2.1, was found by the sum of all fluorescence intensities at each wavelength in the emission spectra ($f_{\lambda Em}$). Fluorescence spectra were normalised to allow for comparison of samples with differing intensities.

$$f_i = \Sigma f_{\lambda Em} \tag{2.1}$$

Measurements were taken in triplicate, by using a fresh sample each measurement, to give a mean intensity.

The effect of photobleaching was found by repeating fluorescence intensity measurements. The degradation, seen in the reduction of total fluorescence intensity. Photobleaching was found to be negligible when 100 µL samples were taken from the bulk sample and returned.

2.2.2.4.1 Fluorescence Ratio

Fluorescence ratio has been used alongside fluorescence intensity. The ratio allowed for a like for like comparison based on raw data, without the need for normalisation. It also permitted a comparison of spectral shape differences.

Fluorescence ratio (f_{330nm}/f_{395nm}) was found by the ratio of the intensity emission at 330nm (f_{330nm}) and intensity emission at 395nm (f_{395nm}), as shown in equation 2.2:

$$f_{330nm}/f_{395nm} = \frac{f_{330nm}}{f_{395}nm} \tag{2.2}$$

The ratio was found by using the tryptophan maxima peak at 330nm emission and 395nm, where a secondary peak was shown to appear in some samples.

2.2.2.4.2 Red Edge Excitation Shift

REES was carried out using the same principles are fluorescence intensity measurements. Samples were excited at 270-310 nm at increments of 5 nm and the emission was taken from 320-500 nm at increments of 1 nm. Emission scan files were batched to allow a faster data acquisition and automate the whole scan.

REES is calculated by plotting the emission intensities at each excitation wavelength. The total fluorescence (f_i) is calculated from the sum of all emission intensities ($f_{\lambda Em}$) at each excitation wavelength (See equation 2.1). Next, the centre of spectral mass

(CSM) is calculated, (equation 1.3). The emission intensities at 320-500nm ($f_{\lambda em}$) are multiplied by the emission wavelength (λ_{Em}). The sum of this is divided by the f_i that was previously calculated.

CSM is then used to calculate the QUBES parameters, which can be used to calculate REES. The CSM for each excitation wavelength is plotted against the excitation wavelength. The plot is fitted to an exponential growth (equation 1.4) curve using OriginPro. The QUBES parameters (R, CSM_0 and A) can be then processed as a 3D plot or as a A/R ratio.

Data analysis was carried out using a customised template on OriginPro to allow for faster data processing, eliminating the need for manually selecting each file. Triplicate measurements were taken, and the mean values were taken.

2.2.2.5 Time Correlated Single Photon Counting

TCSPC uses the FluoroMax-4 spectrofluorometer as a detection system. A 280 nm LED is the excitation light source, and the xenon light source used in fluorescence intensity measurements was turned off. Horiba Datastation software was used for data acquisition and fitting was performed using a customised script on OriginLab. The S-detector bias is set to 950, which accounts for the instrument response.

Before sample measurements, a prompt measurement was required. Ludox (Sigma-Aldrich), silica particles dispersed in an aqueous solution, was used as it scatters light and allows the instrument response to be read. It reflects the distribution of photons from the excitation pulse. The Ludox prompt is excited at 280 nm and an emission of 280 nm. This is first done as it allows for deconvolution by Origin 2018 (OriginLab, MA) from the instrument response function. The prompt cut off is set to 2500 and 10000 to match sample cut off.

Samples were loaded into the 12 µL or the MicroSense cuvettes. Count level cut off is set to 2500 or 10000 for emission at 395 nm and 330 nm, with a 5 nm bandpass, respectively. The cut off was chosen to allow rapid data acquisition while still obtaining a good level of signal to noise (S/N). Data was exported into OriginPro.

Exponential decay was found by deconvoluting the prompt measurement from the TCSPC measurement. A single exponential decay was found using equation 2.3:

$$y = y_0 + A_1 e^{\frac{-t}{\tau_1}} \tag{2.3}$$

Where y_0 is set to 0, A is the pre-exponential factor (the fluorescence intensity at t=0), t is the time (ns) and τ is the time decay (ns).

2.2.2.6 Generating stressed samples and an isothermal time course study

Samples were stressed in accordance to industry standard lead molecule biophysical screening procedures. Vials of 10 mg/mLwere put into incubators at 37°C, 40°C or 45 °C for 14 days. This step aims at creating unfavourable conditions to force aggregates to form provided the molecules are susceptible to aggregate formation. Thermal stressing is a commonly used method in accelerated stability studies. The temperatures are selected to be body temperature and slightly higher than body temperature, and the two week time frame represents the average half-life of most mAbs (Reff et al. 2002).

Time course studies were undertaken to map the aggregation profile of the different mAbs. SEC, FLI, REES and TCSPC were used. One millilitre samples of 0.5mg/mL were incubated at 37 °C and 45 °C for 14 days. Measurements were taken on days: 0, 1, 2, 3, 5, 7, 9, 12 and 14.

Before measurements, samples were cooled to room temperature over 10 minutes. To avoid significant photobleaching from samples, measured samples were returned into the bulk sample and mixed before taking the next measurement.

2.2.2.7 Spearman's Ranking

Spearman's Ranking was used to evaluate the strength and direction of the correlation of two variable data sets, in this case to compare the correlation between two different techniques. Spearman's ranking evaluates the monotonic relationship between two continuous variables. In a monotonic relationship, the variables move in one direction, it either increasing or decreasing, not both. It is based on the ranked values, rather than raw data.

After the time course study, each sample was assigned a rank in descending order, from best to worst. The difference (d_i) in the rankings for each sample between the two techniques were calculated and squared.

Equation 2.4 is used:

$$r_s = 1 - \frac{6 \sum {d_i}^2}{n(n^2 - 1)} \tag{2.4}$$

Where r_s is the Spearman's rank coefficient, d_i is the difference between the rankings for a sample, n= number of data points (in this case 8).

If the Spearman's rank coefficient is above 0.738, a value used for datasets of 8 data points with a 95% level of confidence, then there is a strong correlation between the data sets.

Each technique fluorescence technique (FLI, f_{330nm}/f_{395nm}, REES and TCSPC) was ranked against SEC to evaluate the strength of the correlation and ranked against each other.

2.2.2.8 Cuvette cleaning

Cuvettes were rinsed before each measurement using ultrapure water, produced in-house using a Milli-Q Advantage A10 system (Watford, UK). The cuvettes were dried using compressed air to ensure no interference from left over water.

At the end of each measurement day, the cuvettes were washed with Hellmanex special cleaning concentrate (Hellma) and thoroughly rinsed three times with water. This was performed 3 times and dried with compressed air.

2.2.2.9 Raman Spectroscopy

Each 100µL of 10mg/mL sample in native buffer were loaded into a 96-well quartz microplate (ThermoFischer). Samples were tested using a DXR Smart Raman spectrometer (ThermoFischer) with a DXR 780nm (150mV) laser. Data was acquired using Omic software (ThermoFischer) and analysed using Simca 13 software (Umetrics). Samples were recovered after measurements.

Chapter 3

Biophysical baseline characterisation of aggregates

3.1 Introduction

As it has become clear that the industry struggles with finding an all-in-one high-resolution aggregation detection technique, several approaches have been taken to try to get as close to this as possible.

Currently, companies employ a host of orthogonal techniques to learn as much information about mAb behaviour as possible. This requires a high amount of material for testing (around 20 mg per mAb), which extends the amount of time to get a therapeutic to market.

This chapter aims to simulate the typical orthogonal techniques used, namely: SEC, DLS and AUC, to identify current limitations and generate an aggregation profile on the mAb panel. The information learned from this will act as a basis of comparison for the novel techniques. Various techniques were then evaluated to select the best methods to investigate for comparable or better information at lower concentrations and in a faster data acquisition and processing. The effects of temperature and pH were the conditions explored.

High temperatures (>35 °C) are commonly used in forced degradation. The increased temperature causes thermal stress, allowing an indication of mAb behaviour over time under normal storage conditions. The higher temperature accelerates degradation pathways, instigating the formation of aggregates (insoluble or soluble that are covalent or non-covalent). Fragmentation can also occur where peptide cleavage occurs (Nowak et al. 2017).

Freeze-thaw (-80 °C to 20 °C) is useful to determine the effects of temperature cycling on mAbs. Aggregates can form during the freeze-thaw process. Freeze-thaw induced aggregates are typically non-covalent associated and dependent on pH and concentration (Nowak et al. 2017).

The degradation can also change with pH. At low (<pH 5) and high (>pH 7.5) pHs, typically seen in the purification, neutralisation and administration processes, soluble and insoluble aggregation, and fragmentation can be accelerated (Nowak et al. 2017).

Figure 16 shows the experimental plan followed. The mAb panel was tested to assess developability/ manufacturability. Key criteria for establishing the best techniques for this was the ability to be a high-throughput and low volume platform.

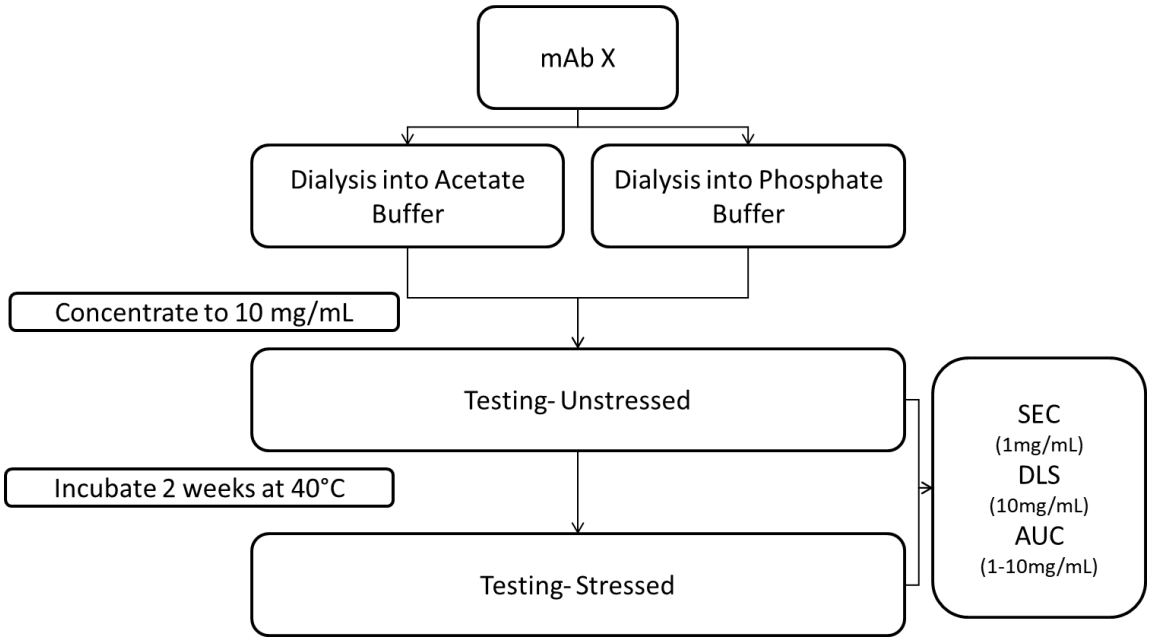

Figure 16 Typical Biophysical screening process for aggregation.

3.2 Results and Discussion

3.2.1 Biophysical Baseline Characterisation

The first mAb panel underwent tests by SEC, DLS and AUC (where required) to create an aggregation profile of the antibodies. Figure 16 shows the methods used for biophysical characterisation.

3.2.1.1 SEC Results

SEC allowed for monomer loss before and after thermal stressing at 40 °C for each mAb in acetate and phosphate at 10 mg/mL and diluting 1 mg/mL for measurements.

Figure 17 shows the percentage monomer obtained by SEC. All the unstressed sample results gave a very high level of monomer present, over 99%. For all mAbs, the samples show a slightly lower level of monomer in phosphate. This suggests that the mAbs are very slightly more stable in the acetate buffer, as expected, as it is designed to mimic the formulation buffer. The small amount of degradation from phosphate buffer suggests that during production, then time spent at higher pHs should be minimised. The mAbs, before thermal stressing, were shown to have 98% monomer by SEC. It is suggested that at 1 mg/mL, all the tested mAbs in both buffers were stable when not stressed.

The samples were then subjected to thermal stressing at 40 °C for 14 days. To avoid evaporation, the lids were secured tightly and covered in a plastic film. Echoing what was observed in the unstressed samples, there was a lower amount of monomer in phosphate buffer across the panel. For mAb B in phosphate buffer, there is a drop in monomer, due to over 23% aggregates being formed. This indicates that the mAbs was

not stable in this buffer, and aggregates formed during the thermal stressing. This was expected from GSK's historical data and confirms the mAbs selection as a positive control.

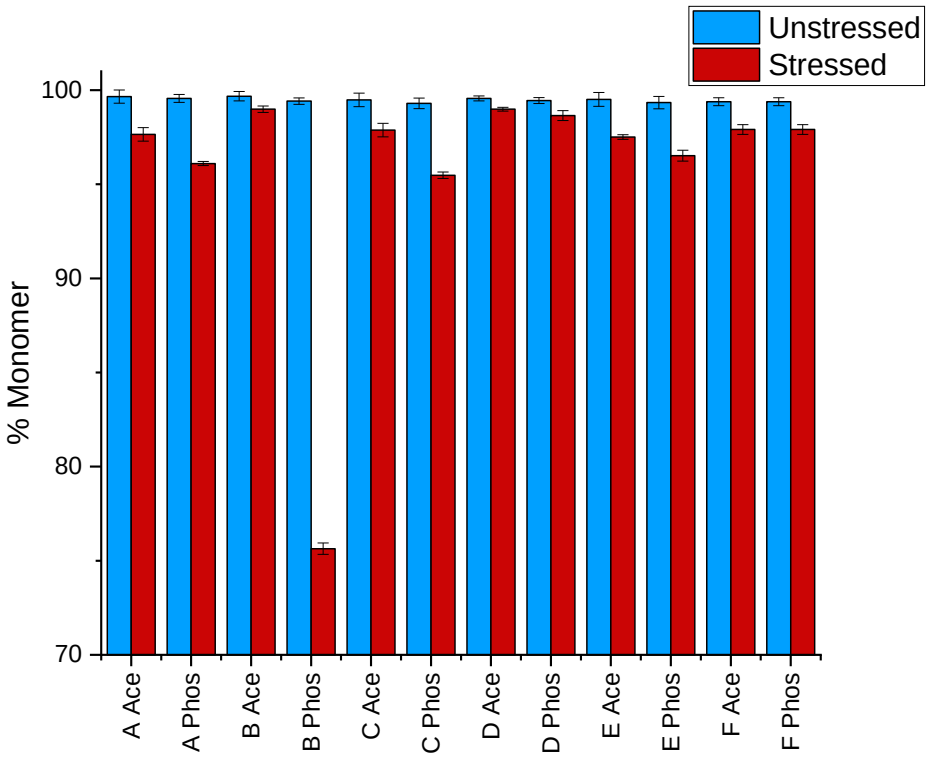

Figure 17 Percentage monomer from SEC measurements. MAbs A-F in acetate and phosphate buffers before and after thermal stressing at 40°C (blue and red respectively). n=3. Error bars show standard deviation.

Figure 18 shows the percentage distribution of each species found from SEC in the stressed samples to investigate the effects of thermal stressing. The level of fragments is higher in phosphate buffer for all mAbs (between 1-2%) than in acetate, as well as the level of aggregates (3-23%). This confirms what is known, i.e. that the phosphate buffer influences fragmentation and aggregation, and that mAbs are not stable in this environment. Fragmentation, while important, was not the focus of the study as fragments are less immunogenic.

Stressing of mAb B in phosphate buffer generated a high level of aggregates (>23%) and relatively low fragmentation (1%). For the other mAbs, there was still a high level of monomer (>95%). IT can be concluded that mAb B is susceptible to aggregation over storage and will be used as our model mAb for this in following experiments.

From SEC alone, measurements at high concentrations and under native conditions cannot be observed. Therefore, DLS, which acts as an orthogonal technique, was used to find this.

The SEC data creates a good baseline for future novel techniques. The new technique should be able to detect similar levels of percentage monomers.

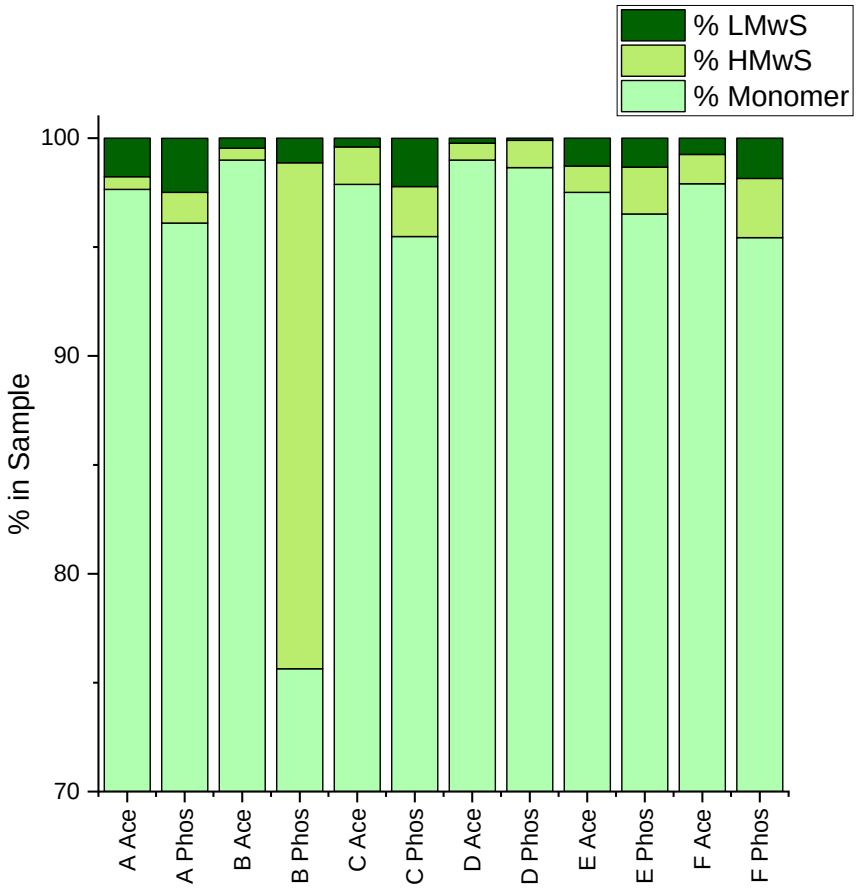

Figure 18 Mean percentage distribution of species in stressed samples. Monomer (Light green), HMwS (high molecular weight species, larger than monomer) and LMwS (low molecular weight species, smaller than monomer) are shown.

3.2.1.2 DLS Results

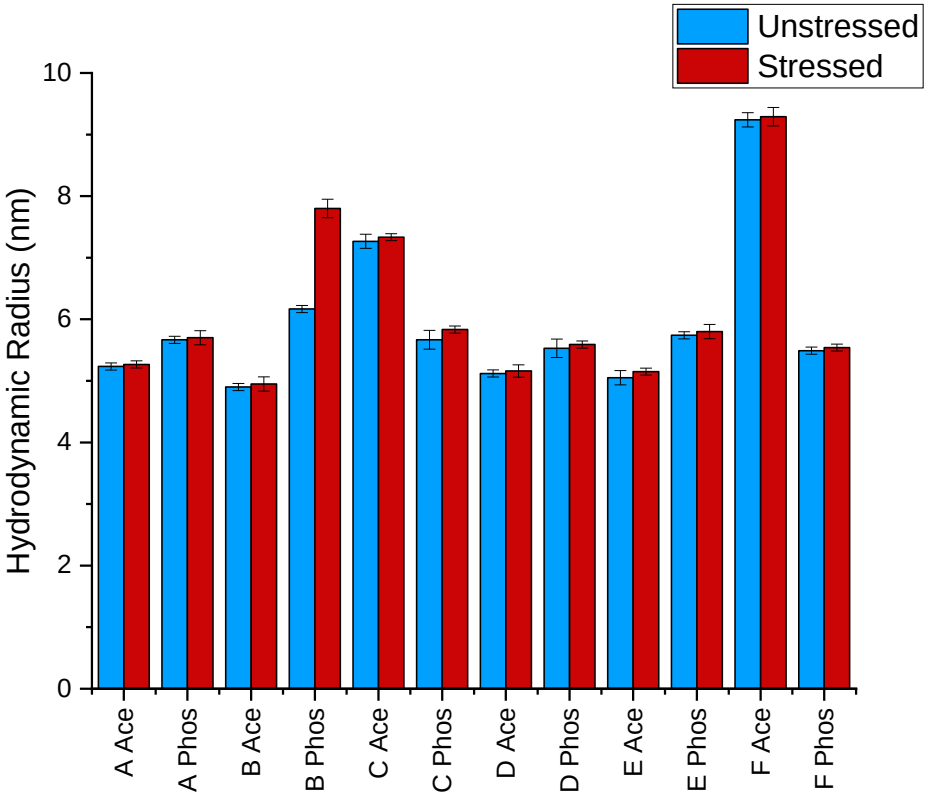

Figure 19 Hydrodynamic radius (nm) from DLS measurements. Monoclonal antibodies A-F in acetate and phosphate buffers before and after thermal stressing at 40°C (blue and red respectively). n=3. Error bars show standard deviation.

DLS was used to further characterise the aggregates, at 10 mg/mL and to observe any differences in size of particles within a certain range. 1-10 nm is measured to pick up monomers (which typically have a hydrodynamic radius of 5-6 nm) and small aggregates (dimers/trimers) present. 10-100 nm and 100-1000 nm ranges are also given, to examine the presence of large aggregates in the sample.

In the unstressed samples, mAbs A, B, D and E show no change between buffers and within the expected monomer range. Therefore, it suggests that they do not experience aggregation in the different buffers at the higher concentration (10 mg/mL). MAb B, showed a larger radius in the phosphate buffer also but still within the expected monomer range.

When examining mAb C, the hydrodynamic radius is 5.67 nm in the phosphate buffer; however, in the acetate buffer it is 7.27 nm. This suggests larger particles than monomers are present in the sample. This is the same for mAb F, showing a hydrodynamic radius of 5.49 nm and 9.24 nm in phosphate and acetate, respectively. As aggregation was not shown in the SEC results in the acetate buffer for mAb C and F, this suggests concentration dependent aggregation. AUC was required to examine this further as SEC is limited to lower concentration measurements.

MAbs A, C, D, E and F did not show any significant size differences between stressed and unstressed samples. This suggests that stressing did not affect the antibody significantly. However, as seen in SEC, this may not be the case unless the running buffer influenced an increase in aggregates and fragments. This highlights the low resolution, characteristic to DLS, in its failure to detect small amounts of small aggregates.

MAb B showed a large increase in hydrodynamic radius, from 6.1 nm to 7.8 nm. This large increase corresponds with the SEC results, suggesting that small aggregates are present in the phosphate buffer. AUC was used to further examine the increase in hydrodynamic radius. For mAb C and F, there appeared to be no significant difference due to stressing the samples.

Table 7 Peak 1 percentage mass from DLS measurements. MAbs A-F in acetate and phosphate buffers before and after thermal stressing at 37°C (blue and red respectively). n=3.

	Peak 1 (1-10 nm) % Mass	
	Unstressed	**Stressed**
A Ace	99.8 ± 0.1	99.9 ± 0.1
A Phos	99.6 ± 0.2	99.5 ± 0.2
B Ace	99.8 ± 0.2	99.8 ± 0.1
B Phos	100 ± 0.1	99.4 ± 0.1
C Ace	99.4 ± 0.2	99.4 ± 0.1
C Phos	99.5 ± 0.2	100 ± 0.2
D Ace	99.8 ± 0.2	99.8 ± 0.2
D Phos	99.6 ± 0.1	99.6 ± 0.2
E Ace	99.6 ± 0.1	99.6 ± 0.1
E Phos	99.4 ± 0.1	99.3 ± 0.2
F Ace	99.7 ± 0.2	99.7 ± 0.1
F Phos	99.7 ± 0.1	99.8 ± 0.1

Table 7 shows the percentage mass of sample between 1-10 nm. It suggests that a vast majority, over 99.4%, of particles found over all conditions were between 1-10 nm. The small percentage found in peak 2 (10-100 nm) and peak 3 (100-1000 nm) suggests larger species, aggregates, and/or dust particulates, respectively. .

Linking to the findings from SEC, DLS could not resolve fragments, as they would fall into the 1-10nm ranges. This is particularly difficult where samples are polydisperse.

From this, DLS is a useful orthogonal technique, which is capable of measuring samples in native buffers and at high concentrations. DLS was able to highlight the differences between mAb C in acetate and phosphate.

3.2.1.3 AUC Results

To explore the results from SEC and DLS further, AUC was used. It is typically used to confirm the data from SEC and DLS and was not performed for each mAb or condition in the panel. MAb F, though also showing concentration dependent aggregation like mAb C, was not tested by AUC due to limited sample availability. It was known that it was a close variant of mAb C, thus behaved similarly. For each sample, one measurement was taken. This data should be viewed as a guideline for the mAb's behaviour.

Figure 20 shows the percentage distributions for the different species found in unstressed mAb C samples, confirming the results seen by SEC and DLS. MAb C, at high concentrations in acetate buffer showed concentration dependent aggregation. SEC results would indicate that a very low level (less than 0.5%) of aggregates was present at 1 mg/mL. The DLS results suggested a larger hydrodynamic radius due to small aggregates at a mAb C concentration of 10 mg/mL. The samples for mAb C were tested in each buffer at concentrations of 1, 5, and 10 mg/mL, to show the aggregation at different concentrations.

In acetate at 1 mg/mL, the AUC show around 99% monomer, corresponding with the SEC results. In phosphate there is a slightly higher level of aggregates present, as expected. At 5mg/mL in acetate, 55% aggregates were seemingly present (0.3% were higher order aggregates). In phosphate the percentage of monomers was slightly lower than that seen for 1 mg/mL but still showed a very high amount, >98%. At 10 mg/mL in acetate, the AUC results show 79% aggregates.

This confirms that mAb C suffers from concentration-dependent aggregation in acetate buffer corresponding to the findings from DLS, where it indicated that the average size of the particles was larger than expected. As all samples were first concentrated to 10 mg/mL and diluted for SEC, it is assumed that the concentration dependent aggregation is reversible.

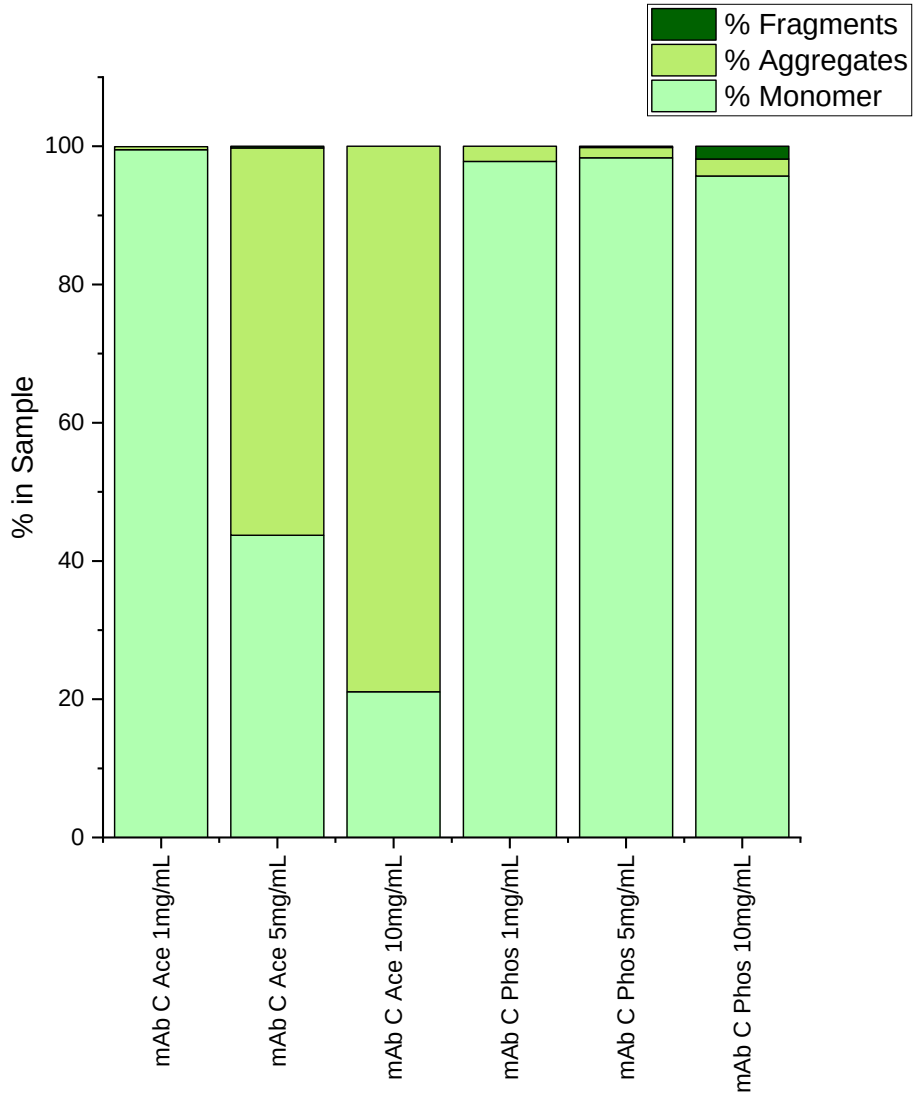

Figure 20 Percentage distributions from AUC for different species present in samples of mAb C in Phosphate buffer and Acetate buffer at 1mg/mL, 5mg/mL and 10mg/mL to show concentration dependence aggregation.

Table 8 shows the percentage distribution of each species, with an estimated molecular weight (MW), derived from experimentally determined sedimentation s-values. It should be noted that the MWs found are an estimate, and prone to bias from the modelling parameters. Where the SEDFIT model could not fit a model accurately, the frictional ratio was set at 1.6. The typical MW for a mAb is around 150 kDa.

At 10 mg/mL in acetate, the larger MW species were dimers. This could offer an explanation for the DLS peak 1 that was still above 99%, despite AUC showing 79% larger species. As this is still within the 1-10 nm range, this further highlights the low resolution observed. At 5 mg/mL, there were various sized species present, in contrast to the monomer and dimer observed at 1 mg/mL and 10mg/mL. However, as this amounts to very small amounts, <0.6%.

Table 8 A summary table of the AUC results for mAb C in Phosphate and Acetate buffers at 1mg/mL, 5mg/mL and 10mg/mL. n=1.

	s-Value	% Distribution	Protein Structure
mAb C Phosphate 1mg/mL	6.1	97.81	Monomer
	10.3	1.92	Dimer
	14.6	0.27	Tetramer
mAb C Phosphate 5mg/mL	3.2	0.17	Fragment
	6.3	98.33	Monomer
	9.9	1.5	Dimer
mAb C Phosphate 10mg/mL	1.5	1.85	Fragment
	5.6	95.7	Monomer
	10.1	1.55	Dimer
	14.7	0.62	Tetramer
	17.7	0.29	Oligomer
mAb C Acetate 1mg/mL	6.5	99.5	Monomer
	11.5	0.45	Dimer
mAb C Acetate 5mg/mL	2.0	0.24	Fragment
	6.3	43.73	Monomer
	7.7	55.73	Dimer
	14.3	0.26	Trimer
	18.2	0.04	Oligomer
mAb C Acetate 10mg/mL	5.9	21.09	Monomer
	7.3	78.91	Dimer

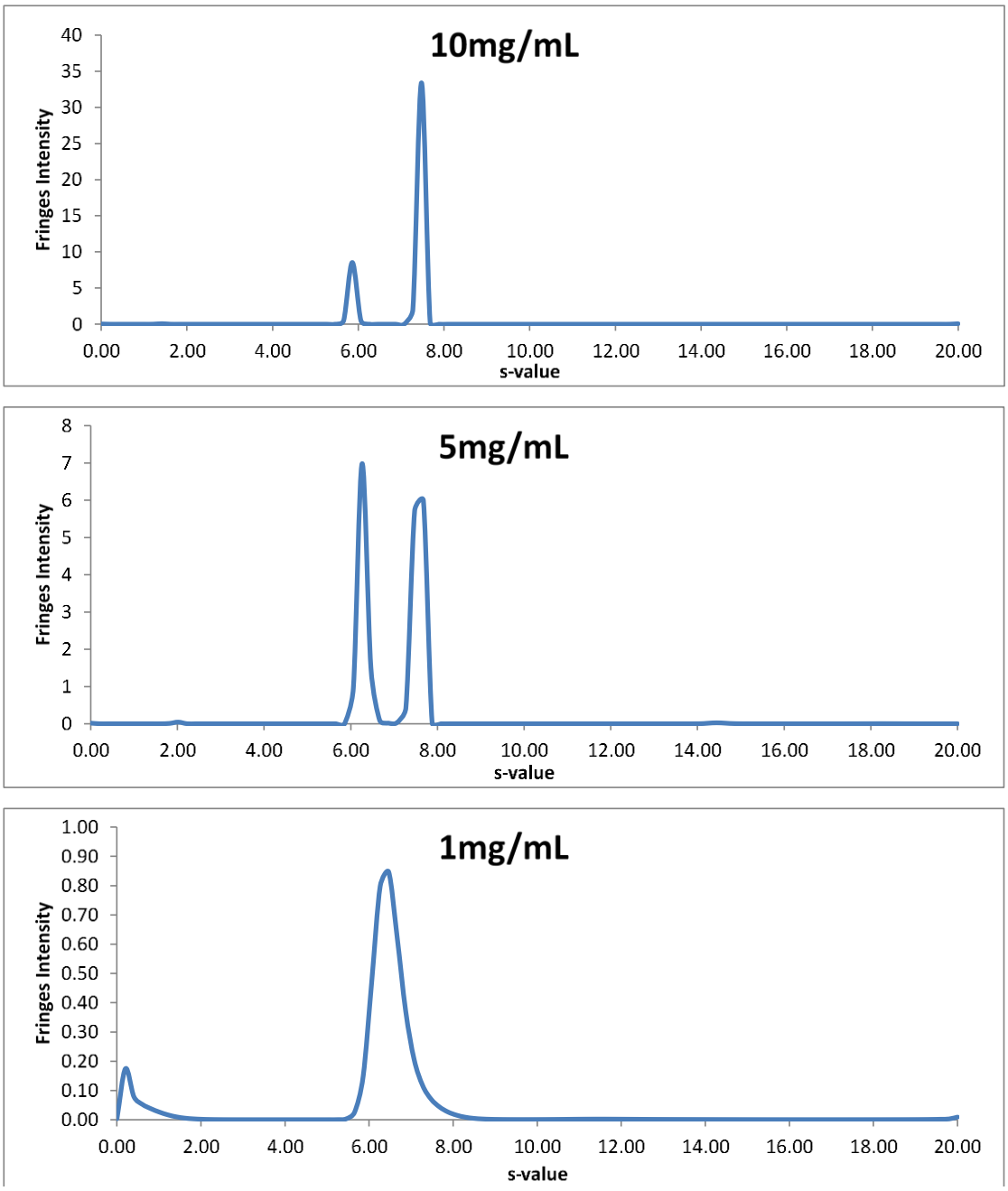

Figure 21 The UV measurements from AUC for 100 µL mAb C in acetate buffer. The different concentrations are shown. s-Value represents the sedimentation coefficient. Fringes intensity is the intensity measured from samples.

Figure 21 shows the raw AUC results for mAb C at different concentrations in acetate buffer. At higher concentrations, the intensity is higher as there is more protein available. The resolution between 5mg/mL and 10mg/mL is comparable, and the s-values for the peaks were located within the same range (6.2 and 6.5 respectively), as were the dimer readings. At 1mg/mL the fringes intensity is much lower, and the resolution could not pick up the small aggregate population, as seen by a slight shoulder to the right of the peak, detected by SEC previously. There is also a small artifact peak at the s-value of 0.5. The software, highlighting limitations with the modelling fit, could not integrate this. However, the results show the concentration dependence aggregation, as the dimer

peak grows relative to the monomer peak with increasing concentration from 5 to 10 mg/mL.

MAb B was also tested in AUC as a model to familiarise with the technique and to confirm the results seen from SEC and DLS. This is shown in Figure 22.

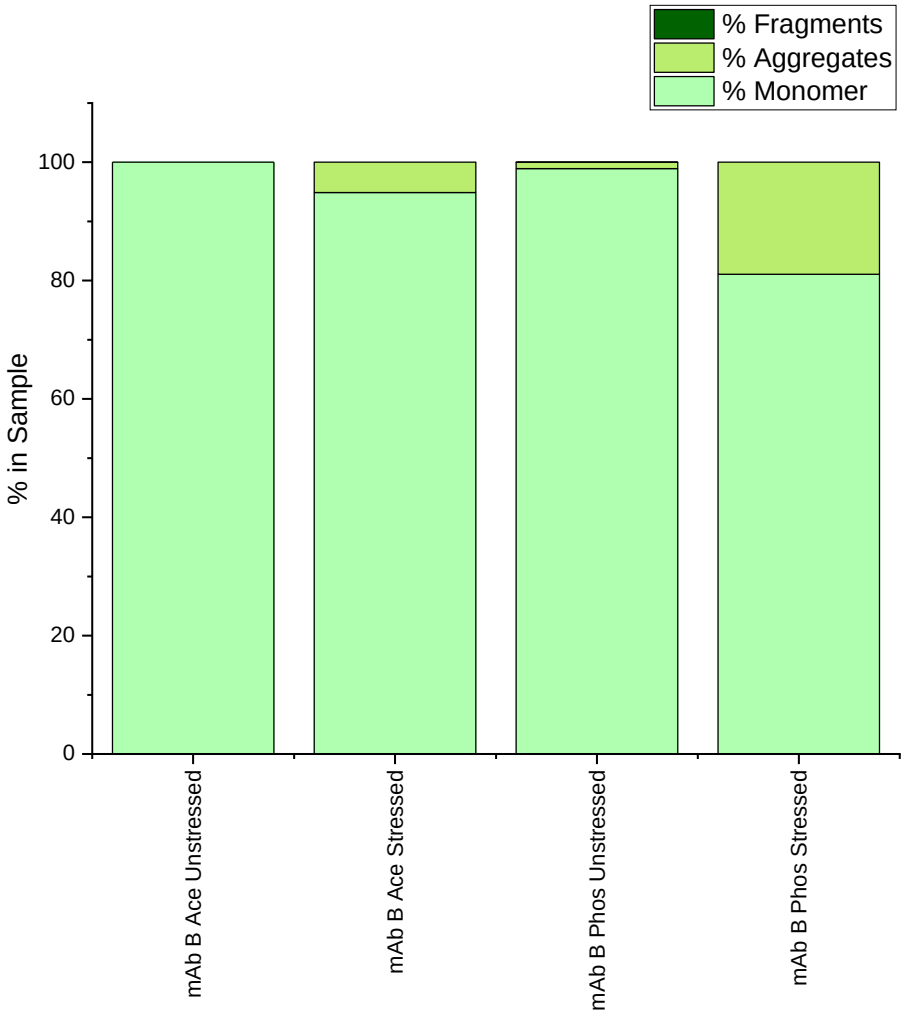

Figure 22 Percentage distribution for different species present in samples of mAb B in Phosphate buffer and Acetate buffer at 10mg/mL to show stress-induced aggregation.

In phosphate buffer, mAb B shows 20%% aggregate when stressed, compared to 1.6% when not. This aggregation was detected in the DLS and SEC (23% aggregates) data. The differences detected by AUC and SEC are negligible.. AUC confirms the baseline data was as expected. The profile, as seen in Table 9, shows a similar sedimentation coefficient for the monomer. Fragments were also detected, as well as the aggregates, which have similar s-values also. Aggregate at with an s-value of 8.7 (dimer) have appeared as the majority. MAb B in phosphate after stressing also showed small levels

of trimers and oligomers. This also suggests that the aggregation is not concentration dependent and is irreversible.

In acetate buffer, there was a 5% aggregation of around a pentamer size for the stressed sample. This level was not seen in DLS or SEC and could be due to the mechanical stress caused by AUC's high rotation speeds causing additional levels of aggregation. This suggests that AUC may not be an appropriate technique for the screening process.

Table 9 Summary table comparing stressed and unstressed samples of the AUC results for mAb B in phosphate buffer and in acetate buffer at 10mg/mL. n=1.

	s-Value	**% Distribution**	**Protein Structure**
mAb B Phos Unstressed	6.3	98.94	Monomer
	10.7	0.91	Dimer
	14.6	0.14	Trimer
mAb B Phos Stressed	2.6	1.82	Fragment
	4.7	2.09	Fragment
	6.3	76.16	Monomer
	8.7	16.24	Dimer
	10.9	3.25	Trimer
	13.3	0.45	Tetramer
mAb B Ace Unstressed	5.3	100.00	Monomer
mAb B Ace Stressed	5.5	94.87	Monomer
	13.3	5.13	Trimer

Overall, AUC had the advantage in being able to confirm the concentration dependent aggregates as identified by DLS. It also allowed for aggregate detection to confirm that seen by SEC. AUC is a very slow method and was not be considered for high-throughput studies.

3.2.1.4 Freeze Thaw Study

Freeze-thaw is commonly used to mimic any stresses that a mAb might encounter during shipping or storage. MAbs A, B and C were tested to evaluate the degradation from each cycle and to test how many times a sample could be used once out of the freezer.

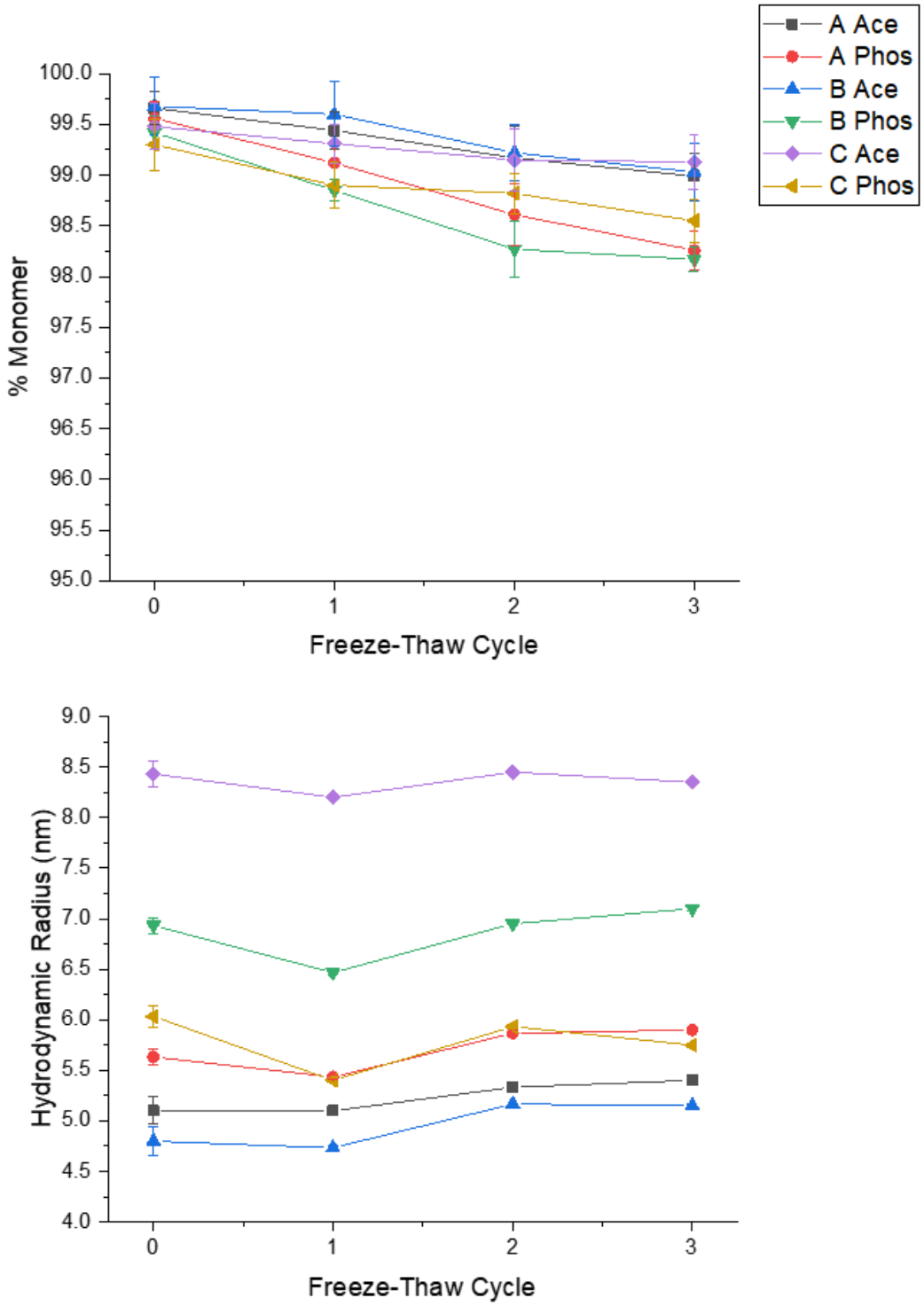

Figure 23 Freeze-Thaw study results from SEC (top) and DLS (bottom) measurements for mAbs A, B and C in Phosphate and Acetate buffers.n=3

This aim for the study was to ensure that the quality does not degrade with time and how best to use the material in future studies. SEC and DLS are used to characterise the aggregation profile for this.

Figure 23 shows the SEC and DLS results from the freeze-thaw study on mAbs A, B and C. MAbs D, E and F were not tested due to availability at the time. The results from SEC suggest a similar pattern as the results in the previous baseline SEC experiments. The percentage of monomers was lower in phosphate buffer than in acetate buffer. As seen in the stressed samples, mAb B showed the most monomer loss. Across all mAbs in each buffer, the trend suggests that around 0.5-1% aggregates are created with each freeze thaw study. The rate of degradation varied, with either the first or second cycle being the most damaging for all three. This may indicate that they are more stable in a lower pH buffer during freezing. However, it has been suggested that the pH changes due to cryoconcentration are not a factor in aggregate formation (Kolhe et al. 2010).

The hydrodynamic radius, found from DLS, is an indication of aggregation. The results indicate that the particles detected are roughly the same size and there is no evidence for an increasing size with each cycle. This correlates to the SEC results, as only a small amount of monomer is lost over the cycles.

From the percentage mass, data not shown, the results were all above 99% in the 1-10 nm peak. It suggests that only a tiny number of larger particles were present and within error. Only mAb B in Phosphate buffer showed a 97% in the 1-10nm peak. 3% was found in peak 3, the 100-1000 nm range. This suggests that the freeze thaw process generated larger aggregate particles in mAb B in phosphate. This correlates to the data found from the baseline SEC and DLS data, showing mAb B to be the most aggregate prone mAb in phosphate. However, from the baseline thermal stressing study, the aggregates formed were still small, confirmed by DLS.

Overall, the results presented here indicate that the freeze-thaw process does influence the size of aggregates forming and could be a useful stressing technique. For storage, to minimise aggregation, small aliquots of 1 mL at 10 mg/mL would be kept at -80 °C. When thawed, the samples would not be frozen again, instead discarded. In between testing, the molecules are kept at 4 °C.

3.2.1.5 Selection of novel methods

Table 10 RAG summary of each technique examined. 1,2 and 3 represents the people (Student and two supervisors, academic and industrial) who ranked the techniques independently. Red= Negative, Yellow= Tentative, Green= Positive, H= high, M= Medium, L= Low, Y= Yes, N= No. Technologies in bold were selected.

Technology	Size Range	Sample Volume	Robustness	Sensitivity	Throughput	Microfluidic	1	2	3
SEC	1-50nm	50-100uL	H	H	H	N			
AUC	1nm-100nm	100µL	M	H	L	N			
FFF (AF4)	1nm-µm	1.5-10mL	M	M	H	N			
MS	Atomic-MDa	1-2 nmol	M	H	H	Y			
SLS	5kDa-MDa	15-120µL	M	H	H	Y			
DLS	1nm-10µm	100µL	M	H	H	Y			
MALS	kDa-Mda	100µL	M	H	H	Y			
RMM	50nm-5µm	0.1-50µm	M	H	M	Y			
NTA	200-1000nm	500µL	M	H	L	N			
SDS-PAGE	5-1000 kDa	15-700µL	M	H	H	Y			
SPR	10-50nm	20-30µL	M	M	M	Y			
CD	N/A	350-750µL	M	M	M	N			
Turbidimetry	100nm- 10 µm	400-500µL	M	H	M	Y			
NMR	kDa	500-600µL	M	H	M	Y			
Raman Spectroscopy	N/A	100-500µL	M	L	L	Y			
FTIR	N/A	10mg	M	L	L	Y			
Coulter Counter	1100µm	4-20mL	L	L	M	Y			
Micro-Flow Imagery	1- 400µm	10-50µL	L	-	M	Y			
Light Obscuration	1-150µm	<25mL	L	M	L	N			
XRD	Atomic-MDa	mg	M	H	L	N			
Fluorescence Spectroscopy	N/A	1-100µL	M	H	H	Y			
Fluorescence Microscopy	N/A	nL	L	H	L	Y			
CE-SDS	5-1000 kDa	15-700µL	M	M	H	Y			
Microscopy	1-100µm	µL	L	L	L				

Once a baseline was established using SEC, DLS and AUC, an extensive literature review was carried out to determine the best techniques to evaluate aggregation. A list of current and novel techniques used to detect and characterise aggregation was created from literature and experience. Table 10 shows a summary table of technologies available to measure protein aggregation and their relative capabilities to incorporate high throughput or microfluidic elements. An orthogonal approach, where multiple different techniques are used that are complementary, is taken. This is due to the limitations in resolution of one technique to characterise different aggregate sizes of numerous orders of magnitude (Den Engelsman et al. 2011).

Several parameters were independently evaluated by the student (1), an academic supervisor (2) and an industrial supervisor (3). A Red-Yellow-Green scoring system was

used based on current knowledge, experience, and availability of the technique for use. The key parameters included low volume and high throughput capabilities.

As a result, the following techniques were carried forward to be examined and adapted to suit the needs of a novel assay: SEC, DLS, Fluorescence spectroscopy and Raman spectroscopy. Fluorescence microscopy was initially selected but not used as the project progressed.

3.2.1.5.1 Evaluation of Raman spectroscopy

Raman spectroscopy was evaluated to assess its ability to detect certain aggregates. The view was to use Raman spectroscopy to assess the suitability of coherent anti-Stokes Raman spectroscopy (CARS). CARS is a novel and powerful technique, which permits the use of small volumes and affords fast data acquisition.

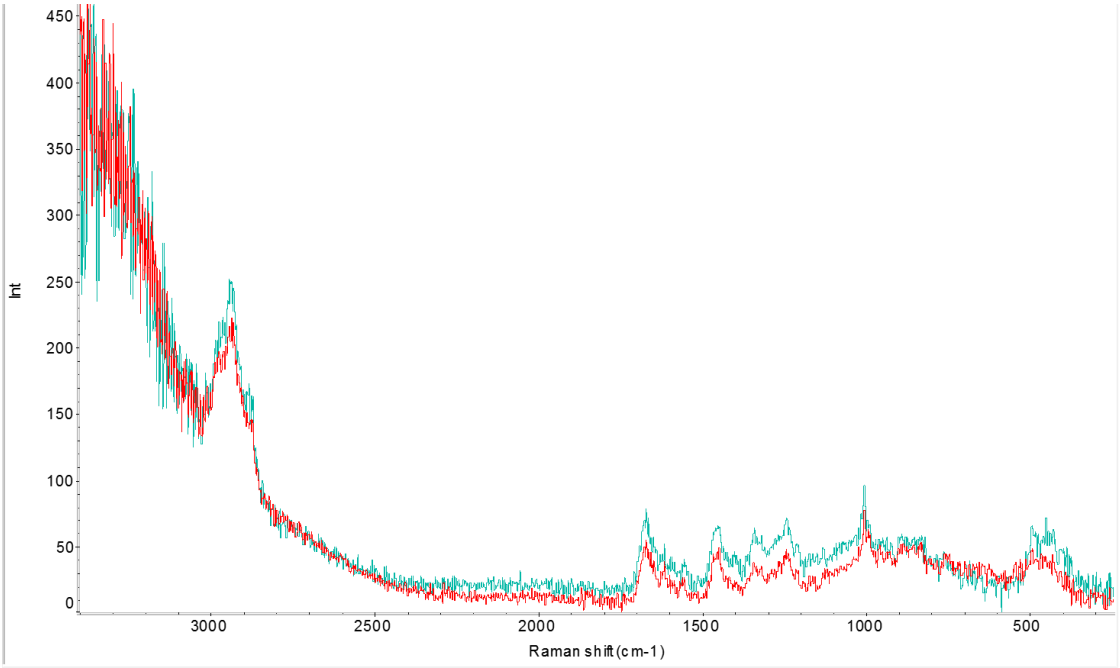

Figure 24 Raman spectrum for mAb B in phosphate before (turquoise) and after stressing at 45°C (red).

Figure 24 shows the Raman spectroscopy measurements for mAb B in phosphate at 1mg/mL before and after thermal stressing. The intensity (y-axis) is plotted against the frequency (Raman shift, x-axis). Raman is typically taken from 1850-600 cm^{-1}. As CARS is active in the 3800-2200 cm^{-1} region, it does not offer any significant value over Raman, as there were little differences between samples. At 10 mg/mL the raw data in the Raman region is relatively noisy, suggesting a higher signal to noise is required. After initial testing, Raman was found to be unsuitable for low volume (minimum requirement of 100 µL of material) and low concentration measurements and was not considered further.

3.2.1.5.2 Evaluation of Fluorescence spectroscopy

Fluorescence spectroscopy was selected for its: ease of use and understanding; equipment and expertise availability; easy sample preparation; low volume capabilities; and fast data acquisition.

Fluorescence spectroscopy was used on mAbs A, B and C to first evaluate the suitability of fluorescence spectroscopy and then compare to the aggregation profiles from the SEC and DLS data. Chapter 4 expands on the fluorescence measurements.

3.3 Conclusions

In this chapter, the mAb panel was characterised by SEC, DLS and AUC.

SEC: SEC is a high-throughput technique to quantify the amount of monomer, fragment and aggregate in a sample. It requires 30 µL at 1 mg/mL and around 15 minutes per sample. From SEC, we conclude that mAb B in phosphate is susceptible to aggregation by thermal stressing as around 23% aggregate was detected after stressing. All other samples satisfied the cut-off of 95% monomer. Overall, samples in phosphate exhibited a lower level of monomer at day 0 and day 14 suggesting the mAbs are less stable in phosphate. This is to be expected as phosphate is designed to mimic the highest pH the mAb will encounter (during purification). SEC is limited in its capacity to measure a wide concentration range.

DLS: The DLS system is high throughput as it is a plate-based system. It can measure samples in native buffer conditions and is able to measure across a relatively wide range of concentrations. It is a qualitative technique that measures the hydrodynamic radius of samples. Typically, standard mAbs exhibit hydrodynamic radii of 5-7 nm. It showed a negligible difference before and after stressing, except in the case of mAb B in phosphate, (hydrodynamic radius of 7.8 nm), but showed differences between buffers, suggesting that there is a size difference in mAbs in different buffers. DLS has several drawbacks including the high material requirement, 300 µL at 10 mg/mL and the prescence of dust, bubbles and other particulates can affect measurements. It requires around 5 minutes per well and is typically run in triplicate due to variable results. The reversible concentration dependent aggregation from mAb C and D in acetate was detected with a hydrodynamic radius of 7.3 and 9.3 nm respectively. DLS works orthogonally to SEC and detects concentration dependent aggregation, as well as confirming the results from SEC.

AUC: AUC is considered the “gold standard” for aggregate detection. It uses sedimentation velocity to accurately quantify the number of monomers, fragments, and aggregates in a sample. It is highly sensitive and able to detect the sizes of species. AUC confirmed the concentration dependent aggregation seen in mAb C in acetate, identified

by DLS. The main drawbacks of AUC are that: it is a time-consuming technique, capable of reading only 8 samples over the course of one day; and it requires complex data analysis.

Techniques to investigate: The main advantages and disadvantages were identified by using current methods to detect different types of mAb aggregation. While AUC gives the most accurate reading, the low-throughput technique hinders its adoption as a mAb screening tool. Therefore, the need for a low material, low volume and high-throughput screening assay is paramount and its use in industry is welcomed.

A literature survey was carried out and techniques were ranked using a Red-Amber-Green method to identify the best methods to investigate for the purposes of detecting protein aggregation.

The standout technique to investigate was fluorescence-based techniques, due to their low volume, low material requirements, ease of use and potential to be employed for high throughput analytics.

Chapter 4

Evaluating fluorescence-based techniques

4.1 Introduction

Fluorescence-based techniques have been used to measure and detect the presence of aggregates in small samples. They are also used to study protein folding, dynamics, and interactions. Fluorescence occurs when a fluorescent molecule is excited by a laser/lamp, raising the electron excitation state and, as a molecule returns to its ground state fluorescence is emitted.

Fluorescence offers many benefits over the currently used SEC, DLS and AUC, as briefly described in Table 11. Fluorescence allowed for a much smaller, recoverable sample size at lower concentrations than SEC and DLS, with faster measurement times too.

Table 11 Benefits of fluorescence techniques over SEC, DLS and AUC.

Parameter	SEC, DLS & AUC	Fluorescence Techniques
Sample Size Required	SEC: 30µL at 1mg/mL DLS: 300µL at 10mg/mL AUC: 100µL at 1-10mg/mL	1-100µL at 0.05-10mg/mL
Measurement Time	SEC: 15min DLS: 5min per well AUC: 8 hours	5 seconds to 3 minutes
Ease of Use	SEC: Easy (Automated) DLS: Unpredictable measurements and complex analysis AUC: Complex analysis	No sample preparation Recoverable sample Easy data analysis

The methods investigated in this chapter are: Fluorescence spectroscopy (including f_{330nm}/f_{395nm} and Red Edge Excitation Shift), and Time Correlated Single Photon Counting (330 nm and 395 nm emission). These methods were compared to SEC throughout to validate the findings.

4.2 Results and Discussion

4.2.1 Evaluation of fluorescence-based techniques

Fluorescence-based techniques have broad applications when detecting protein aggregation. Different techniques may reveal different elements to protein behaviour.

The first steps in establishing fluorescence as a technique was to evaluate the parameters in which to run the scan, measurement time, ease of data analysis and interpretation, establish a working concentration range and assess viability as a novel technique for a lead panel ranking screen.

4.2.1.1 Assessing Fluorescence Intensity Suitability

Tryptophan excitation, based on literature, is the most widely used. This is because of its higher quantum yield. Therefore, excitation was first explored at 280 nm, with emission recorded between 290-500 nm. The expectation was that the overall fluorescence intensity should drop due to buried tryptophan residues as more aggregates are formed. The initial experiments were taken using the samples from the baseline study and diluting from 10 mg/mL to 0.5 mg/mL and 100 µL sample volume. A 100 µL quartz cuvette was used, with a pathlength of 10 mm.

The initial fluorescence intensity experiments are shown in Figure 25. A-D show mAbs A and B in acetate or phosphate and unstressed or stressed (40 °C for 14 days). MAb A in both buffers and mAb B in acetate followed the same trend, in that there was a small decrease in fluorescence intensity after stressing, suggesting that a small amount of tryptophan is being buried due to aggregation. Table 12 shows the total FLI and the percentage change from stressing. The FLI in acetate is also much higher for all samples, suggesting a more exposed tryptophan and therefore perhaps indicating that the mAbs are more stable in acetate. The tail region (around 375-500 nm) after stressing has a higher intensity suggesting that intermediates or aggregates could influence fluorescence at higher wavelengths.

MAb B in phosphate showed a few points contrary to expectations from literature. The overall FLI increased with increased aggregation. At first glance, this could suggest that the tryptophan is more exposed in certain intermediate or pre-aggregate states. By looking at the shape, there appears to be a secondary peak forming around 395 nm. The tail causes an increase in overall FLI, possibly skewing the result, as SEC showed over 20% aggregates present. This secondary peak could be due to the pre-aggregates or aggregates species, fluorescing at a different emission wavelength. As this peak is still relatively small, it is unlikely that this is due to Fluorescence Resonance Energy Transfer (FRET), and the distance between the fluorophores is still relatively large. FRET is the mechanism of energy transfer between two light sensitive chromophores

Overall, FLI results were promising as a quick (<5 second measurements), qualitative and low volume method. These experiments formed the basis and point of reference for subsequent fluorescence spectroscopy experiments.

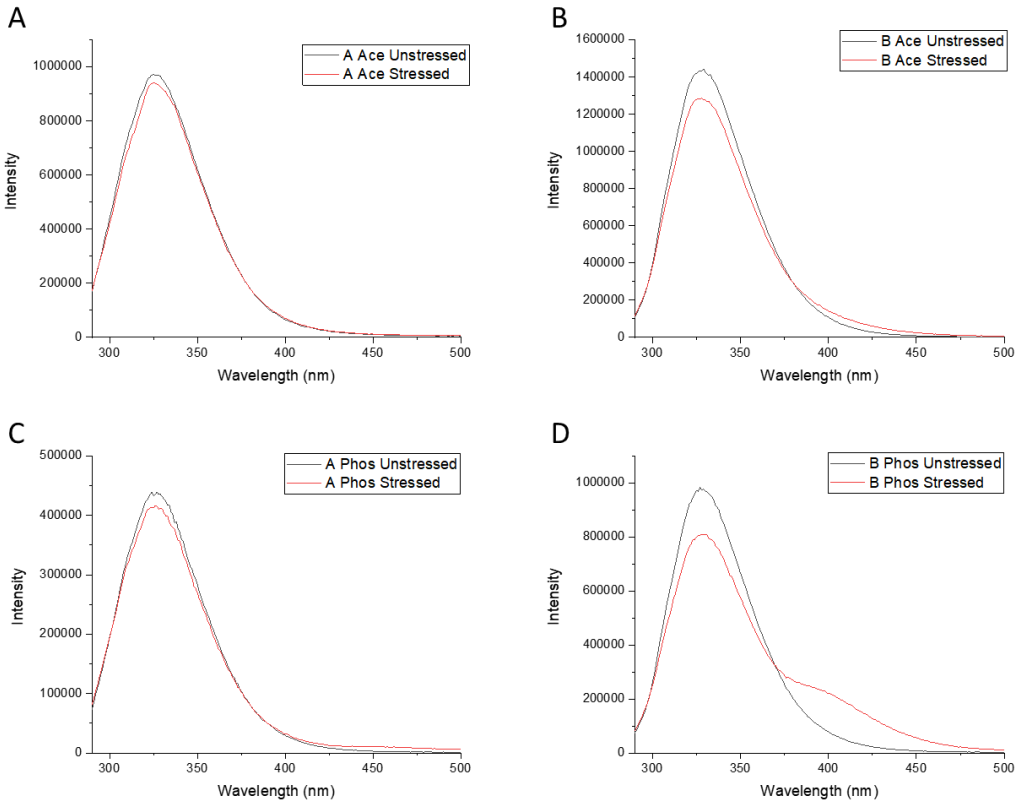

Figure 25 Comparison of mAbs A and B before and after thermal stressing for 14 days at 40°C. A- mAb A in acetate. B- mAb B in acetate. C- mAb A in phosphate. D- mAb B in phosphate. Excitation at 280nm. Emission wavelength from 290-500nm.

Table 12 Total FLI and % change from stressing.

mAb, Buffer and State	FLI ($x10^7$)	% Change
A Ace Unstressed	5.83 ± 0.24	-
A Ace Stressed	5.68 ± 0.28	-2.68
A Phos Unstressed	2.60 ± 0.12	-
A Phos Stressed	2.58 ± 0.13	-1.25
B Ace Unstressed	8.29 ± 0.35	-
B Ace Stressed	7.83 ± 0.32	-5.51
B Phos Unstressed	5.65 ± 0.28	-
B Phos Stressed	5.84 ± 0.29	3.37

4.2.1.1.1 Concentration Range and the Inner-Filter Effect

To assess the working concentration range, a concentration calibration curve was made to determine the relationship between fluorescence and concentration. A range of concentrations from 0.1-10 mg/mL was tested using mAb A in acetate and phosphate buffers, as an example mAb. This allows for the best parameters to be obtained for use in subsequent fluorescence experiments.

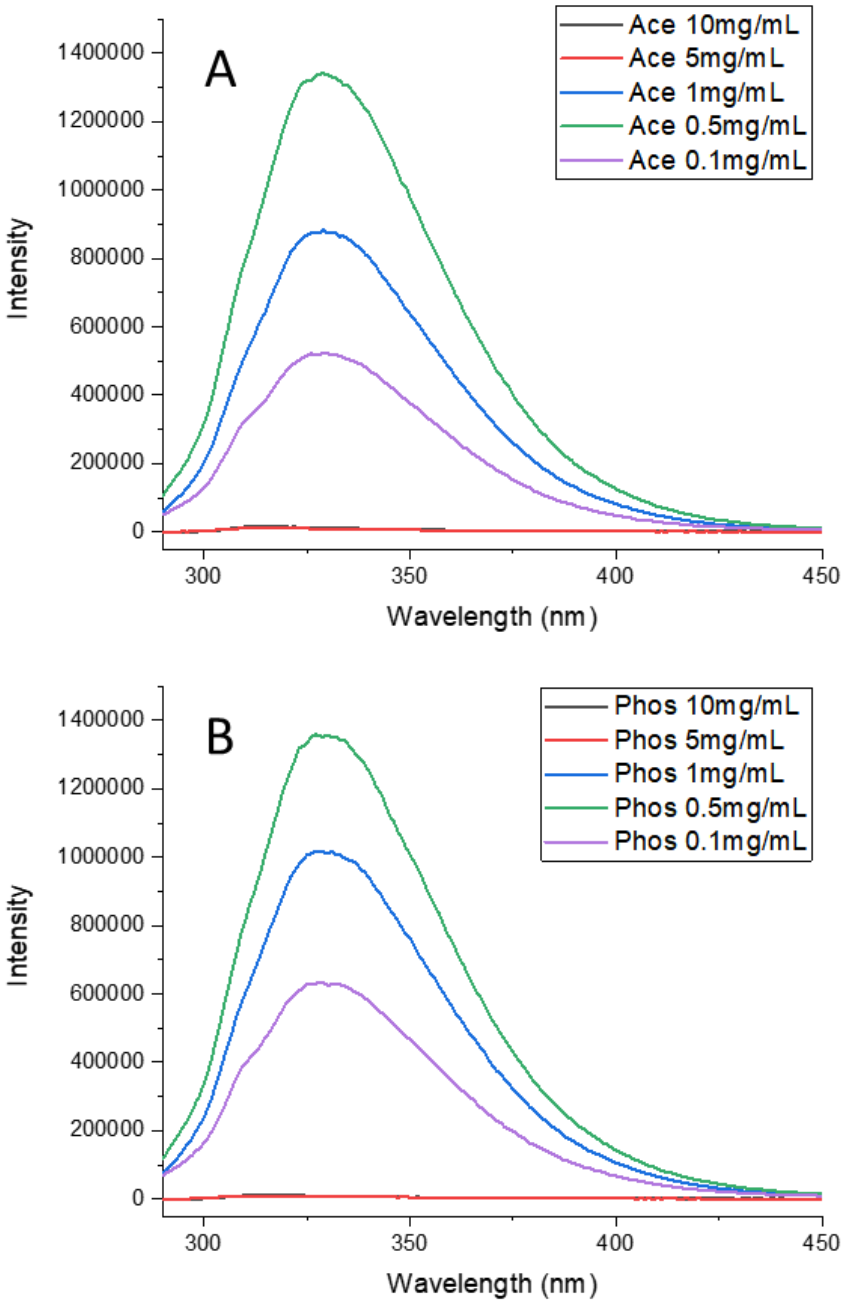

Figure 26 Comparison on the effects of 0.1-10mg/mL concentration range in acetate (A) and phosphate (B) buffers on FLI for mAb C. Excitation at 280nm. Emission wavelength from 290-500nm.

Figure 26 shows the effects of increasing concentration from 0.1-10 mg/mL, for mAb A in both acetate (A) and phosphate (B) buffers using the 100 µL cuvette. At 0.1 mg/mL to

0.5 mg/mL, there is an increase in intensity. However, from 0.5 mg/mL to 1 mg/mL there is a large decrease in intensity. At high concentrations, 5-10 mg/mL, the signal is dramatically reduced. A zoomed in graph for these concentrations is shown in Figure 27. The low signal to noise makes the readings unusable, with the peak being less than 2% of that seen at 0.5 mg/mL. This could be due to the inner-filter effect phenomenon. The inner filter effect is the result of higher concentration samples affecting spectral measurements. Primary filter effect occurs as the excitation beam is attenuated by the high concentrated sample, only exciting the surface molecules that face the excitation beam exciting strongly. Secondary inner filter effect occurs as the emitted fluorescent light is reabsorbed by the sample itself because of the high concentration.

The inner-filter effect poses problems when trying to evaluate whether fluorescence is a viable technique to assess concentration-dependent aggregation. Two options to reduce the inner filter effect were considered: (1) choosing a different excitation wavelength to reduce self-absorbance (this option was less viable as tryptophan is excited at a specific wavelength). (2) using a low volume or differently shaped cuvette. This option was the most viable as it allowed for the same parameters to be used throughout the experiments. This was explored further in Chapter 5.

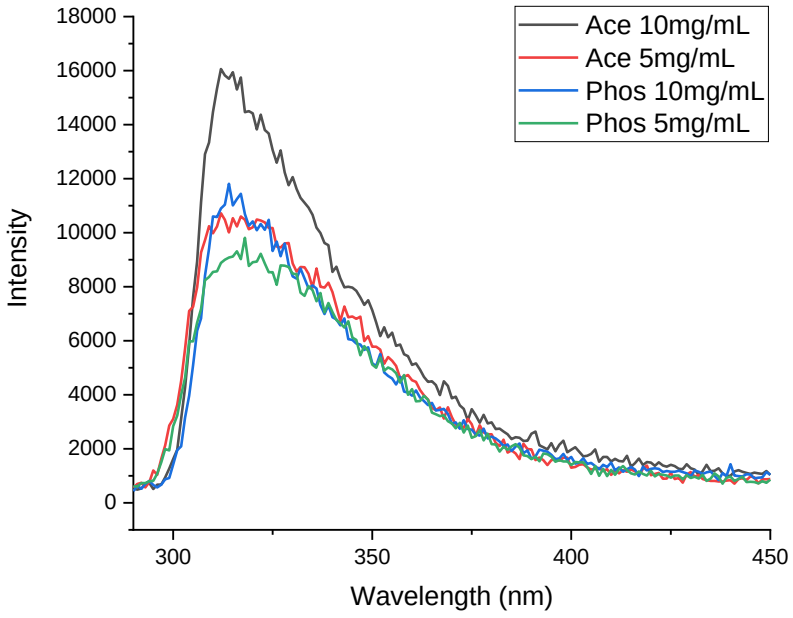

Figure 27 Example of the inner filter effect at higher concentrations (5-10mg/mL) for mAb C in acetate and phosphate buffer. Excitation at 280nm. Emission wavelength from 290-450nm.

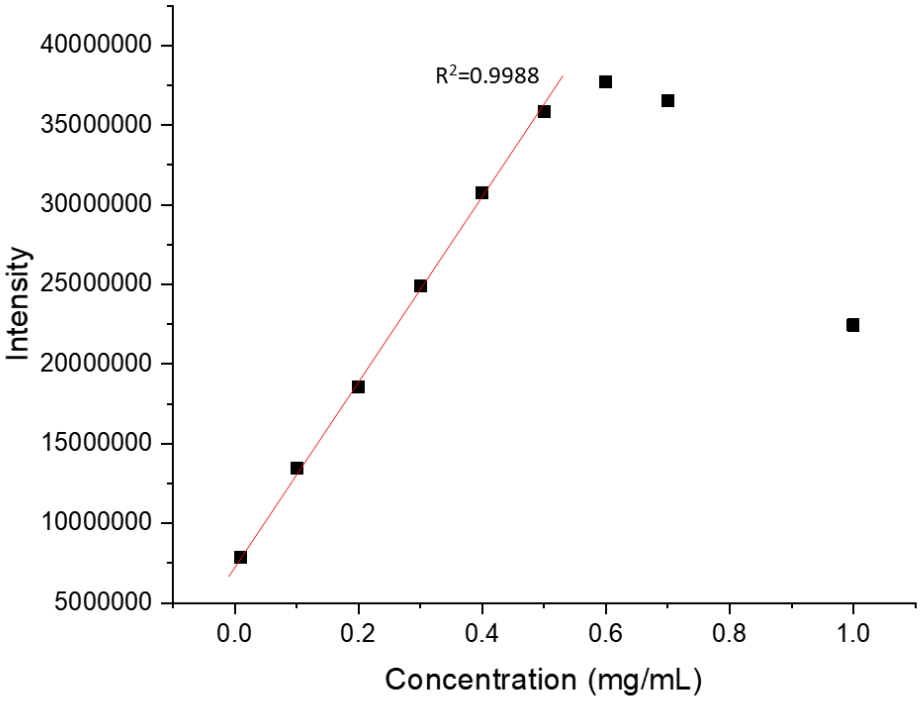

Figure 28 Concentration calibration curve using mAb A in acetate as an example. The red line indicates the line of best fit, highlighting the linearity between total intensity and concentration. The R^2 value was very high, 0.9988, suggesting a strong correlation between 0.01-0.5 mg/mL.

Figure 28 shows the total FLI at 0.01-1.0 mg/mL. At lower concentrations, 0.01-0.5 mg/mL, there is a strong linear relationship between FLI and concentration. This is because the absorption is small. As the concentration increases, the relationship becomes non-linear due to certain deviations, such as the inner filter effect which can reduce the excitation light coming through to the rest of the cell and/or reduce the emitted fluorescence intensity. As the detector is perpendicular to the incident beam, the distortion occurs from early absorption of surface molecules, rather than at the centre of the cell where the emission produced is detected.

For the purposes of the fluorescence experiments, 0.5 mg/mL was chosen for the following fluorescence experiments. It allows us to reduce the amount of material required, while also maintaining a good signal-to-noise ratio. While it is possible to use lower concentrations, mAbs are less stable during storage.

4.2.1.2 Fluorescence Ratio (f_{330nm}/f_{395nm})

To avoid the problems encountered from FLI, such as the secondary peak from stressed mAb B in phosphate, a fluorescence ratio was explored. This then considered shape changes and could evaluate and amplify any intensity rises in the longer wavelengths (395 nm) and any drops seen in the primary peak (330 nm). It alleviated the need for normalisation allowing a fast data analysis from raw data.

Table 13 Fluorescence ratio results for mAb A and B in acetate and phosphate before and after thermal stressing at 40°C for 14 days.

mAb	Buffer	Stress	f_{330nm}/f_{395nm}
A	Acetate	Unstressed	11.0 ± 0.3
A	Acetate	Stressed	10.1 ± 0.2
A	Phosphate	Unstressed	11.4 ± 0.5
A	Phosphate	Stressed	10.0 ± 0.4
B	Acetate	Unstressed	10.3 ± 0.4
B	Acetate	Stressed	7.4 ± 0.3
B	Phosphate	Unstressed	9.7 ± 0.3
B	Phosphate	Stressed	3.4 ± 0.4

Table 13 shows the results from using the fluorescence ratio. There is a clearer method of detecting potentially difficult mAbs when comparing to the total FLI measurements, MAb A in both acetate and phosphate showed a relatively small decrease in fluorescence ratio after stressing. In mAb B acetate samples, the reduction in fluorescence ratio was more than that seen in mAb A, contrary to what was seen by SEC. The most dramatic reduction in ratio can be seen in mAb B phosphate, as expected. The increased secondary peak amplifies the ratio to highlight dramatic shape changes. This could suggest that fluorescence ratio is best employed as a quick qualitative method to rapidly identify problems. Additionally, an early indication could be to compare the initial ratio values. MAb A in both buffers have a small difference between phosphate to acetate in ratio values before stressing. When comparing mAb B, on the other hand, the fluorescence ratio in phosphate is already smaller than in acetate. This could act as a very early suggestion that mAb B is more prone to aggregation. However, further analysis would be required.

4.2.1.3 Red Edge Excitation Shift

REES offers a unique approach to standard FLI and has been used to study the structure of proteins. By changing the excitation wavelength from 270-310 nm in 5 nm increments, REES can selectively excite red-shifted fluorophores towards the red-edge. This shifts the emission maxima, giving information about the protein dynamics.

Figure 29 shows the REES measurements for mAb B in acetate and phosphate before and after thermal stressing. MAb B in acetate buffer, which did not aggregate more than 5% as seen in the SEC results, showed a small spectral shape change at higher excitation wavelengths. All stressed measurements showed a heightened tail from 380 nm onwards. When exciting the stressed samples at 295 nm and higher, the tail (seen in FLI mAb B phosphate aggregated samples) is more pronounced and easily seen, suggesting that aggregates, or pre-aggregate intermediate forms are excited at higher wavelengths and emit at higher wavelengths. This could prove useful when detecting the presence of aggregates, as an alternative to f_{330nm}/f_{395nm}.

For mAb B in phosphate, the tail can be seen more clearly after stressing (Figure 29). The higher amount of aggregates could be the reason for this. The tail forms a secondary peak at all excitation wavelengths tested. As the 330 nm peak decreases, the secondary peak increases at from 295-310 nm excitation.

This can be more clearly seen in Figure 30, which shows the FLI for both mAb A and B when excited at 310 nm. In mAb A acetate, the stressed sample does not show a secondary peak around 395 nm emission but does show a relatively higher intensity after the initial sharp peak. This is the Water Raman peak. During data analysis, blank samples were taken, then subtracted from the spectra to allow for a more accurate measurement, without distortion. In phosphate after stressing, a small secondary peak appears. For mAb B, this peak can be seen for both acetate and phosphate samples after stressing. It should be noted that there is a secondary peak in the unstressed phosphate sample present before stressing. This could be due to the formation of a pre-aggregate form and could be considered as an early indication of a mAb that is susceptible to aggregation.

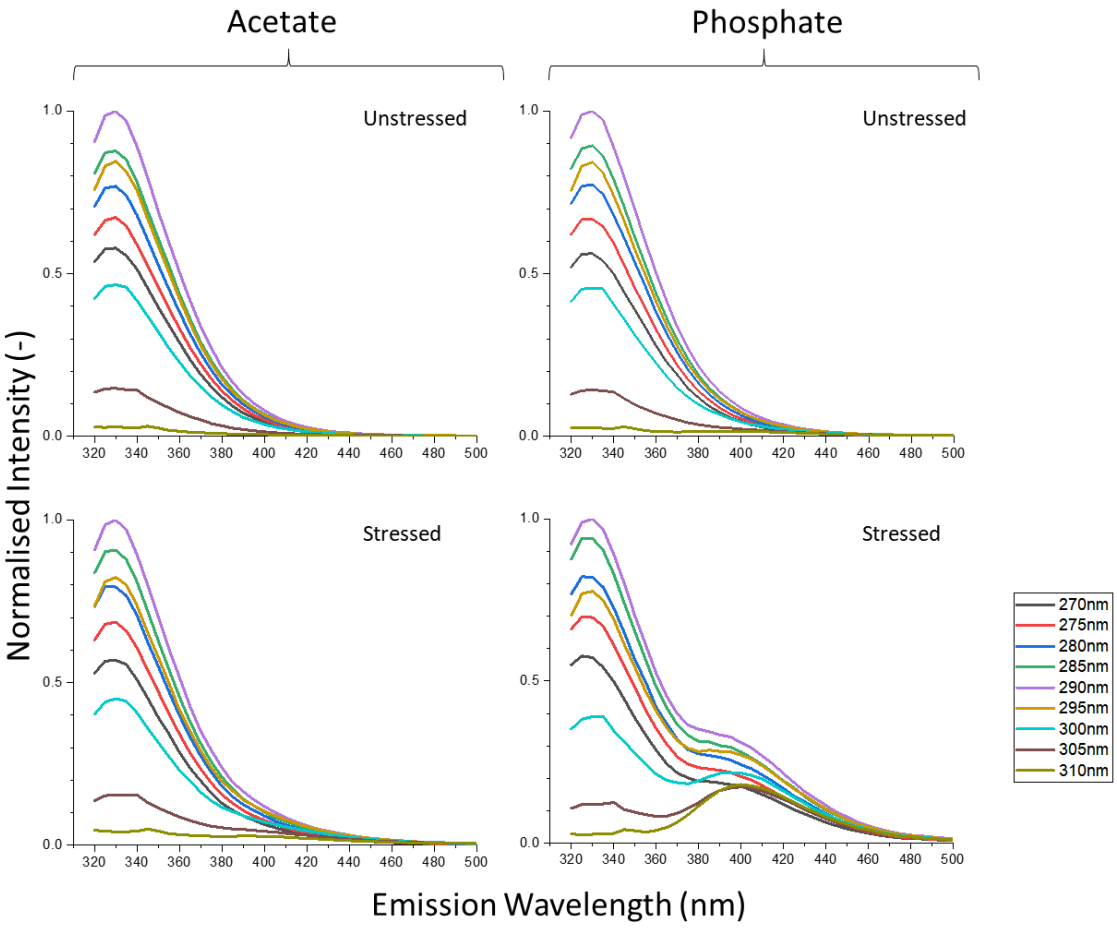

Figure 29 Normalised intensity results to show the effect of REES for mAb B in acetate and phosphate buffers before and after stressing at 40°C for 14 days. Top left- mAb B in acetate unstressed. Top right- mAb B in phosphate unstressed. Bottom right- mAb B in phosphate stressed, Bottom left- mAb B in acetate stressed. Excitation wavelengths at 270-310nm. The box legend corresponds to the excitation wavelength. Emission wavelength from 320-500nm. Samples were at 0.5mg/mL.

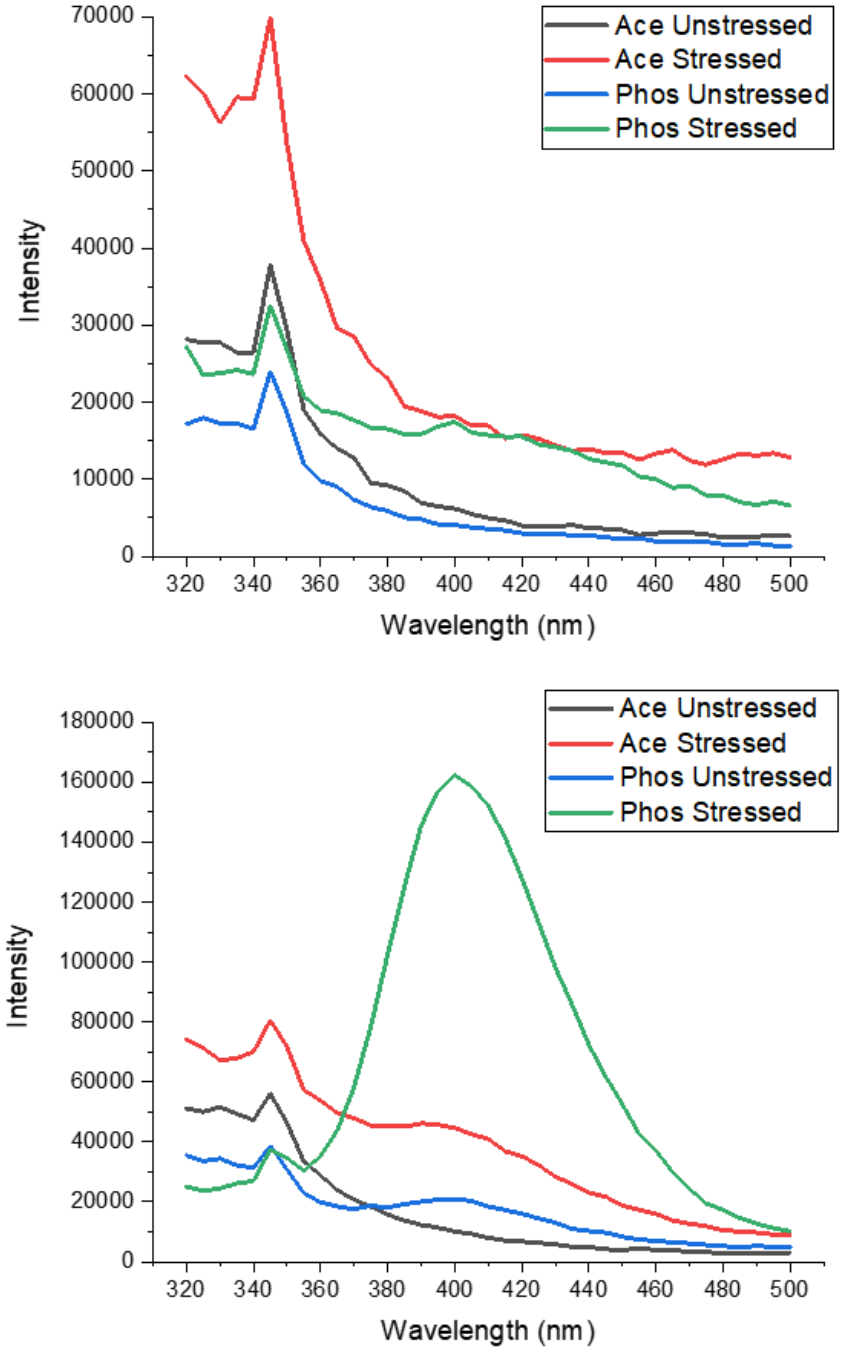

Figure 30 Fluorescence intensity graph for mAb A (A) and B (B). Excitation is 310nm. Emission wavelength taken from 320-500nm.

From the FLI emission scans from REES, the centre of spectral mass (CSM) can be calculated. This considers the whole spectrum, rather than just the emission maximum. This method accounts for shape changes, for example the secondary peak and any influence the higher tail would have, which gives a better indication of the red shift. The change in CSM is used to measure the magnitude of REES.

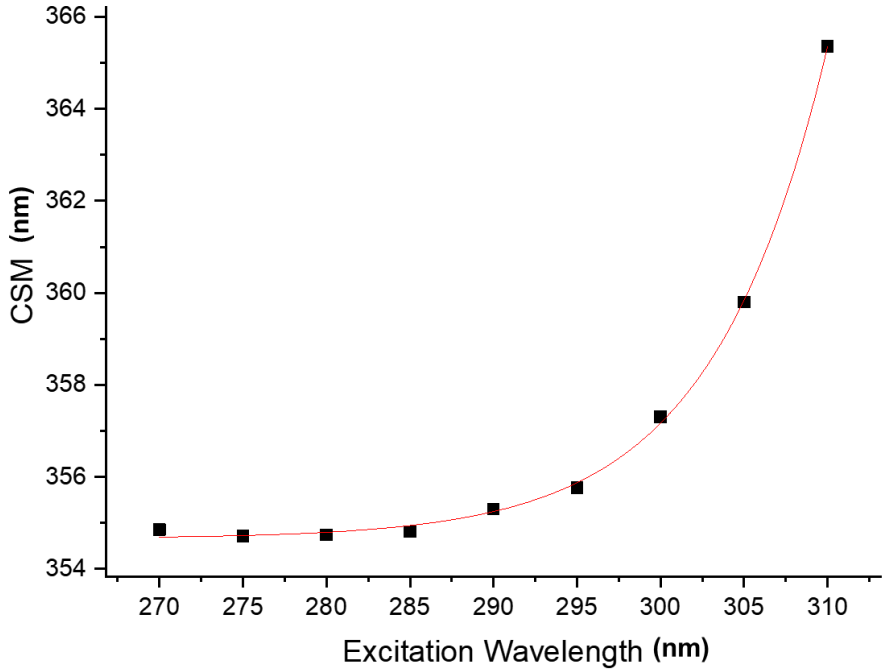

Figure 31 Example of CSM plotted against excitation wavelength. The red line indicated the fitted data which is used to find the QUBES parameters.

Figure 31 is an example of the CSM fitting. CSM values are plotted against the excitation wavelength and fitted using an exponential growth equation. The parameters CSM_0, R and A are calculated from the exponential equation.

Figure 32 shows how CSM changes with a change in excitation wavelength. For mAb A, the stressed samples in both buffers have a higher CSM than unstressed samples for each excitation wavelength, suggesting that there is a REES effect. The heightened tail end of the spectra with this method is shown to have an effect, due to the red shift. Both acetate and phosphate are very close, as seen in the SEC results also. For mAb B, the difference between unstressed and stressed samples is more obvious. The highly aggregated sample (stressed in phosphate) has a much higher CSM across all excitation wavelengths than all the other samples. An increase in CSM suggests that there is a shift in the equilibrium towards an unfolded state, from monomer state. This is promising as another method to detect aggregate, or aggregate prone samples.

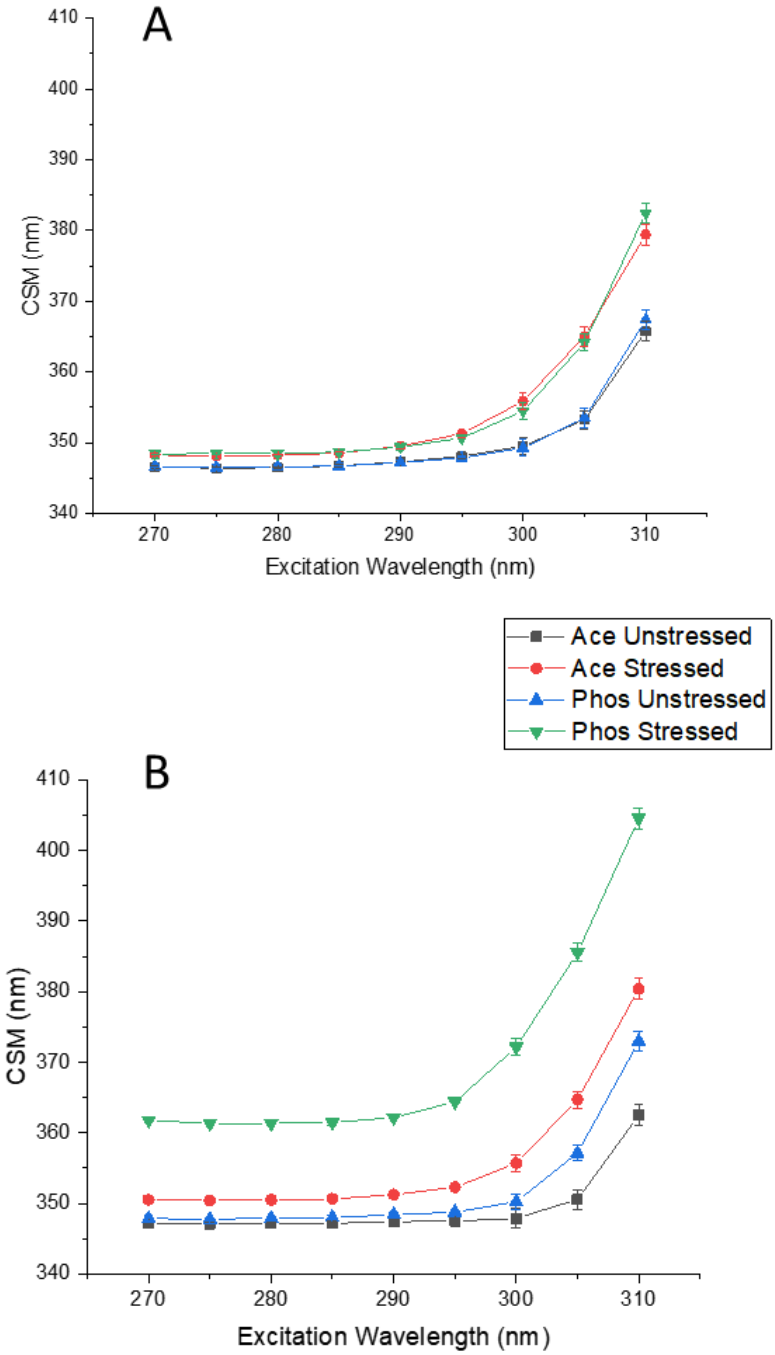

Figure 32 The centre of spectral mass (CSM) plotted with the respective excitation wavelengths. (A) mAb A. (B) mAb B. n=3

The REES phenomenon, excitation at lower energy which causes a red shift in the peak maxima, is used to give information on the conformational states and the equilibrium of these states. This effect is caused by the interactions between a fluorophore and the surrounding solvent, between excited and ground states. REES is due to the change in dipole moments in the fluorophore following excitation and the speed of solvent reorganisation around the fluorophore. By using a lower excitation energy (longer wavelengths) near the red edge of the excitation spectrum, the photo-selection allows fluorophores in a solvent relaxed surrounding environment to require less energy to be

activated (Catici et al. 2016). Therefore, the magnitude of REES can help to provide a measure of the rigidity of the area surrounding the fluorophore.

Table 14 highlights the magnitude of REES. The values were found by calculating the difference between CSM when excited at 270 nm and CSM when exciting at 310 nm. The larger the difference the larger the effects of REES. There is a difference from unstressed to stressed samples in mAb A of 12.0 and 13.4 in acetate and phosphate respectively. This suggests that mAb A in phosphate has more conformations possible, and therefore more likely to aggregate than in acetate. This was case, as seen in SEC. For mAb B, the differences from unstressed to stressed were 14.6 and 17.7 in acetate and phosphate respectively. This is more than seen in the stressed mAb A acetate samples, despite showing less aggregate in SEC. This could be due to the conformations being of similar size, therefore not being detected in SEC. Additionally, when comparing the unstressed samples across both buffers and mAbs, the change in CSM could already be a useful early indicator of its behaviour during thermal stressing.

Table 14 Change in CSM (magnitude of REES) results for mAb A and B in acetate and phosphate before and after thermal stressing at 40°C for 14 days.

mAb	Buffer	Stress	ΔCSM [REES] (nm)
A	Acetate	Unstressed	19.2 ± 1.6
A	Acetate	Stressed	31.1 ± 1.7
A	Phosphate	Unstressed	20.7 ± 1.6
A	Phosphate	Stressed	34.1 ± 2.0
B	Acetate	Unstressed	15.3 ± 1.8
B	Acetate	Stressed	29.9 ± 2.0
B	Phosphate	Unstressed	25.1 ± 1.9
B	Phosphate	Stressed	42.8 ± 1.6

Table 15 REES results for mAb A and B in acetate and phosphate before and after thermal stressing at 40°C for 14 days. CSM_0, A and R were found by fitting the CSM data from Figure 32.

mAb	Buffer	Stress	CSM_0 (nm)	A (nm)	R (nm^{-1})	A/R (nm^2)
A	Acetate	Unstressed	346.6 ± 0.1	0.018 ± 0.005	0.199 ± 0.009	0.090 ± 0.029
A	Acetate	Stressed	348.3 ± 0.1	0.200 ± 0.010	0.148 ± 0.001	1.358 ± 0.077
A	Phosphate	Unstressed	346.7 ± 0.1	0.012 ± 0.002	0.215 ± 0.005	0.054 ± 0.011
A	Phosphate	Stressed	348.0 ± 0.1	0.132 ± 0.012	0.160 ± 0.002	0.830 ± 0.085
B	Acetate	Unstressed	347.1 ± 0.1	0.001 ± 0.001	0.298 ± 0.001	0.002 ± 0.003
B	Acetate	Stressed	350.7 ± 0.2	0.121 ± 0.008	0.159 ± 0.003	0.764 ± 0.064
B	Phosphate	Unstressed	347.0 ± 0.1	0.004 ± 0.002	0.259 ± 0.005	0.015 ± 0.007
B	Phosphate	Stressed	360.7 ± 0.2	0.629 ± 0.015	0.123 ± 0.003	5.132 ± 0.247

Table 15 processed data from fitting an exponential to the mean CSM data. Three parameters: CSM_0, A and R are then found, which give an indication of the REES effect. A larger A/R typically indicates a more pronounced REES effect, the mAb is more flexible and more likely to have various conformations available to it as described by Catici et al. (2016). This could then lead to the assumption that these mAbs are more aggregate prone, as conformations reveal areas for aggregates to form.

MAb A when stressed shows a small increase in A/R, roughly the same percentage increase in both buffers. Comparing to mAb B in phosphate, where there is a large A/R, mAb A is relatively stable. The increase in A and small decrease in R suggests that the REES effect is due to a small amount of aggregates present, causing the shift. The small increase in CSM_0 indicates a small amount of unfolding occurring.

MAb B in phosphate, has a relatively high REES, which suggests that there are more conformations available. There is a larger increase in A, and a larger decrease in R, suggesting that the aggregates influence REES. The larger increase in CSM_0 indicates unfolding.

REES was able to detect the differences between each sample and clearly show mAb B in phosphate to be the outlier. This suggests that REES could be a useful tool in detecting how susceptible a mAb is to aggregation.

4.2.1.4 Time Correlated Single Photon Counting

TCSPC uses the principles of fluorescence decay and aims to measure the time a fluorophore spends in the excited state before returning to the ground state as a photon is emitted. The decay changes in different environments, making it a useful indicator of aggregation. Typical fluorescence decay times for proteins range from 0.1- 4 ns, and for tryptophan is around 3.03 ns. (Berezin & Achilefu 2010).

Figure 33 shows an example of how TCSPC data is fitted. The counts are plotted against the time. An exponential decay is fitted to the data.

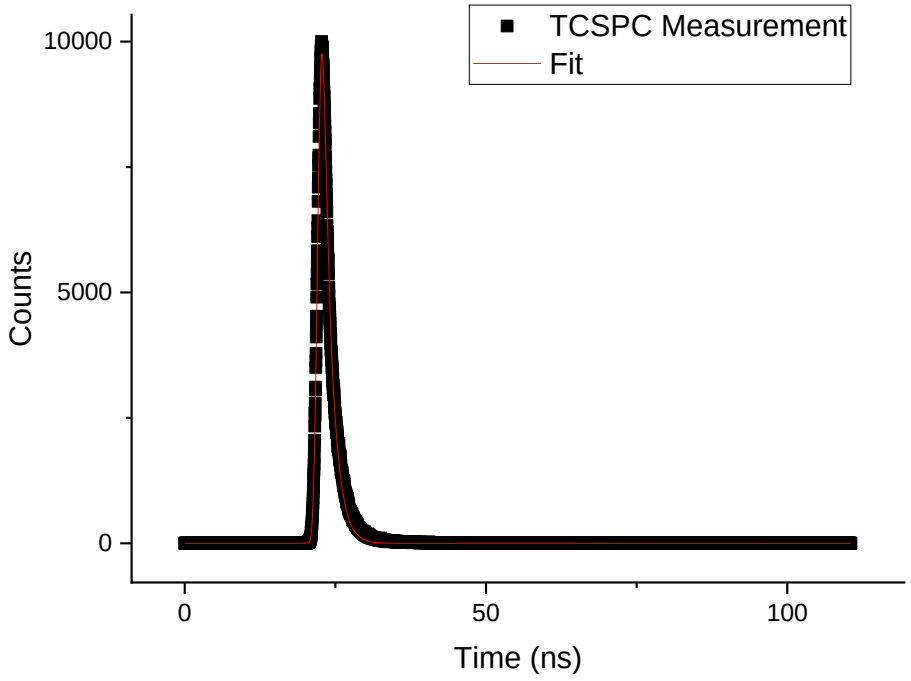

Figure 33 Example of TCSPC fitted exponential decay.

For TCSPC, an LED is used at 280 nm, instead of a xenon lamp as it allows very rapid pulsing. Emission was taken at 330 nm and 395 nm. This allowed for the emission peak to be measured at 330 nm and allowed an investigation into the raised tail at 395 nm. The following data analysis uses a single exponential fit, which is the weighted average decay time, shown in equation 4.1.

$$\tau_{Mean} = \frac{\sum A_i \tau_i}{\sum A_i \tau_i} \tag{4.1}$$

Where: τ is the fluorescence decay and A is the preexponential factor (related to the fraction of each lifetime). Typically a higher time decay suggests more tryptophan are at the surface and a lower decay suggests a buried tryptophan in the core (Kayser et al. 2011; Sahoo et al. 2008).

Figure 34 shows the TCSPC time decay measurements at emission 330 nm and 395 nm. The measurements at 330 nm show a general trend of increased time decay after stressing, except for mAb B phosphate. For mAb A in both buffers and mAb B in acetate, it suggests that the stressing caused more solvent exposure to tryptophan, hence the higher time decay. This could mean that the molecules are unfolding or being partially exposed to the environment slightly due to the thermal stress, possibly as a pre-cursor for aggregation. This is contrary to what was found during the FLI experiments, where intensity dropped after stressing due to less exposure. From SEC, there was a degree of fragmentation, which could influence the increase in time decay.

For mAb B in phosphate, there was a decrease from 1.50 ns to 1.43 ns, a decrease of just under 5%. This suggests that a larger amount of aggregates (around 23% according to SEC) decreases the time decay, when compared to the other samples (which were all less than 5% according to SEC). The lower time decay suggests that the tryptophan residues are being buried in the hydrophobic core as the mAbs aggregate.

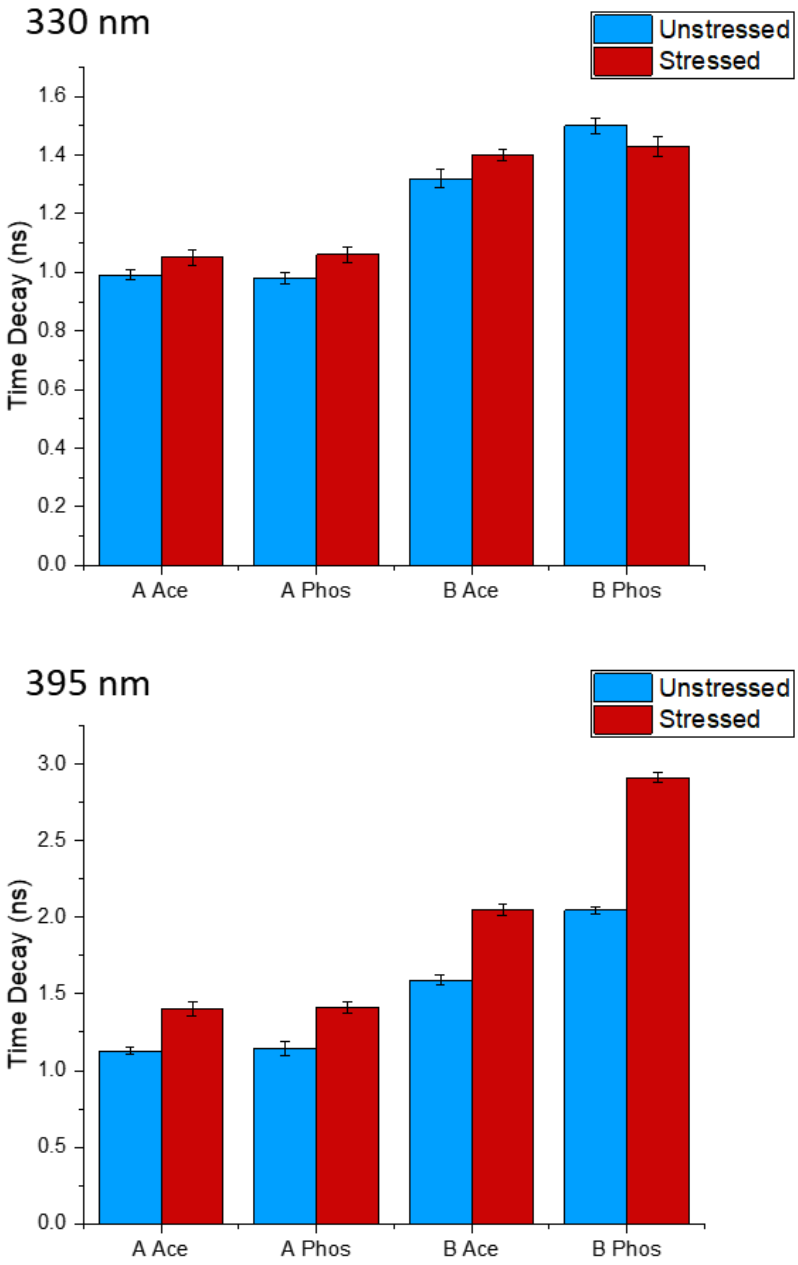

Figure 34 Time decays from TCSPC (Excitation 280nm) at 330nm emission (top) and 395nm emission (bottom) for mAb A and B in acetate and phosphate buffers before and after stressing at 40°C for 14 days. n=3. Error bars show standard deviation.

At 395 nm emission, there is a larger increase across all samples after thermal stressing, the largest change being seen in mAb B in phosphate with a 43% increase. This could suggest that at 395 nm, the technique more sensitive to monomer loss or changes to the mAb structure. For mAb in phosphate, the emission at 330 nm and 395 nm do not follow the same path. This could be due to the influence of the secondary peak, seen in FLI. At the secondary peak, there is more exposure to the solvent, hence the higher time decay. The emission at 395 nm could be influenced by the amount of aggregates present, as seen in FLI with the more intense tail measurement.

An early indication of an aggregate prone mAb could be found by comparing mAb behaviour in each buffer. This was suggested by the f_{330nm}/f_{395nm} described earlier. Comparing mAb A in both buffers, they have very similar time decays, with insignificant differences. However, we see immediately that mAb B in phosphate has a significantly higher time decay than in acetate, even before stressing. This could suggest, that from its structure and the exposure of tryptophan to the environment, it is already more prone to aggregation.

Overall, TCSPC could offer a quick method to detect higher levels of aggregates or to highlight samples that are more prone to aggregation. There are similarities in the results when comparing TCSPC with 395 nm emission and DLS. As TCSPC runs with a much smaller sample volume and measurement time is much lower, it could offer a useful alternative.

4.2.2 Time Course Fluorescence Study

Once each fluorescence technique (FLI, f_{330nm}/f_{395nm}, REES and TCSPC) was evaluated for its usefulness in comparison to SEC. SEC was used as the basis for comparison during the time course study as it offered readings at the same concentration and was used in the degradation study.

DLS was not used for this comparison as it is typically used to examine concentration dependent aggregation and it requires a high amount of material, which was unavailable.

The time course study was carried out to investigate early signs of aggregate prone mAbs and to test the effects of temperature. To investigate the effects of using a lower material requirement, samples at 0.5 mg/mL were thermally stressed. This sample was then used in each technique, eliminating the need to dilute. Temperatures of 37 °C and 45 °C was investigated. The sample volume used was 12 µL taken from the bulk 500 µL. The 12 µL quartz cuvette, with a pathlength of 1.5 mm, was used. The sample was returned to the bulk and new sample was drawn for the replicate measurements. MAbs A, B, D and E were tested in acetate and phosphate buffers.

The aim of this study was to evaluate the suitability of fluorescence techniques while reducing the sample volume, concentration and time taken for measurements. The techniques were evaluated on whether they reveal the same, or more, information as the currently used techniques.

4.2.2.1 SEC Comparison

To ensure the fluorescence-based techniques can be compared to current methods in detecting aggregation, SEC was run alongside the fluorescence samples.

Samples at two concentrations, 0.5 mg/mL and 10 mg/mL, and at different temperatures, 37 °C and 45 °C, were compared to evaluate any problems which may skew results by stressing at different concentrations. Samples were diluted to 0.5 mg/mL for SEC measurements.

The aim of this experiment was to test if by reducing the concentration and/or changing the temperature, the reduction could still give the same information as the lead panel ranking, stressing at 40 °C at 10 mg/mL for two weeks. If at a certain time point, SEC could identify significant differences between the samples, it could lead to an immediate time and material reduction for future assays.

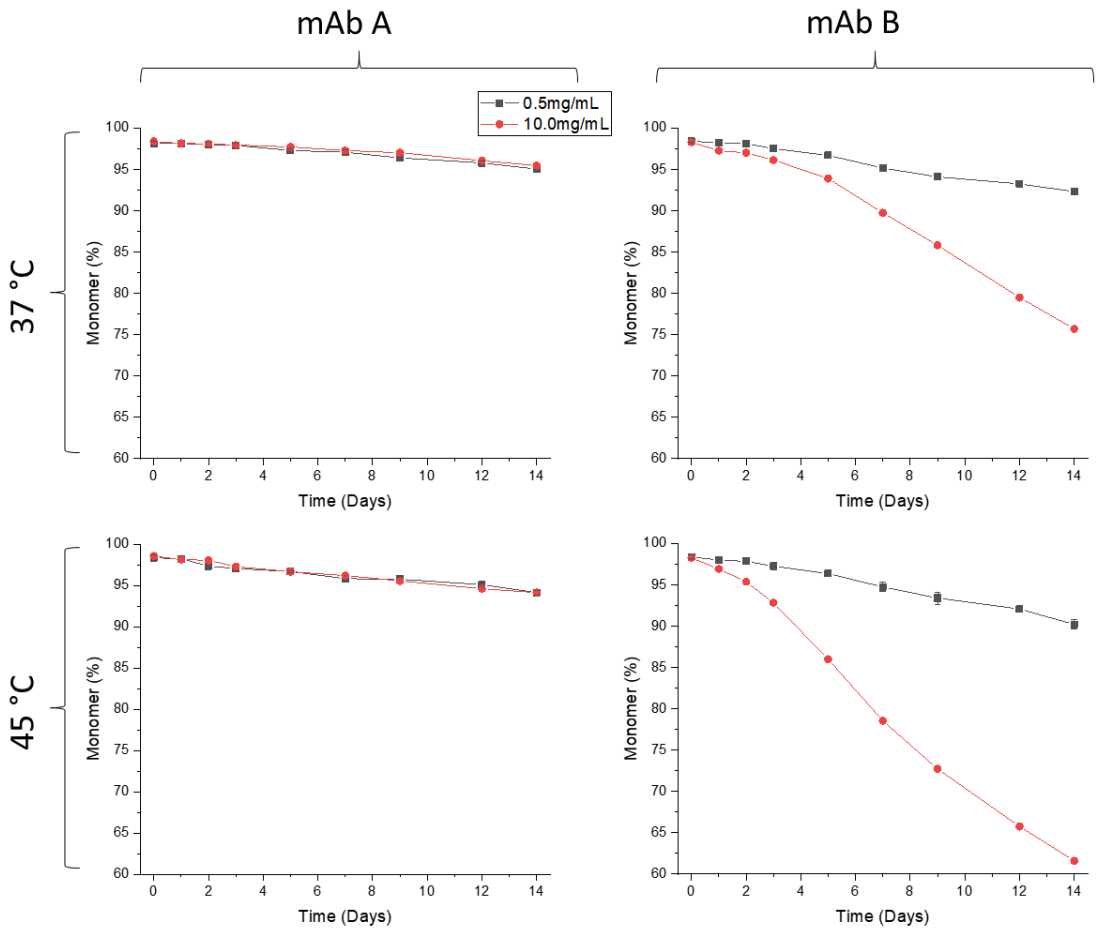

Figure 35 Time course SEC results for mAb A and B in phosphate buffer held at 37°C and 45°C at 0.5mg/mL and 10mg/mL. Black= 0.5mg/mL and Red= 10mg/mL. Error bars show standard deviation (n=3).

Figure 35 shows the percentage monomer change over time at different temperatures and concentrations. For mAb A in phosphate at both temperatures, there is overlap within the error bars between the 0.5 mg/mL and 10 mg/mL. This suggests that there was no significant difference between the two, therefore a lower concentration could be considered for the future testing. However, for mAb B in phosphate, there is a very

significant difference between the two concentrations. This was most likely due to the probability of two monomers meeting to aggregate is much lower in more dilute samples.

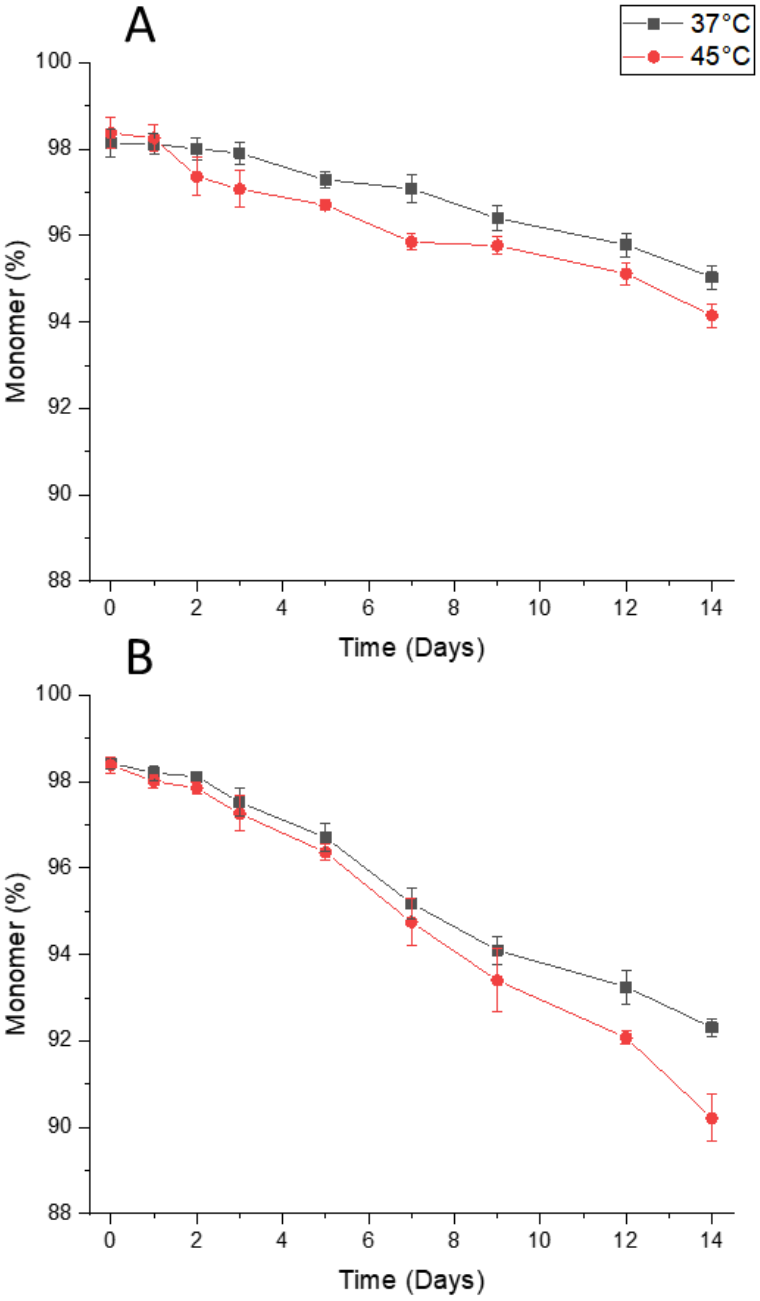

Figure 36 Comparison of time course SEC results for mAb A and B in phosphate buffer at 37°C and 45°C to highlight the differences between stressing at two temperatures. Concentration is 0.5mg/mL. n=3. Error bars show standard deviation.

Figure 36 better shows the differences of the effects of temperature on the mAbs, while concentration is the same. In both samples, there is a higher monomer loss at 45 °C. This shows that, while the differences are relatively small, a higher temperature causes

more monomer loss. Stressing at 45 °C could be better to highlight and exaggerate more aggregate prone mAbs.

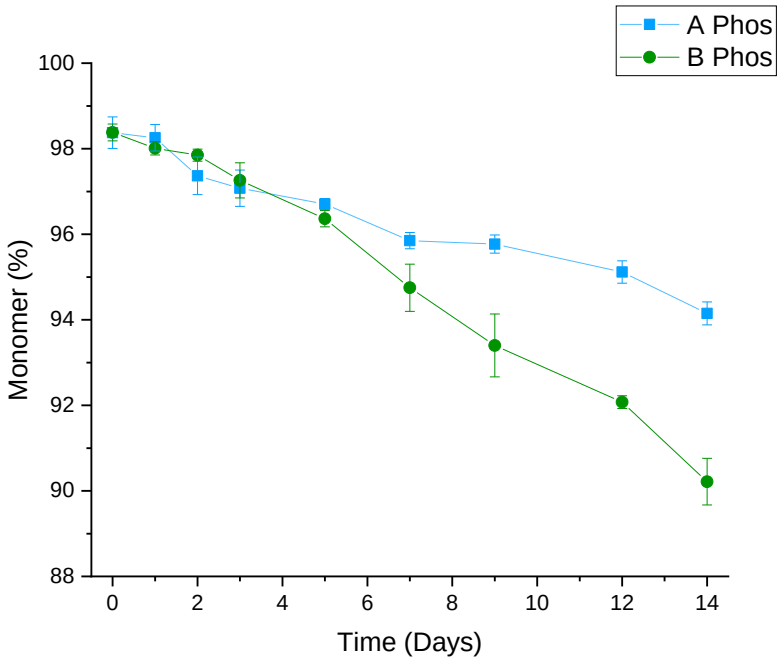

Figure 37 Comparison of time course SEC results for mAb A and B in phosphate buffer at 45°C to highlight the differences between the two mAbs. n=3. Error bars show standard deviation.

Figure 37 shows a direct comparison between mAb A and B in phosphate buffer at 45 °C. There is overlap between the two until day 7, which suggest that SEC may not be capable of early identification of more aggregate prone mAbs. Based purely on SEC, it could prove useful to wait until day 14 rather than reducing the time frame. This highlights the need for a technique that can give the same information in less time.

The initial SEC results showed that at lower concentrations, it could still identify the more aggregate prone mAb during stressing. This formed the basis for comparison and the following fluorescence experiments were all compared at 0.5 mg/mL. Both 37 °C and 45 °C were still compared to investigate small differences between samples.

Figure 38 shows the SEC results for mAbs A, B, D and E in in acetate and phosphate after stressing for 14 days. MAb B in phosphate, at both temperatures suffered from the most monomer loss overall, dropping 6% and 8% monomer at 37 °C and 45 °C respectively. When comparing the results from the GSK panel to these experiments, there is a relatively good amount of success, with the time course study, at both temperatures being able to identify the samples with the highest and lowest monomer loss.

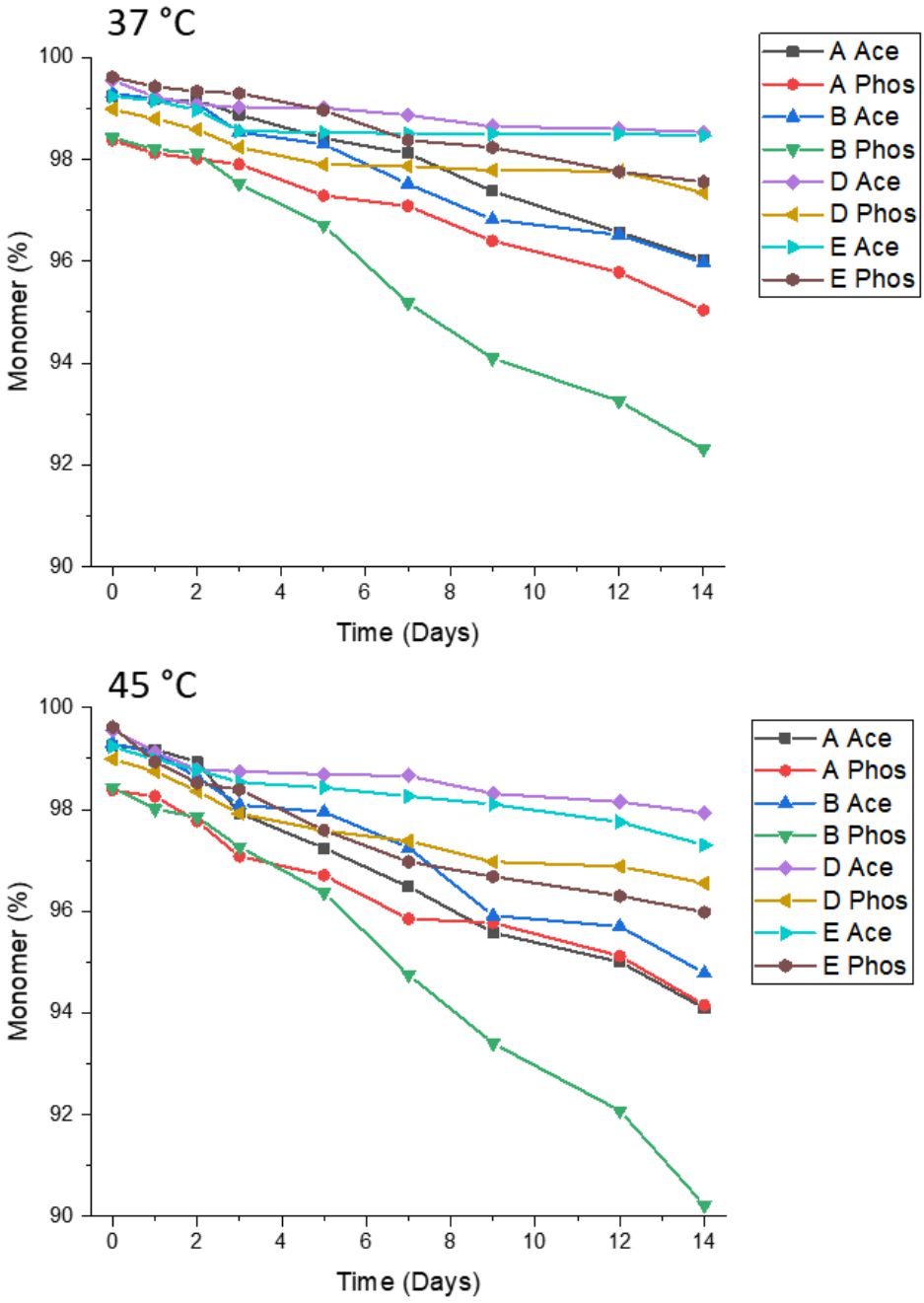

Figure 38 Time course SEC results. MAbs A, B, D and E were isothermally held at 37 °C and 45 °C for 14 days at 0.5mg/mL in 500µL vials. n=3.

Overall, SEC successfully detected mAb B in phosphate to aggregate more highly around day 8 compared to the other samples. The results vary greatly from the baseline SEC data due to the difference in stressing parameters used, temperature and concentration. These differences caused more monomer loss in all samples except mAb B in phosphate, where a there was over 20% more monomer in the more dilute samples. This shows different aggregation kinetics influencing the amount of monomer loss. As SEC was still able to detect the aggregate prone mAb, stressed at 5% of the original sample requirement, it could still be a useful method, that the fluorescence techniques

will be compared. To measure monomer loss by SEC, 30 µL at 0.5 mg/mL was used, taking 15 minutes per sample on average (1 minutes to load, 14 minutes in column).

4.2.2.2 Fluorescence Intensity

Fluorescence intensity measurements were taken by exciting the sample at 280 nm and taking the emission from 290 nm to 500 nm. Measurements were taken at 0.5 mg/mL.

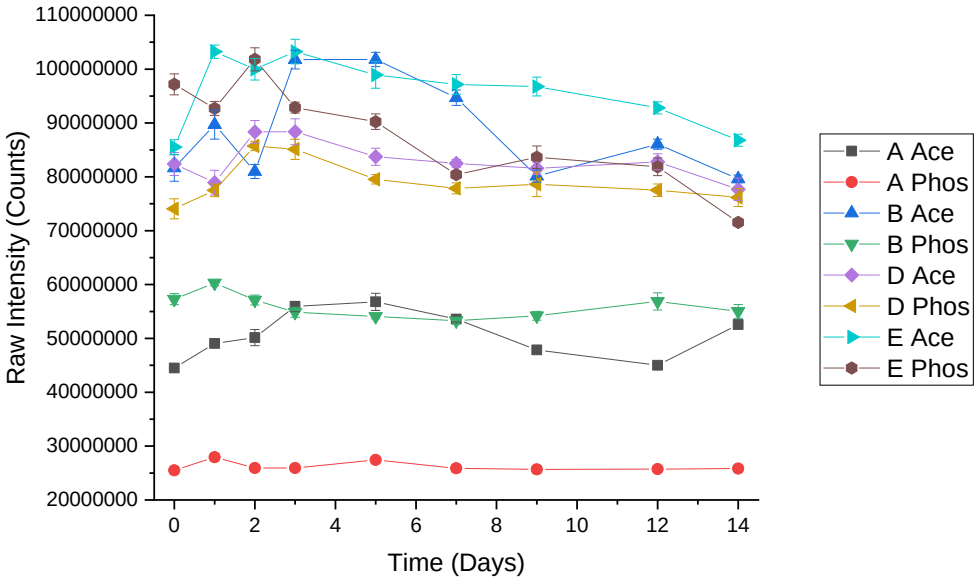

Figure 39 Raw intensity graphs before data processing. MAbs A, B, D and E were isothermally held at 45 °C for 14 days at 0.5 mg/mL in 500 µL vials. n=3. Error bars show standard deviation.

The raw data from total fluorescence intensity shows large fluctuations, and inconsistent results. Despite taking water and fluorescein calibrations, the results from raw FLI were not as expected when compared to the initial FLI experiments in Figure 25. An overall decrease in FLI was expected, apart from mAb B in phosphate (due to the secondary peak forming skewing total FLI). Initial thoughts lead to the possibility of tryptophan residues being buried and/or exposed to the environment as a mAb undergoes conformational changes due to the temperature stressing. Upon repetition of the experiment, data was inconclusive.

Consequently, FLI raw data results were normalised to the emission intensity at 270nm. This allowed a much clearer method for comparing samples day-to-day and allowed the fluctuations to be eliminated more readily. Figure 40 shows the shape changes, more clearly once the FLI scans were normalised. The decrease in fluorescence intensity at the peak (around 330nm) can be seen, as tryptophan residues react to the change in environment. As the mAb conformation changes or some aggregate, some tryptophan residues are buried in the hydrophobic core, lowering their intensity. The second peak could be due to aggregate prone intermediates. As SEC did not suggest a high amount

of aggregates present, this could be indicative of aggregate prone intermediates present in the sample.

All mAbs show the same trend, with increased time, the peak fluorescence decreases. In most samples, as the samples are stressed, the heightened tail appears from 400nm onwards, as seen in the baseline FLI experiments. MAb D is the only mAb not to show this trend in either acetate or phosphate. When comparing this to the time course SEC results, we know that mAb D is the most stable suggesting this could be the reason for the lack of heightened tail, as there are less intermediates of aggregates present. MAb A shows the tightest spread, especially in acetate.

The FLI scans were not able to detect any shape changes or indications that mAb E may precipitate, as had been recorded by GSK historically.

Figure 41 shows the normalised total FLI. The units are arbitrary as they are not true intensity due to the normalisation process. The starting position is mAb specific and is due to the position and the amount of tryptophan residues present in the sample. At 37°C, the differences in mAb behaviour in both buffers is insignificant, all samples showing a general decrease in total fluorescence with increased time stressing. MAb D shows a large decrease in total FLI in both temperatures, differing to the SEC results previously.

The differences in behaviour in each buffer are more apparent in the samples stressed at 45°C. In mAb A, the decrease in fluorescence in phosphate is more obvious by day 9, where there is no overlap in error bars. This is also seen in mAbs D and E after day 5. This suggests that FLI could pick up the differences between the samples, as seen in SEC previously. However, with mAb B in phosphate, for both temperature samples, there is an increase in overall fluorescence due to the secondary peak skewing results. This hinders this technique from fully determining the loss of monomer over time as it would suggest that mAb B in acetate had a lower percentage of monomer than in phosphate, contradicting the results from SEC.

Total FLI was not able to detect mAb B as the more aggregate prone sample, instead suggesting mAb D had lost the most intensity (and therefore tryptophan is being buried) over time. However, it should be considered as a method to determine conformational changes and to identify possible anomalies in mAbs.

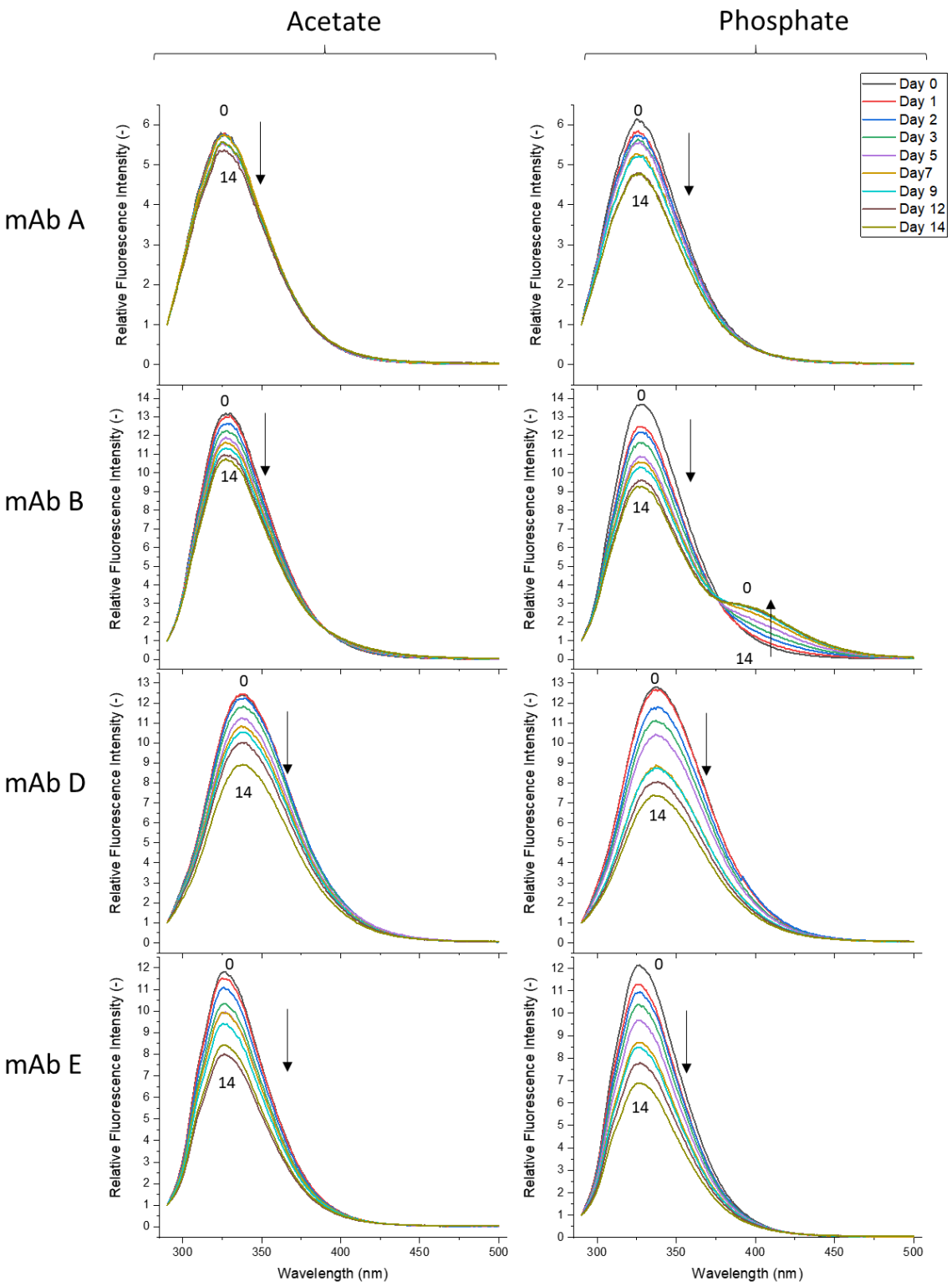

Figure 40 FLI scans over 14 days for mAbs A, B, D and E in acetate and phosphate buffers. Samples held at 45°C. All points are made relative to the intensity at 270nm, to allow the shape change and day-to-day comparisons to be made. Excitation from xenon lamp at 280nm and emission collected from 290nm to 500nm.

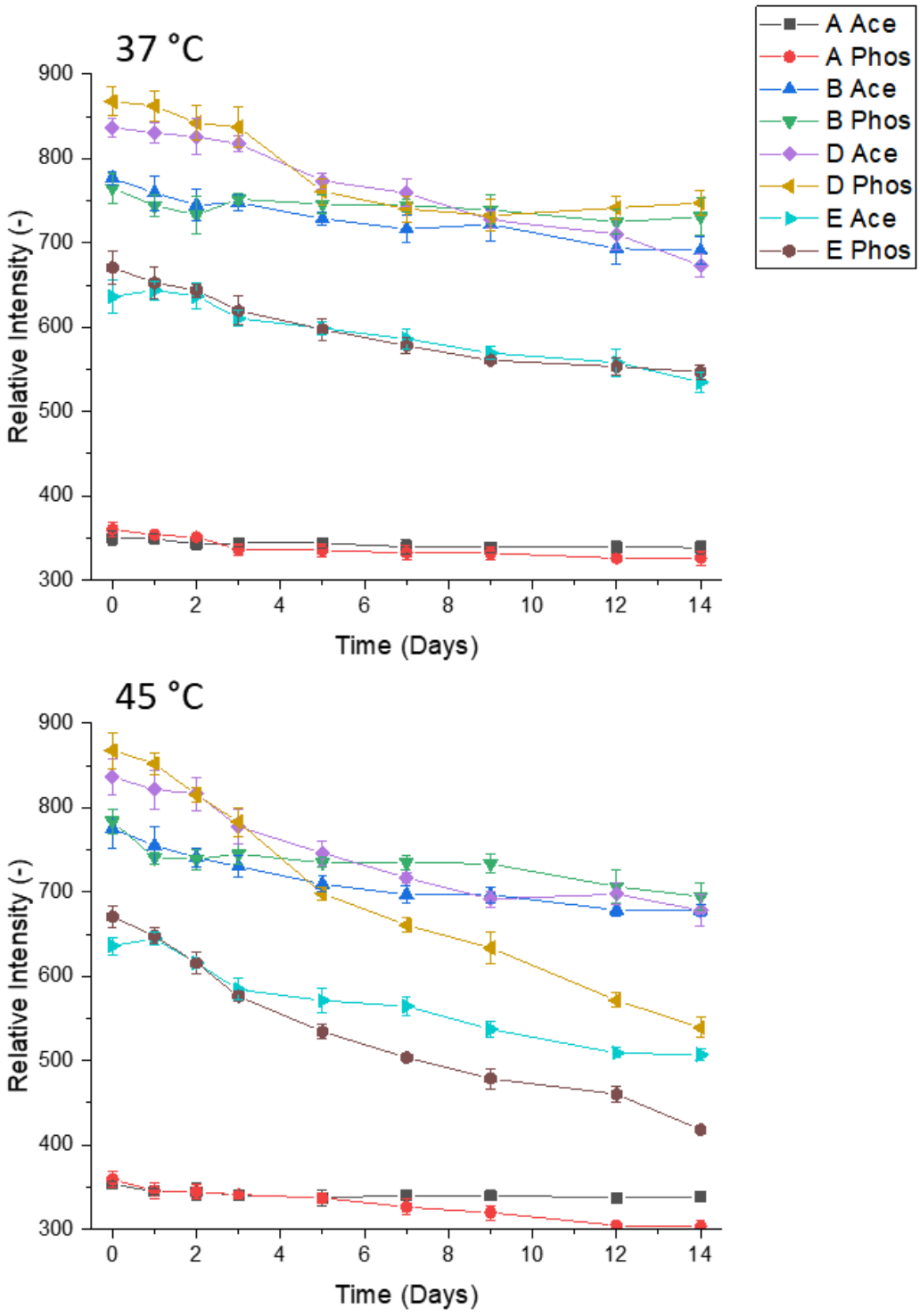

Figure 41 Time-course fluorescence intensity comparison between 37°C and 45°C for mAbs A, B, D and E in acetate and phosphate buffers. All time points are normalised to their 270nm emission intensity. Error bars show standard deviation. n=3.

4.2.2.3 Fluorescence 330:395nm Ratio (f_{330nm}/f_{395nm})

f_{330nm}/f_{395nm} was considered to consider the changes seen in the emission spectra, namely the heightened tail appearing around 390-500nm.

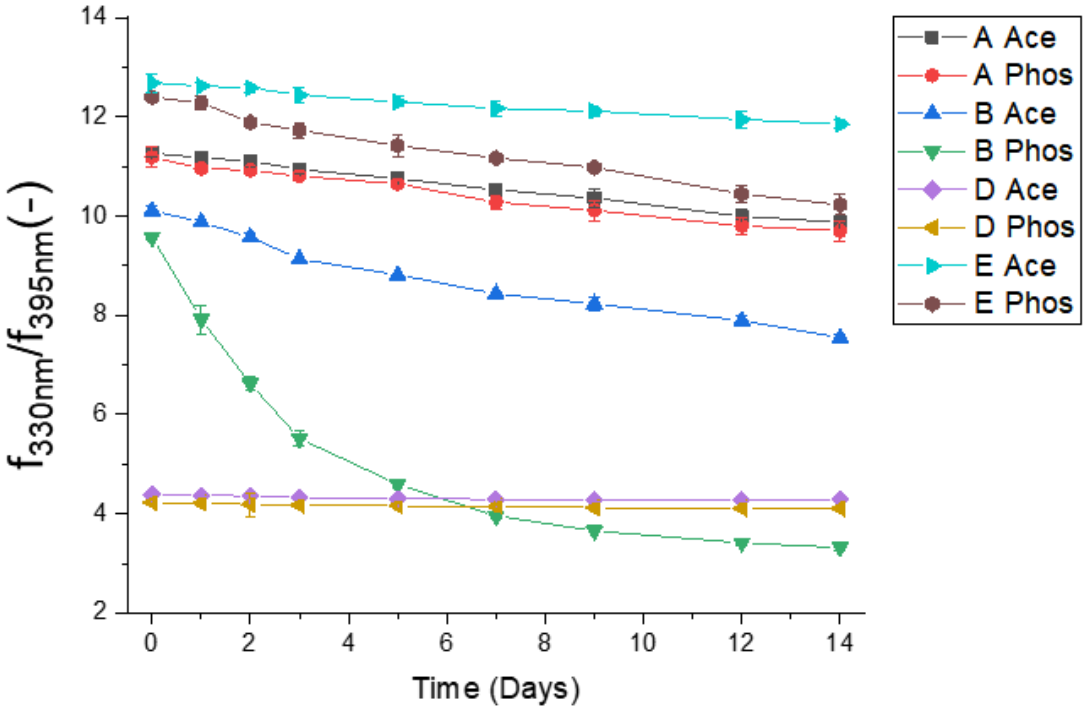

Figure 42 Time-course f_{330nm}/f_{395nm} at 45°C for mAbs A, B, D and E in acetate and phosphate buffers. Error bars show standard deviation. n=3.

Figure 42 shows the f_{330nm}/f_{395nm} results from the time course study at 45°C stressing. The results for samples stressed at 37°C are not shown but it followed an identical trend. Each mAb starts of slightly lower in phosphate on day 0, as expected from the initial lower monomer levels seen in the SEC results. MAbs B and E show a significant difference between samples in phosphate, as the ratio drops with time, compared to samples in acetate. This was expected as both mAbs show a relatively large decrease in percent monomer. With mAb B, the differences between acetate and phosphate can be clearly seen within the first day, with a drop from 9.58 to 8.15, compared to 10.17 to 9.84 in acetate. For mAb E, within the first two days.

MAbs A and D show little difference between samples in acetate and phosphate. This again was expected as they were the negative controls. The samples in phosphate were slightly lower, as seen in SEC previously. MAb D has a relatively low starting f_{330nm}/f_{395nm}, 4.38 and 4.22 in acetate and phosphate respectively. This suggests a much wider spectrum. It is the most stable mAb according to the ratio, dropping less than 3% over 14 days in both buffers.

As fluorescence is typically a method that relies on detecting a change relative to an original, all measurements were also normalised to day 0. This allowed a direct comparison between mAbs and buffers ignoring the raw ratio, as seen in Figure 41, where samples with an inherently high fluorescence skew the measurement.

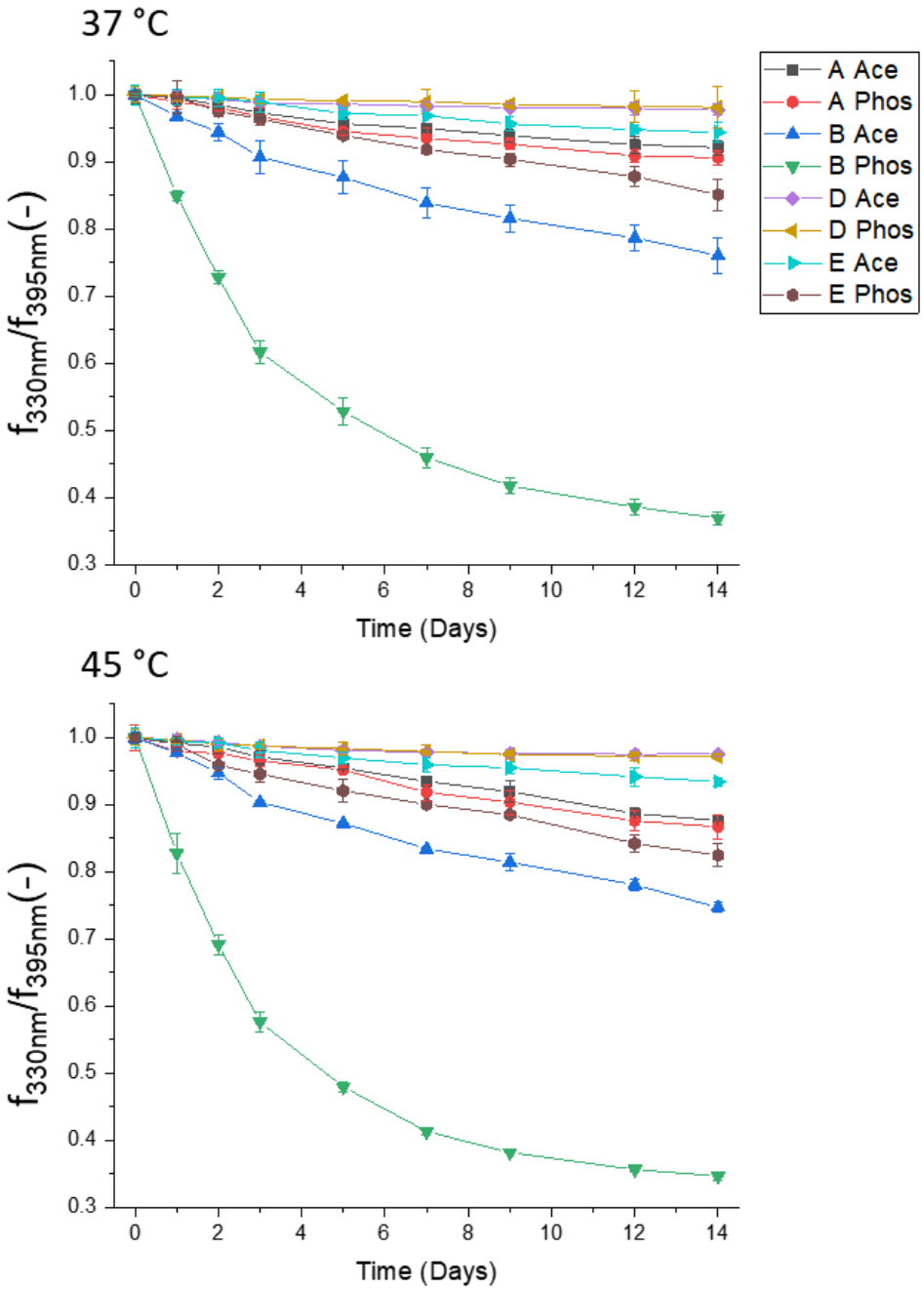

Figure 43 Time-course fluorescence f_{330nm}/f_{395nm} comparison between 37°C and 45°C for mAbs A, B, D and E in acetate and phosphate buffers. All data points are relative to Day 0 measurement. N=3. Error bars show standard deviation.

Using the f_{330nm}/f_{395nm}, mAb B in phosphate is immediately identified as the outlier. Immediately from day 1, it experiences a drop of more than 15% at both temperatures. This could be a promising detection method if other aggregate-prone mAbs share the same shape change.

In most samples, the f_{330nm}/f_{395nm} is lower in phosphate, as confirmed by SEC previously. With mAbs A and D, the negative controls, there was little difference between the two buffers in terms of f_{330nm}/f_{395nm}. However, comparing to the SEC results, the monomer percentage in mAb D phosphate was lower by 1% than in acetate.

Overall, the f_{330nm}/f_{395nm} is a simple and effective method to identify potentially problematic mAbs in the panel, that does not require complex analysis. Data acquisition takes around 1 minutes per sample (10 seconds data acquisition and 55 seconds to load sample), much quicker than SEC. It was able to identify the two mAbs that were flagged in the lead panel ranking within the first day after stressing. Therefore, it could be a potentially easy and powerful technique to carry forward for early prediction.

4.2.2.4 Red Edge Excitation Shift

REES was previously shown to be promising in identifying mAb B in phosphate as having a large A/R ratio and an increased CSM after stressing, indicating that it is a sensitive technique and able to identify that the mAb is more aggregate prone. The REES effect is sensitive to the equilibrium of conformational states and can be used as a proxy to reflect the distribution of conformational states (Catici et al. 2016).

Figure 44 shows the change in CSM graphs during the time course study. In general, an increase in CSM indicates the equilibrium movement from monomer towards an unfolded state. MAb A in acetate shows a slightly less tight spread over time than in phosphate and mAb D and E. This suggests that it is slightly further shifted towards the unfolded state. Comparing this with the SEC data, it could suggest that while the confirmation may be changing, the size does not change. Both mAbs D and E in both buffers have a relatively tight CSM during thermal stressing. This suggest that these mAbs are relatively stable during the thermal stressing, less so in phosphate, as expected. On day 12 and 14 for mAb D in phosphate, we see a sudden steepened curve, which suggests a sudden increase in the amount of unfolding. MAb B in phosphate shows a much higher increase in CSM across the time. This suggests that the equilibrium has shifted towards the unfolded state, opening the mAbs to aggregation. Despite not showing signs of high aggregation from SEC, it can be identified as an aggregation-prone mAb very clearly, that is less stable over time.

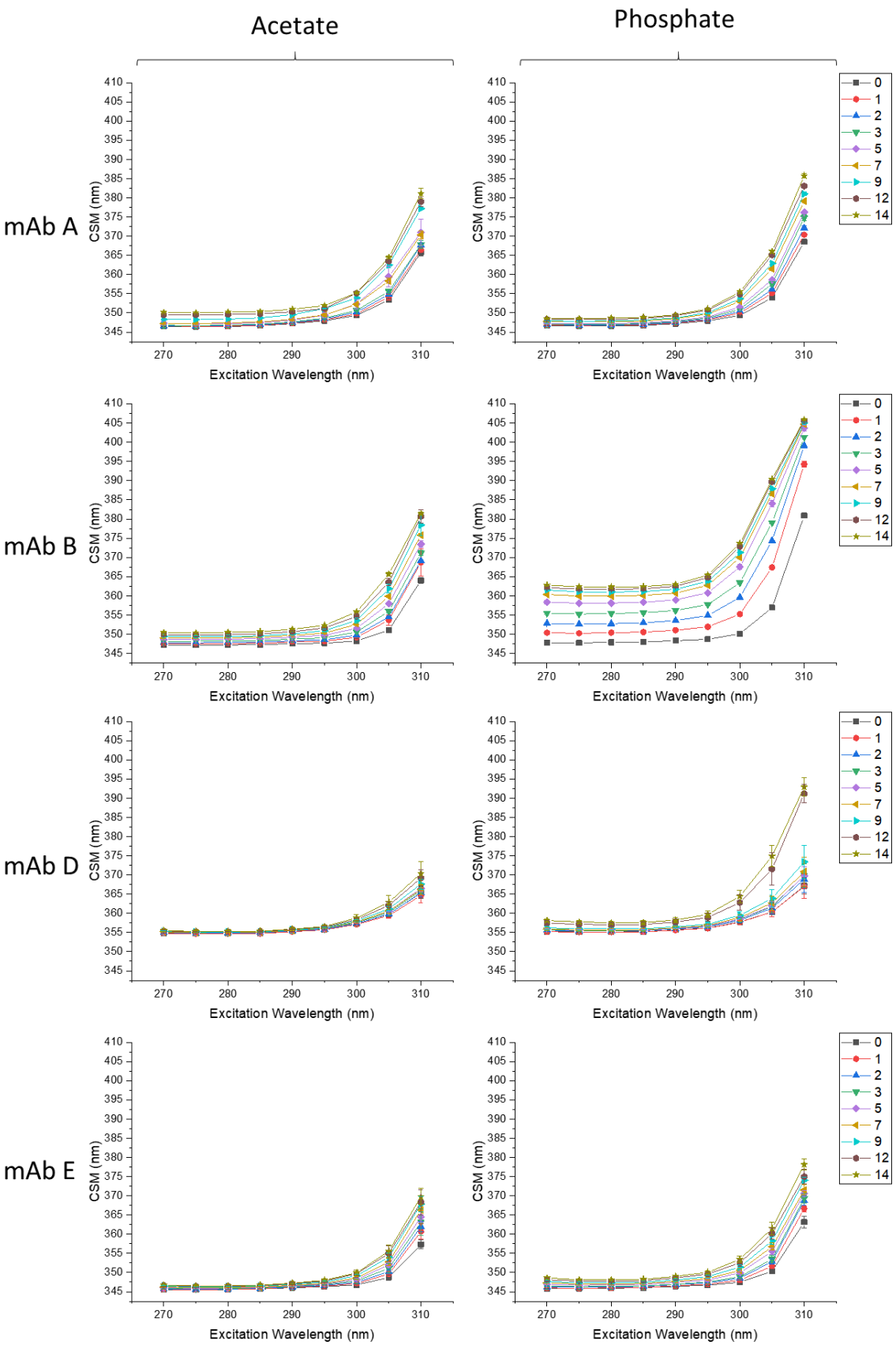

Figure 44 Time-course CSM comparison for samples thermally stressed at 45°C for mAbs A, B, D and E in acetate and phosphate buffers. The colours correspond to the day during the study that the measurements were taken. Error bars show standard deviation. n=3.

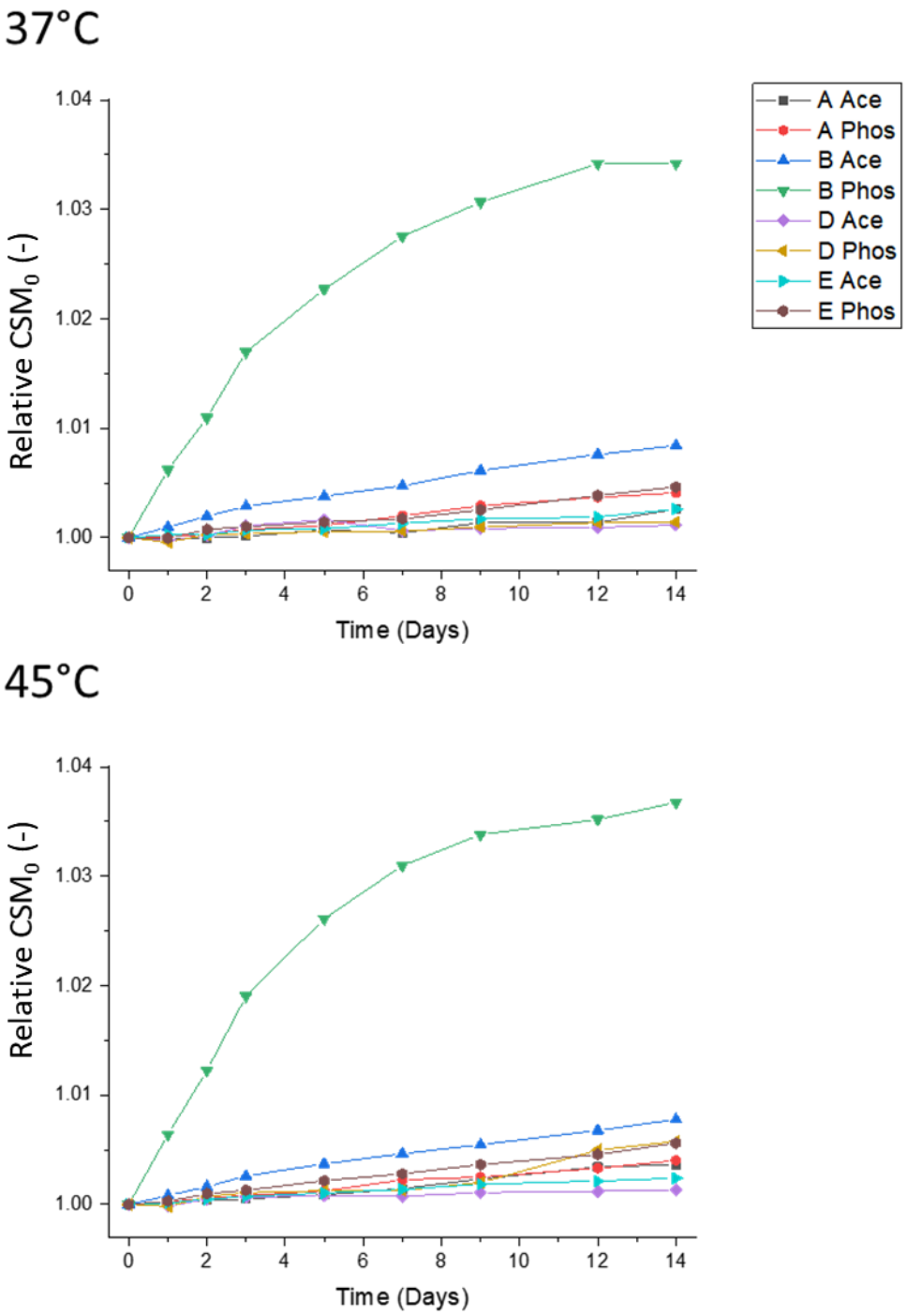

Figure 45 Time-course of parameter CSM_0 from fitted REES data comparison for samples thermally stressed at 37°C and 45°C for mAbs A, B, D and E in acetate and phosphate buffers. The colours correspond to the day during the study that the measurements were taken. Results are calculated relative to Day 0.

Once the CSM data from Figure 44 was fitted to a single exponential, three parameters are found, A, R and CSM_0. These give a good indication of the conformation equilibrium and likelihood of aggregating. MAb A, D and E are relatively flat, showing small changes over the 14 days. It should be noted that mAb D in phosphate at 37 °C does not show a sudden increase in CSM_0 that was previously seen at 45 °C. This could suggest that there is another conformation forming at this slightly elevated temperature.

As expected, MAb B in phosphate shows a relatively large increase in CSM_0, around 3.7% overall, compared to less than 1% in the over samples. It is possible to detect mAb B as problematic from day 1. All CSM values for 45 °C samples are very slightly higher than in 37°C, suggesting that mAbs are less stable at higher temperatures, as confirmed by the other techniques.

Figure 46 shows A vs R parameters over the 14-day thermal stressing. Plotting A vs R better shows the relationship between the two parameters. A high A/R ratio gives a more pronounced REES effect, where the mAb is more susceptible to a shift in the equilibrium towards different conformations. This occurs towards the bottom right hand side quadrant. MAbs A, B and E follow a similar shape over time, an inverse relationship which is decreasing in R and increasing A. The relationship is not linear.

MAb B in phosphate shows a much larger increase in A than any other sample over time. Within the first day of stressing, the sample has a higher A and lower R value, suggesting that this method can be used as an early indication of identifying the aggregate prone mAb.

At both temperatures, the most stable mAb D in acetate, shows a cluster, not following any path with increase time under stressing. In phosphate, the change in A and R is relatively small. This suggests that mAb D has a more rigid structure, less prone to unfolding, also seen by the CMS results. The rigidity of the surrounding environment means that the mAb is likely to have an equilibrium tending towards the native monomer. This makes the mAb less prone to aggregation. MAb B in phosphate follows the same path as the other samples but to a much lesser degree, showing a change in A of around 0.2 and 0.6 in 37 °C and 45 °C respectively.

REES is a powerful and complex tool with many parameters to consider. The most useful appears to be CSM and CSM_0, which shows the progression and changes in the mAb as it unfolds over time. It also does not require data fitting and acts as a true value. Compared to the f_{330nm}/f_{395nm}, it does not require a reliance on specific peaks, 330 nm and 395 nm for example, instead relying on the overall shape change and shift towards the red. Each scan required 9 scans lasting 5 seconds each, 5 nm intervals were used rather than 1 nm in FLI scans, and 1 minute to load the samples for a total of 2 minutes per REES scan.

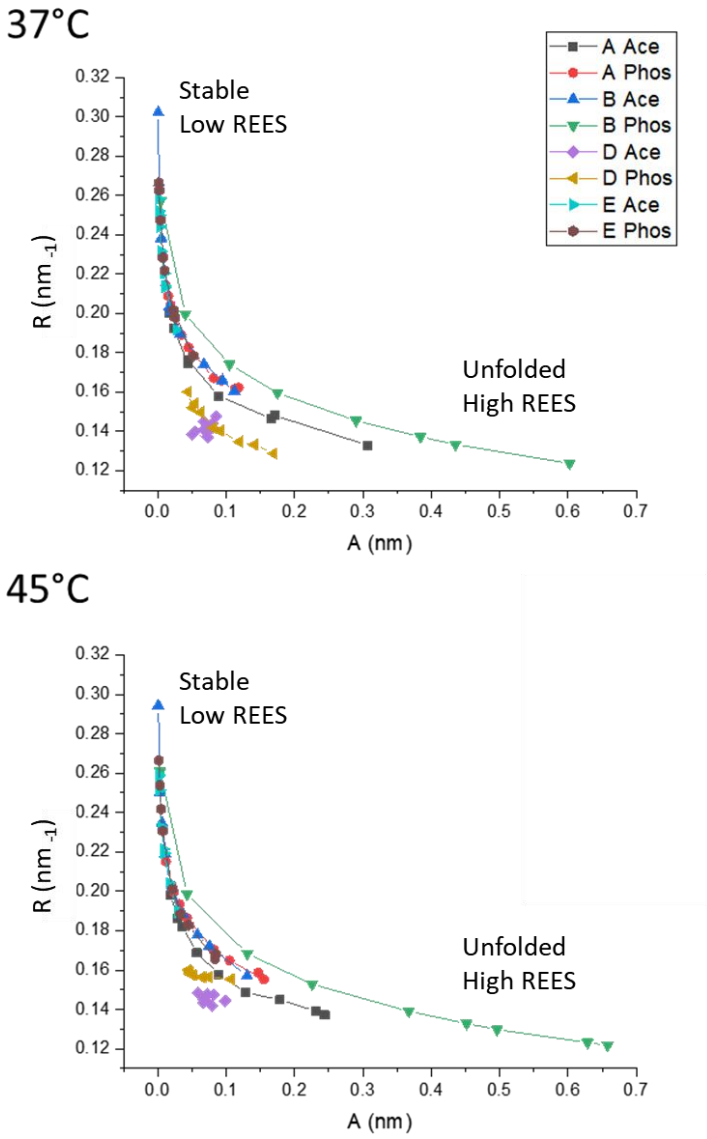

Figure 46 A vs R from fitted REES data comparison for samples thermally stressed at 37°C and 45°C for mAbs A, B, D and E in acetate and phosphate buffers. The colours correspond to the day during the study that the measurements were taken. Results are calculated relative to Day 0.

4.2.2.5 Time Correlated Single Photon Counting

TCSPC was previously shown to increase for mAbs A and B in both buffers at 330 nm and 395 nm, except for mAb B in phosphate, where the time decay at 330 nm emission decreased.

Figure 47 shows the time course fluorescence lifetime results at emission 330 nm. At 330 nm, the mAbs generally showed relatively small changes, fluctuating between ±15% change over the whole time-course. For all mAb samples except mAb B, there is an overall increase in time decay. This suggests that the Tryptophan residues are partially exposed, indicating an unfolding state. In mAb B samples, there is a decrease in time decay, suggesting the tryptophan residues are being buried within the hydrophobic core, albeit to a relatively small amount. It was expected that the time decay at 330 nm emission would change relatively little, as most of the sample (>90%) is still in the native monomer form.

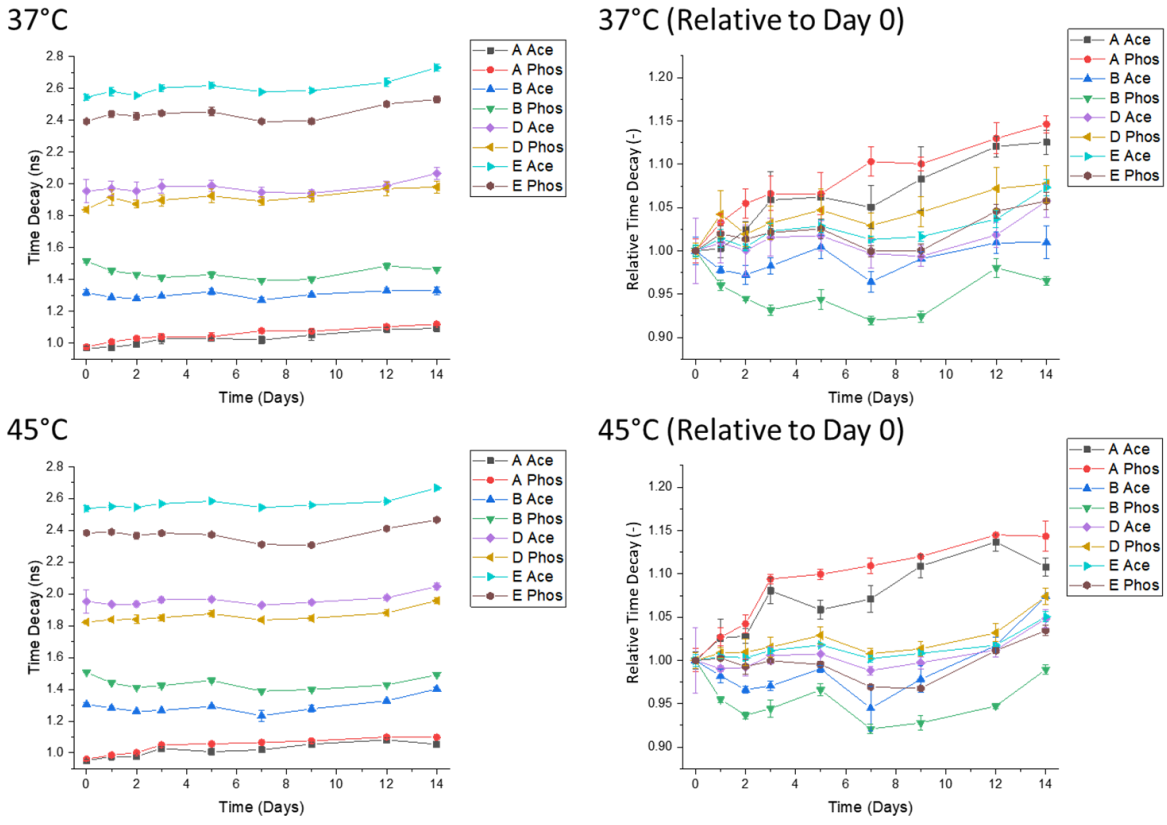

Figure 47 Time-course TCSPC (330 nm emission) comparison between 37 °C and 45 °C for mAbs A, B, D and E in acetate and phosphate buffers. N=3. Error bars show standard deviation. The left side shows the TCSPC 330 nm emission data and the right side shows the data relative to day 0.

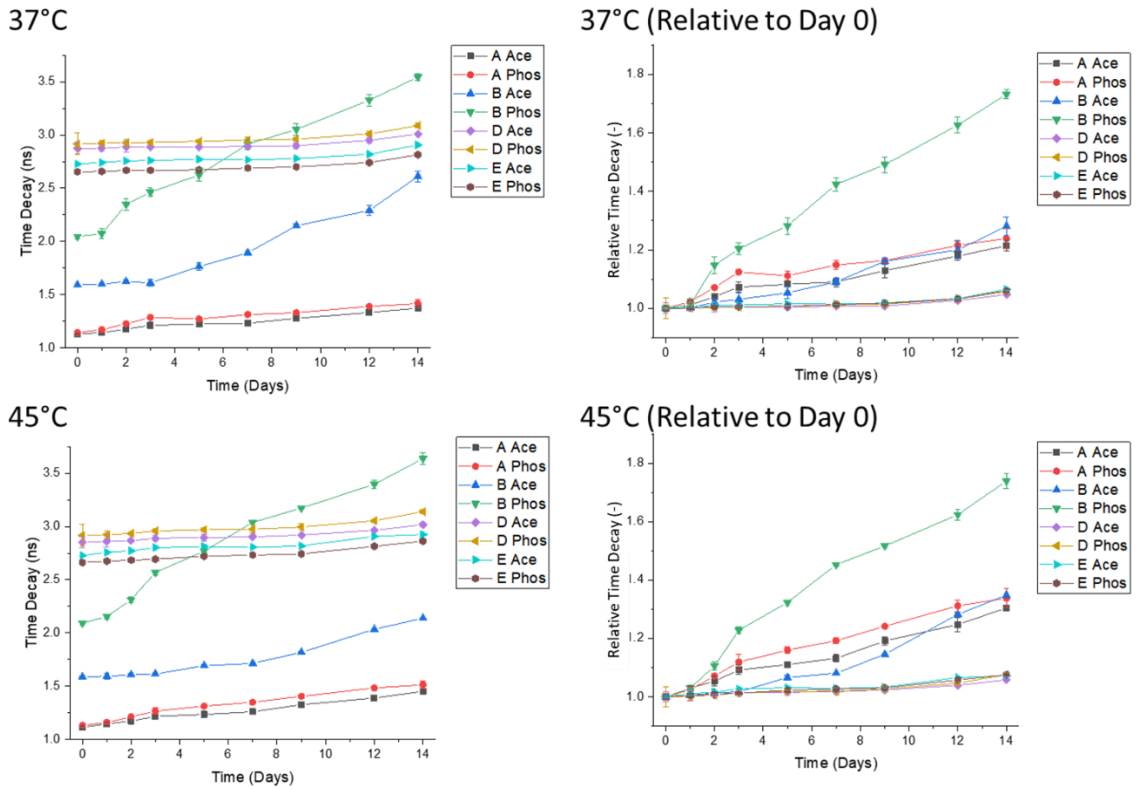

Figure 48 Time-course TCSPC (395 nm emission) comparison between 37 °C and 45 °C for mAbs A, B, D and E in acetate and phosphate buffers. N=3. Error bars show standard deviation. The left side shows the TCSPC 395 nm emission data and the right side shows the data relative to day 0.

The time decay at emission 395 nm revealed much larger changes, possibly due to the species or conformation responsible for the heightened tail seen in the FLI experiments after stressing. There is a relatively small difference between the samples at 37 °C and 45 °C, with the time decay being very slightly higher at the higher temperature stressing.

MAb D and E is relatively flat over the 14 days, increasing in both buffers by less than 7% overall. This suggests that there was little change in the tryptophan environment around this emission. TCSPC is unable to detect any properties in mAb E phosphate that could indicate its tendency to precipitate.

MAb A in both buffers shows a similar profile, with phosphate having slightly higher time decays than in phosphate. The time decay for mAb A increases by around 30% and 34% in acetate and phosphate respectively, roughly the same as mAb B in acetate.

MAb B in phosphate shows a big increase after an initial lag period after day 1. This could suggest that as an early indicator of aggregation or intermediates forming. TCSPC could be useful to detect these species forming.

Notably, the time decay is typically similar in all samples between the buffers except for mAb B. For mAb A, D and E, the time decay difference at day 0 between the two buffers is less than 0.1ns. In phosphate the time decay is 2.1 ns, which is 0.5 ns higher than for

the sample in acetate. This could be an immediate indication that the mAb is more prone to aggregation, as the tryptophan suggests that it is already exposed to the environment in phosphate buffer. This has not been detected by any other fluorescence technique. In SEC, the percentage monomer is less in phosphate samples for all mAbs, with no exception to mAb B.

Overall TCSPC is a rapid and robust method of detecting aggregates, or changes in conformations that cause aggregates. It does not rely on fluorescence intensity, instead using fluorescence lifetime. Taking the emission at 395 nm reveals more information about the changing mAb structure when stressed than 330 nm, where there was little change overall. It was able to detect and identify mAb B in phosphate by day 3 compared to the other samples. It is useful to observe the difference in initial time decay between buffers that could act as a very early indication of instability. TCSPC measurements took 5 seconds when measuring emission at 330 nm, and 30 seconds for 395 nm emission samples.

4.2.3 Cross Correlation of Fluorescence Techniques and SEC

Once all methods and techniques had been evaluated, each technique was cross correlated to SEC in order to better compare their value against currently used methods. It is important to evaluate the novel techniques against the current techniques in order to assess whether there is a benefit of using a fluorescence-based technique. Spearman's ranking was used to discover the strength and direction of the correlation between two variables.

The techniques that were ranked against each other were: SEC, Relative f_{330nm}/f_{395nm}, Relative REES CSM_0, Relative TCSPC at 395 nm emission. FLI, REES parameters A and R and TCSPC emission 330 nm were not considered. While they provided useful information, they did not show the same sensitivity to changes as the other techniques.

Table 16 Spearman's ranking for SEC, f_{330nm}/f_{395nm}, CSM_0 and TCSPC (395nm emission) for time-course results at 37°C after 14 days. Green indicates a strong correlation, above the 0.738 threshold for a 95% level of confidence. Red indicates a weak correlation.

37 °C	SEC	f_{330nm}/f_{395nm}	CSM_0	TCSPC (395 nm)
SEC	-	0.690	0.762	0.881
f_{330nm}/f_{395nm}	-	-	0.976	0.833
CSM_0	-	-	-	0.857
TCSPC (395 nm)	-	-	-	-

Table 17 Spearman's ranking for SEC, f_{330nm}/f_{395nm}, CSM_0 and TCSPC (395nm emission) for time-course results at 45°Cafter 14 days. Green indicates a strong correlation, above the 0.738 threshold for a 95% level of confidence. Red indicates a weak correlation.

45 °C	SEC	f_{330nm}/f_{395nm}	CSM_0	TCSPC (395 nm)
SEC	-	0.690	0.786	0.857
f_{330nm}/f_{395nm}	-	-	0.905	0.833
CSM_0	-	-	-	0.738
TCSPC (395 nm)	-	-	-	-

Table 18 Comparison of Spearman's ranking for SEC, f_{330nm}/f_{395nm}, CSM_0 and TCSPC (395nm emission) to determine the correlation between 37 °C and 45 °C. Green indicates a strong correlation, above the 0.738 threshold for a 95% level of confidence. Red indicates a weak correlation.

Technique	r_s
SEC	0.881
f_{330nm}/f_{395nm}	1.000
CSM_0	0.952
TCSPC (395nm)	0.905

Tables 16, 17 and 18 show the results from the Spearman's ranking comparing the techniques. For 8 pairs of data, the Spearman's ranking coefficient must be higher than 0.738 to satisfy a p=0.05 significance level. The significance level is the likelihood of the correlation occurring 95% of the time.

In both Table 16 and Table 17, SEC correlated well to CSM_0 and the time decay at 395 nm emission. The values exceeded the 0.738 required to give the 95% confidence. This suggests that CSM_0 and TCSPC are useful techniques and should be considered for use in the lead panel ranking.

There was a weak correlation with the f_{330nm}/f_{395nm}, which would satisfy a significance level of 10%. While f_{330nm}/f_{395nm} does not as strongly correlate to SEC, it does correlate very well with CSM_0 and time decay at emission 395nm.

With respect to the f_{330nm}/f_{395nm} and mAb B in phosphate, it should be noted that Spearman's rank does not consider how close certain data points may be or any cut offs. We can clearly see by day 1 that a large change in happening, regardless of its

correlation to SEC. As it is purely a ranking mechanism, it does not account for cut offs (such as 95% monomer used with SEC). Instead it should only be used to evaluate if there is a correlation between the techniques. It is, however, useful as a comparison method with respect to ranking mAbs on their likelihood to aggregate.

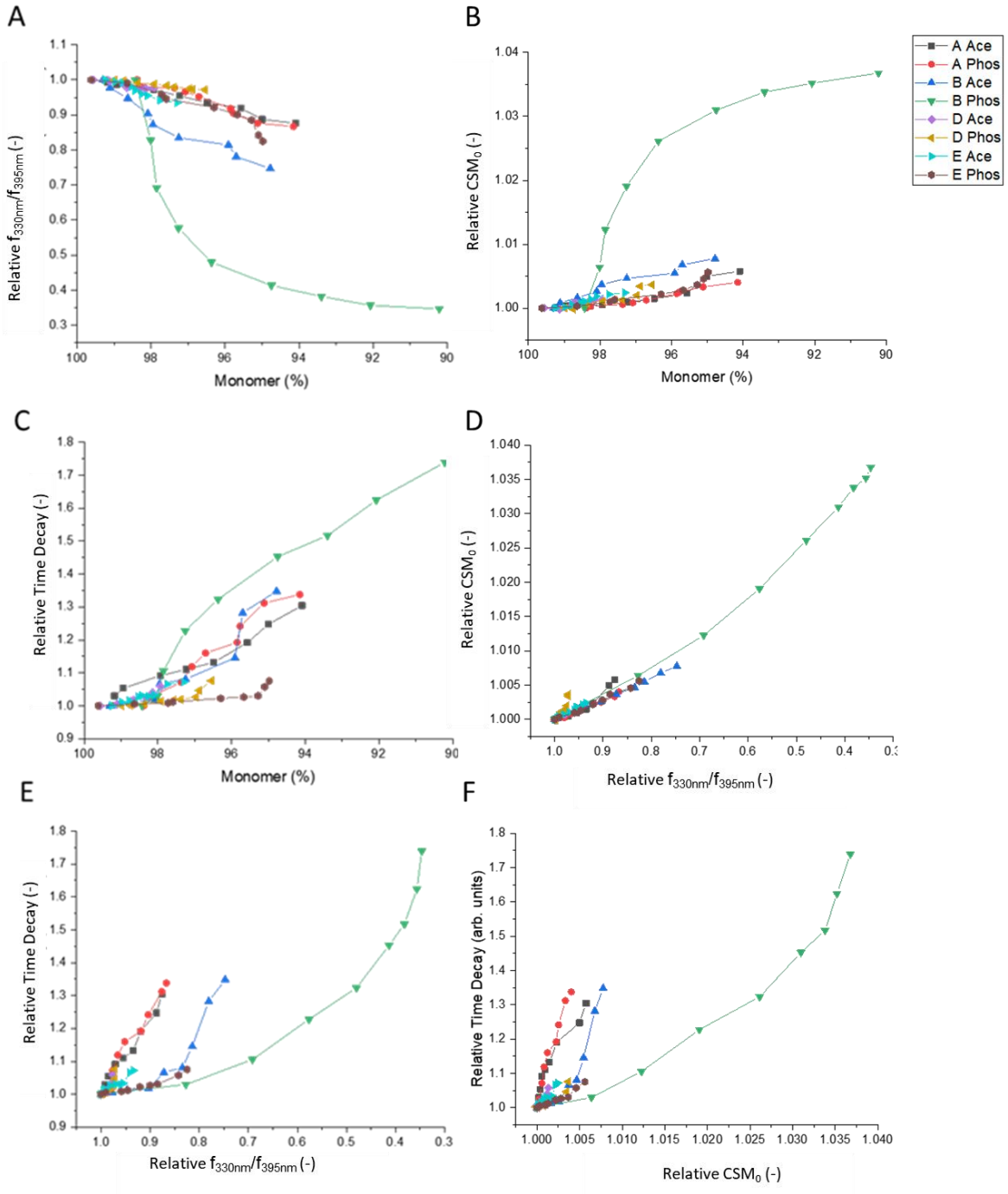

Figure 49 Cross-correlation of techniques (SEC, f_{330nm}/f_{395nm}, Time decay at 395nm emission and CSM_0) for samples stressed at 45°C. A: SEC vs f_{330nm}/f_{395nm}. B: SEC vs REES CSM_0. C: SEC vs TCSPC (395nm emission). D: f_{330nm}/f_{395nm} vs REES CSM_0. E: f_{330nm}/f_{395nm} vs TCSPC (395nm emission). F: REES CSM_0 vs TCSPC (395nm emission).

Figure 49 shows a cross correlation for all techniques when stressed at 45 °C. The results for 37 °C are not shown as they followed the same trend. This demonstrates the correlation between the methods, without using Spearman's ranking. In Figure 49 A,

SEC is compared to the f_{330nm}/f_{395nm}. All samples, except mAb B follow a similar linearity, as monomer percent decreases, the f_{330nm}/f_{395nm} decreases. From day 1, mAb B in phosphate can be identified as an outlier and therefore, f_{330nm}/f_{395nm} could be a useful tool to detect early indications of an aggregate-prone mAb, reducing the need for a 14-day period. The same applies to SEC vs CSM_0, as shown in Figure 49 B.

CSM_0 could be indicating that a mAb is changing structure and as it reaches a critical point, aggregates start to form. In Figure 49 C, SEC vs time decay, mAb B in phosphate follows the same trend as the other samples. This suggests that TCSPC could be a useful method as a means of detecting aggregates, or other conformations which cause the increase in time decay. Combined, f_{330nm}/f_{395nm} and CSM_0 could be a useful method for early detection of conformation changes leading to aggregates, while time decay (395nm emission) could be a useful technique to detect aggregates as the equilibrium shifts.

Figure 49 D follows the tightest spread of data. The similarities between these two methods is due to the data processing. As the equilibrium shifts away from monomers and samples are stressed, the peak at 330 nm decreases, while a heightened tail appears. This tail influences the centre of spectral mass by shifting it towards the red. The f_{330nm}/f_{395nm} simply uses two points, the decrease in the peak and the heightening of the tail, to measure the same phenomenon.

For all the fluorescence-based methods, mAb B in acetate is also identified as an outlier, away from the rest of the samples. This suggests that the environment surrounding the tryptophan is indicative of an aggregate susceptible mAb, regardless of the buffer. These techniques can be used to then predict aggregation. With this information, in silico studies can be carried out to identify common traits in the sequence that may be causing it to aggregate. TCSPC (395nm emission) and CSM_0 could work as orthogonal methods replacing SEC as a non-destructive, low volume, high-throughput, native condition measuring technique for detecting aggregates of aggregate prone mAbs.

The fluorescence-based techniques were not able to detect any anomalies in mAb E phosphate. This sample sometimes precipitates, recorded visually.

4.2.4 Investigating 1-day time course

As each fluorescence technique which was able to quickly detect the susceptibility to aggregate in mAb B, an experiment was carried out to investigate whether the same level of information was possible within 4 hours. Measurements were taken every 30 minutes at 45 °C. Relative f_{330nm}/f_{395nm} and Relative REES CSM_0 at 395 nm emission were chosen to investigate, as they showed significant changes after one day.

The aim of this experiment was to evaluate how quickly the rise in f_{330nm}/f_{395nm} and the CSM_0 is after 4 hours. This provided a good insight into early detection of aggregate prone mAbs.

Figure 50 and Figure 51 show the results from the f_{330nm}/f_{395nm} and CSM_0 study over 4 hours, stressed at 45 °C. The results are very similar to that seen in the 14-day time course study, where samples are stressed at 45 °C and cooled for measurements to 22 °C. The profiles between both f_{330nm}/f_{395nm} and CSM_0 suggests that mAbs are unfolding at the elevated temperature. When allowed to cool, the mAbs seem to relax into a folded state shifting the equilibrium back towards the monomer state when the measurements are taken for the 14-day time course study. With increased days, and therefore more time at higher temperatures, the equilibrium each day shifts towards an unfolding or aggregate state slightly. As previous measurements were taken with samples at room temperature, the overall shift in state is measured, rather than the state of the mAbs at 45 °C. Photobleaching experiments were taken previously and was not considered to impact the results greatly, due to the similar amount of time points taken.

If measurements are taken at 45 °C, real time unfolding was measured. Immediate unfolding, according to the results from CSM_0 occurs within the first 30 minutes. This suggests that using a real-time accelerated study could give a very early prediction for possible aggregation-prone mAbs.

Table 19 shows the results from the Spearman's ranking, comparing the results from 1-day time course and 14-day time course experiments. The strong correlation suggests that within the first few hours, mAbs can be identified or flagged as aggregate prone, providing a useful and rapid means of screening for aggregate prone mAbs over time.

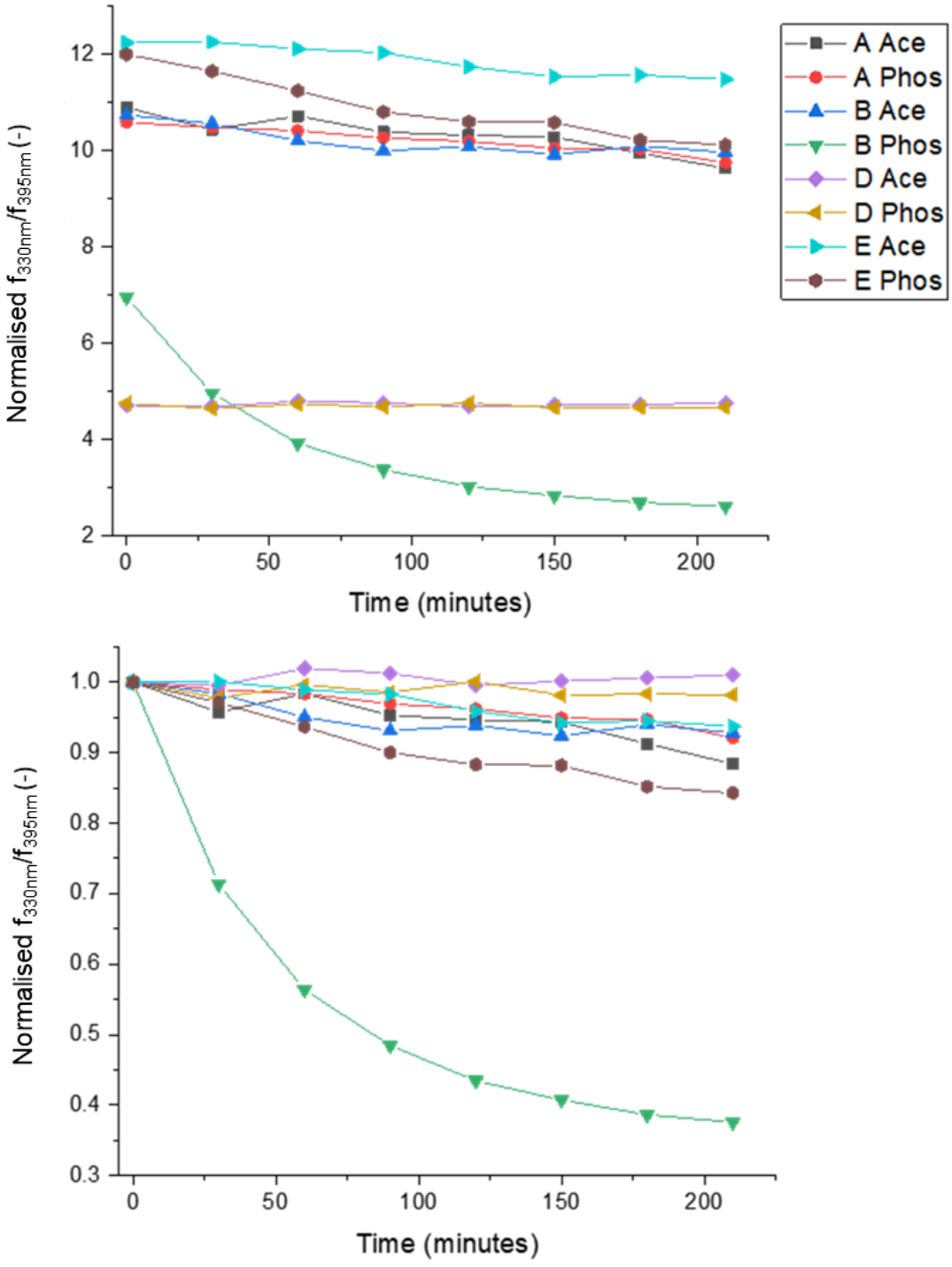

Figure 50 1-day time course of f_{330nm}/f_{395nm} (top) and relative f_{330nm}/f_{395nm} (relative to time point 0 - bottom) thermally stressed at 45 °C for mAbs A, B, D and E in acetate and phosphate buffers.

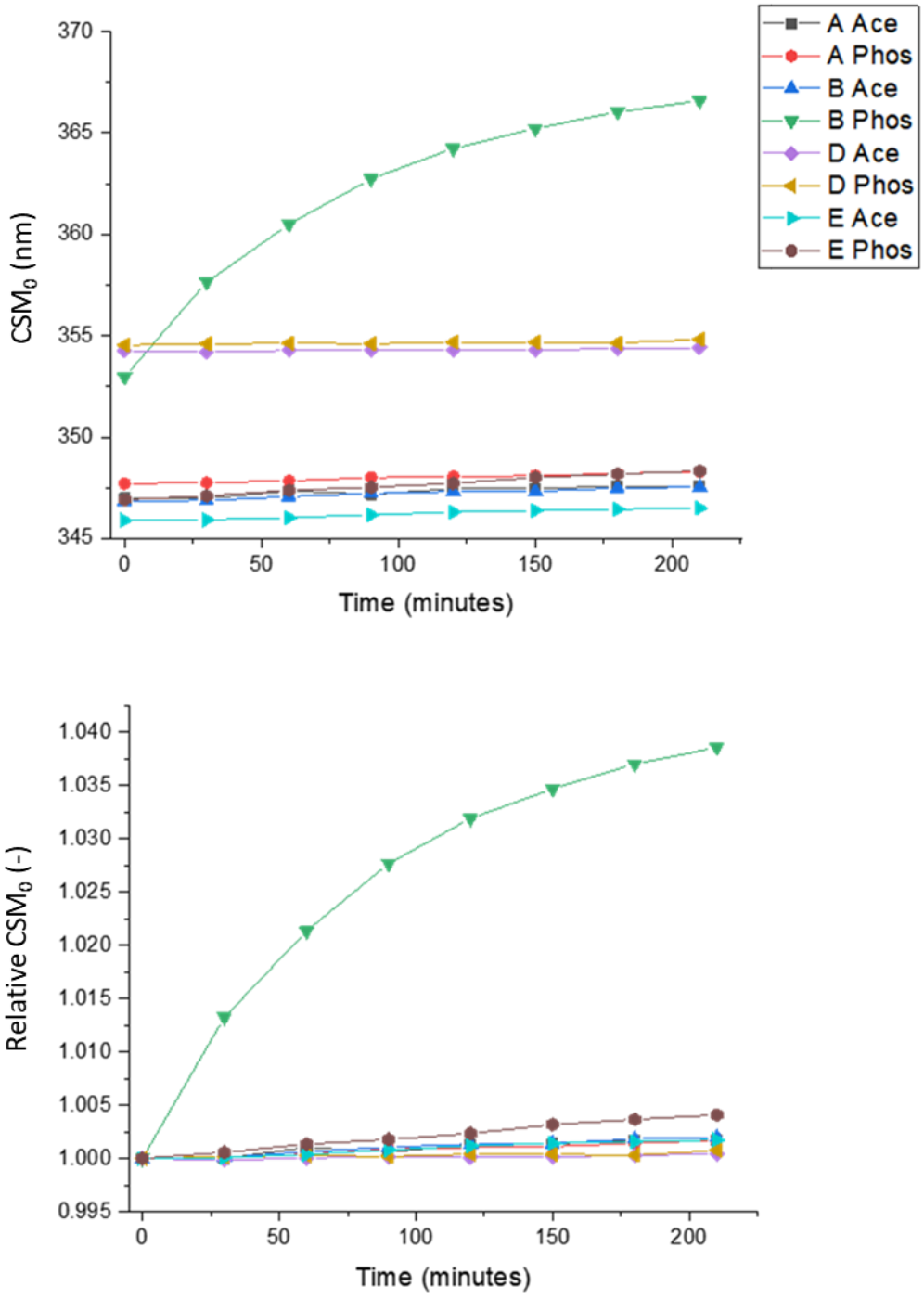

Figure 51 1-day time course of CSM_0 (top) and relative CSM_0 (relative to time point 0 - bottom) thermally stressed at 45 °C for mAbs A, B, D and E in acetate and phosphate buffers

Table 19 Comparison of Spearman's ranking for relative f_{330nm}/f_{395nm} and relative CSM_0 to determine the correlation between 1-day time course and 14-day time course studies. Green indicates a strong correlation, above the 0.738 threshold for a 95% level of confidence. Red indicates a weak correlation.

Parameter	r_s
Relative f_{330nm}/f_{395nm}	0.810
Relative CSM_0	0.833

4.3 Comparison of each method

The techniques were also evaluated regarding throughput, ease of use, measurement time, and data processing. All methods provided a low volume and low concentration option. This is summarised below:

- **FLI**
  - Simple, quick and robust data acquisition and processing.
  - Suitable for low concentrations. Not suitable for high concentrations due to the inner filter effect.
  - Shape changes lost in total fluorescence intensity.
- f_{330nm}/f_{395nm}
  - Simple, quick, and robust data acquisition and processing
  - Able to detect small changes in the shape, a decrease in peak at 330 nm and increase at 395 nm. Provides information on new species or intermediates very early on.
  - Was not able to correlate well to SEC measurements but was able to detect changes in conformation within 4 hours and identify mAb B as problematic.
  - Could be useful as a prediction method.
- **REES**
  - Simple data acquisition but complex data analysis. Slower data acquisition than FLI. Relies on fitted data. More robust method than f_{330nm}/f_{395nm}.
  - Able to detect small shape changes and shifts in centre of spectral mass. Provides valuable information on conformational states.
  - A and R did not provide additional information. CSM_0 is used. Able to detect changes quickly and early on within 4 hours. Able to identify mAb B.

- **TCSPC**
    - Operates differently to the other fluorescence methods, as it measures time decay rather than intensity. Time decay at 395 nm more useful to detect changes.
    - Simple data acquisition and relatively simple data processing.
    - Most strongly correlated to SEC.
    - Immediately identified mAb B as time decays were different in both buffers.

4.3.1 Recommendation for novel assay

Based on the time course experiments, using a combination of both REES and TCSPC could provide a low volume, low concentration alternative to SEC. Both methods were able to correlate well with SEC and could quickly identify mAb B as the most aggregate prone, confirming it as the negative control, from the positive control mAb A.

For TCSPC or REES, 12 µL of sample at 0.5 mg/mL should be loaded into the 12 µL cuvette. Time decay measurements at 395 nm should be taken for each sample in each buffer. If the time decays are different by 10% or more, these mAbs should be flagged. To detect aggregate prone mAbs, a 4-hour isothermal hold at 45 °C with REES measurements taken every 30 minutes. With a data template, results can be obtained in real time. Figure 52 summarised the proposed assay.

These two fluorescence techniques are shown to be useful in predicting aggregate prone mAbs early on. Once aggregation-prone mAbs are identified, the sequence should be examined for any common sequence trends.

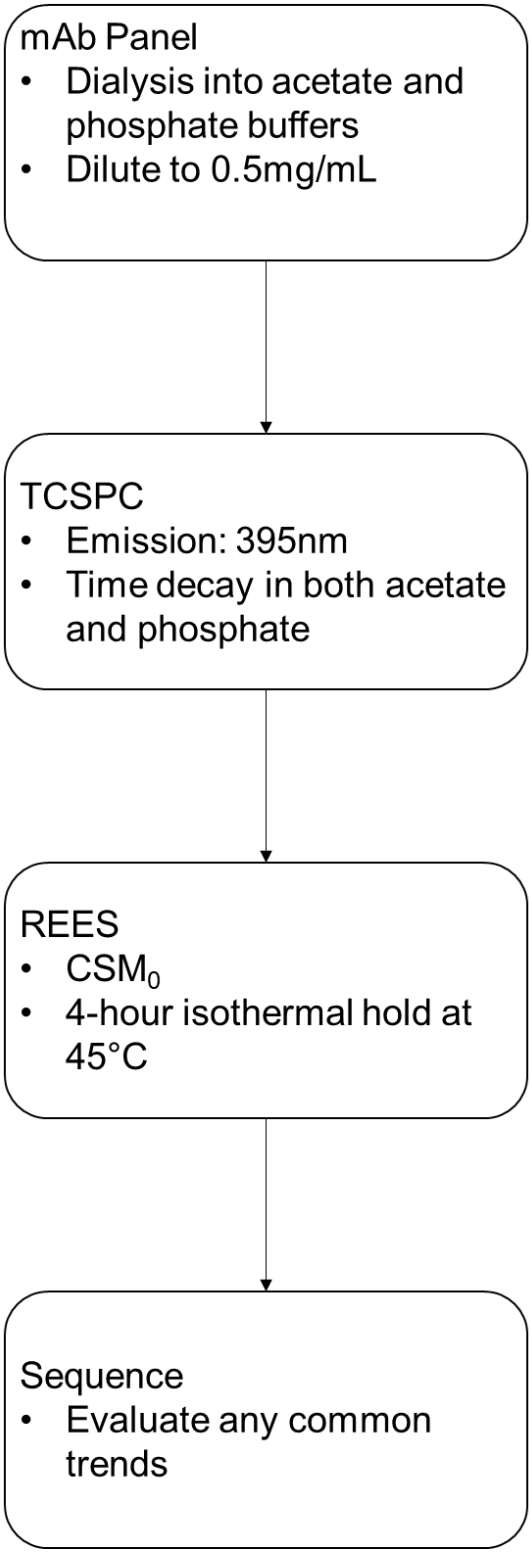

Figure 52 Proposed fluorescence-based assay to predict mAb aggregation over time.

Chapter 5

Fluorescence at high concentrations

5.1 Introduction

A common problem in industry is the detection of concentration dependent aggregation. The requirement for high amounts of materials and lengthy times in currently adopted methods is a limiting factor. Generating high amounts of material for a potential therapeutic candidate is also a bottleneck to streamlining the screening process. If a method can be developed to detect concentration dependent aggregate prone mAbs at lower concentrations, valuable time and costs in the development process are reduced.

During formulation, high concentrations are required. Aggregation at 10 mg/mL is generally indicative to how the mAb will behave at very high concentrations, 50 mg/mL and above.

This chapter aims to investigate the feasibility of using fluorescence-based methods to identify concentration dependent aggregation. In section 4.2.1.1.1, the effects of the inner filter effect (IFE) were noticed. The IFE occurs when the emitted photons from an excited fluorophore are absorbed by a fluorophore on another molecule of the same type. This results in a drastic loss in fluorescence intensity (Lakowicz 2006).

Using the same principles as examined in Chapter 4, f_{330nm}/f_{395nm}, CSM_0 and time decay (at 395 nm) was used. Due to the IFE, fluorescence struggles to measure across a dynamic concentration range, limiting its capabilities to measure concentration dependent aggregates. A new ultra-low volume cuvette was evaluated in order to limit the effects of IFE by reducing the path length. The ability of the new cuvette to detect irreversible aggregates was evaluated to confirm that it can detect aggregates. Then, it was used to evaluate concentration dependent aggregation.

DLS was used to compare across the different concentrations. AUC was not considered as, although it is an absolute method of measuring molecular size, it is too time consuming and requires a high level of expertise and data analysis.

5.2 Results and Discussion

5.2.1 Creating a baseline

In Chapter 3, concentration dependent aggregation prone mAbs, C and F, were characterised. The two mAbs had high hydrodynamic radii, 7.3 nm and 9.2 nm respectively, in acetate, compared to 5.2 nm and 5.5 nm in phosphate. An increased hydrodynamic radius could indicate the presence of larger species in the sample. MAbs A, B, D and E did not show the same characteristic. MAb A and B were used as a comparison for mAbs that did not show signs of aggregation due to concentration in the baseline characteristic study.

Evaluation of the currently used techniques (SEC and DLS) ability to detect concentration dependent aggregates was carried out to assess their strengths and weaknesses.

5.2.1.1 SEC Concentration Study

SEC was evaluated over 0.01 mg-10 mg/mL concentration range. This was to compare its use against the lowest range for fluorescence measurements tested and the typical DLS concentration range.

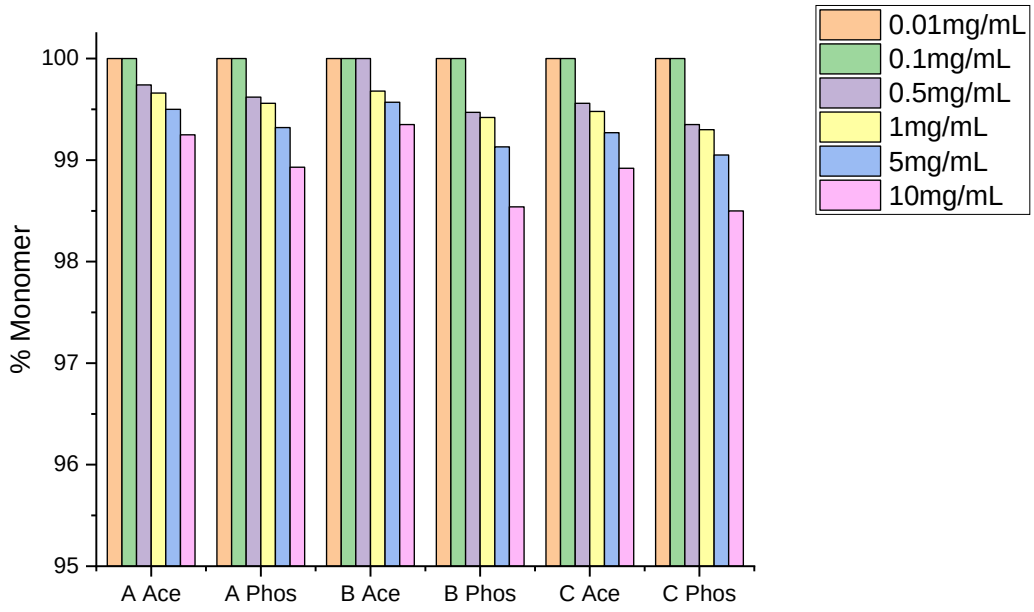

Figure 53 SEC percentage monomer shown for mAbs A, B and C in phosphate and acetate buffer over a range of concentrations: 0.01, 0.1, 0.5, 1, 5, 10 mg/mL to examine the current capabilities for predicting aggregation.

Figure 53 shows the percent of monomers at a range of concentrations. It should be noted that the system is optimised for the SEC at 1 mg/mL due to the detection limits. All the conditions and mAbs exhibit the same trend that the percentage monomer decreases with an increased concentration, instead of showing the same reading. At 0.01 and

0.1 mg/mg, values given were 100% monomer, which may be due to the high signal to noise ratio and failure to distinguish noise from signal. This means that any aggregate or fragment peak that may be present could not be detected as the signal was not high enough. The poor readings at higher concentrations may be due to protein overloading, causing peak broadening and exceeding the detection limit so a less accurate reading is given. From the baseline study, only mAb C should experience a fall in monomer level with increasing concentration, as shown by the previous studies in DLS and AUC. This was not the case, suggesting the SEC is either limited in the concentration it can effectively measure at or due to the concentration dependent nature of mAb C in acetate, the dimers dissociated due to sample dilution in the column. In this case, the rate of dissociation is very fast.

SEC was limited in its ability to detect across a wide range of concentrations. At lower concentrations (0.01 mg/mL and 0.1 mg/mL), the signal was very weak and therefore the signal to noise ratio is low. Figure 54 shows a close view of the chromatogram for mAb A in acetate. Upon close inspection, there appears to be a small aggregation curve. However, as the noise baseline fluctuates it is difficult to draw a solid conclusion and estimate the amount of aggregate present.

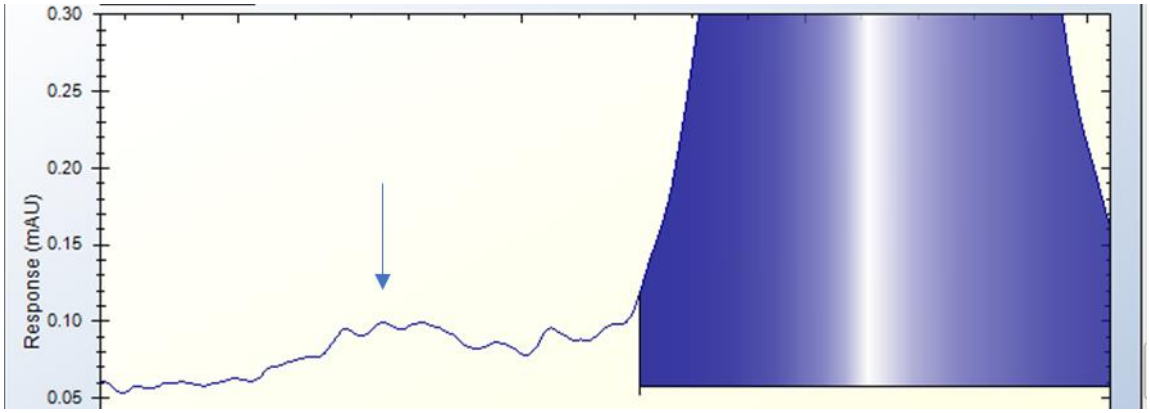

Figure 54 A zoomed in chromatogram showing 0.01mg/mL of mAb A in Acetate buffer. The appearance of an aggregate peak as a very faint weak signa (see arrow).

Figure 55 shows that SEC is sensitive when a higher level of aggregation (and therefore a higher signal) is present at lower concentrations. By diluting the stressed mAb B phosphate sample, the monomer percentages were comparable. This suggests that where aggregates levels are high, at lower concentrations, SEC is sensitive. However, as this project aims to detect and predict behaviour from low populations of aggregates, this technique, in its current form, could not be used.

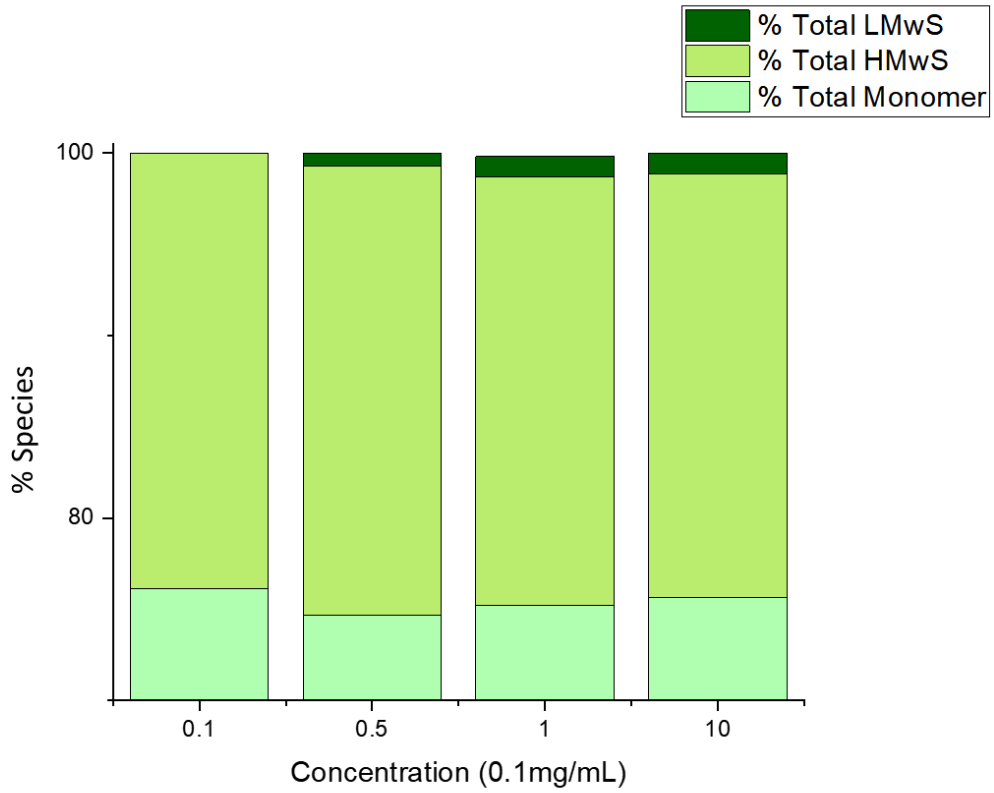

Figure 55 Percentage distribution of species from SEC for mAb B in Phosphate buffer in stressed conditions over different concentrations (0.1, 0.5 and 1mg/mL). LMwS = Low molecular weight species. HMwS= High molecular weight species. 0.01mg/mL was not included as the aggregate peak was not clear.

Figure 56 shows the chromatograms for mAb A in in acetate from 0.01 mg/mL to 10 mg/mL. At 0.01 mg/mL, we see a very weak signal detected at the peak, less than 5 mAU. At the higher concentrations (10 mg/mL), the signal was very strong, and the column was overloaded, indicated by the peak broadening in the chromatograms. The overloading and broadening exceeded detection limits, reducing the accuracy of the readings for each species in the sample. Overall, only 0.5 and 1 mg/mL were within the same area and could be investigated further if SEC were to be readily used.

The inability to pick up concentration dependent readings illustrates SEC to not be viable in its current set up to predict aggregation at the lowest concentrations. SEC could not pick up the concentration dependence exhibited by mAb C. Adjustments to the system could make this possible.

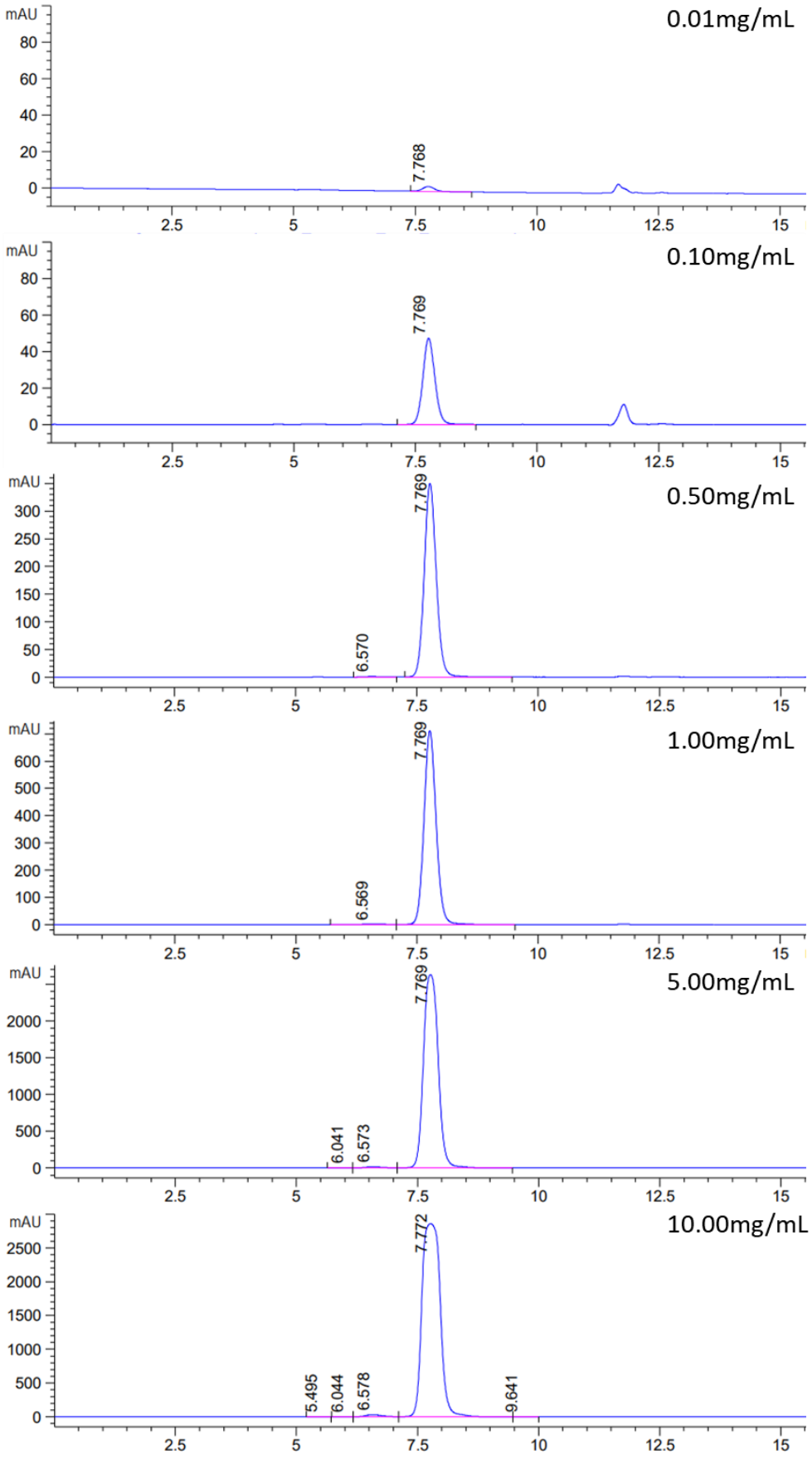

Figure 56 Raw chromatograms for mAb A in acetate buffer at 0.01-10 mg/mL.

5.2.1.2 DLS Concentration Study

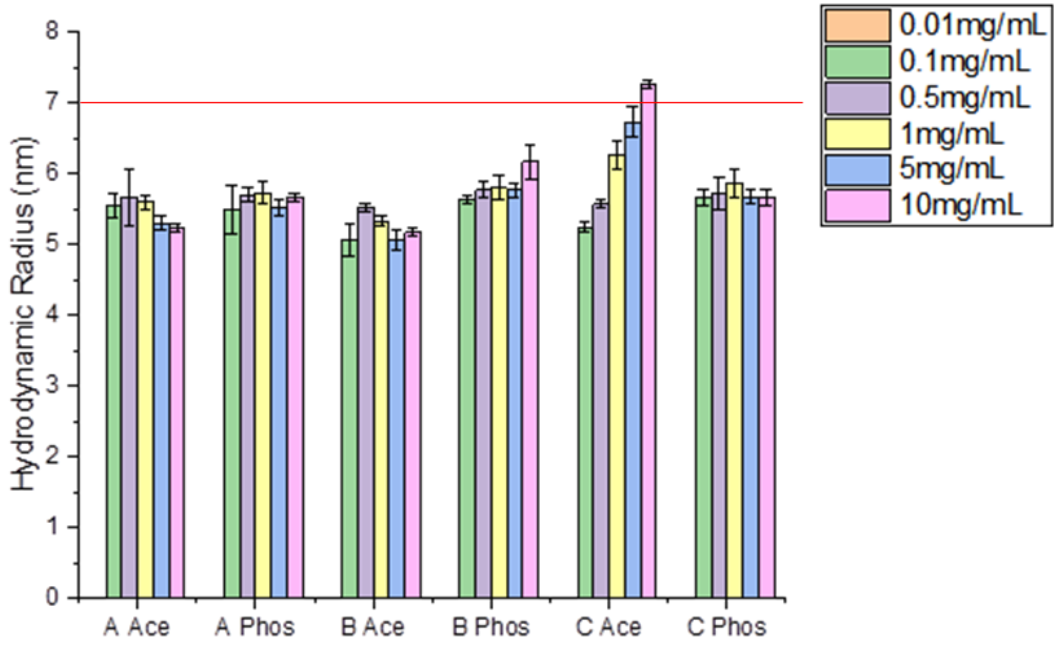

Figure 57 Hydrodynamic radius shown for mAbs A, B and C in acetate and phosphate buffers over a range of concentrations: 0.01, 0.1, 0.5, 1, 5, 10mg/mL to examine the current capabilities for predicting aggregation. The red line indicates the general monomer/aggregate threshold. Error bars represent standard deviations. n=3.

The DLS was more successful than the SEC in terms of detecting low volumes. Only 0.01 mg/mL could not be read due to the low signal. Figure 57 shows the results from the DLS concentration study, using mAbs A, B and C in acetate and phosphate buffer at concentrations ranging from 0.01 mg/mL to 10 mg/mL.

For mAb A, at lower concentrations, the error bars are larger indicating a more varied data. In phosphate buffer, all radii are between a range of 0.23 nm, and for acetate buffer, between 0.43 nm. This suggests that the results are reproducible and that the radii between 0.1 and 10 mg/mL are possible. There may be a slight indication that mAb A fragments at high concentrations in acetate.

Data for the MAb B in the phosphate buffer, suggest that the radii are roughly the same, within a 0.6 nm range, with the exception of at 10 mg/mL, which could be due to the inherent error in DLS. It could also suggest that mAb B in phosphate experiences some degree of concentration-dependent aggregation. However, due to the relatively large error bars and the results from AUC (see Figure 22), this is more like an error in the measurement. In acetate buffer, there appears to be a wide variation within a range of 0.6 nm also. There may be indications of fragmenting at high concentrations in acetate.

For mAb C, DLS showed the concentration dependence aggregation in mAb C clearly, as concentration increases. In the phosphate buffer, the hydrodynamic radius is roughly

similar, within a similar range, with exception of 5 mg/mL. Another reading may be required to fully confirm the linearity of results. With the others, the error bars overlap indicating that there is no significant difference between the points. In the acetate buffer, the increasing hydrodynamic radius is very clearly shown to increase with an increased concentration. Testing at 0.1 to 1 mg/mL may allow a reduction in material required for the DLS. AUC had previously suggested less than 1% aggregates. The increase in hydrodynamic radius could suggest conformation change, that is not picked up by SEC.

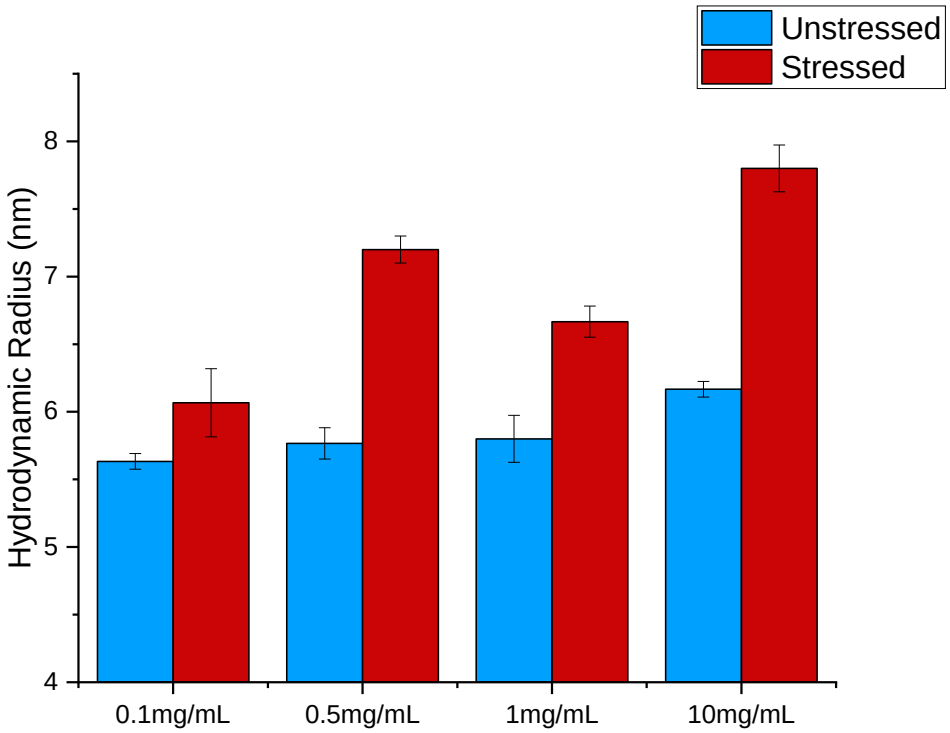

Figure 58 Hydrodynamic radius shown for mAb B in phosphate buffer stressed and unstressed at 0.1, 0.5 1 and 10 mg/mL. Error bars represent standard. n=3.

To examine the ability to detect the irreversible aggregation from stressed phosphate samples from mAb B, various concentrations were also tested. At low concentrations, it very clearly showed the differences between the stressed and unstressed samples. This suggests that it can distinguish the presence of a high amount of aggregates at low concentrations.

However, while it did not measure the same value as obtained previously at 10 mg/mL or consistently, it does present a significant increase in hydrodynamic radius that can be used to predict its behaviour in different conditions. DLS in this case could be used as a basic screening process to detect only the presence of aggregation in different conditions.

5.2.2 Testing fluorescence-based techniques to detect high concentration aggregation

Following the relative success in suggesting fluorescence-based methods as a method of detecting early aggregation signs due to thermal stressing, the same principles were tested to investigate concentration dependent aggregation.

The f_{330nm}/f_{395nm}, CSM_0, and time decay ay 395 nm emission were used. As it was established that due to the IFE at high concentrations (0.6 mg/mL and above), a range of cuvettes were tested. Once this was established, a time course study was carried out to determine if the cuvette could detect aggregates as they form at high concentration under thermal stressing. Then, the cuvette was used to evaluate the detection of higher molecular species in the samples due to concentration dependent aggregation.

5.2.2.1 Testing new cuvettes to decrease the inner filter effect

The three cuvettes available were:

- 100 µL Ultra-Micro Far UV quartz cuvette with a 10 mm (pathlength) by 2 mm window (Hellma).
- 12 µL Ultra-Micro Far UV quartz cuvette with a 1.5 mm (pathlength) by 1.5 mm window (Hellma).
- MicroSense microlitre TrayCell (0.7-10 µL sample size) (Hellma).

As shown in Chapter 3 with the 100 µL cuvette, IFE hinders fluorescence readings at high concentrations. The IFE is due to the absorption of incoming excitation, and/or emitted light by a fluorophore. This reduces the fluorescence intensity. In general, fluorescence intensity is proportional to absorption, provided the concentration range is within linearity. Using the principles of the Beer-Lambert Law, see equation 5.1, where: A_{280} = absorption at 280nm; ε = absorption coefficient; C= concentration of sample; and L= optical pathlength.

$$A_{280} = \varepsilon C L \tag{5.1}$$

As fluorescence is proportional, if the optical pathlength is reduced, the linearity of concentration to absorption is increased. Therefore, the working concentration range is increased by reducing the path length.

Other methods to avoid the IFE include using a different excitation wavelength so absorbance is reduced or using a low volume cuvette or a different window mechanism.

The use of the 12 µL cuvette, previously used to reduce the material requirement for the lead panel, was a good option to test higher concentrations. To investigate this further,

the MicroSense microlitre TrayCell (Hellma) was also used. This cuvette operates in a different way to traditional cuvettes. The MicroSense cuvette uses prisms and fibre optic wave guides to lead the excitation light through the sample. The emission light is reflected by the mirror and is lead out of the window (perpendicular to the excitation light entrance) also guided by prisms and fibre optic waveguides. The path length is determined by the gap between the cuvette and the cap and is fixed at 0.2 mm.

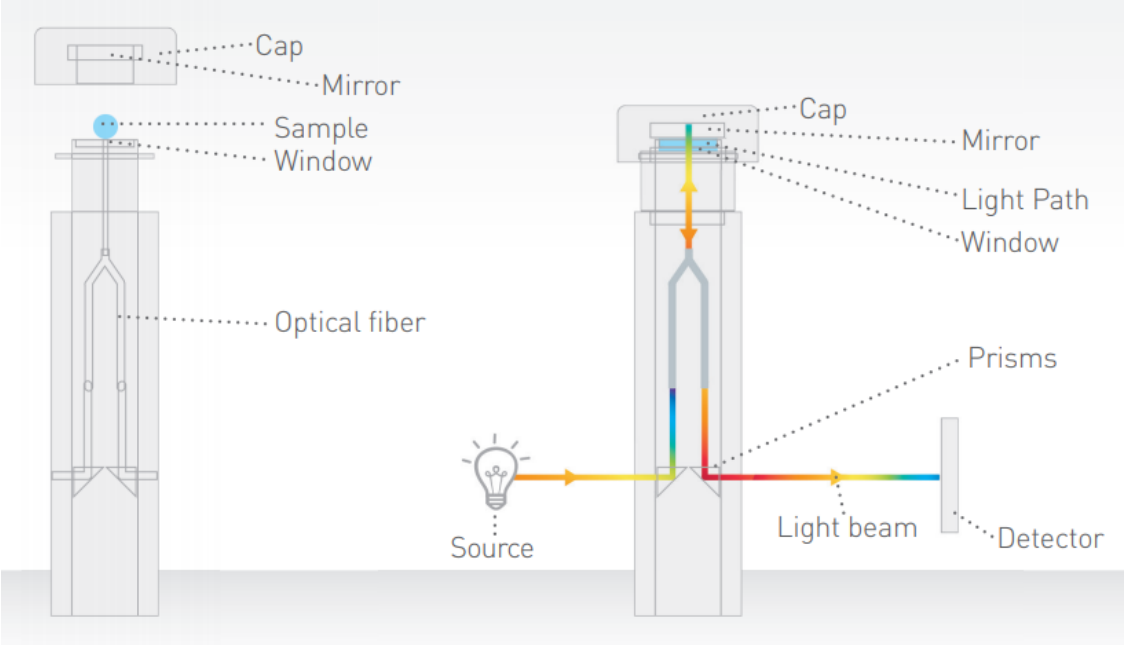

Figure 59 Schematic of the MicroSense cuvette. From Hellma Analytics TrayCell User Manual.

As mAb B in phosphate did not show concentration-dependent aggregation, from AUC, it was used as the model for testing the new cuvettes. Intensity was measured over a range of concentrations to assess the best cuvette for high concentrations (>1 mg/mL). Figure 60 shows the results from the cuvette comparison trial. The 100 µL cuvette showed linearity until 0.5 mg/mL. This cuvette was not considered further as it was not suitable for high concentration measurements. The 12 µL cuvette showed linearity until 1 mg/mL, but lost linearity for 5 mg/mL and 10 mg/mL. For the MicroSense, the intensities are much lower than that seen in the 12 µL cuvette and there is a good linearity between 1 mg/mL and 10 mg/mL.

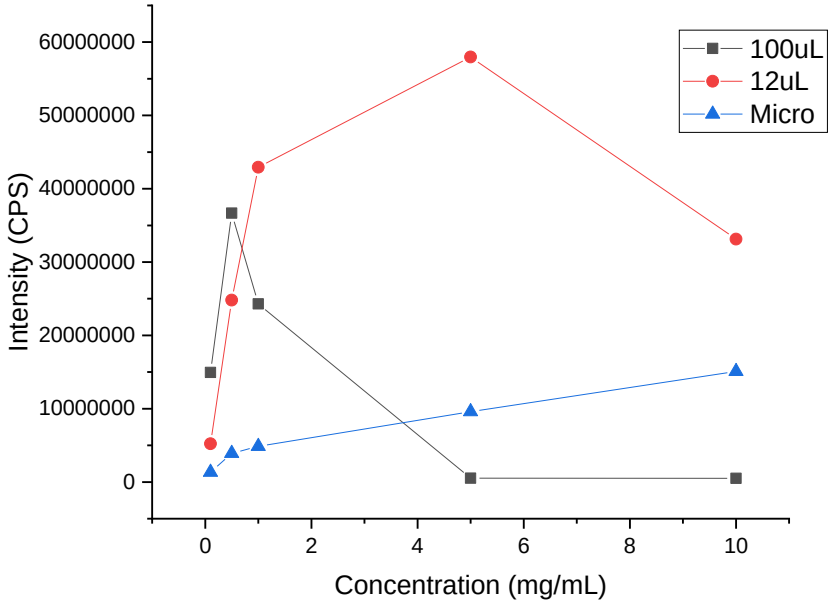

Figure 60 Intensity vs concentration for mAb B in phosphate in each cuvette: 100 µL, 12 µL and MicroSense.

Figure 61 shows the relative fluorescence emission scans, all measurements were relative to their 290nm fluorescence intensity. At 0.1 mg/mL, there was a complete shape change in fluorescence spectrum, with the peak shifting towards 310 nm, from 330 nm in the MicroSense cuvette. As the shape change was not seen by the other cuvettes, it can be assumed that this could be due to the low concentration being at the lowest limit of the suggested measuring range. Also, there was a relatively high amount of noise at the lower concentrations when using the MicroSense cuvette. This suggests that the MicroSense is more suitable to higher concentrations, where the signal would be much higher. The MicroSense cuvette was taken forward to evaluate the effectiveness at high concentrations. There is a drop off at 5mg/mL where the IFE causes a drop in intensity for the 12µL cuvette. The same is seen at 1 mg/mL in the 100 µL cuvette. This is most likely due to the pathlength

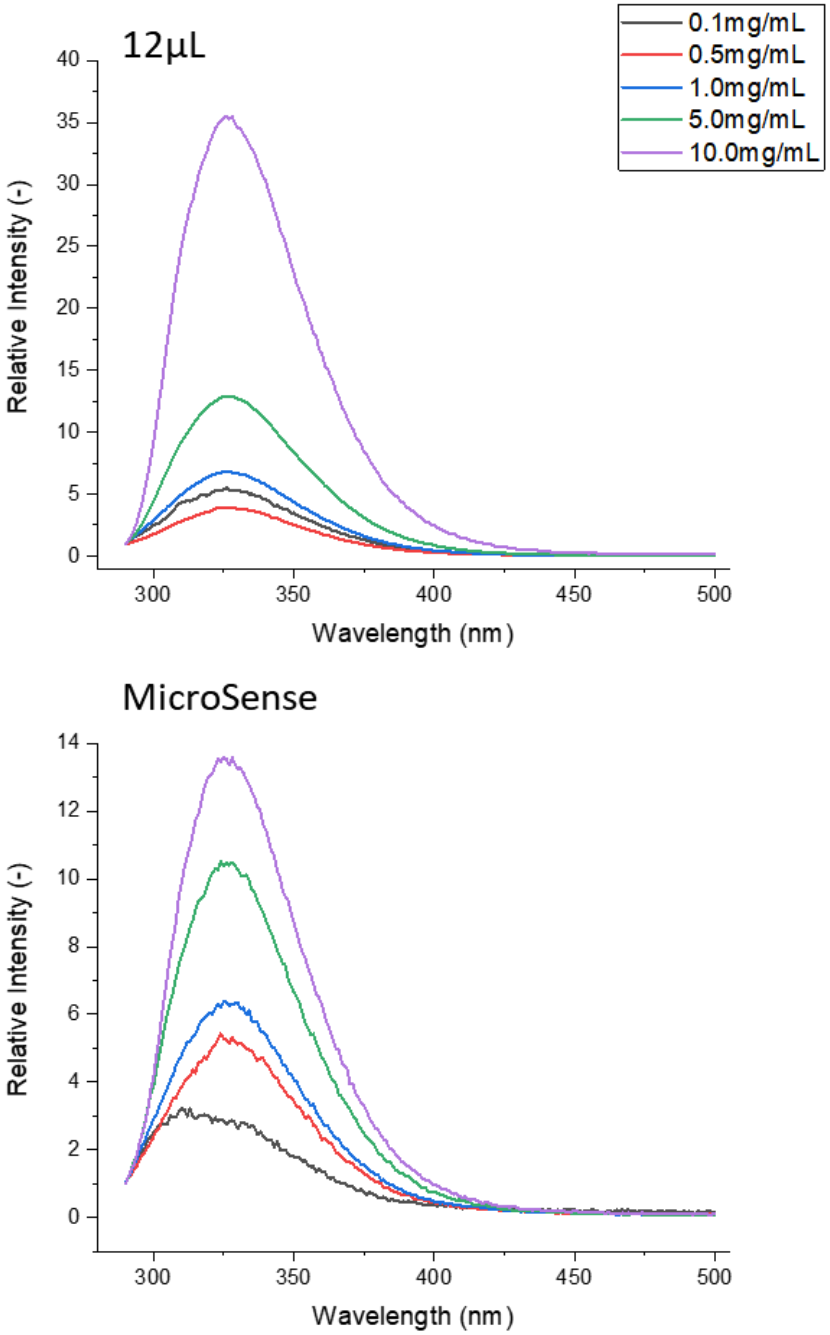

Figure 61 Relative fluorescence intensity scans for mAb B in phosphate buffer at a range of concentrations from 0.1 mg/mL to 10 mg/mL. Intensity is normalised to 1.0 at 290nm. Excitation at 280 nm and emission taken from 290 nm to 500 nm. Top- Fluorescence scans in 12 µL cuvette Bottom- Fluorescence scans in MicroSense cuvette.

5.2.2.2 Low volume time course study

In order to assess the MicroCuvette further, a time course study was conducted to assess whether it could detect irreversible thermally induced aggregation. If small aggregates could be detected, it could prove the ultra-low volume fluorescence was possible. 100 µL of 1 mg/mL and 10 mg/mL samples of mAb C and F in acetate and phosphate were thermally stressed at 45 °C. 2 µL of each sample was used in the MicroSense where f_{330nm}/f_{395nm} and CSM_0 was measured. These two methods were shown to detect conformational changes in the mAb.

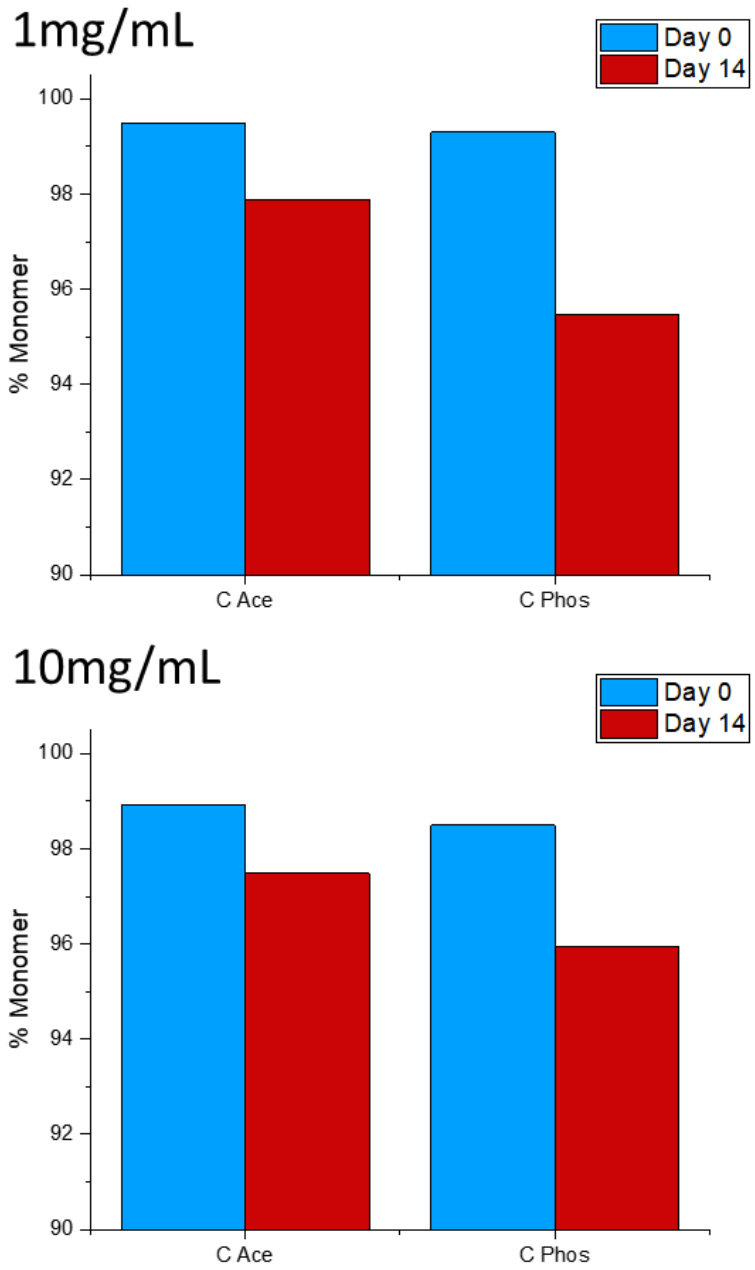

Figure 62 The variation in % monomer for mAb C in acetate and phosphate at 1mg/mL and 10mg/mL.

Figure 62 shows the SEC results from the time course study for mAb C in acetate and phosphate at 1 mg/mL and 10 mg/mL. The results show a small decrease in the amount of monomer after 14 days of thermal stressing. The samples behaved as expected, with mAb C in phosphate having a lower percentage of monomers after stressing. The 10 mg/mL samples suffered from peak broadening which could skew the amount of monomer present. Resolution by SEC was best at the suggested concentration, of 1 mg/mL. The amount of monomer after stressing at both 1 mg/mL and 10 mg/mL was very similar.

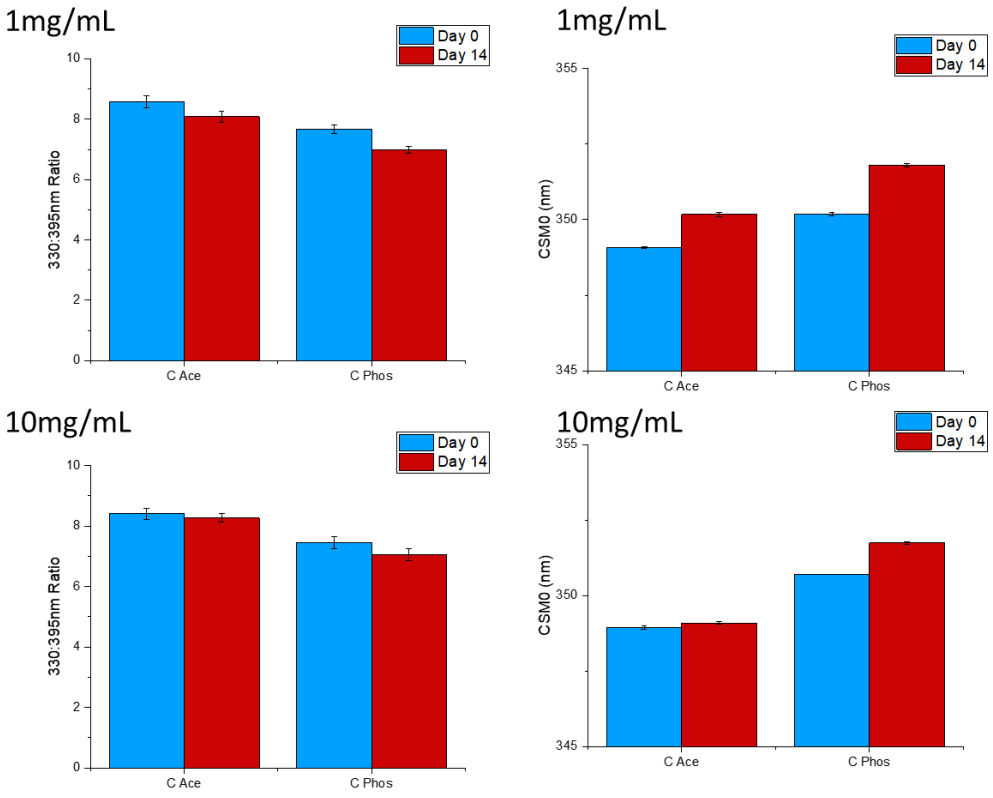

Figure 63 The variation in f_{330nm}/f_{395nm} (left) and CSM_0 (right) over the 14-day time course study of mAb C in acetate and phosphate at 1mg/mL and 10mg/mL. Error bars show standard deviation. n=3.

Figure 63 shows the results for the f_{330nm}/f_{395nm} (left) and the CSM_0 (right) in the time course study. For the f_{330nm}/f_{395nm}, we see a small drop for all samples, correlating with the SEC results. From the previous time course study, as time increased under stress, the ratio decreased suggesting a change in shape to the fluorescence spectra and therefore a change in conformation.

There is an increase in CSM_0 of around 1 nm at 1 mg/mL and 10 mg/mL, suggesting that the mAbs are unfolding and the equilibrium has shifted slightly away from the monomer state, mirroring the SEC results.

Based on these results, it can be concluded that the MicroSense cuvette was able to detect changes due to thermal stressing.

5.2.2.3 Testing detection of concentration-dependent aggregates

From AUC and DLS in the baseline characterisation, mAb C in acetate buffer undergoes dimerization at concentrations higher than 1 mg/mL. As the MicroSense cuvette was able to distinguish stressed samples from unstressed samples, it was considered for use to detect any fluorescence changes between the 1 mg/mL and 10 mg/mL. MAb A was tested as a control sample, as according to DLS it did not show concentration-dependent aggregation, and mAb F was tested as positive control, as it showed concentration-dependent aggregation in the baseline characterisation study.

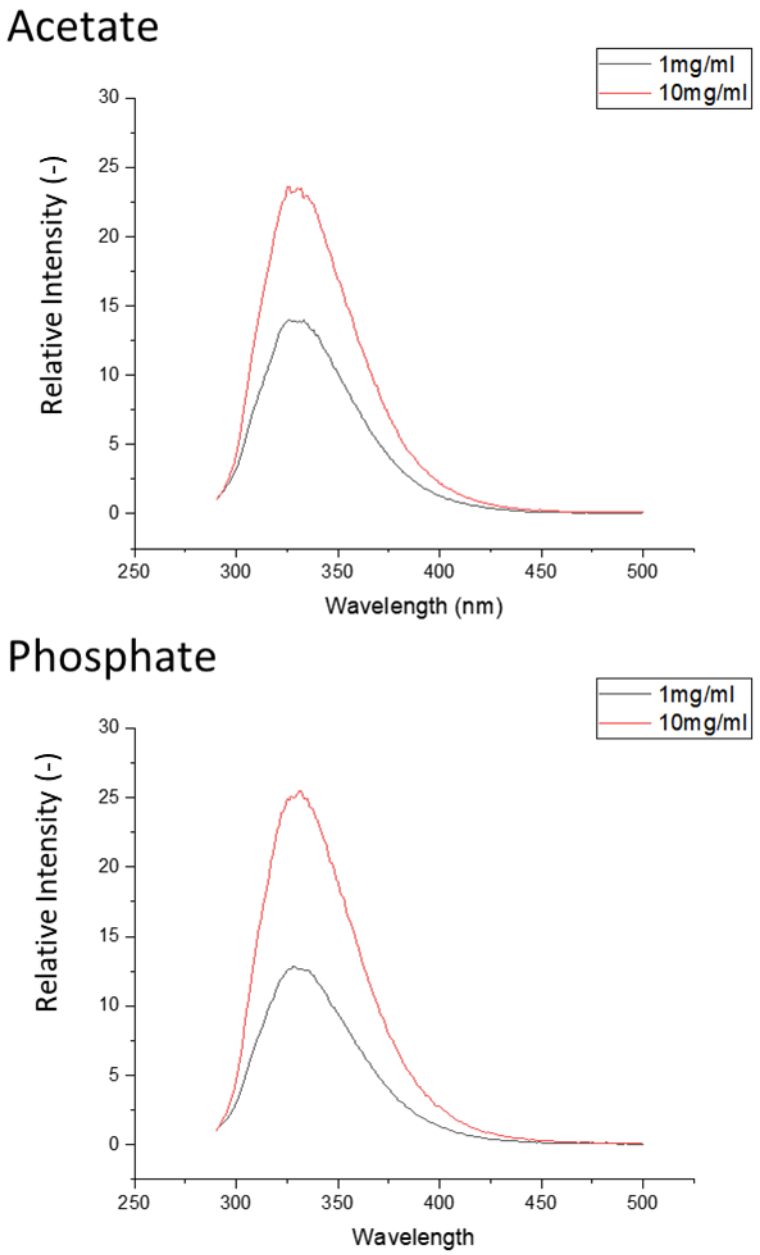

Figure 64 Relative fluorescence spectra (excitation: 280nm, emission: 290-500nm) for mAb C in acetate (top) and phosphate (bottom) at 1 mg/mL (black) and 10 mg/mL (red). Intensity is normalised to 1.0 at emission wavelength 290nm.

Figure 64 shows the relative fluorescence spectra for mAb C in acetate and phosphate at 1 mg/mL and 10 mg/mL. The spectra are relative to their emissions at 290 nm to allow for a comparison between buffers and concentrations. The samples at 10 mg/mL are relatively higher than those at 1 mg/mL as expected, as the intensity is higher overall. The formation of the secondary peak, as seen from the conformation change in mAb B phosphate after thermal stressing, is not seen, suggesting that there is a different aggregation mechanism for mAb C in acetate. The dimerization could contribute to part of the main peak, rather than having its own emission spectra around 400 nm.

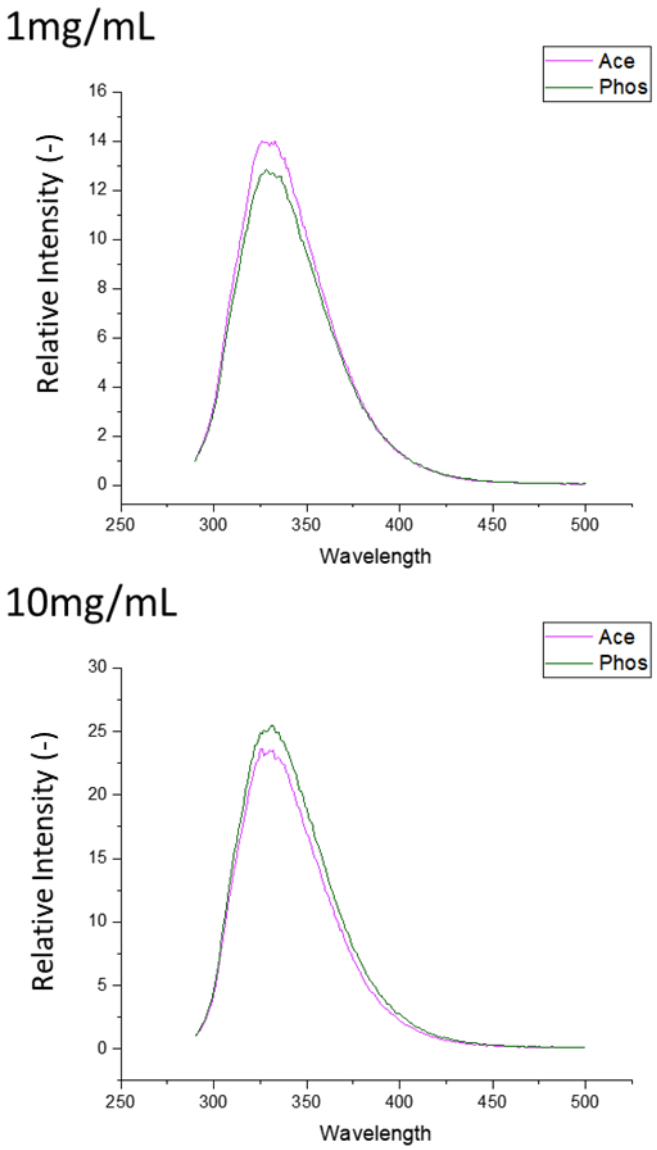

Figure 65 Relative fluorescence spectra (excitation: 280nm, emission: 290-500nm) for mAb C in acetate and phosphate at 1mg/mL (top) and 10mg/mL (bottom). Intensity is normalised to 1.0 at emission wavelength 290nm.

Figure 65 shows the fluorescence spectra with the two buffers against each other. At 1 mg/mL acetate there was a relatively higher peak than in phosphate. This is expected as from earlier fluorescence experiments mAbs are generally more stable in acetate at

1 mg/mL. However, at 10 mg/mL the peak for mAb C in acetate is slightly lower than the peak for mAb C in phosphate. This suggests that the tryptophan is being buried and could confirm the dimerization seen by AUC. However, due to small effects of IFE at high concentrations, it is difficult to conclude that the fall in the peak is due solely to dimerization.

Comparing to mAb A, which did not show signs of concentration dependent aggregation, this was not the case. Figure 66 shows the relative fluorescence spectra for mAb A and F in acetate and phosphate at 1 mg/mL and 10 mg/mL. For mAb A, there is a consistent trend, that acetate has a higher intensity than phosphate between the two concentrations. This suggests that mAb A in acetate behaves similarly at each concentration. For mAb F, a similar pattern to mAb C appears. At 10 mg/mL, the intensity for acetate is less than for phosphate. As mAb F has similar properties to mAb C, it could be due to the tryptophan residues being buried within the aggregates. It should be noted, as AUC showed a highly aggregated sample at 10 mg/mL for mAb C, that the intensity loss is lower than expected.

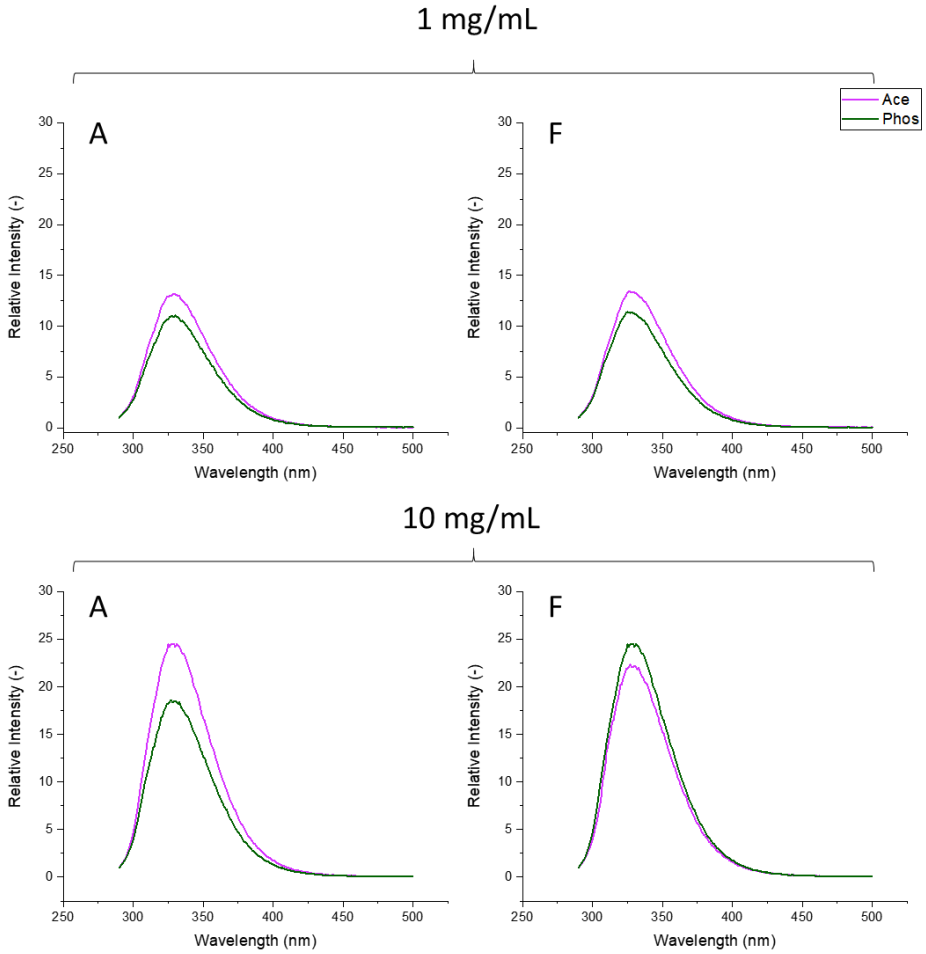

Figure 66 Relative fluorescence spectra (excitation: 280nm, emission: 290-500nm) for mAb A (left side) and mAb F (right side) in acetate and phosphate at 1mg/mL (top) and 10mg/mL (bottom). Intensity is normalised to 1.0 at emission wavelength 290nm.

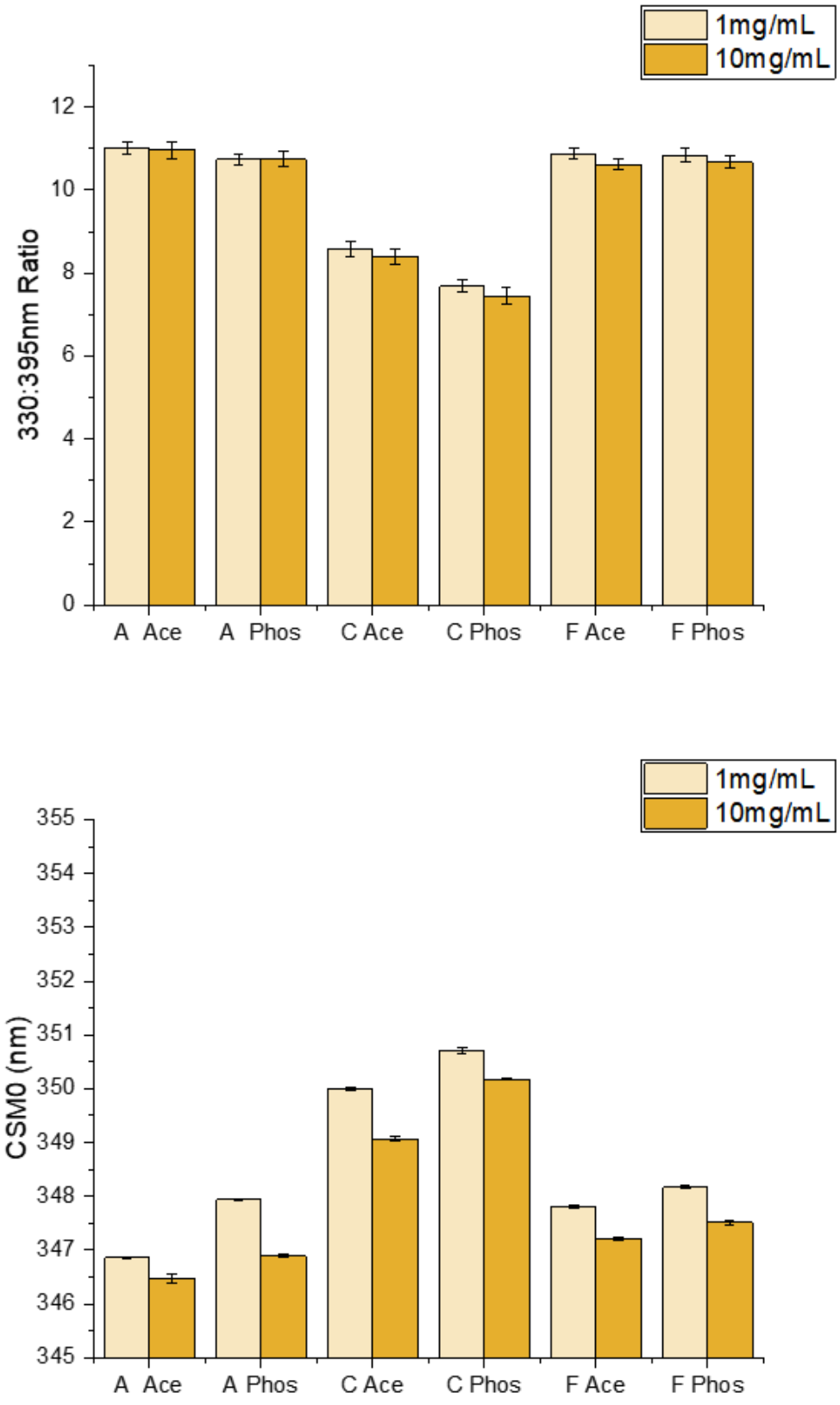

Figure 67 Comparison of f_{330nm}/f_{395nm} (top) and CSM_0 (bottom) at 1mg/mL and 10mg/mL for mAb A, C and F in acetate and phosphate buffers. Error bars show standard deviation. n=3.

Figure 67 shows the results from the f_{330nm}/f_{395nm} and the CSM_0 for mAbs A, C and F. The f_{330nm}/f_{395nm} did not show significant changes between the concentrations. This suggests that the ratio was not as useful or suitable as the raw spectra in determining a more aggregated sample. With the time-course experiments, there was a heightened tail forming due to aggregates or different conformations from 380 nm to 500 nm. This was not seen in the concentration-dependent aggregated samples, suggesting that the ratio is more suitable for identifying aggregate prone mAbs over time, from conformational changes. Therefore, relative intensity could prove a more useful method of detecting aggregation due to concentration.

All mAbs showed a decrease in CSM_0 at 10 mg/mL compared to at 1 mg/mL. This suggests that the mAbs are more stable and folded at higher concentrations, confirming the results from the time course SEC study. Using the trend observed from the 14-day time course study, an increased CSM_0 was expected for mAb C and F in acetate as they are more aggregated. However, it could suggest that mAb C and F in acetate are in a more stable conformation in their dimer forms.

Overall, f_{330nm}/f_{395nm} and CSM_0 do not seem suitable as a low volume method to detect concentration-dependent aggregation due to the IFE. While FLI provided useful information in showing a decrease in fluorescence in mAb C and F in acetate, as the measurements suffer from a small amount of IFE, it is not definitive.

5.2.2.3.1 Testing higher excitation wavelengths for detection of concentration dependent aggregates

An alternative to lowering the pathlength is to use a lower energy excitation wavelength. By investigating the effects of excitation at 310 nm, the effects of the IFE could be reduced, allowing higher concentrations to be measured more effectively.

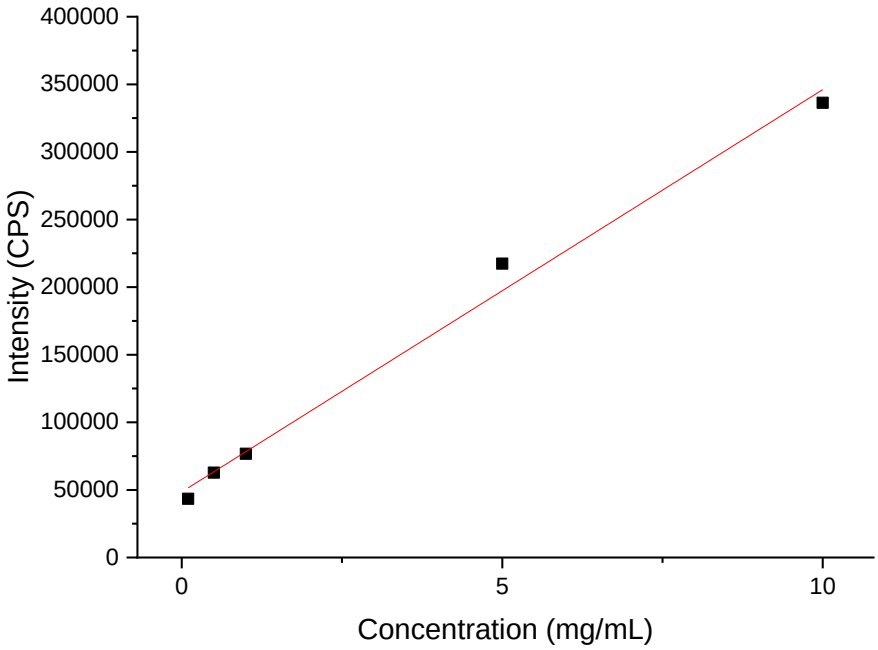

Figure 68 Intensity vs concentration for mAb B in phosphate. Excitation at 310 nm. Emission from 320-500 nm. R^2= 0.991.

shows the fluorescence intensity against concentration when a sample of mAb B in phosphate is excited at 310 nm. The results show a linearity from 0.1 to 10 mg/mL, showing that the sample does not suffer from loss of fluorescence due to IFE. The signal is noticeably lower than that at 280 nm, as expected. The lower signal caused a low signal to noise ratio at low concentrations as seen in Figure 69.

Figure 69 shows a comparison of mAb C in acetate and phosphate buffers at 1 mg/mL and 10 mg/mL. At 1 mg/mL, the noise is much higher than at 10 mg/mL. This causes difficulties in making direct comparisons between the concentrations. At 10 mg/mL, a peak is more prominent around 330 nm due to the better resolution. The shape difference between the two concentrations could contribute to the differences observed in CSM_0 from REES studies as the shape is flatter, causing the spectral mass to shift to the right.

Excitation at 320 nm may help to extend the linearity of samples, however there was low signal at the concentration range of this study. The fluorescence spectra for 1 mg/mL do not show a distinct peak, making it difficult to conclude any changes are due to aggregates due to the inability to compare concentrations directly. Therefore, fluorescence spectra with an excitation of 320 nm was not considered further.

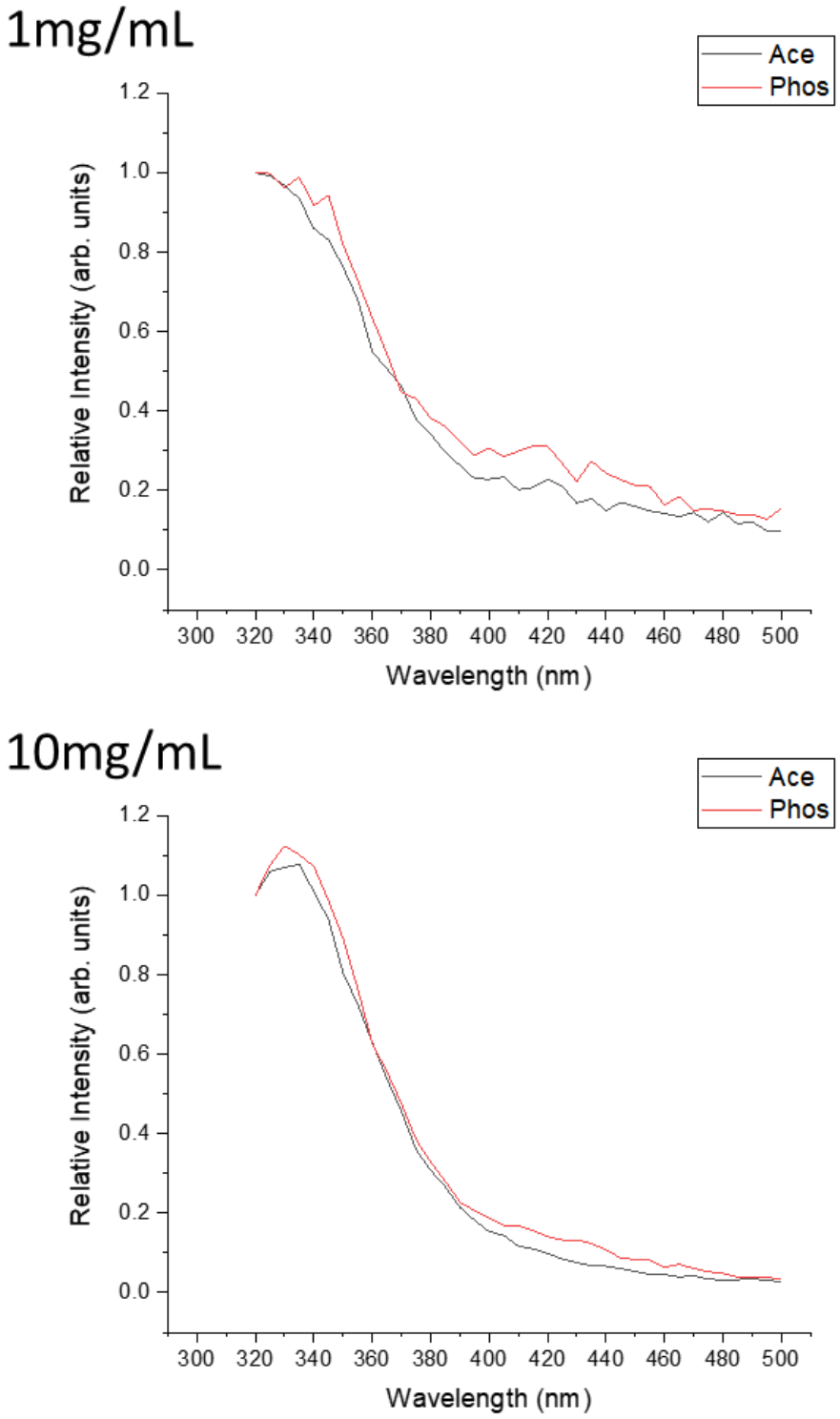

Figure 69 Relative fluorescence spectra (excitation: 310nm, emission: 320-500nm) for mAb C in acetate and phosphate at 1mg/mL (top) and 10mg/mL (bottom). Intensity is normalised to 1.0 at emission wavelength 290nm.

5.2.2.3.1 Testing TCSPC for detection of concentration dependent aggregates

TCSPC was also considered to investigate the effects of concentration, as it is not intensity based. As time decay is a true value, it could provide more insight into the mAb

behaviour. Based on the previous experiments in Chapter 4, an increase in time decay suggests the tryptophan is more exposed to the environment, as it unfolds. As tryptophan is buried within the hydrophobic core, the time decay decreases.

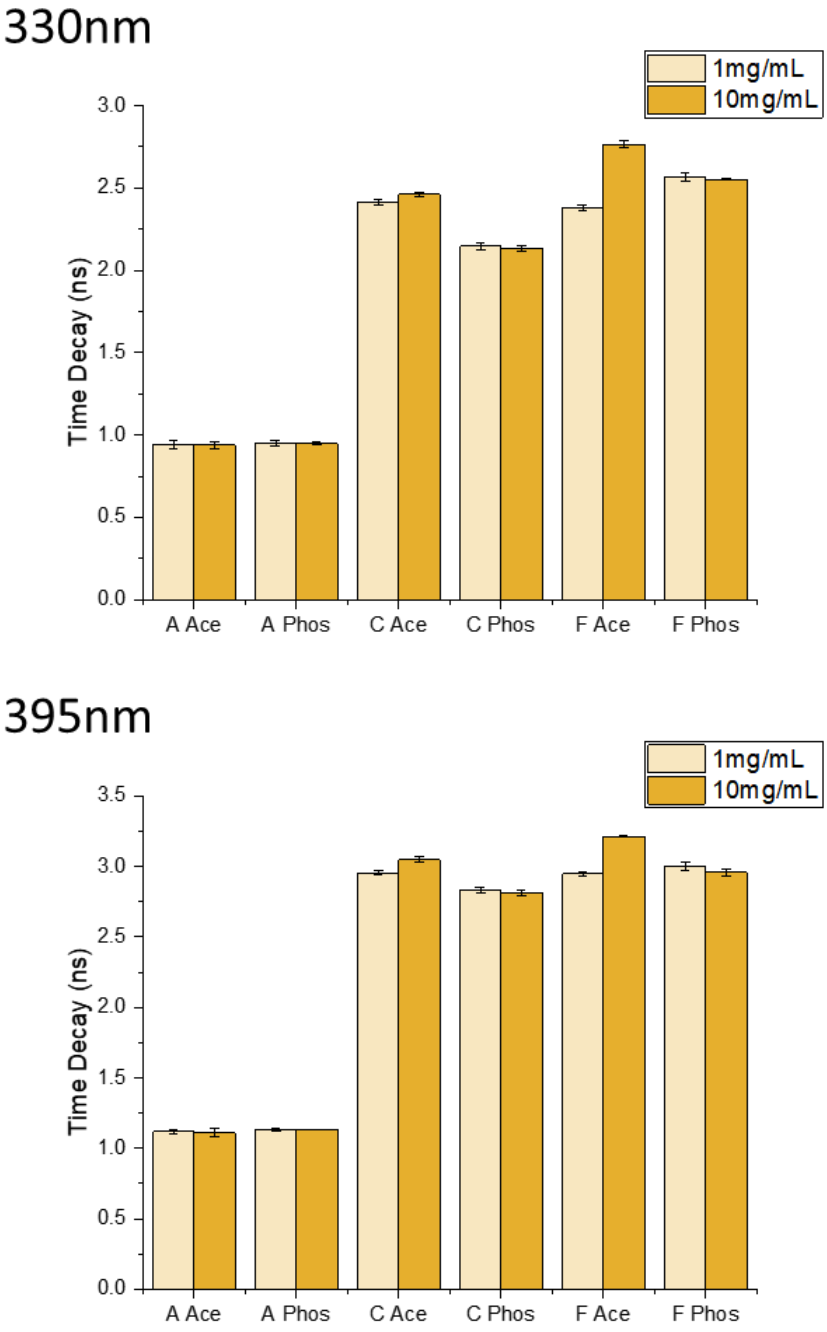

Figure 70 Comparison of time decay at emission of 330nm (top) and 395nm (bottom) at 1mg/mL and 10mg/mL for mAb A, C and F in acetate and phosphate buffers. Error bars show standard deviation. n=3.

Figure 70 is a comparison of the time decays at 330 nm and 395 nm for mAbs A, C and F in acetate and phosphate. In general, the differences between 1 mg/mL and 10 mg/mL are relatively insignificant. This suggests that there is little change in the location of the tryptophan as concentration increases. As expected, the samples that did not suffer from

concentration dependent aggregation showed little change in time decays at both 330 nm and 395 nm. In the time course experiments, a very small increase in time decay was observed at 330 nm with unfolding and aggregation and a larger relative increase was seen at 395 nm. With mAb C and F in acetate, there is a change at 330 nm and 395 nm, suggesting solvent exposure to tryptophan. MAb F in acetate showed the largest change in time decay at 330 nm upon increasing concentrations, from 3.37ns to 2.76 ns, an increase of almost 16%. MAb C in acetate showed a relatively smaller increase in time decay, increasing around 2% at 330 nm and 3% at 395 nm. The increase in time decays was unexpected as AUC showed dimerization in mAb C, suggesting that tryptophan would be buried as seen by mAb B in phosphate.

The initial differences in time decay at both 330nm and 395nm between buffers, observed with mAb B previously, are also seen with mAb and F. Though, mAb F shows this time decay difference between buffers to a lesser degree at 395nm. MAb F also shows a higher time decay at 395nm in phosphate rather than acetate at 1 mg/mL. The initial time decay differences at 1 mg/mL strengthens the initial suggestion that aggregate prone mAbs have different time decays in different buffers. This could be useful as an initial flagging tool to identify more prone mAbs.

Overall, TCSPC is a more robust method of measuring samples at different concentrations. It was more robust than fluorescence intensity methods as it does not suffer from IFE.

5.3 Recommendation for novel assay

A new cuvette, the MicroSense, allowed for higher concentrations to be reached due to the IFE. REES and FLI were initially considered following the time-course study findings. However, both methods were not able to identify mAb C and F as aggregated from mAb A, the negative control molecule. This suggested that there was not a shape change in the fluorescence spectra in aggregated samples. The shape change could be due to conformational changes to the monomer, rather than aggregates.

TCSPC was investigated as an alternative, as time decay is an absolute value, and should not change dramatically with concentration in samples that would not aggregate at higher concentrations. The time decay at 330nm showed little change between the concentrations in mAb A, and mAb C and F in phosphate. The same phenomenon was observed for the time decay at 395nm, albeit to a lesser extent. Again, the differences in time decay between acetate and phosphate for mAb C and F was measured. This could act as a rapid, low volume method to flag mAbs that may behave differently in different buffers.

Chapter 6

Conclusions

This project aims to reduce the gap between the discovery of a therapeutic and its manufacture by characterising protein aggregation

The main objectives of this thesis were to: select and evaluate appropriate methods to investigate monoclonal antibody aggregation at low volumes and to evaluate the ability of the selected methods to detect early signs of aggregation to aid in the development of a prediction model based on the protein sequence.

6.1 Baseline characterisation and method selection

Through a baseline characterisation of the mAb panel, the strengths and weaknesses of each currently employed method was carried out. SEC is a robust, quick method to quantify species in a sample. It was limited in its ability to measure across different concentrations, and samples were not recoverable. The measurements are also not carried out in native buffers. DLS is a qualitative method that was able to measure in native buffers and across a wide range of concentrations allowing it to detect concentration dependent aggregation. However, it requires a high amount of material and is susceptible to dust and bubble interference. Each measurement also requires around 5 minutes per sample. AUC was also evaluated. As it is a time-consuming method, it was only used to confirm concentration dependent aggregation.

A literature survey was carried out to assess the best methods to investigate as low material requirement and high throughput method. Fluorescence-based techniques and Raman spectroscopy were selected, based on availability and a ranking system by the student and two supervisors. Raman spectroscopy was found to require high material requirement and low signal. Therefore, it was not taken forward. Fluorescence was more promising and so was assessed further.

6.2 Evaluation of fluorescence-based methods at low volumes to detect early signs of aggregation

FLI, f_{330nm}/f_{395nm}, REES and TCSPC were evaluated due to their ease of use, ability to measure in native conditions, ability to measure at low concentrations, fast measurements, and no requirement for sample preparation. All fluorescence methods were tested using the same samples as used in the baseline characterisation to measure aggregate propensity. All methods, except FLI, were successful in identifying mAb B as the aggregate prone. FLI was unable to detect the shape change (secondary peak formation around emission wavelength 395nm) in mAb B in phosphate as there was little change in overall intensity.

A time course study was conducted to assess the earliest time point mAb B in phosphate could be significantly identified amongst the other samples. Samples were isothermally

held at 37°C and 45°C and measurements were taken on day 0, 1, 2, 3, 5, 7, 9, 12 and 14. SEC was also used as a baseline for the novel methods. CSM_0 from REES and the fluorescence ratio were quickly able to distinguish mAb B from the other samples within one day. Through the fluorescence methods, mAb B in phosphate shows signs of shifting towards an aggregate prone partially unfolded intermediate, indicative of an aggregating sample. The time decay at 395nm emission was identified as the most strongly correlated to SEC based on Spearman's ranking and was able to identify mAb B within the first 2 days. It should be noted that all techniques were unable to identify mAb E in phosphate to precipitate.

Following the success of the time course study, a 4-hour time course at 45°C was carried out. CSM_0 and f_{330nm}/f_{395nm} was used. Both methods were successful in identifying mAb B from the rest of the samples within the first hour. REES had a better correlation to SEC and was taken forward. This study formed the basis of the novel assay. It reduced the time required to obtain stressed samples, needing less material and could identify the aggregate prone mAb quicker than SEC (which could by day 7).

6.3 Evaluation of fluorescence-based methods to detect concentration-dependent aggregation

Using the same principles as found by REES, concentration dependent aggregates were investigated. Due to the IFE, it was limited in its success to differentiate mAbs C and F in acetate from the negative control, mAb A. A new microvolume cuvette was used to combat the IFE. This cuvette reduced the pathlength, allowing for higher concentrations to be measured. TCSPC was assessed as it showed to be unaffected by the increased concentration. The time decay at 330 nm showed a difference in time decay between acetate and phosphate for mAbs C and F, as well as showing an increased time decay at higher concentrations. As a quick flagging method, TCSPC was able to identify mAbs C and F in acetate from the samples in phosphate and mAb A.

6.4 Proposed fluorescence-based novel assay

Through these initial studies, a novel assay can be put forward. The lead panel mAbs are dialysed into acetate and phosphate buffers. Around 50 µL at 10 mg/mL is recommended for the assay. There are two paths: (1) Taking 12 µL of 0.5 mg/mL diluted sample, the time decay at 395nm emission at room temperature is measured at each buffer. Any samples with large differences (around 5%) between buffers should be flagged preliminarily. Samples are then heated to 45 °C via the connected water bath. A REES scan is taken every 30 minutes for 4 hours. A large rise in CSM_0 is indicative of an aggregate prone mAb. MAbs that have a large difference in time decays and show a significant increase in CSM_0 are flagged and their sequence should be evaluated to find

common trends. (2) Take 2µL of 1mg/mL sample in acetate and measure the time decay at 330nm emission. Repeat in phosphate buffer. Repeat with 10mg/mL samples and compare the time decays. Any differences between buffers and concentrations indicates a change between concentration. These mAbs are then sequenced to find common trends. Figure 71 shows a rough schematic of the novel assay.

It should be noted that the novel assay requires further validation by testing more mAbs of different behaviour. A large amount of data should be collected in order to fully validate the assay and confirm the findings from this project.

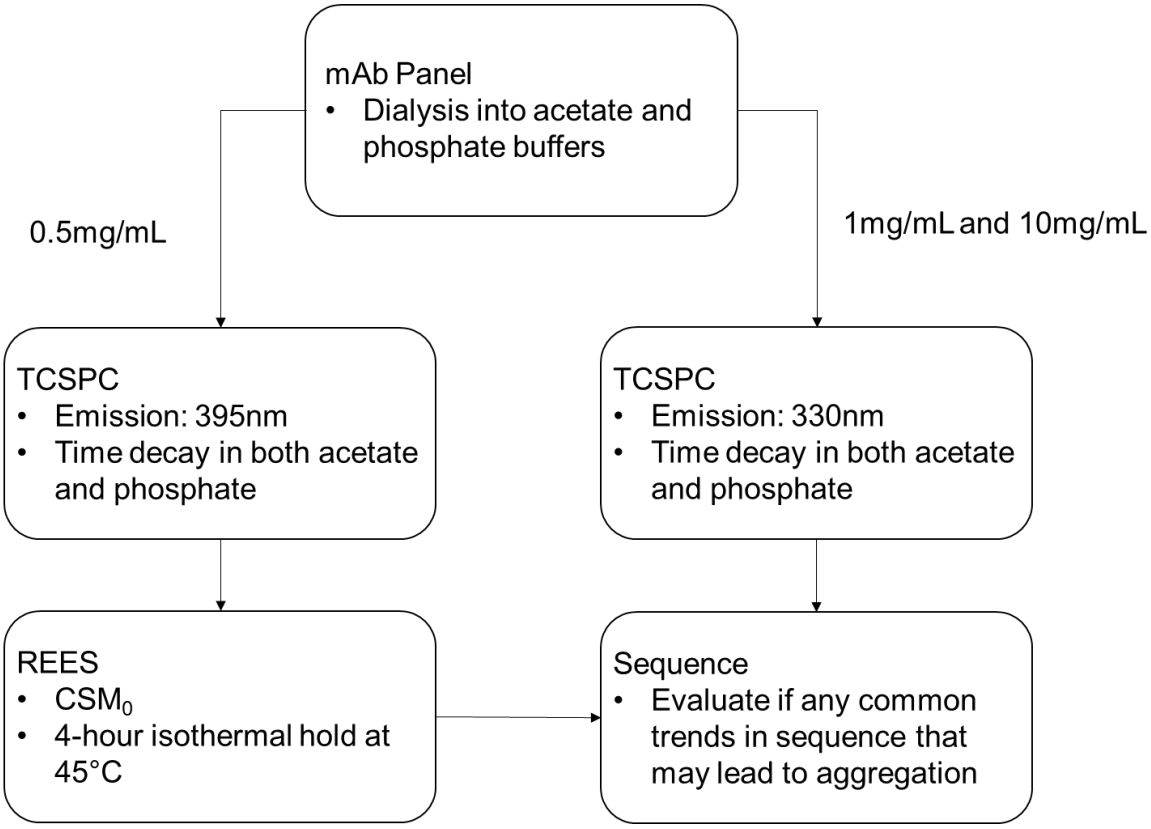

Figure 71 Schematic diagram of proposed low volume novel assay

Chapter 7

Future Work

Several findings in this thesis lead to further areas of research. The key areas are summarised below:

7.1 Increase throughput of fluorescence measurement

The fluorescence methods allow for an increased throughput by reducing the material requirements for each technique. The cuvette-based system used throughout this thesis is time consuming and labour intensive. Using robotics, such as the Tecan liquid handler, dilutions and sample loading can be faster. It is possible to increase throughput by adapting the fluorescence-methods to a plate-based platform.

Another approach to increasing throughput would be to link high throughput material generation techniques of suitable mAbs to the novel assay described in this thesis. Using high-throughput commercial cell culture systems such as the Ambr15 (TAP Biosystems) and the Micro-24 MicroReactor (Pall) and combining with high throughput purification techniques such as, Atoll's Mini-Columns and Phytips (Phynexus), high throughput concentration and dialysis techniques, more candidates can be made available for manufacturability testing. The whole system could be automated, allowing the throughput to increase dramatically. By increasing throughput, in silico methods can be created to allow an aggregation prediction model based on sequence.

7.2 Investigation into secondary peak

From the fluorescence spectra, mAb B in phosphate had a secondary peak appear upon thermal stressing. This is hypothesised to be an aggregate prone partially unfolded intermediate state, which can be useful in predicting mAbs that may aggregate in long term storage. This peak contributed to the large changes seen in REES and the f_{330nm}/f_{395nm}. The species also had a much faster time decay at 395nm than other samples.

This would need confirmation from other mAbs that behave similarly, in order to fully understand the mechanisms observed by fluorescence. The reasons were outside the scope of the thesis; however, it could lead to further understanding of the mechanisms of aggregation.

To probe this intermediate species further, fractionation vis SEC could aid to investigate the properties of pure aggregate and pure monomers. Obtaining similar mAbs to increase the scope of the panel is also useful to determine if this is unique to mAb B, or indicative of other badly aggregating mAbs. As mAb B was chosen at random, this approach would strengthen the case of the novel assay.

7.3 Additional Stresses

The proposed novel assay covers three factors that contribute to aggregation: pH, temperature and concentration. Each of these stresses influences the amount and mechanisms of aggregation each mAb undergoes.

There are other stressed that may be investigated. Other common stresses that a mAb would encounter during the bioprocess manufacture process include free-thawing (during storage), shear stress (during cell culture mixing) and oxidation.

Freeze-thaw was investigated as a method of long-term storage for the project. However, it could be a useful exercise to assess these samples using the same fluorescence principles to examine the effects. Along with shear stress, these physical stresses are not well characterised and may influence aggregate propensity. Oxidation, during aeration may also occur influencing aggregation later in the bioprocess. Fluorescence methods may aid in the fast determination of the effects of these stresses by revealing intermediates that may be missed in initial SEC tests.

References

Agenet, N., Perriat, P., Brichart, T., Crowther, N., Martini, M. & Tillement, O., 2012. Fluorescent Nanobeads: a First Step Toward Intelligent Water Tracers. In *SPE International Oilfield Nanotechnology Conference and Exhibition*. Society of Petroleum Engineers. Available at: http://www.onepetro.org/doi/10.2118/157019-MS [Accessed July 8, 2019].

Alford, J.R., Kendrick, B.S., Carpenter, J.F. & Randolph, T.W., 2008. High Concentration Formulations of Recombinant Human Interleukin-1 Receptor Antagonist: II. Aggregation Kinetics. *Journal of Pharmaceutical Sciences*, 97(8), pp.3005–3021. Available at: http://www.ncbi.nlm.nih.gov/pubmed/17924426 [Accessed June 20, 2019].

Amin, S., Barnett, G. V., Pathak, J.A., Roberts, C.J. & Sarangapani, P.S., 2014. Protein aggregation, particle formation, characterization & rheology. *Current Opinion in Colloid & Interface Science*, 19(5), pp.438–449. Available at: http://www.sciencedirect.com/science/article/pii/S135902941400096X.

Andrews, J.M. & Roberts, C.J., 2007. A Lumry-Eyring Nucleated Polymerization Model of Protein Aggregation Kinetics: 1. Aggregation with Pre-Equilibrated Unfolding. Available at: https://pubs.acs.org/doi/10.1021/jp070212j. [Accessed June 20, 2019].

Banks, D.D., Latypov, R.F., Ketchem, R.R., Woodard, J., Scavezze, J.L., Siska, C.C. & Razinkov, V.I., 2012. Native-State Solubility and Transfer Free Energy as Predictive Tools for Selecting Excipients to Include in Protein Formulation Development Studies. *Journal of Pharmaceutical Sciences*, 101(8), pp.2720–2732. Available at: http://www.ncbi.nlm.nih.gov/pubmed/22648863 [Accessed June 19, 2019].

Le Basle, Y., Chennell, P., Tokhadze, N., Astier, A. & Sautou, V., 2020. Physicochemical Stability of Monoclonal Antibodies: A Review. *Journal of Pharmaceutical Sciences*, 109(1), pp.169–190. Available at: https://www.ncbi.nlm.nih.gov/pubmed/31465737 [Accessed April 21, 2020].

Becker, W., 2005. Advanced Time-Correlated Single Photon Counting Techniques. *Journal of Microscopy*, 81, p.401.

Berezin, M.Y. & Achilefu, S., 2010. Fluorescence lifetime measurements and biological imaging. *Chemical Reviews*, 110(5), pp.2641–2684.

Berkowitz, S. a., Engen, J.R., Mazzeo, J.R. & Jones, G.B., 2012. Analytical tools for characterizing biopharmaceuticals and the implications for biosimilars. *Nature*

Reviews Drug Discovery, 11(7), pp.527–540. Available at: http://dx.doi.org/10.1038/nrd3746.

Bickel, F., Herold, E.M., Signes, A., Romeijn, S., Jiskoot, W. & Kiefer, H., 2016. Reversible NaCl-induced aggregation of a monoclonal antibody at low pH: Characterization of aggregates and factors affecting aggregation. *European Journal of Pharmaceutics and Biopharmaceutics*, 107, pp.310–320. Available at: https://www.sciencedirect.com/science/article/abs/pii/S093964111630323X [Accessed June 24, 2019].

Carpenter, J., Bain, D. & Johnson, G., 2016. Use of Analytical Ultracentrifugation as an Orthogonal Method for Size Exclusion Chromatography: Assuring Quality for Therapeutic Protein Products and Meeting Regulatory Expectations. In S. Uchiyama, F. Arisaka, W. Stafford, & T. Laue, eds. *Analytical Ultracentrifugation*. pp. 389–395.

Carpenter, J.F., Randolph, T.W., Jiskoot, W.I.M., Crommelin, D.J.A., Middaugh, C.R., Winter, G., Fan, Y., Kirshner, S., Verthelyi, D., Kozlowski, S., Clouse, K.A., Swann, P.G., Rosenberg, A.M.Y. & Cherney, B., 2009. Overlooking Subvisible Particles in Therapeutic Protein Products : Gaps That May Compromise Product Quality. , 98(4), pp.1201–1205.

Catici, D.A.M., Amos, H.E., Yang, Y., van den Elsen, J.M.H. & Pudney, C.R., 2016. The red edge excitation shift phenomenon can be used to unmask protein structural ensembles: implications for NEMO-ubiquitin interactions. *The FEBS Journal*, 283(12), pp.2272–2284. Available at: http://www.ncbi.nlm.nih.gov/pubmed/27028374 [Accessed July 8, 2019].

Chapeau, A.L., Silva, J.V.C., Schuck, P., Thierry, A. & Floury, J., 2016. The influence of cheese composition and microstructure on the diffusion of macromolecules: A study using Fluorescence Recovery After Photobleaching (FRAP). *Food Chemistry*, 192, pp.660–667. Available at: https://www.sciencedirect.com/science/article/pii/S0308814615010638 [Accessed July 4, 2019].

Chattopadhyay, A. & Haldar, S., 2014. Dynamic Insight into Protein Structure Utilizing Red Edge Excitation Shift. *Accounts of Chemical Research*, 47(1), pp.12–19. Available at: http://pubs.acs.org/doi/10.1021/ar400006z [Accessed July 5, 2019].

Chen, S., Yu, Y.-L. & Wang, J.-H., 2018. Inner filter effect-based fluorescent sensing systems: A review. *Analytica Chimica Acta*, 999, pp.13–26. Available at: https://www.sciencedirect.com/science/article/pii/S0003267017311856 [Accessed

July 8, 2019].

Chi, E.Y., Krishnan, S., Randolph, T.W. & Carpenter, J.F., 2003. Physical Stability of Proteins in Aqueous Solution: Mechanism and Driving Forces in Nonnative Protein Aggregation. , 20(9), pp.1325–1336.

Chiti, F. & Dobson, C.M., 2009. Amyloid formation by globular proteins under native conditions. *Nature Chemical Biology*, 5(1), pp.15–22. Available at: http://www.ncbi.nlm.nih.gov/pubmed/19088715 [Accessed June 18, 2019].

Chothia, C., 1976. The nature of the accessible and buried surfaces in proteins. *Journal of molecular biology*, 105(1), pp.1–12. Available at: http://www.ncbi.nlm.nih.gov/pubmed/994183 [Accessed July 8, 2019].

Chroma Technology Corporation, 2016. Fluorochrome Spectra. Available at: https://www.chroma.com/knowledge-resources/about-fluorescence/introduction-to-fluorescence/fluorochrome-spectra [Accessed February 12, 2017].

Cleland, J.L., Powell, M.F. & Shire, S.J., 1993. The development of stable protein formulations: a close look at protein aggregation, deamidation, and oxidation. *Critical reviews in therapeutic drug carrier systems*, 10(4), pp.307–77. Available at: http://www.ncbi.nlm.nih.gov/pubmed/8124728 [Accessed June 17, 2019].

Committee for Medicinal Products for Human use (CHMP), 2007. Guideline on immunogenicity assessment of biotechnology-derived therapeutic proteins. *European Medicines Agency (EMEA)*. Available at: http://www.emea.europa.eu [Accessed June 13, 2019].

Craik, D.J., Fairlie, D.P., Liras, S. & Price, D., 2013. The Future of Peptide-based Drugs. *Chemical Biology & Drug Design*, (81), pp.136–147. Available at: https://onlinelibrary.wiley.com/doi/pdf/10.1111/cbdd.12055 [Accessed June 4, 2019].

Creative Proteomics, 2020. Size Exclusion Chromatography (SEC) Service. *Pronalyse*. Available at: https://www.creative-proteomics.com/pronalyse/size-exclusion-chromatography-sec-service.html [Accessed April 23, 2020].

Cromwell, M.E.M., Hilario, E. & Jacobson, F., 2006. Protein aggregation and bioprocessing. *The AAPS Journal*, 8(3), pp.572–579. Available at: http://www.ncbi.nlm.nih.gov/pmc/articles/PMC2761064/%5Cnhttp://www.ncbi.nlm.nih.gov/pmc/articles/PMC2761064/pdf/12248_2008_Article_83572.pdf.

Das, R.S. & Agrawal, Y.K., 2011. Raman spectroscopy: Recent advancements, techniques and applications. *Vibrational Spectroscopy*, 57(2), pp.163–176.

Daugherty, A.L. & Mrsny, R.J., 2006. Formulation and delivery issues for monoclonal antibody therapeutics. *Advanced Drug Delivery Reviews*, 58(5–6), pp.686–706. Available at: http://www.ncbi.nlm.nih.gov/pubmed/16839640 [Accessed June 18, 2019].

Demchenko, A.P., 2008. Chapter 4 Site-Selective Red-Edge Effects. In *Methods in enzymology*. pp. 59–78. Available at: http://www.ncbi.nlm.nih.gov/pubmed/19152856 [Accessed July 5, 2019].

Demchenko, A.P., 2002. The red-edge effects: 30 years of exploration. *Luminescence*, 17(1), pp.19–42. Available at: http://www.ncbi.nlm.nih.gov/pubmed/11816059 [Accessed July 5, 2019].

Demeule, B., Lawrence, M.J., Drake, A.F., Gurny, R. & Arvinte, T., 2007. Characterization of protein aggregation: The case of a therapeutic immunoglobulin. *Biochimica et Biophysica Acta - Proteins and Proteomics*, 1774(1), pp.146–153.

Dobson, C.M., 2003. Protein folding and misfolding. *Nature*, 426(6968), pp.884–890. Available at: http://www.nature.com/articles/nature02261 [Accessed June 18, 2019].

Dobson, C.M. & Karplus, M., 1999. The fundamentals of protein folding: bringing together theory and experiment. *Current opinion in structural biology*, 9(1), pp.92–101. Available at: http://www.ncbi.nlm.nih.gov/pubmed/10047588 [Accessed June 18, 2019].

Ecker, D.M., Jones, S.D. & Levine, H.L., 2015. The therapeutic monoclonal antibody market. *mAbs*, 7(1), p.9. Available at: https://www.ncbi.nlm.nih.gov/pmc/articles/PMC4622599/ [Accessed June 13, 2019].

Den Engelsman, J., Garidel, P., Smulders, R., Koll, H., Smith, B., Bassarab, S., Seidl, A., Hainzl, O. & Jiskoot, W., 2011. Strategies for the assessment of protein aggregates in pharmaceutical biotech product development. *Pharmaceutical Research*, 28(4), pp.920–933.

Fekete, S., Goyon, A., Veuthey, J.-L. & Guillarme, D., 2018. *Size Exclusion Chromatoraphy of Protein Biopharmaceuticals: Past, Present and Future*, Russell Pub. Available at: https://archive-ouverte.unige.ch/unige:103247 [Accessed June 25, 2019].

Fekete, S. & Guillarme, D., 2014. Ultra-high-performance liquid chromatography for the characterization of therapeutic proteins. *TrAC Trends in Analytical Chemistry*, 63,

pp.76–84. Available at: http://www.sciencedirect.com/science/article/pii/S0165993614001836.

Fernandez-Escamilla, A.-M., Rousseau, F., Schymkowitz, J. & Serrano, L., 2004. Prediction of sequence-dependent and mutational effects on the aggregation of peptides and proteins. *Nature Biotechnology*, 22(10), pp.1302–1306. Available at: http://www.nature.com/articles/nbt1012 [Accessed June 21, 2019].

Fink, A.L., 1998. Protein aggregation: folding aggregates, inclusion bodies and amyloid. *Folding and Design*, 3(1), pp.R9–R23. Available at: http://www.ncbi.nlm.nih.gov/pubmed/9502314 [Accessed June 18, 2019].

Fowler, A., Swift, D., Longman, E., Acornley, A., Hemsley, P., Murray, D., Unitt, J., Dale, I., Sullivan, E. & Coldwell, M., 2002. An evaluation of fluorescence polarization and lifetime discriminated polarization for high throughput screening of serine/threonine kinases. *Analytical Biochemistry*, 308(2), pp.223–231.

Gabrielson, J.P., Randolph, T.W., Kendrick, B.S. & Stoner, M.R., 2007. Sedimentation velocity analytical ultracentrifugation and SEDFIT/c(s): Limits of quantitation for a monoclonal antibody system. *Analytical Biochemistry*, 361(1), pp.24–30.

Garcia-Pardo, J., Graña-Montes, R., Fernandez-Mendez, M., Ruyra, A., Roher, N., Aviles, F.X., Lorenzo, J. & Ventura, S., 2014. Amyloid Formation by Human Carboxypeptidase D Transthyretin-like Domain under Physiological Conditions. *Journal of Biological Chemistry*, 289(49), pp.33783–33796. Available at: http://www.ncbi.nlm.nih.gov/pubmed/25294878 [Accessed June 24, 2019].

GE Healthcare, *Size Exclusion Chromatography: Principles and Methods*, Available at: https://cdn.gelifesciences.com/dmm3bwsv3/AssetStream.aspx?mediaformatid=10061&destinationid=10016&assetid=11639 [Accessed April 23, 2020].

Gil-Garcia, M., Bañó-Polo, M., Varejão, N., Jamroz, M., Kuriata, A., Díaz-Caballero, M., Lascorz, J., Morel, B., Navarro, S., Reverter, D., Kmiecik, S. & Ventura, S., 2018. Combining Structural Aggregation Propensity and Stability Predictions To Redesign Protein Solubility. *Molecular Pharmaceutics*, 15(9), pp.3846–3859. Available at: http://pubs.acs.org/doi/10.1021/acs.molpharmaceut.8b00341 [Accessed June 21, 2019].

Goldberg, D.S., Bishop, S.M., Shah, A.U. & Sathish, H.A., 2011. Formulation Development of Therapeutic Monoclonal Antibodies Using High-Throughput Fluorescence and Static Light Scattering Techniques: Role of Conformational and Colloidal Stability. *Pharmacists Association J Pharm Sci*, 100, pp.1306–1315. Available at: https://onlinelibrary.wiley.com/doi/pdf/10.1002/jps.22371 [Accessed

June 25, 2019].

Grilo, A.L. & Mantalaris, A., 2019. The Increasingly Human and Profitable Monoclonal Antibody Market. *Trends in Biotechnology*, 37(1), pp.9–16. Available at: https://www.sciencedirect.com/science/article/pii/S0167779918301495 [Accessed June 4, 2019].

Gun'ko, V., Klyueva, A., Levchuk, Y. & Leboda, R., 2003. Photon correlation spectroscopy investigations of protein. *Advances in Colloid and Interface Science*, 105(1–3), pp.201–328.

Haldar, S., Chaudhuri, A. & Chattopadhyay, A., 2011. Organization and Dynamics of Membrane Probes and Proteins Utilizing the Red Edge Excitation Shift. *The Journal of Physical Chemistry B*, 115(19), pp.5693–5706. Available at: https://pubs.acs.org/doi/10.1021/jp200255e [Accessed July 5, 2019].

Hamrang, Z., Rattray, N.J.W. & Pluen, A., 2013. Proteins behaving badly: Emerging technologies in profiling biopharmaceutical aggregation. *Trends in Biotechnology*, 31(8), pp.448–458. Available at: http://dx.doi.org/10.1016/j.tibtech.2013.05.004.

Harrison, J.S., Gill, A. & Hoare, M., 1998. Stability of a single-chain Fv antibody fragment when exposed to a high shear environment combined with air-liquid interfaces. *Biotechnology and bioengineering*, 59(4), pp.517–9. Available at: http://www.ncbi.nlm.nih.gov/pubmed/10099366 [Accessed June 17, 2019].

He, F., Razinkov, V., Middaugh, C.R. & Becker, G.W., 2013. High-Throughput Biophysical Approaches to Therapeutic Protein Development. *Biophysics for therapeutic protein development*, pp.7–31. Available at: http://link.springer.com/10.1007/978-1-4614-4316-2.

Healey, J.F., Parker, E.T. & Lollar, P., 2018. Identification of aggregates in therapeutic formulations of recombinant full-length factor VIII products by sedimentation velocity analytical ultracentrifugation. *Journal of Thrombosis and Haemostasis*, 16(2), pp.303–315. Available at: http://doi.wiley.com/10.1111/jth.13917 [Accessed June 25, 2019].

Hermeling, S., Schellekens, H., Maas, C., Gebbink, M.F.B.G., Crommelin, D.J.A. & Jiskoot, W., 2006. Antibody Response to Aggregated Human Interferon Alpha2b in Wild-type and Transgenic Immune Tolerant Mice Depends on Type and Level of Aggregation. *Journal of Pharmaceutical Sciences*, 95(5), pp.1084–1096. Available at: http://www.ncbi.nlm.nih.gov/pubmed/16552750 [Accessed June 20, 2019].

Hernandez, R., 2015. Detecting Protein Aggregates and Evaluating their

Immunogenicity. *BioPharm International*, 28(3). Available at: http://www.biopharminternational.com/detecting-protein-aggregates-and-evaluating-their-immunogenicity [Accessed January 19, 2015].

Hong, P., Koza, S. & Bouvier, E.S.P., 2012. Size-Exclusion Chromatography for the Analysis of Protein Biotherapeutics and their Aggregates. *Journal of liquid chromatography & related technologies*, 35(20), pp.2923–2950. Available at: http://www.pubmedcentral.nih.gov/articlerender.fcgi?artid=3556795&tool=pmcentrez&rendertype=abstract.

Hwang, W.Y.K. & Foote, J., 2005. Immunogenicity of engineered antibodies. *Methods*, 36(1), pp.3–10.

Jakubek, R.S., Handen, J., White, S.E., Asher, S.A. & Lednev, I.K., 2018. Ultraviolet resonance Raman spectroscopic markers for protein structure and dynamics. *TrAC Trends in Analytical Chemistry*, 103, pp.223–229. Available at: https://www.sciencedirect.com/science/article/pii/S0165993617303953 [Accessed July 8, 2019].

James, L.C. & Tawfik, D.S., 2003. Conformational diversity and protein evolution – a 60-year-old hypothesis revisited. *Trends in Biochemical Sciences*, 28(7), pp.361–368. Available at: http://www.ncbi.nlm.nih.gov/pubmed/12878003 [Accessed June 18, 2019].

Jarasch, A., Koll, H., Regula, J.T., Bader, M., Papadimitriou, A. & Kettenberger, H., 2015. Developability Assessment During the Selection of Novel Therapeutic Antibodies. *Journal of Pharmaceutical Sciences*, 104(6), pp.1885–1898. Available at: https://www.sciencedirect.com/science/article/pii/S0022354915300848 [Accessed June 24, 2019].

Johann, C., 2012. Characterization of proteins and protein conjugates by Multi-Angle Light Scattering coupled to SEC. , pp.1–27. Available at: http://www.waters.com/webassets/cms/events/docs/LC Biopharma_Characterization of proteins and protein conjugates by MALS-SEC.pdf.

Jones, H.B.L., Wells, S.A., Prentice, E.J., Kwok, A., Liang, L.L., Arcus, V.L. & Pudney, C.R., 2017. A complete thermodynamic analysis of enzyme turnover links the free energy landscape to enzyme catalysis. *The FEBS Journal*, 284(17), pp.2829–2842. Available at: http://doi.wiley.com/10.1111/febs.14152 [Accessed July 8, 2019].

Jose, N., Deshmukh, G.P., Ravindra, M.R. & Review, M., 2019. *Dynamic Light Scattering: Advantages and Applications*, Available at: https://www.actascientific.com/ASNH/pdf/ASNH-03-0194.pdf [Accessed June 25,

2019].

Kalonia, C., Toprani, V., Toth, R., Wahome, N., Gabel, I., Middaugh, C.R. & Volkin, D.B., 2016. Effects of Protein Conformation, Apparent Solubility, and Protein-Protein Interactions on the Rates and Mechanisms of Aggregation for an IgG1 Monoclonal Antibody. *The Journal of Physical Chemistry B*, 120, pp.7062–7075. Available at: https://www.researchgate.net/publication/304910107 [Accessed June 18, 2019].

van der Kant, R., Karow-Zwick, A.R., Van Durme, J., Blech, M., Gallardo, R., Seeliger, D., Aßfalg, K., Baatsen, P., Compernolle, G., Gils, A., Studts, J.M., Schulz, P., Garidel, P., Schymkowitz, J. & Rousseau, F., 2017. Prediction and Reduction of the Aggregation of Monoclonal Antibodies. *Journal of Molecular Biology*, 429(8), pp.1244–1261. Available at: https://linkinghub.elsevier.com/retrieve/pii/S0022283617301183 [Accessed June 24, 2019].

Kapusta, P., Wahl, M., Benda, A., Hof, M. & Enderlein, J., 2007. Fluorescence lifetime correlation spectroscopy. *Journal of Fluorescence*, 17(1), pp.43–48.

Kayser, V., Chennamsetty, N., Voynov, V., Helk, B. & Trout, B.L., 2011. Tryptophan-tryptophan energy transfer and classification of tryptophan residues in proteins using a therapeutic monoclonal antibody as a model. *Journal of Fluorescence*, 21(1), pp.275–288.

Kelley, B., 2009. Industrialization of mAb production technology: the bioprocessing industry at a crossroads. *mAbs*, 1(5), pp.443–52. Available at: http://www.ncbi.nlm.nih.gov/pubmed/20065641 [Accessed June 14, 2019].

Kesik-Brodacka, M., 2017. Progress in biopharmaceutical development. *Biotechnology and Applied Biochemistry*, 65(3), pp.306–322. Available at: https://iubmb.onlinelibrary.wiley.com/doi/pdf/10.1002/bab.1617 [Accessed June 4, 2019].

Kessler, M., Goldsmith, D. & Schellekens, H., 2006. Immunogenicity of biopharmaceuticals. *Nephrology Dialysis Transplantation*, 21(suppl_5), pp.v9–v12. Available at: http://academic.oup.com/ndt/article/21/suppl_5/v9/1906130/Immunogenicity-of-biopharmaceuticals [Accessed June 13, 2019].

Kolhe, P., Amend, E. & Singh, S.K., 2010. Impact of freezing on pH of buffered solutions and consequences for monoclonal antibody aggregation. *Biotechnology Progress*, 26(3), pp.727–733.

Krishnamurthy, R. & Manning, M.C., 2002. The stability factor: importance in formulation development. *Current pharmaceutical biotechnology*, 3(4), pp.361–71. Available at: http://www.ncbi.nlm.nih.gov/pubmed/12463418 [Accessed June 20, 2019].

Kubista, M., Sjoback, R., Eriksson, S. & Albinsson, B., 1994. *Experimental Correction for the Inner-filter Effect in Fluorescence Spectra*, Available at: https://pubs.rsc.org/en/content/articlepdf/1994/an/an9941900417 [Accessed July 8, 2019].

Kunert, R. & Reinhart, D., 2016. Advances in recombinant antibody manufacturing. *Applied microbiology and biotechnology*, 100(8), pp.3451–61. Available at: http://www.ncbi.nlm.nih.gov/pubmed/26936774 [Accessed June 17, 2019].

Lakowicz, J.R., 2006. *Principles of Fluorescence Spectroscopy* 3rd ed., Springer US.

Lakowicz, J.R. & Keating-Nakamoto, S., 1984. Red-edge excitation of fluorescence and dynamic properties of proteins and membranes. *Biochemistry*, 23(13), pp.3013–3021. Available at: http://pubs.acs.org/doi/abs/10.1021/bi00308a026 [Accessed July 8, 2019].

Lakowitz, J., 2006. *Principles of fluorescence spectroscopy* 3rd ed.,

Laue, T.M. & Stafford, W.F., 1999. Modern applications of analytical ultracentrifugation. *Annual review of biophysics and biomolecular structure*, 28, pp.75–100.

Lauer, T.M., Agrawal, N.J., Chennamsetty, N., Egodage, K., Helk, B. & Trout, B.L., 2012. Developability Index: A Rapid In Silico Tool for the Screening of Antibody Aggregation Propensity. *Journal of Pharmaceutical Sciences*, 101(1), pp.102–115. Available at: https://www.sciencedirect.com/science/article/pii/S0022354915317780 [Accessed June 18, 2019].

Lebowitz, J., Lewis, M.S. & Schuck, P., 2002. Modern analytical ultracentrifugation in protein science: A tutorial review. *Protein Science*, 11(9), pp.2067–2079.

LeSaout, X., Costioli, M., Jordan, L., Lambert, J., Beighley, R., Provencher, L., Gerwe, B., McGuire, K., Verlinden, N. & Barry, A., 2015. Automated small-scale protein purification and analysis for accelerated development of protein therapeutics. *Engineering in Life Sciences*, p.n/a-n/a. Available at: http://doi.wiley.com/10.1002/elsc.201400252.

Li, M., Xu, J., Romero-Gonzalez, M., Banwart, S.A. & Huang, W.E., 2012. Single cell Raman spectroscopy for cell sorting and imaging. *Current Opinion in Biotechnology*, 23(1), pp.56–63.

Li, W., Prabakaran, P., Chen, W., Zhu, Z., Feng, Y., Dimitrov, D., Li, W., Prabakaran, P., Chen, W., Zhu, Z., Feng, Y. & Dimitrov, D.S., 2016. Antibody Aggregation: Insights from Sequence and Structure. *Antibodies*, 5(3), p.19. Available at: http://www.mdpi.com/2073-4468/5/3/19 [Accessed June 18, 2019].

Lichtman, J.W. & Conchello, J.-A., 2005. Fluorescence microscopy. *Nature Methods*, 2(12), pp.910–919. Available at: http://www.nature.com/articles/nmeth817 [Accessed July 2, 2019].

Lindgren, M., Sörgjerd, K. & Hammarström, P., 2005. Detection and Characterization of Aggregates, Prefibrillar Amyloidogenic Oligomers, and Protofibrils Using Fluorescence Spectroscopy. *Biophysical Journal*, 88(6), pp.4200–4212.

Liu, R., Liu, J. fu, Zhou, X. xia, Jiang, G. bin & Liu, R., 2011. Applications of Raman-based techniques to on-site and in-vivo analysis. *TrAC - Trends in Analytical Chemistry*, 30(9), pp.1462–1476.

Lowe, D., Dudgeon, K., Rouet, R., Schofield, P., Jermutus, L. & Christ, D., 2011. Aggregation, stability, and formulation of human antibody therapeutics. *Advances in Protein Chemistry and Structural Biology*, 84, pp.41–61. Available at: https://www.sciencedirect.com/science/article/pii/B9780123864833000045?via%3Dihub [Accessed June 18, 2019].

Maddux, N.R., Iyer, V., Cheng, W., Youssef, A.M.K., Joshi, S.B., Volkin, D.B., Ralston, J.P., Winter, G. & Middaugh, C.R., 2014. High Throughput Prediction of the Long-Term Stability of Pharmaceutical Macromolecules from Short-Term Multi-Instrument Spectroscopic Data. *Journal of Pharmaceutical Sciences*, 103(3), pp.828–839. Available at: http://www.ncbi.nlm.nih.gov/pubmed/24421157 [Accessed June 21, 2019].

Mahler, H.-C., Friess, W., Grauschopf, U. & Kiese, S., 2009. Protein Aggregation: Pathways, Induction Factors and Analysis. *Journal of Pharmaceutical Sciences*, 98(9), pp.2909–2934.

Mahler, H.C., Müller, R., Frieß, W., Delille, A. & Matheus, S., 2005. Induction and analysis of aggregates in a liquid IgG1-antibody formulation. *European Journal of Pharmaceutics and Biopharmaceutics*, 59(3), pp.407–417.

Manning, M.C., Chou, D.K., Murphy, B.M., Payne, R.W. & Katayama, D.S., 2010. Stability of protein pharmaceuticals: An update. *Pharmaceutical Research*, 27(4), pp.544–575.

Marcu, L., Grundfest, W.S. & Maarek, J.M., 1999. Photobleaching of arterial fluorescent

compounds: characterization of elastin, collagen and cholesterol time-resolved spectra during prolonged ultraviolet irradiation. *Photochemistry and photobiology*, 69(6), pp.713–21. Available at: http://www.ncbi.nlm.nih.gov/pubmed/10378012 [Accessed July 4, 2019].

Mie, G., 1908. Beiträge zur Optik trüber Medien, speziell kolloidaler Metallösungen. *Annalen der Physik*, 330(3), pp.377–445. Available at: http://doi.wiley.com/10.1002/andp.19083300302 [Accessed April 23, 2020].

Millar, D.P., 1996. Time-resolved fluorescence spectroscopy. *Current Opinion in Structural Biology*, 6(5), pp.637–642. Available at: http://www.sciencedirect.com/science/article/pii/S0959440X96800303.

Misra, M., 2012. Biosimilars: Current perspectives and future implications. *Indian Journal of Pharmacology*, 44(1), p.12. Available at: http://www.ncbi.nlm.nih.gov/pubmed/22345862 [Accessed June 13, 2019].

Möller, M. & Denicola, A., 2002. Protein tryptophan accessibility studied by fluorescence quenching. *Biochemistry and Molecular Biology Education*, 30(3), pp.175–178. Available at: http://doi.wiley.com/10.1002/bmb.2002.494030030035 [Accessed July 4, 2019].

Mori, S. & Barth, H., 2013. *Size-Exclusion Chromatography*, Springer Berlin Heidelberg.

Morrison, S.L., Johnson, M.J., Herzenberg, L.A. & Oi, V.T., 1984. Chimeric human antibody molecules: Mouse antigen-binding domains with human constant region domains. *Proceedings of the National Academy of Sciences of the United States of America*, 81(21 I), pp.6851–6855.

Moussa, E.M., Panchal, J.P., Moorthy, B.S., Blum, J.S., Joubert, M.K., Narhi, L.O. & Topp, E.M., 2016. Immunogenicity of Therapeutic Protein Aggregates. *Journal of pharmaceutical sciences*, 105(2), pp.417–430. Available at: http://www.ncbi.nlm.nih.gov/pubmed/26869409 [Accessed June 18, 2019].

Munishkina, L.A. & Fink, A.L., 2007. Fluorescence as a method to reveal structures and membrane-interactions of amyloidogenic proteins. *Biochimica et Biophysica Acta - Biomembranes*, 1768(8), pp.1862–1885.

Nowak, C., K. Cheung, J., M. Dellatore, S., Katiyar, A., Bhat, R., Sun, J., Ponniah, G., Neill, A., Mason, B., Beck, A. & Liu, H., 2017. Forced degradation of recombinant monoclonal antibodies: A practical guide. *mAbs*.

Oladepo, S.A., Xiong, K., Hong, Z., Asher, S.A., Handen, J. & Lednev, I.K., 2012. UV Resonance Raman Investigations of Peptide and Protein Structure and Dynamics.

Chemical Reviews, 112(5), pp.2604–2628. Available at: http://www.ncbi.nlm.nih.gov/pubmed/22335827 [Accessed July 8, 2019].

Oliva, A., Llabrés, M. & Fariña, J.B., 2004. Applications of multi-angle laser light-scattering detection in the analysis of peptides and proteins. *Current drug discovery technologies*, 1(3), pp.229–242.

Oshinbolu, S., Wilson, L.J., Lewis, W., Shah, R. & Bracewell, D.G., 2018. Measurement of impurities to support process development and manufacture of biopharmaceuticals. *TrAC Trends in Analytical Chemistry*, 101, pp.120–128. Available at: https://www.sciencedirect.com/science/article/pii/S0165993617303242 [Accessed June 4, 2019].

Otsuka Electronics Co., 2015. Zeta-potential & Particle Size Analyzer ELSZ-2000 Series. Available at: http://www.otsukael.com/product/detail/productid/1/category1id/2/category2id/1/category3id/29 [Accessed February 12, 2017].

Owicki, J.C., 2000. Fluorescence Polarization and Anisotropy in High Throughput Screening: Perspectives and Primer. *Journal of biomolecular screening*, 5(5), pp.297–306. Available at: http://www.uam.es/personal_pdi/ciencias/mvelez/Research_archivos/Owicki.pdf.

Paborji, M., Pochopin, N.L., Coppola, W.P. & Bogardus, J.B., 1994. Chemical and physical stability of chimeric L6, a mouse-human monoclonal antibody. *Pharmaceutical research*, 11(5), pp.764–71. Available at: http://www.ncbi.nlm.nih.gov/pubmed/8058650 [Accessed June 17, 2019].

Palais, C., Machaidze, G., Gurny, R. & Arvinte, T., 2009. New methods allowing the detection of protein aggregates. *mAbs*, 1(2), pp.142–150.

Peronio, P., Acconcia, G., Rech, I. & Ghioni, M., 2015. Improving the counting efficiency in time-correlated single photon counting experiments by dead-time optimization. *The Review of scientific instruments*, 86(11), p.113101. Available at: http://www.ncbi.nlm.nih.gov/pubmed/26628115 [Accessed July 11, 2019].

Philo, J.S., 2003. Characterizing the Aggregation and Conformation of Protein Therapeutics Characterizing the Aggregation and Conformation of Protein Therapeutics. , (October), pp.1–3.

Philo, J.S. & Arakawa, T., 2009. *Mechanisms of Protein Aggregation*, Available at: https://pdfs.semanticscholar.org/155b/44d0416c84231d0615feba1da803284e0d6

b.pdf [Accessed June 20, 2019].

Philo, J.S., Liu, J., Andya, J.D. & Shire, S.J., 2006. A critical review of analytical ultracentrifugation and field flow fractionation methods for measuring protein aggregation. *Aaps Journal*, 8(4), pp.E580–E589.

Poole, R.A., Hawe, A., Jiskoot, W. & Braeckmans, K., 2012. Fluorescence Spectroscopy to Characterize Protein Aggregates and Particles. *Analysis of Aggregates and Particles in Protein Pharmaceuticals*, pp.201–226.

Pudney, C., 2017. Protein structure analysis based on red-edge excitation shift (REES) spectroscopy. , pp.1–81. Available at: https://patentimages.storage.googleapis.com/16/12/8c/0aceed8baa7604/WO2017158371A1.pdf [Accessed July 8, 2019].

Raghuraman, H., Kelkar, D.A. & Chattopadhyay, A., 2005. Novel Insights Into Protein Structure and Dynamics Utilizing the Red Edge Excitation Shift Approach. In *Reviews in Fluorescence 2005*. pp. 199–222. Available at: http://citeseerx.ist.psu.edu/viewdoc/download?doi=10.1.1.723.8149&rep=rep1&type=pdf [Accessed July 5, 2019].

Razinkov, V.I., Treuheit, M.J. & Becker, G.W., 2013. Methods of high throughput biophysical characterization in biopharmaceutical development. *Current drug discovery technologies*, 10(1), pp.59–70. Available at: http://www.ncbi.nlm.nih.gov/pubmed/22725690.

Reff, M.E., Hariharan, K. & Braslawsky, G., 2002. Future of monoclonal antibodies in the treatment of hematologic malignancies. *Cancer control : journal of the Moffitt Cancer Center*, 9(2), pp.152–66. Available at: http://www.ncbi.nlm.nih.gov/pubmed/11965235.

Rosenthal, T.B., 1947. The effect of temperature on the pH of blood and plasma in vitro. *Journal of Biological Chemistry*.

Sahoo, B., Balaji, J., Nag, S., Kaushalya, S.K. & Maiti, S., 2008. Protein aggregation probed by two-photon fluorescence correlation spectroscopy of native tryptophan. *The Journal of chemical physics*, 129(7), p.075103. Available at: http://www.ncbi.nlm.nih.gov/pubmed/19044804 [Accessed August 16, 2019].

Schein, C.H., 2010. Protein Aggregation and Precipitation , Measurement and Control. *Encyclopedia of Industrial Biotechnology*, pp.1–29. Available at: http://onlinelibrary.wiley.com/doi/10.1002/9780470054581.eib052/full.

Schuck, P., Zhao, H. & Zhao, H., 2017. *Sedimentation Velocity Analytical*

Ultracentrifugation, Boca Raton, FL : CRC Press, Taylor & Francis Group, [2017]: CRC Press. Available at: https://www.taylorfrancis.com/books/9781351976848 [Accessed June 25, 2019].

Senisterra, G. a & Finerty, P.J., 2009. High throughput methods of assessing protein stability and aggregation. *Molecular bioSystems*, 5(3), pp.217–223. Available at: http://jbx.sagepub.com/content/13/5/337.full.pdf.

Sharma, V.K. & Kalonia, D.S., 2010. Experimental Detection and Characterization of Protein. , pp.205–256.

Shire, S.J., 2009. Formulation and manufacturability of biologics. *Current Opinion in Biotechnology*, 20(6), pp.708–714. Available at: http://www.ncbi.nlm.nih.gov/pubmed/19880308 [Accessed June 18, 2019].

Shire, S.J., Shahrokh, Z. & Liu, J., 2004. Challenges in the development of high protein concentration formulations. *Journal of Pharmaceutical Sciences*, 93(6), pp.1390–1402.

Smith, C., 2007. Tools for drug discovery: tools of the trade. *Nature*, 446(7132), pp.219–22. Available at: http://dx.doi.org/10.1038/446219a.

Song, L., Hennink, E.J., Young, I.T. & Tanke, H.J., 1995. Photobleaching kinetics of fluorescein in quantitative fluorescence microscopy. *Biophysical journal*, 68(6), pp.2588–600. Available at: http://www.ncbi.nlm.nih.gov/pubmed/7647262 [Accessed July 4, 2019].

Sormanni, P., Aprile, F.A. & Vendruscolo, M., 2018. Third generation antibody discovery methods: *in silico* rational design. *Chemical Society Reviews*, 47(24), pp.9137–9157. Available at: http://xlink.rsc.org/?DOI=C8CS00523K [Accessed June 24, 2019].

Soumpasis, D.M., 1983. Theoretical analysis of fluorescence photobleaching recovery experiments. *Biophysical Journal*, 41(1), pp.95–97. Available at: http://www.ncbi.nlm.nih.gov/pubmed/6824758 [Accessed July 4, 2019].

Spidel, J.L., Vaessen, B., Chan, Y.Y., Grasso, L. & Kline, J.B., 2016. Rapid high-throughput cloning and stable expression of antibodies in HEK293 cells. *Journal of Immunological Methods*, 439, pp.50–58. Available at: https://www.sciencedirect.com/science/article/pii/S0022175916302113 [Accessed June 24, 2019].

Steger, K., Brady, J., Duskin, M. & Donato, K., 2016. Literature Review : CHO versus HEK Cell Glycosylation. Available at:

http://www.maxcyte.com/resources/AppNotes-TechPapers/CHO_HEK.pdf.

Stetefeld, J., McKenna, S.A. & Patel, T.R., 2016. Dynamic light scattering: a practical guide and applications in biomedical sciences. *Biophysical Reviews*, 8(4), pp.409–427.

Stokes, G., 1845. On the theories of internal friction of fluids in motion. *Trans Cam Philos Soc.*, 8, pp.287–305.

Subramaniam, K. V., 2016. Perspectives on Technology Trends in Biopharmaceuticals Manufacture. In *The Mind of an Engineer*. Singapore: Springer Singapore, pp. 433–439. Available at: http://link.springer.com/10.1007/978-981-10-0119-2_56 [Accessed June 4, 2019].

Tartaglia, G.G., Pawar, A.P., Campioni, S., Dobson, C.M., Chiti, F. & Vendruscolo, M., 2008. Prediction of Aggregation-Prone Regions in Structured Proteins. *Journal of Molecular Biology*, 380(2), pp.425–436. Available at: https://www.sciencedirect.com/science/article/pii/S0022283608005676 [Accessed June 21, 2019].

Teale, F.W. & Weber, G., 1957. Ultraviolet fluorescence of the aromatic amino acids. *The Biochemical journal*, 65(3), pp.476–82. Available at: http://www.ncbi.nlm.nih.gov/pubmed/13412650 [Accessed July 4, 2019].

Temel, D.B., Landsman, P. & Brader, M.L., 2016. Orthogonal Methods for Characterizing the Unfolding of Therapeutic Monoclonal Antibodies: Differential Scanning Calorimetry, Isothermal Chemical Denaturation, and Intrinsic Fluorescence with Concomitant Static Light Scattering. *Methods in Enzymology*, 567, pp.359–389.

Thomas, D.W., Burns, J., Audette, J., Carroll, A., Dow-Hygelund, C. & Hay, M., 2016. Clinical development success rates 2006-2015. *BIO Industry Analysis Report*, (June), p.https://www.bio.org/sites/default/files/Clinical%2. Available at: https://www.bio.org/sites/default/files/Clinical Development Success Rates 2006-2015 - BIO, Biomedtracker, Amplion 2016.pdf [Accessed June 13, 2019].

Thompson, R.B. & Scarlata, S., 2017. Fluorescence Made Easier: Fluorescence Techniques for the Novice. Episode 1: The Basics. In Springer, Cham, pp. 1–8. Available at: http://link.springer.com/10.1007/978-3-319-48260-6_1 [Accessed July 2, 2019].

Tous, G.I., Wei, Z., Feng, J., Bilbulian, S., Bowen, S., Smith, J., Strouse, R., McGeehan, P., Casas-Finet, J. & Schenerman, M.A., 2005. Characterization of a Novel Modification to Monoclonal Antibodies: Thioether Cross-link of Heavy and Light

Chains. *Analytical Chemistry*, 77(9), pp.2675–2682. Available at: http://www.ncbi.nlm.nih.gov/pubmed/15859580 [Accessed June 17, 2019].

Trovato, A., Seno, F. & Tosatto, S.C.E., 2007. The PASTA server for protein aggregation prediction. *Protein Engineering Design and Selection*, 20(10), pp.521–523. Available at: http://www.ncbi.nlm.nih.gov/pubmed/17720750 [Accessed June 24, 2019].

Tsumoto, K., Isozaki, Y., Yagami, H. & Tomita, M., 2019. Future perspectives of therapeutic monoclonal antibodies. *Immunotherapy*, 11(2), pp.119–127. Available at: https://www.futuremedicine.com/doi/10.2217/imt-2018-0130 [Accessed June 4, 2019].

Tuma, R., 2005. Raman spectroscopy of proteins: from peptides to large assemblies. *JOURNAL OF RAMAN SPECTROSCOPY J. Raman Spectrosc*, 36, pp.307–319. Available at: www.interscience.wiley.com [Accessed July 9, 2019].

Vendruscolo, M. & Paci, E., 2003. Protein folding: bringing theory and experiment closer together. *Current opinion in structural biology*, 13(1), pp.82–7. Available at: http://www.ncbi.nlm.nih.gov/pubmed/12581664 [Accessed June 18, 2019].

Ventura, S., Cristina Vega, M., Lacroix, E., Angrand, I., Spagnolo, L. & Serrano, L., 2002. Conformational strain in the hydrophobic core and its implications for protein folding and design. *Nature Structural Biology*, 9(6), pp.485–493. Available at: http://www.ncbi.nlm.nih.gov/pubmed/12006985 [Accessed June 24, 2019].

Vermeer, A.W. & Norde, W., 2000. The thermal stability of immunoglobulin: unfolding and aggregation of a multi-domain protein. *Biophysical journal*, 78(1), pp.394–404. Available at: http://www.ncbi.nlm.nih.gov/pubmed/10620303 [Accessed June 18, 2019].

Vincente, N., Diaz Zamboni, J., Adur, J., Paravani, E. & Casco, V., 2007. Photobleaching correction in fluorescence microscopy images Related content Photostability of thiol-capped CdTe quantum dots in living cells: the effect ofphoto-oxidation. *Journal of Physics: Conference Series*, 90. Available at: https://iopscience.iop.org/article/10.1088/1742-6596/90/1/012068/pdf [Accessed July 4, 2019].

Vlasak, J. & Ionescu, R., 2011. Fragmentation of monoclonal antibodies. *mAbs*, 3(3), pp.253–263.

Wahl, M., 2014a. Time-Correlated Single Photon Counting. *Technical Note*, pp.1–14. Available at:

http://www.picoquant.com/images/uploads/page/files/7253/technote_tcspc.pdf.

Wahl, M., 2014b. Time-Correlated Single Photon Counting The Principle of Time-Correlated. , pp.1–14.

Walsh, G., 2018. Biopharmaceutical benchmarks 2018. *Nature Biotechnology*, 36(12), pp.1136–1145. Available at: http://www.nature.com/articles/nbt.4305 [Accessed June 4, 2019].

Wang, W., 2005. Protein aggregation and its inhibition in biopharmaceutics. *Int J Pharm*, 289(1–2), pp.1–30. Available at: http://ac.els-cdn.com/S0378517304006908/1-s2.0-S0378517304006908-main.pdf?_tid=f6717102-5a2a-11e4-9e68-00000aacb35e&acdnat=1414010309_744d3603dc8c35001b75bdcc25959fe1.

Wang, W. & Roberts, C.J., 2010. *Aggregation of Therapeutic Proteins*, Hoboken, NJ, USA: John Wiley & Sons, Inc. Available at: http://doi.wiley.com/10.1002/9780470769829 [Accessed June 21, 2019].

Wang, W., Singh, S., Zeng, D.L., King, K. & Nema, S., 2007. Antibody Structure, Instability, and Formulation. *Journal of Pharmaceutical Sciences*, 96(1), pp.1–26. Available at: https://linkinghub.elsevier.com/retrieve/pii/S0022354916321633 [Accessed June 4, 2019].

Wang, Y., Rae, B.R., Henderson, R.K., Gong, Z., Mckendry, J., Gu, E., Dawson, M.D., Turnbull, G.A. & Samuel, I.D.W., 2011. Ultra-portable explosives sensor based on a CMOS fluorescence lifetime analysis micro-system. *AIP Advances*, 1(3), p.032115. Available at: http://aip.scitation.org/doi/10.1063/1.3624456 [Accessed July 5, 2019].

Weise, M., Kurki, P., Wolff-Holz, E., Bielsky, M.-C. & Schneider, C.K., 2014. Biosimilars: the science of extrapolation. *Blood*, 124(22), pp.3191–3196. Available at: http://www.bloodjournal.org/cgi/doi/10.1182/blood-2014-06-583617 [Accessed June 13, 2019].

Wolf Pérez, A.-M., Sormanni, P., Andersen, J.S., Sakhnini, L.I., Rodriguez-Leon, I., Bjelke, J.R., Gajhede, A.J., De Maria, L., Otzen, D.E., Vendruscolo, M. & Lorenzen, N., 2019. In vitro and in silico assessment of the developability of a designed monoclonal antibody library. *mAbs*, 11(2), pp.388–400. Available at: https://www.tandfonline.com/doi/full/10.1080/19420862.2018.1556082 [Accessed June 24, 2019].

Wriggers, W., Introduction to Spectroscopy and Fluorescence What is Spectroscopy ? *The University of Texas School of Health Information Sciences at Houston*.

Wu, H., Kroe-Barrett, R., Singh, S., Robinson, A.S. & Roberts, C.J., 2014. Competing aggregation pathways for monoclonal antibodies. *FEBS Letters*, 588, pp.936–941. Available at: http://dx.doi.org/10.1016/j.febslet.2014.01.051 [Accessed June 18, 2019].

Wurm, F.M., 2004. Production of recombinant protein therapeutics in cultivated mammalian cells. *Nature Biotechnology*, 22(11), pp.1393–1398. Available at: http://www.nature.com/articles/nbt1026 [Accessed June 17, 2019].

Wyatt Technology, 2016. Understanding Dynamic Light Scattering. Available at: http://www.wyatt.com/library/theory/dynamic-light-scattering-theory.html [Accessed February 12, 2017].

Yammine, A., Gao, J. & Kwan, A., 2019. Tryptophan Fluorescence Quenching Assays for Measuring Protein-ligand Binding Affinities: Principles and a Practical Guide. *BIO-PROTOCOL*, 9(11). Available at: https://bio-protocol.org/e3253 [Accessed July 4, 2019].

Ye, H., 2006. Simultaneous determination of protein aggregation, degradation, and absolute molecular weight by size exclusion chromatography-multiangle laser light scattering. *Analytical Biochemistry*, 356(1), pp.76–85.

Yuan, P. & Walt, D.R., 1987. Calculation for fluorescence modulation by absorbing species and its application to measurements using optical fibers. *Analytical Chemistry*, 59(19), pp.2391–2394. Available at: http://pubs.acs.org/doi/abs/10.1021/ac00146a015 [Accessed July 8, 2019].

Yuraszeck, T. & Gibbs, M., 2016. Drug development strategies for therapeutic biologics: industry perspectives. In H. Zhou & F. Theil, eds. *ADME and Translational Pharmacokinetics / Pharmacodynamics of Therapeutic Proteins*. Hoboken, NJ: Wiley, pp. 369–383.

Zhou, J., Ren, K., Zhao, Y., Dai, W. & Wu, H., 2012. Convenient formation of nanoparticle aggregates on microfluidic chips for highly sensitive SERS detection of biomolecules. *Analytical and Bioanalytical Chemistry*, 402(4), pp.1601–1609.